

Copyright © by
Arakali L. Ravimohan
1971

I. EXPERIMENTAL TESTS ON THE POSITIVE COLUMN
IN PURE RARE GASES AND THEIR BINARY MIXTURES

II. KINETICS OF HYDROCARBON REACTIONS IN THE
POSITIVE COLUMN OF D.C. AND PULSED D.C. DISCHARGES

Thesis by

Arakali L. Ravimohan

In Partial Fulfillment of the Requirements

For the Degree of

Doctor of Philosophy

California Institute of Technology

Pasadena, California

1971

(Submitted Feb. 16, 1971)

This thesis is dedicated to
my parents
who see in it a significance
that goes beyond its contents

ACKNOWLEDGMENTS

It is with great pleasure that I acknowledge the guidance of Professor Fred Shair during the course of this project. His constant encouragement and insistence on meticulousness have played a large role in the development of my scientific personality over the past few years. My graduate studies at Caltech have been immeasurably enriched by my contact with him.

The project would not have gone very far without the contributions of many excellent people on the technical support staff. I am especially indebted to John Yehle for helping in the development of the microwave circuitry and other electronics. George Griffith, Chick Nakawatase and Bill Schuelke of the Chemical Engineering Instrument Shop have cheerfully met the impossible deadlines I imposed on them with no sacrifice of excellence. Erich Siegel and Sig Jenner of the Chemistry Glass Blowing Shop have been very helpful in the fabrication of the glassware.

I am grateful to the U.S. Atomic Energy Commission and the California Institute of Technology for supporting me with a Graduate Research Assistantship and a tuition scholarship. The USAEC support was under Project Agreement No. 1 under AT(04-3)-767. Thanks are also due to the Jet Propulsion Laboratory of Caltech for the loan of some of the electronic equipment.

I have had the good fortune of having my thesis typed with exceptional competence by Ruth Stratton. June Gray's help with the illustrative material is also thankfully acknowledged.

ABSTRACT

Part I:

A TM_{011} microwave cavity was used to measure the radially averaged electron density \bar{n}_e and the electron-neutral collision frequency ν_{en} in d.c. glow discharge positive columns of pure rare gases and their binary mixtures. Electric field E was measured by measuring the floating potential across pairs of probes in the plasma. The pure gases studied were He, Ne and Ar at pressures of 1-8 torr and discharge currents I of 5-20 mA. The calculated values of the electron drift velocity v_d in He and Ne are substantially lower than the Bradbury and Nielson drift tube values, indicating substantial ionization via metastables in the range of p and I investigated. Discharges in He-Ar and He-Ne mixtures at $p = 2-5$ torr and $I = 15$ mA exhibit time and space dependent values of \bar{n}_e , ν_{en} and E due to the effect of cataphoresis. The results indicate that the Shair and Remer model is a reasonable description of the phenomenon of cataphoresis in these mixtures where the impurity (Ar or Ne) content is in the range of 2-20%.

Part II:

By employing a positive column flow reactor with low residence times (< 100 msec) in d.c. discharges with low currents (< 5 mA), it is possible to convert up to 5% of the feed methane into ethane, ethylene and hydrogen with negligible formation of solid and liquid products. The percent methane in the argon or helium feed C_0 affects the

product distribution, with good selectivity for $C_o > 5\%$. Average steady-state electron densities in the discharge were simultaneously measured by perturbation of the resonance of a TM_{010} microwave cavity. A pulsed d.c. discharge enabled the residence time to be effectively reduced even further. The pulsed discharge experiments were conducted at 3-9 torr with pulse durations ~ 1 msec and pulse intervals of 20-50 msec. Pulse current was measured as a function of time with a current probe. The TM_{010} cavity was used to obtain transient electron densities in the discharge, which varied between 10^9 and 10^{10} electrons/cm³.

The kinetic results are consistent with a free radical mechanism with electron-impact dissociation as the initiating step. Derived values of the integrated cross-section for $CH_4 + e \xrightarrow{\alpha} CH_3 + H + e$ and $CH_4 + e \xrightarrow{\beta} CH_2 + H_2 + e$ are in the range $3.6 - 15.5 \times 10^{-11} \text{ cm}^3 \text{ sec}^{-1}$, and that for $C_2H_4 + e \xrightarrow{\gamma} C_2H_2 + H_2 + e$ is $\sim 9 \times 10^{-10} \text{ cm}^3 \text{ sec}^{-1}$. α and β fall with C_o in the range 4.0-12.6%, indicating a shift of the electron energy distribution function $f_e(\epsilon)$ to lower values of ϵ . Calculations are presented for the case of H_2 dissociation to illustrate the strong effect of the tail end of $f_e(\epsilon)$ on the rate of chemical reaction.

TABLE OF CONTENTS

ACKNOWLEDGMENTS	iii
ABSTRACT	iv
TABLE OF CONTENTS	vi
LIST OF FIGURES	x
LIST OF TABLES	xiv
NOMENCLATURE	xvi
PROLEGOMENA	1
PART I. EXPERIMENTAL TESTS ON THE POSITIVE COLUMN IN PURE RARE GASES AND THEIR BINARY MIXTURES	
1. Introduction	4
1.1 The Glow Discharge in Pure Gases and Mixtures	
1.2 Review of Literature	
1.2a) Microwave cavity resonance	
1.2b) Electric field measurements	
2. Experimental Technique (I)	11
2.1 Two-Bulb Discharge Tube and Vacuum System	
2.2 D.C. Power Supply and Electric Field Measurements	
2.3 Microwave System	
2.3a) Principle of operation	
2.3b) Microwave apparatus	
2.3c) Calibration of the microwave cavity	
3. Measurements in Pure He, Ne, and Ar	17
3.1 Aim of Experiments	
3.2 Procedure	
3.3 Presentation of Results	
3.3a) Longitudinal electric field E	
3.3b) Electron density n_e and drift velocity v_d of the electrons	
3.3c) Electron-neutral collision frequency ν_{en}	
3.4 Discussion of Results in Pure Rare Gases	
3.5 Suggestions for Future Work in Pure Rare Gases	
4. Measurements in Binary Gas Mixtures: He-Ar, He-Ne	24
4.1 Cataphoresis	
4.2 Aim of Experiments	
4.3 Procedure	

- 4.4 Presentation and Discussion of Results
 - 4.4a) Steady-state results
 - 4.4b) Transient results
- 4.5 Suggestions for Future Work

End of Part I

PART II. KINETICS OF HYDROCARBON REACTIONS IN THE POSITIVE COLUMN OF D.C. AND PULSED D.C. DISCHARGES

- 5. Introduction 31
 - 5.1 Review of Literature
 - 5.1a) Chemical reactions in equilibrium and non-equilibrium plasmas
 - 5.1b) Gas chromatography of the light hydrocarbons
 - 5.2 Scope of the Present Measurements in Terms of Plasma Kinetic Theory
- 6. Experimental Technique (II) 42
 - 6.1 Carry-Over of Previously Developed Systems
 - 6.2 The Reactor and Gas Handling System
 - 6.2a) The D.C. discharge flow reactor
 - 6.2b) Flow system for gas handling
 - 6.3 The Gas Chromatograph System
 - 6.4 The Pulse Generator and Adaptation of the Microwave Circuit
- 7. Measurements in CH₄-Ar Mixtures with a D.C. Discharge Flow System 56
 - 7.1 Aim of Experiments
 - 7.2 Description of Procedure Used
 - 7.3 V-I Characteristics of Choked Flow Orifice System
 - 7.4 Composition Measurements of the Effluent Stream
 - 7.5 Microwave Measurements on the Discharge
 - 7.6 Treatment of Data and Discussion of Results
- 8. Measurements in CH₄-Ar and CH₄-He with a Pulsed D.C. Discharge Flow System 68
 - 8.1 Aim of Experiments
 - 8.2 Description of Procedure Used
 - 8.3 Fine Structure of the Pulsed D.C. Discharge and Its Variation with Gas Composition
 - 8.4 n_e as a Function of Time within the Pulse
 - 8.5 Composition Measurements of Effluent Stream
 - 8.6 Treatment of Data and Discussion of Results

9.	A Proposed Chemical Mechanism to Explain the Kinetic Data	80
9.1	The Mechanism	
9.2	Agreement with Fundamental Work in Free Radical Chemistry	
9.3	Tests of the Proposed Mechanism on the D.C. Discharge Data	
9.4	Tests of the Proposed Mechanism on the Pulsed Discharge Data	
9.5	Integrated Cross-Sections for	
	$\text{CH}_4 + e \longrightarrow \text{CH}_3 + \text{H} + e$	
	$\text{CH}_4 + e \longrightarrow \text{CH}_2 + \text{H}_2 + e$	
	$\text{C}_2\text{H}_4 + e \longrightarrow \text{C}_2\text{H}_2 + \text{H}_2 + e$	
9.6	Order of Magnitude Calculations to Rule Out Ionic and Photochemical Mechanisms	
10.	The Role of the Electron Energy Distribution Function $f_e(\epsilon)$	97
10.1	Calculations on H_2 Dissociation with Maxwellian and Druyvesteyn Distributions	
10.1a)	Frequency of inelastic collision processes involving electrons with a Maxwellian distribution of energy	
10.1b)	Frequency of inelastic collision processes involving electrons with a Druyvesteyn distribution of energy	
10.1c)	A comparison of the rate of dissociation of H_2 using i) Maxwellian and ii) Druyvesteyn distribution	
10.2	Difficulties in Experimentally Measuring $f_e(\epsilon)$ especially in Reacting Systems	
10.3	Difficulties in Solving Boltzmann's Equation for $f_e(\epsilon)$	
11.	Suggestions for Future Work in Reacting Non-Equilibrium Plasmas	107

End of Part II		
12.	Summarized Conclusions of Parts I and II	109
13.	Tables for Chapters 1-11	112
14.	Figures for Chapters 1-11	158
APPENDICES		241
A-1	Error Analysis	
A-2	Nature of Solution of Cataphoresis Equations for the Steady-State Profile for Given Values of $\langle n_e \rangle$ and E	

A-3	Neutral Temperature Estimation	
A-4	Linear Perturbation Analysis of a Resonant Microwave Cavity	
A-5	Electron-Ion Recombination in the Afterglow of a Pulsed Discharge	
A-6	Evaluation of the Integral \bar{I}	
A-7	Similarity Criteria for Glow Discharges	
A-8	Non-Equilibrium Plasma Reactor for Natural Gas Processing	
A-9	Procedure for Operation of the Flame Ionization Detector	
LIST OF REFERENCES		264
AUTHOR INDEX		273
PROPOSITIONS		
P-1	The Accuracy of Kinetic Parameters Estimated from Batch and Integral Reactor Data	278
P-2	Application of Microwave Cavity Perturbation Techniques to a Study of the Kinetics of Reactions in the Liquid Phase	287
P-3	Optimization of Chemical Reactor Networks with Respect to Flow Configuration	292

MISCELLANEOUS PUBLICATIONS AND CONFERENCE PRESENTATIONS		309

* * *

LIST OF FIGURES

1. Typical view of a d.c. glow discharge at $p = 1-10$ torr	5
2. Breakdown potential V_s and maintenance potential V_g in a d.c. glow discharge	6
3. Schematic V-I characteristic of d.c. discharges	6
4. Glow discharge tube 1	159
5. The microwave cavity	160
6. Coaxial circuit for automatic plotting of transmission characteristic of microwave cavity with glow discharge plasma	161
7. Electric field in the positive column of helium	162
8. Electric field in the positive column of neon	163
9. Electric field in the positive column of argon	164
10. Electron densities in the positive column of pure helium	165
11. Electron densities in the positive column of pure neon	166
12. Electron densities in the positive column of pure argon	167
13. Drift velocities of electrons in helium	168
14. Drift velocities of electrons in neon	169
15. Drift velocities of electrons in argon	170
16. Electron-neutral collision frequency in helium	171
17. Electron-neutral collision frequency in neon	172
18. Electron-neutral collision frequency in argon	173
19. Levels of ionization in a He-Ar mixture	174
20. Electron density and collision frequency vs. time in helium-argon mixtures at cathode end	175
21. Nature of solution to cataphoresis equations--normal case	176
22. Nature of solution to cataphoresis equations--anomalous case	177
23. Wall temperatures in He discharges	178

24.	Dissociation mechanisms in H_2 , O_2 and N_2 according to Franck-Condon principle	41
25.	The gas flow system	179-180
26.	D.C. power supply and measuring circuit	181
27.	Circuit for electric field measurement	182
28.	Schematic diagram of choked flow orifice system	43
29.	Comparison of residence time distribution in idealized reactors	183
30.	Effect of varying amounts of longitudinal dispersion on the residence time distribution	184
31.	Glow discharge tube 2	185-186
32.	Positive column isolation system	187
33.	Simple design of the orifice	187
34.	Throughput of Ar and residence time vs. pressure p_1	188
35.	Gas flow in the chromatographic system	189-190
36.	LOENCO 6-way valve for sample injection into chromatograph	191
37.	Quantitative calibration of the flame ionization detector	192
38.	Typical separation of lower hydrocarbons	193
39.	Atypical separation of lower hydrocarbons	194
40.	Voltage v_3 as a function of time	195-196
41.	Schematic of pulse generator	53
42.	Pulse generator circuit	197-198
43.	Electrical measurements on pulsed discharge	199-200
44.	Resonance curves of microwave cavity with and without pulsed discharge	201
45.	V-I characteristics of He discharge in a choked flow orifice system	202
46.	V-I characteristics of Ar discharge in a choked flow orifice system	203
47.	% of methane converted vs. I --preliminary results	204

48.	Product distribution of converted methane--preliminary results	205
49.	% ethane in effluent stream vs. mean residence time	206
50.	% of reactant converted to ethane vs. initial % CH ₄ (C ₀)	207
51.	Ethane/ethylene vs. initial % CH ₄ (C ₀)	208
52.	Electron density in reacting CH ₄ -Ar d.c. glow vs. discharge current I	209
53.	% ethane in effluent stream vs. discharge current I	210
54.	(C ₂ H ₂)/(C ₂ H ₄) vs. discharge current I	211
55.	% C ₂ H ₆ in effluent vs. $\tau I^{0.8}$	212
56.	(C ₂ H ₂)/(C ₂ H ₄) vs. $\tau I^{0.8}$	213
57.	Test of first order decay of reacting CH ₄	214
58.	i _m vs. t in pure Ar pulsed discharge	215
59.	i _m vs. t for 0.91% CH ₄ in Ar pulsed discharge	215
60.	i _m vs. t for 17.7% CH ₄ in Ar pulsed discharge	216
61.	i _m vs. t for pure He pulsed discharge	216
62.	i _m vs. t for 0.82% CH ₄ in He pulsed discharge	217
63.	i _m vs. t for 16.4% CH ₄ in He pulsed discharge	217
64.	i _m vs. t for pure CH ₄ pulsed discharge	218
65.	Qualitative explanation of the measured current i _m in pulsed discharge circuit	71
66.	Electron density as a function of time in the afterglow of CH ₄ and Ar	219
67.	Effect of C ₀ on (n _e) ₀ vs. t in CH ₄ -Ar mixtures	220
68.	Effect of C ₀ on (n _e) ₀ vs. t in CH ₄ -He mixtures	221
69.	Effect of pulse width τ_w on (n _e) ₀ vs. t in CH ₄ -Ar mixtures	222
70.	Effect of total pressure p ₁ on (n _e) ₀ vs. t in CH ₄ -Ar mixtures	223
71.	% conversion to C ₂ H ₆ vs. ξ^* in pulsed discharge	224

72.	% conversion to C_2H_4 vs. ξ^* in pulsed discharge	225
73.	Effect of τ , τ_w , τ_I variation on % conversion to C_2H_6 vs. ξ^*	226-227
74.	Effect of τ , τ_w , τ_I variation on % conversion to C_2H_4 vs. ξ^*	228-229
75.	Effect of total pressure p_1 on pulsed discharge reaction of CH_4	230
76.	Slopes of ethane and ethylene conversion curves in pulsed discharge vs. C_0	231
77.	% CH_4 converted to all products vs. C_0 with different carrier gases	232
78.	Minimum ethane/ethylene ratio vs. C_0 with different carrier gases	233
79.	Integrated cross-sections for electron-impact dissociation reactions	234
80.	Inelastic collision cross-section for H_2 dissociation	235
81.	The Maxwellian distribution of electron energies	236
82.	The Druyvesteyn distribution of electron energies	237
83.	A comparison of the "tails" of the Maxwellian and Druyvesteyn distributions	238
84.	A simple double Langmuir probe circuit for T_e measurement	239
85.	Measured double probe characteristics in Ar at $p = 5.0$ torr	240
A-5.1	Test of recombination control in CH_4 and Ar afterglows	256

LIST OF TABLES

1. Calibration of the TM_{011} mode	113
2. Dielectric constants of organic liquids determined with the TM_{010} mode	114
3. Measurements in helium-argon mixtures	115-117
4. Measurements in helium-neon mixtures	118-119
5. Some typical reactions occurring in plasmas	33
6. Mean electron energies calculated from equation (18)	38
7. Reynolds number for flow in the reactor	120
8. Limiting cases of the residence time distribution in laminar flow reactors	46
9. Calculated pressure drop in flow reactor with pure argon at 295°K	121
10. Retention times of C_1-C_3 hydrocarbons on silica gel column at various column temperatures	122
11. Relative response factors of C_1-C_3 hydrocarbons on silica gel column	123
12-18. Preliminary runs #1-35 in a d.c. glow discharge	124-130
19-20. Preliminary runs #36-43 in an a.c. glow discharge	131-132
21-36. Kinetic runs #1-71 in d.c. glow discharges in CH_4 -Ar mixtures at $p_1 = 5.0$ torr	133-148
37. Effects of radial and longitudinal diffusion in the experimental reactor	149
38-39. Pulsed discharge runs #1-8: effect of varying gas residence time	150-151
40. Pulsed discharge runs #2,9,10: effect of varying total pressure	152
41. Pulsed discharge runs #11-14: effect of varying pulse interval	153
42. Pulsed discharge runs #15-20: effect of varying pulse width τ_w , and τ , τ_I and τ_w simultaneously	154
43. Pulsed discharge runs #21-30: effect of varying rare gas carrier	155

44.	Calculated values of electron-impact cross-sections for reactions (1), (3) and (6)	156
45.	Values of $(1-\theta)$ in the Maxwellian energy distribution	89
46.	A comparison of the rate of dissociation of H_2 using i) Maxwellian, and ii) Druyvesteyn distributions	157

NOMENCLATURE

B'	constant in equation (54)
C	symmetrical bell-shaped distribution of equation (29)
C_o	% methane in the feed on a molar basis
C'	constant in equation (54)
$C_{\lambda m}$	parameter in equation (71)
D	diffusion coefficient cm^2/sec
D'	defined in equation (58)
D_c	diameter of microwave cavity cm ($= 2R_o$)
D_R	inside diameter of reactor cm ($= 2R$)
D_a	ambipolar diffusion coefficient cm^2/sec
E	electric field, volts/cm
\vec{E}, \vec{E}_o	electric field vectors in Appendix A-4
E_z	electric field along the axis of a cylinder, volts/cm
$E(\theta)$	exit age residence time distribution of particles in the reactor
\vec{H}	magnetic field intensity in Appendix A-4
I	d.c. discharge current, mA
\bar{I}	integral evaluated in Appendix A-6
J	$\frac{\langle n_+ \rangle}{\langle n_e \rangle}$ in cataphoresis
\vec{J}	current density in Appendix A-4
K	defined in equation (A-2.2)
L	length of discharge tube, cm
L_c	length of microwave cavity, cm
M	mass of neutral molecule

N	neutral particle number density per cm^3
N_i	particle density of i^{th} scatterer in equation (10)
P_c	electron-neutral elastic collision probability
Q	quality factor of resonance
Q_i	cross-section for the i^{th} scatterer in equation (10)
R	plasma radius, cm
R_o	cavity inside radius, cm
R_g	gas constant
Re	Reynolds number, dimensionless
S_{lm}	parameter in equation (71)
T_a	ambient air temperature, $^{\circ}\text{K}$
T_e	electron temperature, $^{\circ}\text{K}$
T_g	gas temperature, $^{\circ}\text{K}$
T_i	diffusion time corresponding to i^{th} mode, sec
T_w	wall temperature, $^{\circ}\text{K}$
V_s	breakdown voltage, volts
V_g	maintenance potential, volts
\dot{V}_f	volumetric flow rate of gas through the reactor, cm^3/sec
V_p	bias voltage on double probe
V_R	volume of positive column reactor, cm^3
a_i	constant of equation (A-5.3)
d	interelectrode distance, cm
e	charge on an electron = 1.6×10^{-19} coulomb
$f_e(\epsilon)$	electron energy distribution function expressed as a fraction

f'_0	resonant frequency of perturbed cavity MHz
f_2, f_1	half power frequencies of microwave resonance MHz
g	relative velocity between electron and neutral molecule
h	heat transfer coefficient for natural convection in Appendix A-2
i	1) level of ionization ($= \frac{\langle n_+ \rangle}{\langle n_0 \rangle + \langle n_+ \rangle}$) in Chapter 4 and Appendix A-2 2) transient discharge current in a pulsed discharge, mA
i_{1+}, i_{2+}	currents in double probe experiment of Chapter 10, μA
i_m	measured current in pulsed discharge circuit, mA
i_s, i_{d_1}, i_{d_2}	transient currents in pulsed discharge circuit
j	current density in d.c. discharge, mA/cm^2
\vec{k}	propagation vector in Appendix A-4
\bar{k}	fraction of input energy converted to air from discharge tube
k_B	Boltzmann's constant ($= 1.38 \times 10^{-16} \frac{\text{joule}}{\text{°K}}$)
m_0	mass of neutral molecule
m_e	mass of an electron $9.1 \times 10^{-28} \text{g}$
n	$(n_e)_0$ in Appendix A-1
$\langle n_0 \rangle$	radially averaged impurity particle concentration in cataphoresis, per cm^3
$\langle n_+ \rangle$	radially averaged positive ion density, per cm^3
n_e	electron density per cm^3
$(n_e)_0$	electron density on the axis of the discharge tube per cm^3
$\langle n_e \rangle$	radially averaged n_e in Part I ($= 0.433 (n_e)_0$)
\bar{n}_e	radially averaged n_e as measured by microwave cavity resonance, Part II ($= 0.433 (n_e)_0$)

p	total pressure in discharge, torr (The symbol P and the equivalent unit mm Hg have been used in some figures)
q	$\frac{i}{n_e}$ in a pulsed discharge
\vec{r}	radius vector in Appendix A-4
r_o	outer radius of discharge tube, cm
t	time. Also internal variable in equation (63)
u_1	internal variable in equations (11) and (12)
\vec{v}	electron velocity in Appendix A-4
v_a, v_c	transient voltages at anode and cathode of pulsed discharge, volts
v_d	electron drift velocity, cm/sec
w	electron speed
x	$\delta(\Delta f_{1/2})$ in Appendix A-1
y	$(f'_o - f_o)$ in Appendix A-1
z	distance along positive column, cm
α	electrostatic Peclet number ($= \frac{\langle n_+ \rangle}{\langle n_o \rangle + \langle n_+ \rangle} \frac{\mu EL}{D}$)
α_{oo}, α_{lm}	parameters in equation (71)
α'	second order recombination coefficient for electrons and ions, $\text{cm}^3 \text{sec}^{-1}$
α_i	primary ionization coefficient of Townsend
β'	$\frac{\alpha' n_o \Lambda^2}{a}$, dimensionless parameter of Ref. (134)
β_{lm}	parameter in equation (71)
δ	cathode end bulb volume divided by discharge tube volume
ϵ	1) anode end bulb volume divided by discharge tube volume in Chapter 4 and Appendix A-2 2) arbitrary energy as in $f_e(\epsilon), \phi(\epsilon)$

$\bar{\epsilon}$	average electron energy, eV
ϵ_0	permittivity of free space
ζ	internal variable in equations (64) and (66) and Appendix A-6
η	1) dimensionless form factor of equations (2) and (3) 2) dimensionless length ($= z/L$) along cataphoresis tube with cathode end zero
θ	1) dimensionless impurity concentration ($= \frac{\langle n_0 \rangle + \langle n_+ \rangle}{\langle n_0^0 \rangle}$) in Chapter 4 and Appendix A-2 2) dimensionless time ($= t/\tau$) in Chapters 5-8 3. fraction of particles with energies below ϵ_θ in Chapters 9 and 10
Λ_i	diffusion length of <i>i</i> th mode, cm
μ	mobility of positive ion, $\text{cm}^2/(\text{volt} \times \text{sec})$
μ'	viscosity, cp
$\bar{\mu}$	refractive index of plasma (complex)
μ_0	permeability of free space
ν	rate of electron-impact process
ν_a	attachment coefficient, sec^{-1}
ν_{en}	average electron-neutral collision frequency per electron per sec
ν_ℓ	relaxation frequency in Chapter 10
ξ	variable defined by equation (31)
ξ^*	practical version of ξ ($= \frac{\tau}{\tau_I} \int_0^{\tau_w} idt$)
σ	molecular radius of neutral A^0
τ	mean residence time in reactor, msec
$\frac{M}{\tau_c}$	dimensionless characteristic time for cataphoresis, as defined in equation (11)
τ_I	pulse interval, msec
τ_x	cutoff value of t within a pulse, msec

τ_w	pulse width, msec
$\phi(\epsilon)$	energy dependent cross-section, \AA^2
ω	applied frequency, rad/sec
ω_{po}	electron plasma frequency defined in equation (4) rad/sec

PROLEGOMENA

It is now being realized that the plasma state is the rule rather than an exception in the physical universe. Plasma may be defined broadly as an ionized gas that conducts electricity and has approximately equal numbers of positive and negative charged particles. In this thesis, we deal with systems with low degrees of ionization $\sim 10^{-6}$ to 10^{-8} , which are typical values in low pressure (~ 1 -10 torr) glow discharges. Such systems exhibit extreme departures from the Maxwell-Boltzmann equilibrium condition. Neutral particle and ion mean energies remain at values close to that corresponding to the ambient temperature ($\sim 300^\circ\text{K}$), although the light electrons attain very high "temperatures" ($\sim 10^4$ $^\circ\text{K}$). This property distinguishes non-equilibrium plasmas from the equilibrium plasmas, e.g., arcs and induction torches, where neutral temperatures are typically 10^3 - 10^4 $^\circ\text{K}$. Laboratory glow discharges have values of E/N , the electric field divided by the neutral particle density in the range of 1.0 to $750 \times 10^{-17} \text{V-cm}^2$, depending on pressure and gas composition. Among the applications of interest to a chemical engineer are cataphoretic separators for obtaining extremely pure gases (impurity levels less than 1 in 10^8), and reactors for conducting irreversible chemical reactions. Part I of the thesis is about non-reacting systems, with measurements in pure rare gases and their binary mixtures. In gas mixtures, it is necessary to consider the effect of cataphoresis, wherein the component with the lowest ionization potential is preferentially ionized and drifts toward the cathode, thus establishing concentration gradients in space and time.

The focus of the work, however, is on Part II, which deals with the possibility of using a non-equilibrium plasma to conduct hydrocarbon reactions. An attempt is made, using plasma kinetic theory, to relate the experimentally observed kinetics to the microscopic processes taking place in the discharge. Future work could proceed along two directions. One is the development of commercially feasible processes to utilize plasmas in general, and non-equilibrium plasmas in particular. The other direction is towards establishing greater contact with more fundamental work, e.g., low-energy beam measurements of electron-impact dissociation cross-sections. The results of the present exploratory investigation indicate that both these approaches are likely to be extremely productive.

PART I

EXPERIMENTAL TESTS ON THE POSITIVE COLUMN
IN PURE RARE GASES AND THEIR BINARY MIXTURES

1. INTRODUCTION

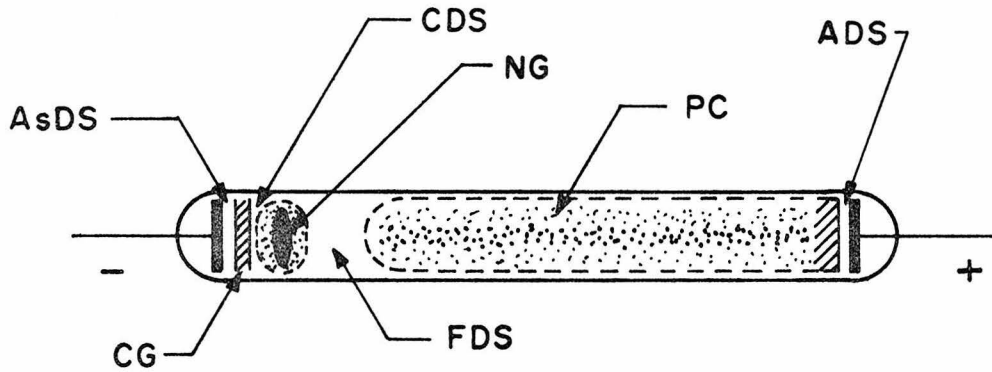
1.1 The Glow Discharge in Pure Gases and Mixtures

A typical d.c. glow discharge is shown in Fig. 1. The cathode glow is a thin layer separated from the cathode by the Aston dark space. The cathode glow is bounded on the other side by the Crookes dark space, following which is another luminous region called the negative glow. The Faraday's dark space leads to a region which is sometimes striated. This is the positive column. The color and intensity of the glow depend on the nature and the pressure of the gas.

The electrical characteristics of a glow discharge are shown in Fig. 2. The lowest value of applied potential difference V_s at which a discharge is established is called the sparking potential or the static breakdown potential. Once the glow discharge is stabilized, the voltage across it is the maintenance potential. This is usually lower than the breakdown potential, but becomes higher at low values of pressure p , or inter-electrode distance d . Paschen's law expresses the results of breakdown studies by the relationship

$$V_s = f(pd) \quad (1)$$

Another instructive electrical characteristic is the voltage-current curve for a discharge (Fig. 3). In the region AB, the gap potential remains fairly constant. As the current increases, the voltage falls and stabilizes at $V_g < V_s$. This is the region CD of the normal glow discharge. At higher values of the current, we have the abnormal glow, and finally the arc discharge region FG.



AsDS	ASTON DARK SPACE
CG	CATHODE GLOW
CDS	CROOKES DARK SPACE
NG	NEGATIVE GLOW
FDS	FARADAY DARK SPACE
PC	POSITIVE COLUMN
ADS	ANODE DARK SPACE

Fig. 1. Typical view of a d.c. glow discharge at $p = 1-10$ torr

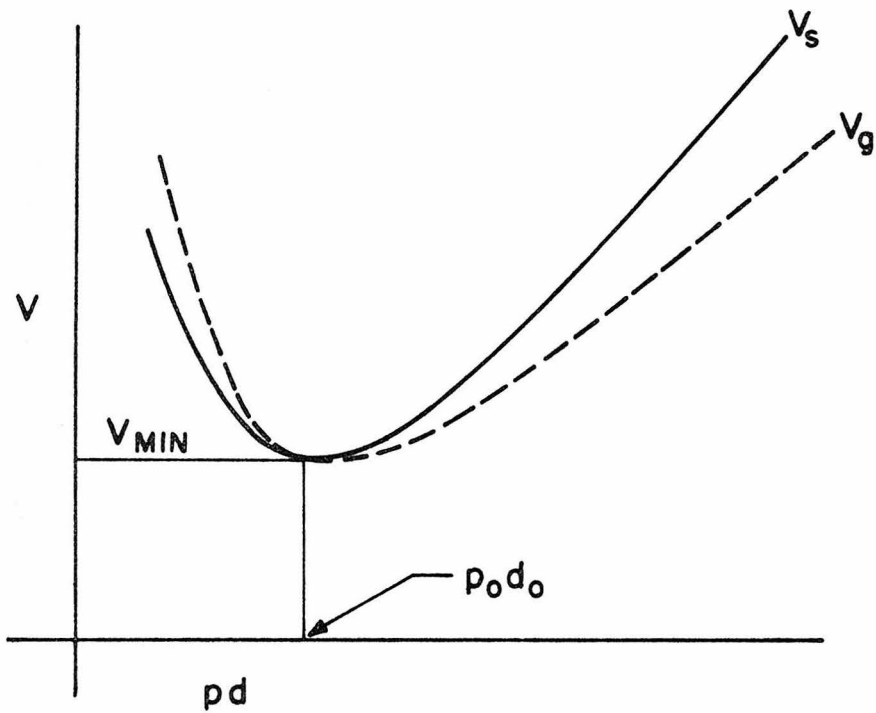


Fig. 2. Breakdown potential V_s and maintenance potential V_g in a d.c. glow discharge

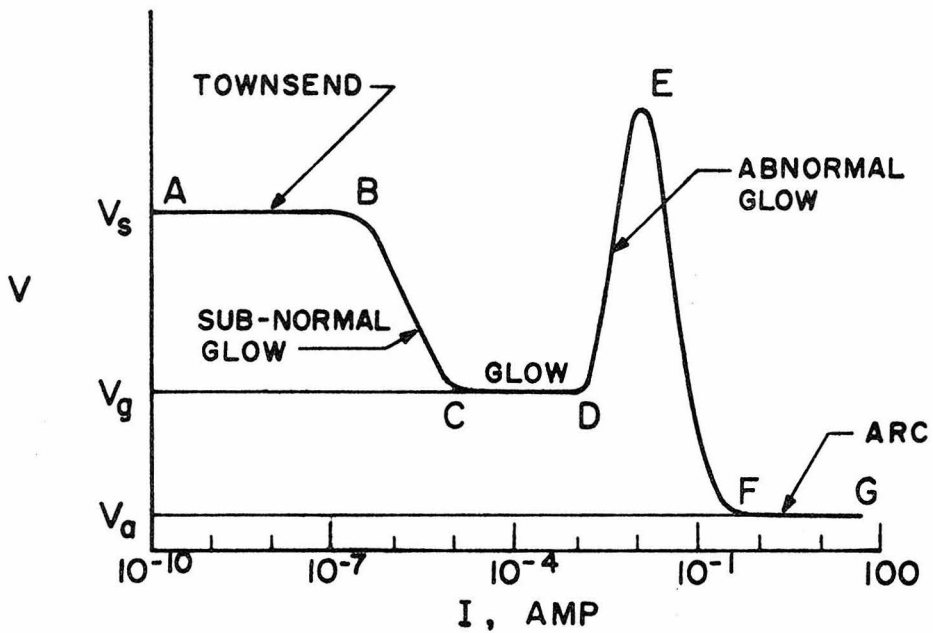


Fig. 3. Schematic V-I characteristic of d.c. discharges

Irving Langmuir⁽¹⁾ was the first to recognize that the positive column of a glow discharge is a fourth state of matter, to which he bestowed the name "plasma". Now it is customary to classify glow discharge phenomena under the general category of "Non-Equilibrium Plasmas" where the molecules are at temperatures close to the ambient, although the electron temperature may be very much higher. Llewellyn-Jones⁽²⁾ gives a good introductory account in his monograph on the subject. Brown's text⁽³⁾ goes into greater detail about the microscopic phenomena taking place in the discharge. Cobine⁽⁴⁾ deals with various electrical engineering applications, after giving a semi-empirical account of the basic processes in the plasma. A comprehensive review of pre-1956 work on the glow discharge is found in the article by Gordon Francis in the Handbuch der Physik.⁽⁵⁾

Under certain conditions of gas composition, current density and pressure, alternate dark and bright "striations" are seen in the positive column. Two types of striations may be recognized--the stationary or standing variety and the moving striations. Often their motion is rapid enough for the column to appear uniform to the naked eye. Pekarek⁽⁶⁾ has attempted to explain the observed behavior from a theoretical standpoint.

The positive column of a cylindrical glow discharge between parallel plates has been a topic of interest ever since its visual properties were first elucidated. In recent years, there has been a resurgence of activity in this area with the discovery of new applications, as in lasers,⁽⁷⁾ cataphoretic tubes,⁽⁸⁾ and reactors for conducting difficult chemical reactions.⁽⁹⁾ Other applications of glow

discharges are in electronic tubes and thin film deposition by sputtering. Past work has concentrated mainly on the unstriated column in pure gases, and a theory is available⁽⁵⁾ that predicts the electric field and electron "temperature" in the positive column of rare gases, e.g., He, Ne, Ar, to within $\pm 20\%$, and simple molecular gases, e.g., H_2 , O_2 , N_2 to within $\pm 50\%$. However, very little systematic and reliable information is available even today about the properties of electrons in such discharges, notably the electron density n_e , the electron-neutral collision frequency ν_{en} , and, on a subtler level, the electron energy distribution $f_e(\epsilon)$. In discharges in gas mixtures, the situation is even more hopeless. The above-mentioned electronic properties enter intimately into any attempted explanation of spectral data,⁽¹¹⁾ cataphoresis,⁽⁸⁾ or chemical reactions in the positive column.⁽¹²⁾ Hence, further development of these applications would seem to demand a concerted effort to understand the behavior of the electronic population in pure gases and mixtures, at least to the extent of being able to develop semi-empirical models.

1.2 Review of Literature

1.2a) Perturbation of microwave cavity resonance by a plasma.

The microwave cavity technique⁽¹³⁻¹⁶⁾ is a powerful recent tool for obtaining the electron density n_e and the electron-neutral collision frequency ν_{en} in plasmas. Actual measurements using this technique are largely confined to the study of microwave discharges and of plasma decay. In glow discharges, n_e is traditionally determined from Langmuir probe data and from spectral observations.⁽¹⁷⁾ These data are difficult to interpret, and the accuracy of the resulting numbers is

uncertain. A recent comparison⁽¹⁸⁾ of the probe and microwave techniques in a Ne positive column concluded that the probe method (single and double) could lead to underestimation of n_e , by a factor of as much as 5, due to the disturbing effect of the probe on the plasma. Prince and Robertson⁽¹¹⁾ report some microwave cavity determinations of n_e ratios in an argon glow discharge, but give no absolute values. Anderson⁽¹⁰⁾ reported the first quantitative microwave cavity measurements in d.c. glow discharges in connection with some Hall effect studies of positive columns in He, Ne, Ar. Labuda and Gordon⁽¹⁹⁾ measured n_e in He-Ne discharges as a function of current and tube diameter, using a TE_{101} cavity; but no attempt was made in their work to pick up spatial or temporal variations which might have been induced due to cataphoresis. Gheorgiu⁽²⁰⁾ has used the technique to measure the "electric susceptibility of an ionized gas".

The work described in the present thesis represents the first application of the microwave cavity technique to

- a) measurements in d.c. glow discharges in very pure He, Ne and Ar (Chapter 3)
- b) measurements in He-Ar and He-Ne mixtures in the range where cataphoresis occurs (Chapter 4)
- c) measurements in chemically reacting CH_4 -Ar and CH_4 -He flows (Part II).

It is also the first recorded instance of the use of the TM_{011} mode for measuring plasma properties.

1.2b) Electric field measurements in the positive column. The measurement of the longitudinal electric field E , on the other hand, is fairly straightforward. The earlier workers differentiated the

voltage across the discharge with respect to the variable distance between the electrodes.⁽⁵⁾ But this was soon given up in favor of measuring, with a high-impedance voltmeter, the voltage drop across two identical probes, placed at a known distance of separation in the plasma.⁽²¹⁾ This method has proved quite reliable and has been used even very recently.⁽²²⁾ The fact that a probe technique leads to good values of E is probably because the disturbing effect of the probes on this parameter is less than their effect on n_e , and because radial gradients⁽⁵⁾ in the longitudinal electric field are weak. In the present work, electric fields measured by this technique were of great assistance in correlating the results.

Part I is organized under four chapters. Chapter 2 dwells on details of the experimental techniques used, with emphasis on departures from standard practice. The question of the accuracy of the measurements is also considered. Chapter 3 describes the measurements in pure He, Ne and Ar, and discusses the implications of the results on theories of the positive column. Finally, Chapter 4 deals with measurements in rare gas mixtures. The effect of cataphoresis on the results is used to elucidate some microscopic aspects of a previous theory of this phenomenon.⁽⁸⁾ It is believed that the results obtained here will be of use in various positive column applications. In particular, Part II considers rare gas plasmas in which organic molecules introduced in small concentrations, undergo various chemical reactions.

2. EXPERIMENTAL TECHNIQUE (I)

2.1 Two Bulb Discharge Tube and Vacuum System

Figure 4 shows the discharge tube that was used for the experiments. The function of the end bulbs was⁽⁸⁾ to enhance cataphoretic effects in the experiments on gas mixtures, but the same tube was used for the measurements on pure gases as well. To minimize interference with cavity resonance, the portion of the tube between the end bulbs was made of quartz instead of pyrex.⁽²³⁾ The electrodes were made of molybdenum and were cooled by a stream of water circulating through the hollow copper leads. A quartz jacket around the copper leads prevented them from acting as electrodes. Copper has a great tendency to sputter, especially at the cathode,⁽⁵⁾ and to avoid contamination of the system it should not be allowed to come in contact with the discharge. Further cooling could be provided, if necessary, by circulating water through the jackets surrounding the pyrex end bulbs. Unfortunately, the quartz portion of the tube within the microwave cavity could not be conveniently cooled, as water is a very good absorber of microwaves, and hence has a deleterious effect on the quality of resonance. However, wall heating was not appreciable, as the discharges were run at low power levels (see Appendix A-3). For higher power levels than the ones used here, it may be necessary to use a non-absorbing cooling liquid, e.g., benzene.

The discharge tube could be connected through valve V and thick-walled TYGON vacuum tubing to the glass manifold of a vacuum system. The manifold had connections for various gas supplies, and

could be evacuated by a CVC 2" diffusion pump (PMCS-2C), backed by a KINNEY rotary vacuum pump. A baffle was located between the mixing chamber (manifold) and the diffusion pump to reduce contamination of the system from the diffusion pump fluid vapors. A CVC vacuum-gate valve, Model VSTM2, was used to isolate the baffle and pumps from the mixing chamber. The pressure in the system could be measured to $\pm 1\%$ with a TODD universal vacuum gauge. The base vacuum was less than 10^{-4} torr.

Matheson Research Grade helium, neon and argon (with no detectable impurities at the 2 ppm threshold) were used for the experiments on pure gases. The pyrex flasks were directly sealed to the glass manifold with no intervening metal lines. However, the 99.99% high purity grade was employed for the experiments on gas mixtures.

2.2 D.C. Power Supply and Electric Field Measurement (Fig. 26,27)

Regulated d.c. power was supplied to the discharge by a CVC-LC031 supply followed by a lab-fabricated π -section filter. Discharge current was measured by a 0-50 mA TRIPLETT Model 420-G ammeter, and could also be monitored on a HP-122AR oscilloscope, which was fed with the voltage drop across a $10.8\Omega \pm 1\%$ resistor in series with the tube. The voltage across the discharge was measured on a 0-5000V TRIPLETT Model 420 voltmeter. Electric field E was measured by a KEITHLEY 601 electrometer with a 6103A 1000:1 divider probe. For a continuous record of the electric field, the electrometer output was fed through a FLUKE A-88 isolation amplifier to a L & N speedomax W strip chart recorder, with 1 mV full scale sensitivity. E was obtained by dividing the measured voltage across a pair of floating molybdenum wire probes (P_1 or P_2) by

the distance of separation between the probes (2.0 cm). The electric field values are accurate to within $\pm 5\%$.

2.3 Microwave System

2.3a) Principle of operation. The two parameters of a discharge that can be obtained from microwave cavity measurements are the electron density n_e and the average electron-neutral collision frequency ν_{en} . A particular cavity resonance is characterized by a resonant frequency f_o , and the loaded quality factor Q . A plasma placed inside a microwave cavity introduces a change in both f_o and Q . As shown by Ingraham and Brown,⁽²³⁾ a first order perturbation calculation yields

$$\frac{f'_o - f_o}{f_o} = \frac{1}{2} \frac{\omega_{po}^2}{\omega^2 + \nu_{en}^2} \eta \quad (2)$$

$$\left(\frac{1}{Q'} - \frac{1}{Q}\right) = \frac{\omega_{po}^2}{\omega^2 + \nu_{en}^2} \frac{\nu_{en}}{\omega} \eta \quad (3)$$

where η is a dimensionless form factor that depends on the geometry of the cavity, the ratio of plasma radius to cavity radius, and the mode of coupling into and out of the cavity. Using the plots of η presented by Ingraham and Brown,⁽²³⁾ it is therefore possible to solve equations (2) and (3) for n_e and ν_{en} . ω_{po} is the electron-plasma frequency which can be expressed as

$$\omega_{po} = \sqrt{\frac{n_e e^2}{m_e \epsilon_o}} = 56.4 \times 10^3 \sqrt{n_e} \quad (4)$$

where n_e is in units of cm^{-3} .

If it is desired to use a mode for which η plots are not available, it may be necessary to determine η experimentally, as shown later in this section.

2.3b) Microwave apparatus. Figure 5 shows the dimensions of the cylindrical resonant cavity that was used. The two modes that were used were TM_{010} and TM_{011} . In these, the magnetic field is in the azimuthal θ direction and the electric field is along the axis of the cavity, varying as $E_z = E_{z0} J_0 \left(2.4 \frac{r}{R_0} \right)$. In the TM_{011} mode there is, in addition, a half wave modulation of the fields along the length, such that they vanish on the side walls. ⁽²⁴⁾ This can be expected to minimize errors due to the holes where the plasma tube enters the cavity. The amount of coupling is determined by the area of the loops (L_1 and L_2), their depth of penetration into the cavity, and the orientation of the loops with respect to the field. ⁽²⁵⁾ Maximum coupling was obtained when the plane of the loops was perpendicular to the magnetic field. As shown in Figure 5, the brass cavity was constructed in two halves which could be joined together after the discharge tube was in place. Figure 6 shows details of the coaxial circuit to plot the resonance curve of the cavity. Attenuators were chosen for flat frequency response in the 2-4 GHz range. The sweeper was chosen for its excellent linearity, frequency stability ($\pm 0.25\%$ over full range of RF power), and its calibrated markers which retain their accuracy even in the narrowest of the three vernier-tuned Δf sweeps.

2.3c) Calibration of the microwave cavity. The method used for the measurement of f_0 and Q was a "transmission" method. ⁽²⁶⁾ With the modes of coupling used, this is more accurate than the SWR method

used before⁽²³⁾ when a high collision frequency in the plasma causes great under-coupling of the cavity. Measurement of f_o and Q , both with and without the plasma, was thus straightforward. In both cases, the resonance curve was obtained on a suitable scale and the resonant frequency f_o and half-power points f_2 and f_1 determined from it.

Now

$$Q = \frac{f_o}{(f_2 - f_1)}$$

The values of Δf_o and $\Delta(1/Q)$ were put into equations (2) and (3) to calculate n_e and v_{en} .

The bulk of the present microwave data was taken with the TM_{011} mode. This is because there was excessive shift as well as broadening of TM_{010} mode, leading to appreciable interference from higher order modes. The resulting distortion of the resonance curve made accurate measurements of Δf_o and $\Delta(1/Q)$ difficult. This problem was minimized with TM_{011} . Calibration of TM_{011} with respect to TM_{010} was done by making simultaneous measurements on a helium discharge under conditions where the latter was still yielding clean resonance curves. As shown in Table 1, the values of v_{en} from the two modes check out, and $\eta_{011} = 0.59 \eta_{010}$. η_{010} for $R/R_o = 0.012$ was determined from Fig. 5-4 of Ingraham and Brown⁽²³⁾ to be 0.017, thus giving $\eta_{011} = 0.0097$. The above calculations are for $n_e = (n_e)_o J_o(\frac{2.4r}{R})$.⁽²⁸⁾ To check the general applicability of the charts of Fig. 5-4 of Ingraham and Brown⁽²³⁾ to the present case, the dielectric constant of pure organic liquids was determined with the TM_{010} mode. As shown in Table 2, the values for benzene and m-xylene agree to within 1% of the accepted values. Even in the case of ethyl ether, where there is appreciable broadening of the

resonance curve, the agreement is within 3.0%. These checks were taken as evidence that the assumptions of the method were not being violated, at least for the case of constant dielectric constant. By extension one may assume that this is true even when the dielectric constant varies with radius. Since the values of

$$\frac{\omega_{po}^2}{\omega^2 + \nu_{en}^2} = \frac{2\Delta f_o}{f_o \eta}$$

with the plasma are comparable to the corresponding values in Table 2, we can expect that n_e and ν_{en} calculated from linear theory (equations 2 and 3) are no more than 5% off from their true values.

3. MEASUREMENTS IN PURE He, Ne AND Ar

3.1 Aim of Experiments

The aim of the experiments described in Chapter 3 was to obtain a set of measurements of the electric field E , electron density n_e , and electron-neutral collision frequency ν_{en} in pure He, Ne and Ar positive columns with the discharge current I and the pressure p as independent variables. The sensitivity of the measurements to small quantities of impurities was sought to be investigated with a view to testing the adequacy of the similarity parameters pR and E/p in the range $p = 1-8$ torr, $I = 5-20$ ma.

3.2 Procedure

In this set of experiments, the discharge tube 1 was evacuated and filled with pure rare gases at various known pressures. Microwave readings were taken at each pressure for different values of the discharge current. Simultaneously, the electric field was also measured. The agreement of the readings at different positions on the discharge tube, and the fact that they were reproducible, was taken as evidence of the purity of the gases.

3.3 Presentation of Results

3.3a) Longitudinal electric field, E. Figures 7-9 show the measured electric fields in the three rare gases investigated. The results have been divided by the pressure p and plotted against pR , where R is the radius of the tube. The present results can therefore be compared with those of other workers to see if the similarity rule, ⁽⁵⁾ $(E/p)_{I=\text{constant}} = f(pR)$, is being obeyed. In helium and

neon, E was found to be quite insensitive to I . The measured values of E/p fall on essentially the same curve as those of earlier workers, ^{(21), (29-32)} (Figs. 7 and 8) despite the fact that I and R are different. Hence the similarity rule is valid in the range investigated. The values of E are very sensitive to impurities, the slightest leak of air into the system makes itself evident at once by a sharp increase in E .

There was a qualitative difference between the results in argon and those in helium and neon described above. For one thing, E in Ar is a strongly decreasing function of I , a result which has been observed by others. ^{(5) (21)} Further, in the case of Ar, strong oscillations were observed in the current. Below 1.9 mm Hg, these had a time period of a few microseconds, and above 3.6 mm Hg, they were in the millisecond range. Between 1.9 mm Hg and 3.6 mm Hg, both types of oscillations were present. The amplitude of the oscillations was often as high as 25% of I for low values of I . Figure 9 shows that the present values of E/p are higher than those found in wider tubes for the same I . ^{(21) (33)} Moreover, there are discontinuities in the curve at $p = 1.9$ mm Hg and 3.6 mm Hg, which corresponds exactly to the pressures that mark off the different regimes of oscillation. This suggests that the oscillations play a major role in the breakdown of similarity in the case of argon.

3.3b) Electron density n_e and drift velocity v_d of the electrons. Figures 10, 11 and 12 show the measured values of $(n_e)_0$ plotted against I for different pressures. In a glow discharge, current is carried mostly by the light electrons, so that current density j is

given by

$$j = \langle n_e \rangle e v_d \quad (5)$$

Since⁽²⁸⁾

$$n_e = (n_e)_o J_0\left(\frac{2.4r}{R}\right) \quad (6)$$

$$\begin{aligned} \langle n_e \rangle &= \frac{1}{\pi R^2} \int_0^R 2\pi r (n_e)_o J_0\left(\frac{2.4r}{R}\right) dr \\ &= \frac{2}{2.4} \times J_1(2.4) (n_e)_o \\ &= 0.433 (n_e)_o \end{aligned} \quad (7)$$

From (5) and (7)

$$v_d = \frac{j}{e \times 0.433(n_e)_o} = \frac{I}{0.433\pi R^2 e(n_e)_o} \quad (8)$$

Equation (8) was used to calculate v_d which is plotted against E/p in Figures 13, 14 and 15. The error bars on each point in these figures represent the variation in v_d (and E/p) found experimentally for a given p for different I . In He and Ne the v_d values fall well below those found in drift tube experiments.⁽³⁴⁾⁽³⁵⁾⁽³⁶⁾ Disagreement increases with E/p and is less in Ne than in He. Values of v_d in He and Ne with small amounts of impurity (air) lie much closer to the Allen values.⁽³⁶⁾ In pure Ar, however, the deduced v_d values follow the same general trend as the Bradbury and Nielsen⁽³⁴⁾ measurements in a drift tube for lower E/p .

It is also evident that any linearity in n_e vs. I can be seen only at low pressures and low currents. Hence the conclusion of Prince and Robertson⁽¹¹⁾ and Labuda and Gordon⁽¹⁹⁾ regarding linear n_e vs. I plots is not true in general. From equation (5) it is seen that the necessary condition for linearity is that v_d must not be a function of I , which in turn implies that both E/p and the composition of the discharge are constant. This rules out any changes in metastable concentrations which might occur as I is changed (see discussion section). In gas mixtures, linear n_e vs. I ⁽¹⁹⁾ indicates absence even of cataphoresis.

3.3c) Electron-neutral collision frequency ν_{en} . Figures 16, 17 and 18 show the electron-neutral collision frequency ν_{en} as a function of I for various pressures. Generally speaking, there is a maximum in ν_{en} with respect to I . The other noteworthy feature is that ν_{en} in He and Ne with small amounts of impurity are lower than the values for the corresponding pressure in the pure gas. These impure samples are, of course, the same as the ones that gave v_d values close to the Allen⁽³⁶⁾ curves for He and Ne. However, this phenomenon was not observed in Ar. Collision frequencies in impure Ar (impure enough to yield v_d values 2.5 to 3 times higher than the Allen values, were substantially the same as those in pure Ar. A possible explanation for these anomalies is offered in the discussion section below.

The ν_{en} determined from microwave measurements is an average over the prevailing electron energy distribution $f_e(\epsilon)$ with a weighting factor ϵ .⁽²³⁾

$$v_{en} = \frac{\int_{\epsilon=0}^{\infty} \frac{v_{en}(\epsilon)}{\omega^2 + v_{en}(\epsilon)^2} \epsilon f_e(\epsilon) d\epsilon}{\int_{\epsilon=0}^{\infty} \frac{1}{\omega^2 + v_{en}(\epsilon)^2} \epsilon f_e(\epsilon) d\epsilon} \quad (9)$$

where $v_{en}(\epsilon)$ is the energy dependent collision frequency which, in a mixture of n scatterers, assumes the form

$$v_{en}(\epsilon) = \sqrt{\frac{2\epsilon}{m_e}} \sum_{i=1}^n (Q_i N_i) \quad (10)$$

where Q_i is the cross-section for the i^{th} scatterer and N_i is its density.

3.4 Discussion of Results in Pure Rare Gases

A simplified theory of the positive column⁽²⁾ leads to the conclusions that E/p and T_e are functions of pR , and v_d is a function of E/p only. The first two conclusions have been experimentally checked in glow discharges in pure gases,⁽⁵⁾ but the third has never been directly demonstrated. It is generally assumed that for the E/p 's found in glow discharges, it is the same as the function determined in the experiments of Townsend⁽³⁵⁾ or Bradbury and Nielsen,⁽³⁴⁾ and correlated theoretically by Allen.⁽³⁶⁾ Rigorous theory⁽³⁷⁾ reveals that this is strictly true only in the absence of significant ionization and excitation collisions. Hence, deviations of v_d from the drift tube values would indicate that such collisions are becoming more important in the present case. Equality of E/p alone does not establish similarity of a glow discharge positive

column to the setup of Townsend⁽³⁵⁾ or Bradbury and Nielsen.⁽³⁴⁾

One distinct possibility in glow discharges is the presence of significant amounts of excited metastable states. In particular, it is important to consider ionization by metastables which would tend to increase n_e and lower v_d for the same E/p , e.g., $\text{He} + e \rightarrow \text{He}^* + e$, $\text{He}^* + \text{He} \rightarrow \text{He}_2^+ + e$; $\text{Ne} + e \rightarrow \text{Ne}^*$, $\text{Ne}^* + \text{Ne} \rightarrow \text{Ne}_2^+ + e$. Metastable He^* and Ne^* are known to be rapidly destroyed even by small amounts of impurities,⁽³⁸⁾ so that metastable ionization would be an important process only in discharges in very pure He and Ne. The abnormally low v_d and high v_{en} observed could therefore be due to the effects of ionization by metastable He^* and Ne^* . This tallies with the fact that the smallest amount of impurity (air) raises v_d to near the Allen values⁽³⁶⁾ and lowers v_{en} as described before.

The probe results of Golubovskii et al⁽³²⁾ in neon positive columns also yield v_d values considerably below the Allen values. However, Anderson's v_d values⁽¹⁰⁾ in He and Ne are close to the Allen values indicating that metastables may not have played a very important role in his experiments. This could be due to two reasons. First, there could have been a slight contamination of his system from the electrodes, especially if the discharge was turned on and off a number of times before observations were taken. Second, ionization by metastables might not be significant in his range of pressures and currents (which were typically 0.1-1.0 torr, 0.5-2.0 mA, both a decade lower than present values). All this would seem to indicate that prediction of v_d of electrons in glow discharges (especially in pure He and Ne) is more difficult than hitherto assumed. It would

also suggest that any attempt to extract elastic collision probabilities P_c for electrons and ground state He or Ne atoms from v_{en} data in their positive columns by solution of the integral equation (9) could lead to incorrect values of P_c .

3.5 Suggestions for Future Work in Pure Rare Gases

Based on the results presented in this chapter, the following suggestions may be made for future work in d.c. discharge positive columns of pure rare gases.

(1) Greater attention must be paid to the effects of small amounts of impurities. Even when extremely pure samples are used, electrode contamination makes suspect the most careful work in closed systems. n_e is the parameter most sensitive to this effect, which may be overcome in a baked out system, with flow of gas to sweep impurities away.

(2) A consistent set of n_e , v_{en} , $f_e(\epsilon)$ and E data must be obtained simultaneously in He, Ne, Ar and other gases as a function of p and I .

(3) Mass spectrometric studies of the relative and absolute concentrations of various ionic species, e.g., He^+ , He_2^+ are necessary.

(4) Methods for theoretically predicting extent of ionization by metastables, and v_d , in very pure He, Ne and Ar discharges at $p = 1-10$ torr are required.

4. MEASUREMENTS IN BINARY GAS MIXTURES: He-Ar, He-Ne

4.1 Cataphoresis

D.C. discharges in gas mixtures differ from those in pure gases insofar as the positive column exhibits concentration gradients in space and time. This is the result of a phenomenon known as cataphoresis, in which the component with the lowest ionization potential is selectively ionized and drifts toward the cathode, producing an increase in the concentration of this component near the cathode. The first direct composition measurements on cataphoresis were made by Matveeva.⁽³⁹⁾ Using a system with end bulbs, she studied the effects of initial gas composition, discharge current, discharge pressure and distance between the electrodes on the amount of separation achieved in binary mixtures of He, Ne and Ar. Schmeltekopf⁽⁴⁰⁾ compared optical and mass spectrometer data in He-Ne discharges and found a poor measure of agreement between them. Extensive composition measurements using thermal conductivity gauges have been made in this laboratory⁽⁴¹⁾ in binary mixtures of He with Ar, Ne, N₂, O₂, CO and CO₂.

A survey of the literature indicates a surprising lack of information on electric fields and electron densities in discharges in gas mixtures, especially under conditions in which cataphoretic effects would be noticeable. For instance, the field measurements of Headrick and Duffendack⁽⁴²⁾ and the electron density measurements of Labuda and Gordon⁽¹⁹⁾ neglected cataphoresis entirely. On the other hand, these quantities enter intimately into any quantitative model that attempts to correlate the data.⁽⁸⁾⁽⁴³⁾ Hence it is to be expected that reliable

determinations of E and n_e as a function of position and time in such systems will be of assistance in establishing the model on a sounder footing.

4.2 Aim of Experiments

The aim of the experiments of Chapter 4 was (1) to measure n_e , v_{en} and E as functions of time in d.c. discharge in He-Ar and He-Ne mixtures until steady state was attained. The range of parameters was to be $p = 2-5$ torr, $I = 15$ mA and the Ar or Ne content 2-20%; (2) to qualitatively explain the steady-state and transient results in terms of the phenomenon of cataphoresis (Section 4.1); (3) to use the steady-state data and the Shair and Remer model⁽⁸⁾ to back calculate the composition profiles in the discharge tube with two end bulbs, and to check for agreement with the measured profiles in similar systems.

4.3 Procedure

Gas mixtures of known composition were prepared by introducing helium into a sample of neon or argon at known partial pressure, and subsequently measuring the total pressure. Adequate time (~ 30 min) was provided to insure thorough mixing. The discharge tube was evacuated and filled with mixtures at different pressures. The discharge was struck and microwave readings were obtained as a function of time at a given position. The sweep time was 20 seconds, and f_0 and Q were determined from the resonance curve as outlined before. Electric field E was recorded as a function of time at P_1 and P_2 . Steady-state was reached within 15-20 minutes, whereupon the microwave cavity was moved to two other positions on the discharge tube to obtain the resonance curves there. Current I was kept constant at 15 mA

throughout this set of experiments.

4.4 Presentation and Discussion of Results

4.4a) Steady-state results. Tables 3 and 4 show the steady-state results in He-Ar and He-Ne mixtures of various compositions and total pressures. It is seen that $(n_e)_0$ (and v_{en}) are functions of position, and that E toward the cathode is always higher than that toward the anode. The results of Tables 3 and 4 were used to check how much the level of ionization i and the parameter $\alpha = \frac{\langle n_+ \rangle}{\langle n_o \rangle + \langle n_+ \rangle} \frac{\mu EL}{D}$ vary with position in a given discharge. i and α are assumed to be constant in the model.⁽⁸⁾ The calculations (Appendix A-2) involved an iterative solution for the concentration of the minority component. In cases when this concentration was low, especially in He-Ar, it became necessary to assume $J = \frac{\langle n_+ \rangle}{\langle n_e \rangle} < 1$. The fact that this is always less than 1 indicates that other ions besides Ar^+ and Ne^+ may be playing a role in cataphoresis, as charge neutrality cannot be violated.

The concentration profiles $\theta(\eta, \infty)$ show a decrease as we move away from the cathode, as might be expected. The profiles are flatter when the initial concentration of the minority component is high. The monotonic character of the solution is in agreement with the spectroscopic results of Riesz and Diecke⁽⁴⁴⁾ in rare gas mixtures. The resulting i 's and α 's, both of which represent a combination of measured and calculated parameters, vary somewhat with position. This variation is less when cataphoretic effects are small (as with high initial compositions of Ar or Ne). The fact that the variation is less than 50% (except at 2.45 torr with 2.4% Ar) suggests that it is a valid procedure to use a mean value to explain cataphoresis, as done

in the model.⁽⁸⁾ Also, the i values agree to within an order of magnitude with those calculated from direct composition measurements at the anode in a similar system⁽⁴¹⁾ (see Fig. 19). Variations of v_{en} with position do not correlate very well with composition changes, suggesting that the electron energy distribution $f_e(\epsilon)$ may not be the same at different points in the discharge. However, as shown by Sosnowski⁽⁴³⁾ the Shair and Remer model⁽⁸⁾ can be successfully used to predict composition profiles in cataphoretic systems even when $f_e(\epsilon)$ is known to be varying with time and position.

4.4b) Transient results. Figure 20 shows some typical cases of transients of $(n_e)_o$ and v_{en} that were observed in the experiments on gas mixtures. The values have been plotted against dimensionless time Dt/L^2 . The final points on these curves correspond to a real time of 15-20 minutes, which is sufficient for steady-state to be reached. There were, in addition to the smooth curves shown in the figure, sudden non-reproducible deviations, especially in v_{en} at low values of $\langle n_o \rangle$. Also, the transient variations in v_{en} did not correlate very well with transient composition variations that might be expected from cataphoresis, again pointing to the possibility of changes in the electron energy distribution $f_e(\epsilon)$. Electric field values after the first minute did not change much with time. Generally speaking, the variation in E was less than 10%. E on the cathode side remained higher than that on the anode side throughout this period.

The dimensionless characteristic time for cataphoresis⁽⁸⁾ is given by

$$\tau_c^M = \frac{1}{\frac{\alpha^2}{4} + u_1^2} \quad (11)$$

where u_1 satisfies the transcendental equation

$$\tan u_1 = \frac{-(\delta + \epsilon)u_1}{1 + \frac{\alpha}{2}(\delta - \epsilon) - \delta\epsilon\left(\frac{\alpha^2}{4} + u_1^2\right)} \quad (12)$$

When u_1 is small enough for $\tan u_1 \approx u_1$, we can solve equation (12) directly for $\left(\frac{\alpha^2}{4} + u_1^2\right) = 1/\tau_c^M$

$$\left(\frac{\alpha^2}{4} + u_1^2\right) \approx \left[1 + \frac{\alpha}{2}(\delta - \epsilon) + (\delta + \epsilon)\right] / \delta\epsilon \quad (13)$$

Therefore,

$$\tau_c^M \approx \frac{\delta\epsilon}{1 + \frac{\alpha}{2}(\delta - \epsilon) + (\delta + \epsilon)} \quad (14)$$

Putting $\delta = 30.7$, $\epsilon = 19.2$, $\alpha = 1$, leads to $\tau_c^M \approx 10.4$, which is not inconsistent with the transient results of Fig. 20. However, since n_e and v_{en} do not vary monotonically, a more exact comparison was not possible.

4.5 Suggestions for Future Work in Gas Mixtures

1) The microwave measurements may be repeated with controlled wall temperature using benzene as cooling liquid as suggested in Chapter 2.

2) n_e , v_{en} and E must be measured as a function of time in a two-bulb system in which simultaneous composition measurements are

being taken. The technique of Remer and Shair⁽⁴¹⁾ is a convenient one for making such composition measurements in a cataphoretic system.

3) The range of the present measurements could be extended to values of I greater than 15 mA and to mixtures with molecular gases e.g., O_2 , N_2 , CO_2 , CO . Collision frequency in such situations may be high enough to swamp out the TM_{010} and TM_{011} modes, but TE_{011} might be tried.

4) Measured transient values of n_e and E can be used to reconcile transient composition measurements within the framework of the model for cataphoresis proposed by Shair and Remer.⁽⁸⁾

PART II

KINETICS OF HYDROCARBON REACTIONS IN THE POSITIVE
COLUMN OF D.C. AND PULSED D.C. DISCHARGES

5. INTRODUCTION

5.1 Review of Literature

5.1a) Chemical reactions in equilibrium and non-equilibrium plasmas. As early as 1874, de Wilde⁽⁴⁶⁾ and P. and A. Thenard⁽⁴⁷⁾ introduced acetylene into an electric discharge and observed the formation of a hard, brittle and amorphous solid. Wood⁽⁴⁸⁾ recognized the role of the newly discovered free radical, and initiated a systematic study of reactions in discharges. Modified forms of Wood's tube were used extensively to dissociate diatomic molecules, e.g., H₂, O₂, N₂ and Cl₂ at pressures of 1-10 torr, with yields of atomic species up to 40%⁽⁴⁹⁾ controlled essentially by wall recombination. Such experiments had, by 1939, resulted in the collection of a large body of more or less empirical information on the subject. Glockner and Lind,⁽⁵⁰⁾ in their comprehensive book, listed the reactions that occur in the various types of discharges known until then. Electric discharges in gases were classified as

- 1) Disruptive--the arc and spark discharges
- 2) Silent or non-disruptive
 - a) Glow discharges--using d.c. or low-frequency a.c.
 - b) Electrodeless discharges--using higher frequency a.c. with inductive or capacitive coupling
 - c) Point and point-plate discharges
 - d) Corona and semi-corona discharges--using a fine wire as electrode.

After World War II, two new techniques were developed for creating laboratory plasmas. One was an offshoot of radar, and made use of microwave power to establish a discharge. Reactions in a microwave

discharge were first studied by McCarthy.⁽⁵¹⁾ The other was the now familiar plasma jet, which uses d.c., a.c., or high frequency field to maintain a plasma that is largely thermal in nature. Hellund⁽⁵²⁾ devotes his book mostly to the plasma jet. The microwave discharge and plasma jet are devices in which power input is readily and continuously controlled, and there are no electrodes to contaminate the system. A recent book by McTaggart⁽⁵³⁾ gives a good account of plasma chemistry experiments, from the earliest to the latest. The American Chemical Society monograph on chemical reactions in electrical discharges⁽⁵⁴⁾ is another useful source of information. A summary of the types of reactions that occur in various discharges is given in Table 5 (compiled from McTaggart⁽⁵³⁾ and Baddour and Timmins⁽⁹⁾).

The processing industry has also made use of chemical reactions in the plasma state. The now obsolete Birkeland and Eyde process⁽⁵⁵⁾ for the fixation of nitrogen, and the Huls process⁽⁵⁶⁾ for converting methane to acetylene use disruptive arcs. The ozonizers, on the other hand, utilize a silent discharge. Patents have been obtained⁽⁹⁾ for plasma processes for the preparation of speciality chemicals such as N_2H_4 , ClO_2 , ClO_3 and B_2Cl_4 . A plasma jet synthesis of pigment grade TiO_2 has been recently suggested.⁽⁵⁷⁾ Vurzel and Polak⁽⁵⁸⁾ give a broad review of plasma chemical technology. Another comprehensive review, concentrating on reactions in non-disruptive discharges, is found in Spedding.⁽⁵⁹⁾

Previous work on hydrocarbon reactions in discharges has generally resulted in a bewildering array of products, including solids and liquids of unknown composition.^(60,61) A review of early

Table 5

Some Typical Reactions Occurring in Plasmas

Type of Discharge	Reactants	Products	References
1) Disruptive discharges--arc	$CF_4 + C$	C_2F_4	Baddour & Bronfin ⁽⁶⁴⁾ (1965)
2) Non-disruptive (silent) discharges			
a) Glow discharges	H_2	oH	Wood ⁽⁴⁸⁾ (1920)
	CH_4	C_2H_2, H_2	Hesp, Halasz, Gerlach ⁽⁶⁰⁾ (1967)
b) Electrodeless discharges(r.f.)	Cl_2	oCl	Rodebusch & Klingelhoefter ⁽⁶⁵⁾ (1933)
	$^oO +$ Solid C	$CO + CO_2$	Blackwood and McTaggart ⁽⁶⁶⁾ (1959)
c) Point-plate discharge	O_2	O_3	Warburg ⁽⁶⁷⁾ (1905)
d) Corona discharge	O_2	O_3	Described by Glockner and Lind ⁽⁵⁰⁾ (1939)
3) Modern plasmas			
a) Microwave discharges	N_2-O_2 mixtures	Various oxides of nitrogen	McCarthy ⁽⁵¹⁾ (1954)
	$HCl + O_2$	$Cl_2 + H_2O$	Described by Baddour and Timmins ⁽⁹⁾ (1967)
b) Plasma-jet	$2C + N_2$	C_2N_2	Stokes and Knipe ⁽⁶⁸⁾ (1960)
	$H_2 + 2C + N_2$	HCN	Grosse, et al ⁽⁶⁹⁾ (1961)

experiments in this area may be found in Thomas et al.⁽⁶²⁾ Starting with methane, Brewer and Kueck⁽⁶³⁾ were able to achieve specificity, but only by cooling the tube to liquid air temperatures in order to condense out the ethylene. Spedding's review⁽⁵⁹⁾ does not indicate any later experiments that yielded a small number of gaseous products only. It is therefore our claim that the present thesis is the first recorded instance of a hydrocarbon reaction in an ambient neutral temperature plasma, which has been made selective enough to obtain some information on the elementary processes in the mechanism.

5.1b) Gas chromatography of the light hydrocarbons. Gas chromatography (GC) may be defined⁽⁷⁰⁾ as a process for the separation and analysis (qualitative and quantitative) of substances in the gas phase by adsorption on and subsequent partitioning with a solid or liquid phase. The method was pioneered by James and Martin⁽⁷¹⁾ in the 1950's. However, some earlier workers, e.g., Schuftan⁽⁷²⁾ had described an elution technique for use with liquid phases. Turner⁽⁷³⁾ began the development of adsorption gas chromatography by the displacement technique. The frontal analysis method of adsorption GC must be credited to Phillips.⁽⁷⁴⁾ Between 1956 and 1962, there was an explosive growth of literature in the field, and a complete literature survey can be made only with the aid of a computer. After 1962, most of the progress has been in perfecting the instrumentation and in extending the range of applications.⁽⁷⁵⁾

Even if we restrict our attention to the $C_1 - C_5$ hydrocarbons, the number of possible compounds is very large, over 30 occurring fairly frequently in hydrocarbon mixtures. Separation of every member

from every other member is impractical as columns become abnormally long. In practice, column conditions can be found to separate any reasonable set of compounds that might occur in the mixture to be analyzed. The low partition coefficients of the $C_1 - C_5$ hydrocarbons necessitates the use of packed columns with a large proportion of stationary phase. The short retention times often permit operation at room temperature. Liquid phases have also been tried with unsatisfactory results. (76)

The complete separation of methane, C_2 and C_3 from each other, from higher hydrocarbons and permanent gases may be achieved on adsorbents. Charcoal, (77) silica gel (78) or alumina (79) can be used. On charcoal, the order of elution is H_2 , O_2 , N_2 , CO , CH_4 , CO_2 , C_2H_2 , C_2H_4 , C_2H_6 . On silica gel and alumina, alkenes and alkynes are selectively retained relative to alkanes. The order of elution is as follows:

silica gel or alumina: H_2 , air, CO , CH_4 , C_2H_6 , CO_2 , C_2H_4 , C_3H_8 ,
cyclo- C_3H_6 , C_3H_6 , C_2H_2

Porous polymers have also been used. (80)

Either thermal conductivity or flame ionization detectors can be employed in the above-mentioned analysis. The flame ionization detector (FID) is preferable from the point of view of sensitivity, but is effective only for the hydrocarbon components of the mixture (81). The basis of FID is the change in the electrical conductivity of a hydrogen flame burning in air when an organic substance is introduced into it.

5.2 Scope of Present Measurements in Terms of Plasma Kinetic Theory

The visual appearance and gross electrical characteristics of a glow discharge were briefly reviewed in Section 1.1. We shall now concern ourselves with the basic theory of the positive column^(2,5,82,83,84) which is the best understood region of the discharge, and therefore is the ideal medium to study plasma chemical reactions in the laboratory.

In an unstriated positive column with negligible cataphoresis and irreversible chemical reaction, the longitudinal electric field E ($= \frac{dV}{dz}$) is independent of position and very nearly independent of the discharge current. E is usually an order of magnitude smaller in the positive column than in the cathode fall, which takes up most of the voltage drop across the discharge. The current is carried mainly by the electrons and is given by

$$I = e \int_0^R v_d n_e(r) 2\pi r dr \quad (15)$$

and $n_e \approx n_+$ due to quasi-neutrality. The radial electric field set up by small departures from the neutrality condition leads to the phenomenon of ambipolar diffusion.^(2,5,84) Equating the rate of particle production to the rate of ambipolar diffusion, Schottky⁽²⁸⁾ showed that the particle density goes as

$$n_e(r) = n_e(0) J_0\left(\frac{2.405r}{R}\right) \quad (16)$$

The distribution of electron energies $f_e(\epsilon)$ can, in principle, be obtained as the solution of the Boltzmann equation for the electrons.

$$\frac{\partial f_e}{\partial t} + v_i \frac{\partial f_e}{\partial x_i} + R_i \frac{\partial f_e}{\partial v_i} = \sum_P \left(\frac{\partial f_e}{\partial t} \right)_{\text{coll}} \quad (17)$$

where the summation on the R.H.S. is over all the elastic and inelastic electron impact processes. This approach was developed by Lorentz, Chapman and Cowling, Druyvesteyn and Margenau, among others. Allis presents a good review of this work in the Handbuch der Physik.⁽⁸⁵⁾ The theoretical solutions have been hampered by a severe lack of knowledge about the rates of inelastic electron-impact processes. Recent attempts, such as those of Engelhardt and Phelps,⁽⁸⁶⁾ and Shaw⁽⁸⁷⁾ have used the computational approach. In gas discharges, it is probably more reliable to try and measure $f_e(\epsilon)$ experimentally, despite the formidable array of practical problems involved.⁽⁸⁸⁾ Chapter 10 presents a more detailed account of the role of the electron energy distribution function. An approximate calculation equating the energy loss in elastic collisions with the gain per electron per second leads to the following expression for mean energy⁽⁸⁴⁾

$$\bar{\epsilon} = \frac{E}{N} \frac{eM^{1/2}}{\sqrt{2} \pi \sigma^2 (3m_e)^{1/2}} \quad (18)$$

from simple kinetic theory. The results for some typical values of E/N are shown in Table 6, with the concept of "temperature", of course, being valid only for a Maxwellian $f_e(\epsilon)$. More exact calculations⁽⁵⁾ for various simple gases indicate that the effect of inelastic collisions is to bring the electron temperatures down into the neighborhood of 10^4 °K.

Table 6

Mean Electron Energies Calculated from Equation (18)

$\frac{E}{N}$ $V = \text{cm}^2$	M	σ \AA	$\bar{\epsilon}$ eV	T_e $^{\circ}\text{K}$	Comment
1.5×10^{-16}	4	2.58/2	10	116,050	T _e values are too high by a factor of approximately 5 because inelastic collisions were neglected.
5×10^{-17}	20	2.80/2	6.35	73,900	
5×10^{-17}	40	3.42/2	6.0	69,600	

The types of inelastic processes that must be considered in the positive column are⁽⁸³⁾

- 1) Electron-impact ionization
- 2) Electron-ion and ion-ion recombination
- 3) Electron attachment and detachment
- 4) Charge transfer and ion-molecule reactions
- 5) Excitation and dissociation
- 6) Secondary reactions of excited species and dissociation fragments.

The general expression for the rate of an electron-impact process is

$$v = n_e N \int_{\epsilon=0}^{\infty} \sqrt{\frac{2\epsilon}{m_e}} \phi(\epsilon) \cdot f_e(\epsilon) \cdot d\epsilon \quad (19)$$

The quantity $\phi(\epsilon)$, which has units of L^2 , is called the cross-section for the process. These cross-sections can, in principle, be calculated if a proper quantum mechanical treatment of the collision is possible. In practice, this has been possible⁽⁸⁹⁾ only for elastic scattering and the simplest types of inelastic process, e.g., rotational excitation of H_2 . The more usual approach is to measure $\phi(\epsilon)$ in electron swarm or beam type of experiments.^(90,91) A recent summary of available data on ionization, excitation and dissociation cross-sections is to be found in Kieffer.⁽⁹²⁾

An irreversible chemical reaction in a plasma can result by electron-impact dissociation followed by various secondary reactions. According to Kaufman,⁽⁸⁴⁾ the principal mechanism for this initial step is the formation of an electronic state with an energy greater than D_d ,

the dissociation energy. The subsequent dissociation, which is governed by the Franck-Condon principle, can come about in three ways: i) a repulsive upper state dissociating on its first pseudo-vibration in about 10^{-13} sec, e.g., Fig. 24a for $H_2 + e \rightarrow H + H + e$; ii) a sufficiently energetic bound upper state formed on the repulsive part of the potential energy curve, also dissociating on its first vibration in about 10^{-13} sec, e.g., Fig. 24b for $O_2 + e \rightarrow O + O + e$; iii) a bound upper state crossing over to a state with lower dissociation energy whereupon dissociation occurs rapidly, e.g., Fig. 24c for $N_2 + e \rightarrow N + N + e$.

Previous attempts to relate plasma chemistry quantitatively to the fundamental processes taking place have dealt with dissociation of H_2 , O_2 , N_2 and CO_2 .^(65,93,94,95) As pointed out in Section 5.1a, hydrocarbon reactions in discharges, even when the reactant is as simple as CH_4 , were too complex to be analyzed in such detail. On the other hand, hydrocarbon reactions are of great commercial interest in the petroleum and natural gas industry. A sufficiently simple hydrocarbon reaction would therefore represent a compromise between the twin objectives of theoretical understanding and practical utility. Chapters 6-11 describe the results of attempts to simplify the kinetics to the point where the fundamental processes can be identified. Simultaneous information on n_e , N and $f_e(\epsilon)$ would then enable us to relate the kinetics to the cross-sections through equation (19). The results we present are a partial fulfillment of the aims just stated.

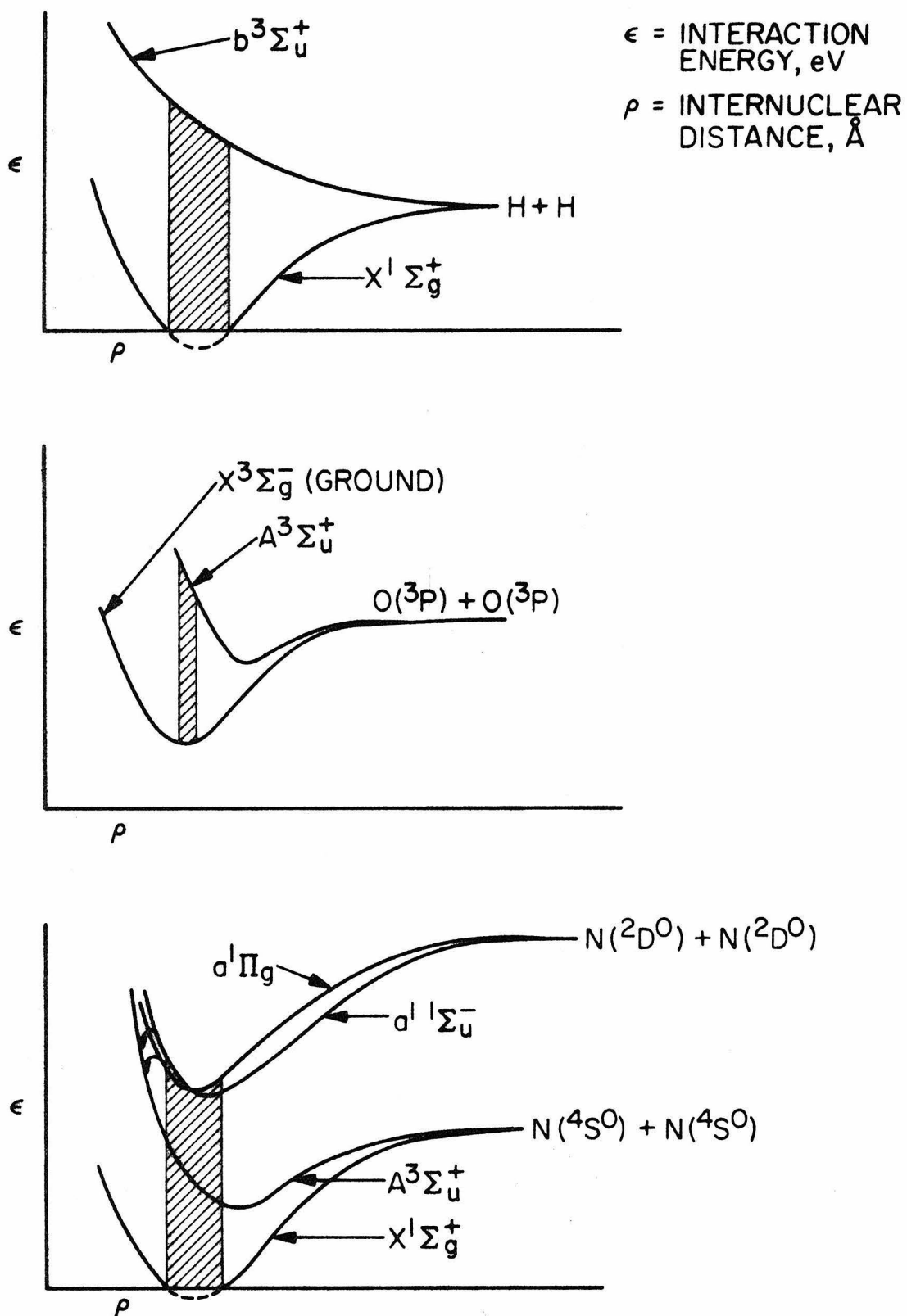


Fig. 24. Dissociation mechanisms in H₂, O₂ and N₂ according to Franck-Condon principle

6. EXPERIMENTAL TECHNIQUE II

6.1 Carry-Over of Previously Developed Systems

A substantial portion of the apparatus described in Chapter 2, Experimental Technique I, was carried over for the experiment on reacting systems. The retained equipment can be summarized as

- i) Vacuum system. Glass manifold, CVC 2" diffusion pump, Kinney rotary vacuum pump and Todd universal vacuum gauge (items 1, 3, P₁ and 4, respectively in Fig. 25).
- ii) D.C. power supply system. CVC-LC031 supply, lab-fabricated π -section filter, ammeters, voltmeter and HP-122AR oscilloscope (Fig. 26).
- iii) Electric field measurement system. Keithley 601 electrometer with 6103A 1000:1 divider probe, leads and switch-box (Fig. 27).
- iv) Microwave cavity and circuit for measurement of \bar{n}_e and v_{en} . There were no changes made in the microwave system described in Section 2.3 (Fig. 5 and Fig. 6) except in the pulsed discharge experiments.

6.2 The Reactor and Gas Handling System

6.2a) The d.c. discharge flow reactor. The positive column of a d.c. discharge was chosen for the chemical reaction experiments because it is the best understood type of non-equilibrium plasma (see Section 5.2). A flow reactor was preferred to a batch reactor for the following reasons: 1) Flow systems permit convenient observation at

low residence times (< 1 sec), thus giving kinetic information on the early stages of a reaction. 2) There is less contamination from the electrodes as compared to a batch system where impurities tend to accumulate (see Section 3.3e). 3) On-line chromatographic analysis of the product stream is possible in a flow reactor, with no disturbance to the system due to sampling. 4) Any practical application of non-equilibrium plasma reactors is likely to involve a flow reactor rather than a batch reactor (see Appendix A-8).

We discovered that an effective method of confining the flow to the positive column is to interpose an insulating plate with a 0.005" to 0.020" orifice in the discharge (see Fig. 28 below).

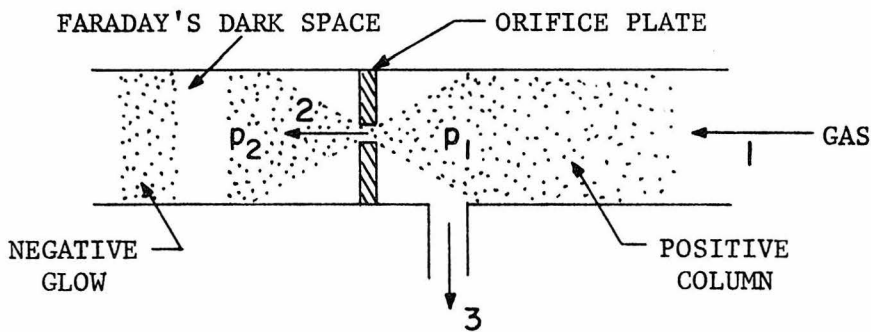


Fig. 28

The discharge passes through the orifice, but only a small fraction ($< 5\%$) of the gas flow does. As long as the plate was made of an insulating material, e.g., baked soapstone, and p_2 was kept less than p_1 by an auxiliary pump, the negative glow never penetrated to the right side of the orifice; hence the gas flow was mainly through the positive column.

The dimensions of the microwave cavity should be approximately $D_c = 10$ cm, $L_c = 8$ cm to get well separated modes in the 2-4 GHz range. Also, the diameter of the plasma tube should not be more than $0.2 D_c$ for linear perturbation theory to be valid.⁽²³⁾ We were therefore restricted to cylindrical reactors with $D_R = 1-3$ cm. The length of the positive column reactor $L > 20$ cm to accommodate the cavity, electric field probes, pressure gauge taps and quartz-pyrex seals. A large value of L also insures that the entrance length equal to $0.035 DRe^{(45)}$ is small compared to the total length. On the other hand, L must not be made so large that there are problems in breaking down the gas with the 0-5000V power supply. Therefore $L < 70$ cm.

Mean residence time in the discharge τ is defined as

$$\tau = \frac{\text{Volume of the reactor}}{\text{Volumetric flow rate}} = \frac{V_R}{\dot{V}_f} \quad (20)$$

The volumetric flow rate for any pressure is limited by the pumping speed of the downstream pump P_1 (see Section 6.2). Hence to keep τ low, it was necessary to select the smallest reactor volume that was yet consistent with the above-mentioned restrictions on D_R and L . The actual volume of the positive column turned out to be 24 cm^3 .

The residence time of the gas molecules in the reactor will, in general, be distributed around the mean value given by equation 20. The exit distributions for three idealized reactors are:

$$\text{Plug flow reactor (PFR): } E(\theta) = \delta(1) \quad (21)$$

$$\text{Ideal laminar flow reactor: } E(\theta) = \frac{1}{4} H(2\theta - 1) \cdot \frac{1}{\theta^3} \quad (22)$$

(Negligible diffusion)

$$\text{Continuous stirred-tank reactor: } E(\theta) = \exp(-\theta) \quad (23)$$

(CSTR) where $\theta = t/\tau$

These distributions are compared in Fig. 29. In order to simplify analysis, and also to minimize consecutive reactions of the products, it is clearly preferable to have a PFR. The actual reactor may or may not permit such idealization. Sample calculations (Table 7) indicate that with the densities obtaining at $p = 1-10$ torr, the flow is invariably laminar. Diffusion coefficients are two orders of magnitude higher than at atmospheric pressure. The residence time distribution in a laminar flow reactor with radial and longitudinal dispersion was derived by Bosworth.⁽⁹⁶⁾ Some limiting cases are summarized in Table 8. A small diameter tube promotes radial dispersion and a long one hinders longitudinal dispersion. The plug flow approximation is therefore more likely to be valid in long slender reactors as shown in Fig. 30.⁽⁹⁷⁾ The approximate residence time distribution realized in the actual reactor is indicated by the heavy line. Analysis of the reactor is described more fully in Section 7.6.

The discharge tube (Fig. 31) had outside diameter of 12 mm and inside diameter of 10 mm, with a quartz section of length 6-1/4" where the microwave cavity went around it. Except for the quartz section, the tube was made of pyrex glass. Inlet 4 and outlet 5 were equipped with wide-bore 6 mm greased stopcocks and 1/4" Kovar seals. Anode A,

Table 8

Limiting Cases of the Residence Time Distribution in
Laminar Flow Reactors

Radial Diffusion	Longitudinal Diffusion	Reactor Idealization
1) Negligible ($R > 18\sqrt{D\tau_0}$)	Negligible ($L > 360\sqrt{D\tau_0}$)	Ideal laminar flow reactor
2) Predominant ($R \ll 18\sqrt{D\tau_0}$)	Negligible ($L > 360\sqrt{D\tau_0}$)	Plug flow reactor (PFR)
3) Predominant ($R \ll 18\sqrt{D\tau_0}$)	Predominant ($L \ll 360\sqrt{D\tau_0}$)	Continuous stirred tank reactor (CSTR)
4) Negligible ($R > 18\sqrt{D\tau_0}$)	Predominant ($L \ll 360\sqrt{D\tau_0}$)	Rare case
5) Predominant	Neither negligible nor predominant	Treated in Bosworth ⁽⁹⁶⁾
6) Neither negligible nor predominant	Neither negligible nor predominant	Treated in Bosworth ⁽⁹⁶⁾

τ_0 = minimum residence time = 2τ

τ = average residence time

which was grounded, was a solid molybdenum rod of 5/16" diameter which entered through a 3/8" Kovar seal and was fitted in place by a Swagelock union. Other features of the positive column side of the orifice were--a pair of 0.020" tungsten electric field probes sealed into the glass 1 cm apart with their tips barely contacting the plasma, a 3/16" diameter Ni disc which may be used as an auxiliary electrode, and a tap with a 2 mm stopcock and a 1/4" Kovar seal where a vacuum gauge was attached to read the pressure in the discharge tube. On the cathode side of the orifice was a 300 ml pyrex bulb with an outlet for connection to the auxiliary pump and a tap for a McLeod gauge to read the pressure on the left side. The off-ground cathode C was also a 5/16" molybdenum rod attached to the tube in the same manner as A with a 3/8" Swagelock union. The cathode bulb served to stabilize the discharge. No attempt was made to cool the electrodes or the tube, as the discharge was run at low power levels. Use of Mo electrodes effectively prevented any sputtering.

Two different designs of the orifice were tried. In the first, an elaborate attempt was made to avoid any bypassing of the positive column. The isolation system (Fig. 32) divided the tube into three compartments, the products passing from the positive column to the middle compartment and out through the exit. The discharge passed through the central orifice. Two cylindrical ends of the isolation system also served to support O-rings for sealing the three parts of the tube together. At low pressures, a tendency was noticed for the discharge to spread into the central compartment, thus vitiating the

purpose of the design. Hence a simpler orifice design with one O-ring (Fig. 33) was adopted. Bypassing was minimized by keeping the outlet 5 as close as practicable to the orifice. No significant difference in performance was noticed between the two designs.

The 0.005" orifice tended to plug up with deposits, especially at high hydrocarbon concentrations and high currents. However, with the 0.020" orifice, a loose deposit would build up in the first few runs, and permit stable operation in the subsequent runs. Such a conditioned orifice also permitted the discharge to be run at currents as low as 0.5 mA, whereas with a fresh 0.020" orifice the lowest possible current was 5 mA. Section 7.3 deals with the V-I characteristics of the choked flow orifice system in greater detail.

6.2b) Flow system for gas handling. Matheson ultra-high purity gases (< 50 ppm impurities) were used in the present set of experiments. The He, Ar and CH₄ were purchased and stored in high pressure cylinders at pressures up to 2000 psig, with 1L-580 or equivalent single stage regulators bringing delivery pressures down to 10-40 psig. As shown in Fig. 25, the gases passed through Brooks R-2-15 rotameters to a Swagelock 1/4" mixing tee, after which they were fed to the discharge tube. The CH₄ could also be supplied through a Circle Seal MV92T1-4CC micrometer valve. Other valves used in the system were Circle Seal M92T1-4CC and Nupro needle valves, Circle Seal 9533B-4CC miniaturized plug shut-off valves, Eck and Krebs greased stopcocks and Edwards valves. Glass-metal connections were achieved through 1/4" Kovar seals and 3/16" I.D. thick-walled tygon tubing slipped on the metal. Tygon ties were clamped around the tygon tube

and the connection sealed with GE glyptal varnish. The bulk of gas flow was through outlet 5 and manifold 1 to pump P_1 (used here with the diffusion pump off). A sample was bled off for injection to the chromatograph through a 6-way valve and pump 3. The pump P_2 maintained a pressure differential across the orifice and had less than 5% of the total gas flow going through it. Pressure at various points in the system was measured with gauges $G_1 - G_6$ (Fig. 25). These gauges were calibrated against the Todd universal vacuum gauge. Due to the variation of rotameter calibration with the pressure at G_4 , the rotameters were used for indication only, and flow rate was actually measured directly at the pump exhausts by water displacement in an inverted burette at atmospheric pressure (less aqueous tension at room temperature).

Throughput of pure Ar is shown in Fig. 34 as a function of pressure p_1 . In the region of interest (1-10 torr), the throughput falls off more than proportionately to p_1 . Hence the minimum attainable residence time in the tube, calculated from equation 20, or equivalently equation 24 below, rises rapidly as p_1 is decreased.

$$\tau = \frac{V_R}{\dot{V}_f} = \frac{\frac{\pi}{4} \times 1^2 \times 30}{\frac{100}{x} \times \frac{760}{p_1}} \text{ sec} = 0.31 p_1^x \text{ msec} \quad (24)$$

where x = time taken to displace 100 cm^3 of water at atmospheric pressure.

Residence times could conceivably be reduced even further in a system with larger diameter tubes and a pump with higher speed.

The pressure drop in the discharge tube was calculated from equation 25 (45)

$$w = \frac{\pi D_R^4}{128} \frac{g_c M}{2R_g T_g \mu'} \left(\frac{p_4^2 - p_1^2}{L} \right) \quad (25)$$

and is shown in Table 9, for pure Ar and the maximum attainable throughput. Δp as a % of p_4 is seen to vary from 10-16%. Hence the discharge tube operates very nearly at constant pressure. This would not be the case if throughput were to be increased to higher values by redesigning the system. For example, Deckers et al⁽⁹⁵⁾ with a 0.7 cm diameter 80 cm length tube had residence times ~ 20 msec at 1 torr, but report pressure drops of up to 70% of the upstream pressures. Another disadvantage of high velocity systems may be flow noise, which was already becoming apparent at the highest flow rates used in the present work.

6.3 The Gas Chromatograph System

The system was developed around a Loenco Model 160 gas chromatograph. It was a dual column, controlled temperature unit, equipped with a dual flame ionization detector and Model 28 electrometer. The signal was recorded on a Leeds and Northrup Speedomax W (1 mV/in) strip chart recorder with a Model 224-4 Disc Integrator. A thermal conductivity detector system was also available for low sensitivity work. A diagrammatic sketch of the unit is shown in Fig. 35. The column was 1/8" O.D., 1/16" I.D., 150" L and was packed with Davison Grade 58-08-08-226 silica gel of mesh size 35-60. Packing was done in

the laboratory by the usual techniques.⁽⁹⁸⁾ The column was conditioned every 3 months by purging it with helium for 24 hours, with the oven temperature maintained at 120°C. A trickling flow of helium was maintained through the column when the system was not being used. Sample introduction was accomplished through the 6-way valve shown in Fig. 36. To draw the sample into the loop, pump P₃ was turned on; valves 7 and 8 (Fig. 25) were then closed to trap the sample in the loop at a pressure read on G₆. When the 6-way valve is pushed in, a constant reproducible sample volume is injected into the column. Volume of the sampling loop was approximately 3.1 cm³.

Calibration consists of two parts:

- a) Column calibration, and
- b) Detector calibration.

Column calibration consists of determining the retention times for various components. The purpose of obtaining the retention times is to be able to identify the peaks in the analysis of an unknown mixture. Table 10 shows the results of this calibration for column temperatures of 49°C, 64°C and 70°C. Carrier gas flow rate was kept constant at 25 cm³/min. Temperature programming was tried but gave unsatisfactory results due to column bleeding which could be seen on the most sensitive detector attenuations.

Detector calibration consists of determining the relative and absolute response factors of the flame ionization detector. Quantitative analysis of unknown mixtures requires a plot of peak area against partial pressure of a component. These plots were made by injecting known partial pressures of various components into the column, and

determining the areas of the resulting peaks. A set of calibration curves for column temperature of 64°C is shown in Fig. 37. The areas are seen to be proportional to the partial pressures in the range 0-2 torr. When the conditions, e.g., temperature or H_2 or air flow rate, are changed, the absolute calibration could change. However, for a given column, the relative response factors should remain unchanged.⁽⁷⁵⁾ The relative response factors are shown in Table 11 with respect to methane = 1.0. Hence, for a new set of conditions, all that has to be done is to determine the absolute calibration for one component, e.g., CH_4 , the rest can be calculated using the relative factors in Table 11. The procedure for operating the flame ionization detector is summarized in Appendix A-9.

A typical separation is shown in Fig. 38. Although the separation was usually as good as that in Fig. 38, there was a tendency for the methane peak to tail into the ethane and ethylene peaks which was noticeable when the methane-to-product ratio exceeded about 10^2 . This was approximately corrected by subtracting the area under the trailing methane peak from the integrator areas (Fig. 39). However, a better, although tedious, procedure may be to fractionally condense out the products from the predominant CH_4 before they are analyzed.⁽⁹⁹⁾ Another problem occasionally encountered was random noise in the flame detector output. A remedy for this is to pass the H_2 and air supplies through silica gel filters.⁽⁹⁸⁾

6.4 The Pulse Generator and Adapted Microwave Circuit

The purpose of using a pulsed discharge rather than a d.c. discharge for conducting chemical reactions is to effectively reduce the residence time to values lower than those attainable by merely increasing the gas velocity (see Section 6.2). An additional effect could be an increase in the mean electron energy.⁽¹⁰⁰⁾ The pulse generator was designed to produce pulses of width 0.2 to 1.6 msec at intervals of 20-50 msec. A typical pulse is shown in Fig. 40 which is a photograph of the oscilloscope traces actually obtained. Faster cutoffs (less than 2 μ sec) are possible for pulse widths less than 100 μ sec in commercially available equipment, e.g., Velonex 570 with V-1083 plug-in. Nevertheless, for the present purpose, the laboratory fabricated unit of Fig. 42, used with the CVC-LC031 supply already available, was found quite adequate.

Design of our pulse generator was extremely simple. The scheme has been used before in discharge work, e.g., Grant's spectroscopic studies of the neon discharge.⁽¹⁰¹⁾ Fig. 41, below, shows the basic principle which is to use a high voltage triode, e.g., 6BK4C/6EL4A to

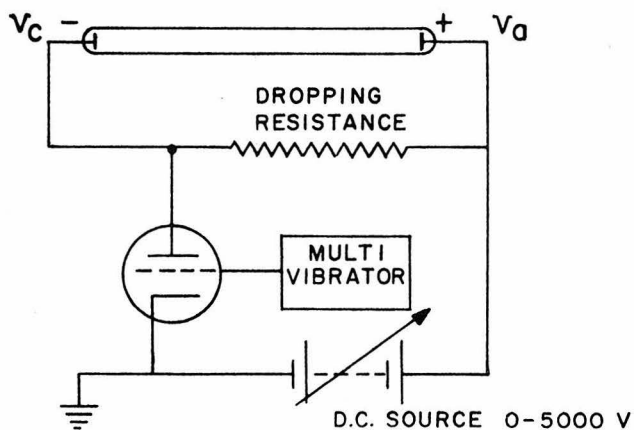


Fig. 41

alternately switch the discharge on and off. The discharge tube conducts only when its cathode voltage v_c is reduced to a near-ground value by the conduction of the triode. Anode voltage v_a always remains at the value set by the d.c. voltage source (0-5000V).

The switching process was controlled by varying the triode grid voltage by means of a free floating astable multivibrator circuit operating at low voltage (225V). Such multivibrator circuits are commonly used in electronic applications such as generating square waves, in timing frequencies and frequency division. As shown in Fig. 42, the multivibrator consists of two alternately conducting 6AG7 tubes and an R-C network to control the time constants. Let us start with T_2 on and T_1 off. The voltage at terminal 4 on T_1 begins to fall as the 0.05 mf capacitor C-3 discharges through R-5 at a rate regulated by the pulse repetition frequency control PRF. At a certain point T_1 starts conducting, leading to a fall in voltage at terminal 4 on T_2 , and cutoff of T_2 at a rate determined by the 1000 pf capacitor C-5 and the pulse width control PW. The high voltage tube T_3 and the discharge tube are therefore on only as long as T_1 is on. The PRF and PW controls interact slightly, so that a variation of only repetition frequency would require some adjustment of PW to keep the pulse width constant, and vice versa.

The microwave circuit had to be adapted (Fig. 43) in order to be used with the pulsed discharge. A Tektronix 541 oscilloscope with Type D plug-in was used instead of the Moseley 7005A recorder of Fig. 6. The sawtooth output of the oscilloscope was divided by a factor of approximately 15 and used to sweep the K & S Model 5000 sweeper at

rates up to 1 msec/sweep, beyond which the sweeper becomes nonlinear. The sweep was triggered in the a.c. slow mode by voltage v_3 from the cathode of tube T_3 , so that the microwave cavity was swept from f_1 to f_2 beginning at the instant the discharge tube turned on. The cavity output was fed to the Y axis of the oscilloscope set on 1 mV/cm. The X axis was on internal sweep. The resonance curve (Fig. 44) appeared at a position on the sweep determined by the Vernier frequency adjustment of f_1 . $(f_2 - f_1)$ was determined by the voltage fed to the sweeper, and could be adjusted in the range 20-50 MHz by varying the control on voltage divider 1.

Pulse current was monitored on the second Y axis of the oscilloscope (set at 50 mV/cm) by means of a Tektronix P-6016 current probe and Type 131 amplifier. Photographs of the oscilloscope traces were taken on Polaroid 3000 film with camera settings of $f/8$ and $1/100$ sec.

7. MEASUREMENTS IN CH₄-Ar MIXTURES WITH

A D.C. DISCHARGE FLOW SYSTEM

7.1 Aim of Experiments

The aim of the present set of experiments was 1) to simplify the kinetics of CH₄ reactions in a rare gas plasma by finding conditions under which there are only a few products, all in the gaseous state; 2) to measure the concentration of these products by gas chromatography, with mean residence time τ , discharge current I , and % methane in the feed C_0 , as independent variables; 3) to simultaneously measure radially averaged steady state electron density \bar{n}_e (and electron-neutral collision frequency ν_{en}) with a TM₀₁₀ microwave cavity; 4) to attempt Langmuir probe measurements that might provide information on the electron energy distribution function $f_e(\epsilon)$; and 5) to plot the data in a form that would suggest a kinetic model correlating the macroscopic kinetics and the microscopic collision processes in the plasma.

7.2 Description of Procedure Used

The system was evacuated by means of pumps P_1 and P_2 (Fig. 25) to about 20 mtorr. No attempt was made to reduce the pressure any further because the flow of gases should rapidly sweep away any remaining impurities in the system. The carrier gas (Ar) flow was started and adjusted so that p_2 was approximately 5 torr. Methane flow was then turned on and the chromatograph brought to operating condition by the procedure outlined in Appendix A-9. The CH₄ peak in

the chromatogram represents the partial pressure of methane in the reactant mixture. A series of trial and error adjustments was then made to simultaneously achieve the desired value of τ , as measured by water displacement in an inverted burette (see Section 6.2), p_1 as indicated on gauge G_1 , and C_o as inferred from the CH_4 peak on the gas chromatograph. To increase τ at constant C_o and p_1 , the Edwards valve E_1 (Fig. 25) was partially closed, and corresponding adjustments of the Ar flow (valves 10,11) and CH_4 flow (valve 12) were made to keep p_1 constant at 5 torr. If it was desired to increase C_o , 12 was partly opened and 10 partly closed, keeping p_1 the same and the Edwards valve E_1 in the same position as before. To increase p_1 , both 10 and 12 were opened; τ and C_o were then kept constant by adjusting E_1 , 10 and 12. This tedious procedure consumed most of the time spent on the experiments described in Chapter 6 and 7. Fortunately, the time constant for the system to reach steady state after any adjustment was less than 2 min., otherwise an even longer time would have been spent in achieving desired values of τ , p_1 and C_o .

The d.c. power supply was turned on and the current I adjusted to the desired value as read on ammeters A_1 and A_2 (Fig. 26). For a certain applied voltage V , I was found to depend on p_2 , the pressure in the cathode bulb (see Section 7.3). In a given run, the lowest current I was first investigated and an increase in I was obtained by increasing p_2 , which was easily achieved by choking off the flow to pump P_2 by means of the Edwards valve E_2 . Thus the total steady state voltage remained approximately constant for $I = 0.5 \text{ mA} - 2.0 \text{ mA}$. Oscillations in current were observed on the

oscilloscope which were independent of the ripple in the d.c. voltage ($< \pm 10\%$). These were often as large in amplitude as 25% of I , and were evident in both the msec/cm and the μ sec/cm ranges. The oscillations seemed to correlate with moving striations in the discharge. Color of the discharge was an almost invisible lavender. After waiting 5 min. for attainment of steady state under constant current conditions, the trigger on the microwave sweeper was pushed to obtain the resonance curve with a sweep time of 60 sec. Some "hash" was observed on the X-Y recorder, but this was not serious enough to affect \bar{n}_e measurements. The product sample was trapped in the sampling loop by closing shut-off valves 7 and 8 (Fig. 25), and injected into the chromatograph after pressure p_6 had been noted on G_6 . V was read on voltmeter V_1 and electric field E on the electrometer K (Fig. 26). The same two probes could also be used as a double Langmuir probe. Attempts to measure $f_e(\epsilon)$ by this method are described in Chapter 10.

Calculation of $(n_e)_0$ and v_{en} from the observed frequency shift and broadening of the TM_{010} mode has been described in Section 2.3a of Part I. The concentration of various gaseous hydrocarbon products was calculated from equations 26 and 27 below, using the measured peak areas in the chromatogram.

$$\% x \text{ in product stream} = \frac{100 \times (\text{area of } x \text{ peak on att. } 1 \times \text{calibration factor for } x)}{(\text{Total pressure of sample})} \quad (26)$$

$\% CH_4$ in the feed (C_0) was calculated analogously.

$$\% \text{CH}_4 \text{ converted to } x = \frac{100 \times (\% x \text{ in product stream})}{C_o \times (\text{No. of C atoms in } x \text{ molecule})} \quad (27)$$

The "number of C atoms in x molecule" divisor accounts for the fact that carbon from $n \text{ CH}_4$ molecules is required to produce one C_nH_m molecule.

Further treatment of the data is explained in Section 7.6.

7.3 V-I Characteristics of the Choked Flow Orifice Discharge

The voltage-current characteristics of the choked flow orifice d.c. discharge tube described in Section 6.2a are shown in Figs. 45 and 46. V is the steady state voltage across the electrodes, as measured on voltmeter V (Fig. 26), and I the steady state current, as indicated by ammeters A_1 and A_2 (Fig. 26). Both in pure He (Fig. 45) and pure Ar (Fig. 46), three main features are clearly evident:

1) V is an increasing function of I ; in terms of the general characteristic of Fig. 2, this means we are in the abnormal glow region of the curve. dV/dI increases as p_2 falls.

2) V increases for the same I as the cathode bulb pressure p_2 is reduced; a result which may be due to the increased cathode fall at lower pressures.

3) At low p_2 , e.g., 0.8 torr in Fig. 45, the discharge is stable down to much lower values of current than normally possible. Hence, by the simple device of lowering p_2 , it is possible to get stable d.c. discharges at currents as low as 0.1 mA in pure rare gases.

The same trends were observed in mixtures of CH_4 with Ar and He, except that stable discharges with $I < 0.5$ mA were difficult to

maintain even at the lowest possible values of p_2 . For constant gas composition and p_1 , p_2 had no effect on the microwave measurements. Therefore, the behavior of the discharge on the positive column side of the orifice (right side of Fig. 28) was quite independent of the phenomena in the cathode bulb.

Orifice size had no effect on the V-I characteristic, except that for given pumping speeds and given p_1 , smaller orifices enabled us to attain lower values of p_2 . The orifice seems, however, to be a region of high chemical reactivity, as evidenced by the tendency toward solid formation especially when it is in a fresh unconditioned state (see Section 6.2a). This may be because it is a region of high electric field and perhaps high electron temperature. In practice the problem was minimized by reducing the amount of backmixing between the orifice and positive column regions, and by using a conditioned 0.020" orifice that did not get totally plugged up with deposits.

7.4 Composition Measurements of the Effluent Stream

After a series of preliminary runs (Tables 12-18), it was found that the desired goal of a small number of gaseous products (selectivity) is achievable under the following conditions

- 1) Lowest possible residence time τ in the discharge tube (~ 100 msec or less)
- 2) Small spread of residence times, i.e., conditions under which the reactor may be modelled as a plug flow reactor.
- 3) Low power inputs, which in a d.c. glow discharge means low discharge currents ($I < 5$ mA). The technique for obtaining steady discharges at low currents was discussed

in Section 7.3

- 4) Concentrations of methane in the feed stream should not be less than about 2%.

The conditions listed above all imply low total conversions of methane (< 10%), so that we are looking at the initial stages of the reactions. Further, it was found that a steady low-current d.c. discharge could be maintained in mixtures of CH_4 and Ar at reasonable voltages (< 5000V) for $p_1 = 5$ torr. Hence the d.c. discharge kinetic experiments (Chapter 7) were performed in CH_4 -Ar mixtures with only τ , I and C_0 as independent variables. The effect of carrier gas and total pressure variation was, however, investigated in pulsed discharges (Chapter 8).

Figure 47 shows the results of the final runs in the preliminary series. It is seen that the hydrocarbon products are ethane and ethylene, with a smaller amount of acetylene. No solid or liquid products were found in the discharge tube. The presence of H_2 may be inferred from the hydrogen balance. In order to perform a legitimate carbon balance at low total conversions of methane, the flow rates of CH_4 and Ar should be held constant to within 1% during the run. Since this was somewhat beyond the capabilities of the system, each point on the "total conversion" curve of Fig. 47 represents an average over three observations of the CH_4 peak in the product stream. Over 80% of the carbon in the methane lost reappears as C_2H_6 , C_2H_4 and C_2H_2 , as seen in Fig. 48. At the lowest currents of 0.1 and 0.2 mA, the carbon reappearing is over 95%, but it must be remembered that this is also the region where the total conversion measurement is least accurate.

In view of the encouraging carbon balance of Figs. 47 and 48, the kinetic experiments were performed under approximately similar conditions.

Tables 21-36 summarize the results of the kinetic experiments. Mean residence time τ was varied in the range 57-117 msec. The percentage CH_4 in the feed stream (C_o) was in the range 4.0-12.6%. Discharge current I was set at 0.75 mA, 1.0 mA, 1.5 mA and 2.0 mA, with a 0.5 mA run whenever a stable discharge could be maintained at that current. Voltage across the tube, V , is not only a function of pressure p_1 and composition C_o , but also the pressure p_2 in the cathode bulb (see Section 7.3). Since I is the desired independent variable, p_2 and V were not rigidly controlled. They were allowed to assume any value that permitted stable operation at a given current level. In general, low p_2 (~ 0.7 torr) resulted in low currents ($\sim 0.5 - 0.75$ mA) for a voltage of 4000-4500V. Equation 26 was used to reduce the chromatographic data to the form reported in columns (f), (g), (h), and (i) of Tables 21-36. The multiplying factors (e.g., 2 for C_2H_6) are the number of C atoms in the respective product molecules, and have been retained with equation 27 in mind. In the range investigated, all the hydrocarbon products are increasing functions of current, as is the % methane converted to these products (column j) which varied from 1.6 to 17.5%. Spot checks on the carbon balance indicated that gaseous hydrocarbon products accounted for over 70% of the CH_4 converted, with the best balances at the lowest currents and residence times. Electric field in the kinetic experiments was in the range 30-60 V/cm.

Figures 49-51 illustrate the behavior of three quantities of interest--the concentration of ethane in the effluent stream, % CH₄ converted to ethane, and the ethane to ethylene ratio for p₁ = 5 torr and C₀ = 12.6% . % C₂H₆ in the product stream (Fig. 49) is seen to be linearly proportional to the mean residence time τ , with the slope increasing with discharge current I . The slope of these straight lines is the rate of formation of the major product ethane if the plug flow approximation is permissible. The percentage of reactant converted to C₂H₆ (Fig. 50) falls as the feed becomes richer in methane. At approximately 10% CH₄, the curves seem to be approaching a limiting lower value. Later experiments with pulsed discharges (Chapter 8) indicated that the limiting value might be the conversion to ethane with a 100% CH₄ feed. On the other hand, the ethane to ethylene ratio (Fig. 51) increases as C₀ is increased, approaching a limiting upper value at a methane concentration of approximately 10%. Thus, low C₀ tends to favor high total conversion, and also the formation of greater amounts of C₂H₄ as compared to C₂H₆. Both the percent conversion to C₂H₆ and [C₂H₆]/[C₂H₄] increase with increasing discharge current I . Section 7.6 deals with further treatment of the data.

7.5 Microwave Measurements on the Discharge

Microwave data on the electron density n_e and electron-neutral collision frequency ν_{en} in reacting CH₄-Ar d.c. glow discharges have been tabulated in Tables 21-36. The quantity of immediate interest in developing kinetic models is \bar{n}_e , since ν_{en} is mainly an indicator of the elastic collisions of the electrons with the various

molecular species in the discharge. $(n_e)_o$ values are seen to increase with I , as might be expected, and lie in the range $1.3 - 9.8 \times 10^9$ per cm^3 for $I = 0.5 - 2$ mA. Corresponding drift velocities, calculated as in Section 3.3b, turn out to be $3 - 5.6 \times 10^6$ cm/sec. These can be compared to v_d 's in pure Ar discharges (Fig. 15) which are $1.4 - 2.2 \times 10^6$ cm/sec for $E/p = 6-10$ V/(cm \times torr). Comparable data in pure CH_4 and CH_4 -Ar mixtures are available for E/p values up to 0.6 V/(cm \times torr) only.⁽¹⁰²⁾ It must, however, be pointed out that our deduced v_d values for $C_o = 4.0 - 12.6\%$ are not in disagreement with the trends visible in Fig. 11 of English and Hanna.⁽¹⁰²⁾

Figure 52 illustrates the behavior of $(n_e)_o$ with discharge current I for $C_o = 12.6\%$. At low values of I the relationship is approximately linear. At $I = 2.0$ mA there is a tendency for $(n_e)_o$ to level off, probably because of composition changes induced by the higher extents of chemical reaction. For the range of τ investigated, no clear relationship between $(n_e)_o$ and τ was observed. Hence it was decided to model $(n_e)_o$ as a function of I only. An empirical correlation of the form $(n_e)_o = (n_{eo})_{I=1 \text{ mA}} I^{0.8}$ may be successfully used to predict electron densities with a precision comparable to that achieved in the measurements ($\pm 6\%$), see Appendix A-1).

7.6 Treatment of Data and Discussion of Results

In Section 6.2a it was mentioned that an elongated slender design for the reactor might permit modelling as a PFR even when the flow is laminar. We shall now discuss the validity of the approximation insofar as it applies to the d.c. discharge flow reactor of Fig. 31 under the conditions used in the kinetic experiments (Tables 21-36).

The binary diffusion coefficient for the CH₄-Ar system at 300°K was calculated by the method recommended by Reid and Sherwood,⁽¹⁰³⁾ and at low pressures is given by

$$D_{12}p = 164 \text{ cm}^2/(\text{sec} \times \text{torr}) \quad (28)$$

For $p = p_1 = 5$ torr, D_{12} is 32.8 cm²/sec. Cleland and Wilhelm⁽¹⁰⁴⁾ computed that for low conversion (< 20%) first order reactions in long reactors, the plug flow approximation is correct to within 0.01% if $D\tau/2R^2 > 1$. Table 37 shows that radial diffusion is certainly predominant in our system as $D\tau/2R^2 > 3$. Levenspiel⁽⁹⁷⁾ gives the following limiting expression for the residence time distribution in a plug flow reactor with longitudinal dispersion for small $D\tau/L^2$.

$$C = \frac{1}{2\sqrt{\pi \frac{D\tau}{L^2}}} \exp \left[-\frac{\left(1 - \frac{t^2}{\tau^2}\right)}{4(D\tau/L^2)} \right] \quad (29)$$

C is therefore the symmetrical, bell-shaped Gaussian distribution and is accurate to within 0.5% for $D\tau/L^2 < 0.001$. From Fig. 30 it is clear that backmixing may be neglected under these conditions where the C curve is centered on 1.0 and is symmetrical. The heavy line in Fig. 30 corresponds to the curve realized in our system for $\tau = 75$ msec.

From the above discussion, the ideal plug flow model should be accurate in the present case to within 2%. It is believed that even a sophisticated analysis, accounting for radially varying reaction rates and diffusion of the products, should reveal an error of no more than 5% due to imperfections in reactor modelling.

Treatment of data proceeds with a plot of the product concentrations against discharge current to uncover possible dependencies on electron density \bar{n}_e . Figure 53 shows typical log-log plots of the percent ethane in the product stream vs. I . The multiplying factors of 3.6 and 2 have been used only to accommodate the data in a 1 cycle \times 1 cycle graph, and are arbitrary. $[C_2H_6]$ is seen to be proportional to I^m , with m , the slope of the straight lines of Fig. 53, in the range 0.8 - 1.0. In view of the approximate $I^{0.8}$ dependence of $(n_e)_0$ on discharge current (Section 7.5) this indicates that $[C_2H_6]$ is linearly proportional to \bar{n}_e in the range investigated. Since it was found earlier (Fig. 49) to be proportional to the mean residence time τ , it was considered worth while to try and use $\tau\bar{n}_e$ or equivalently $\tau I^{0.8}$ as a single group to correlate all the data for a particular value of C_o . Figure 55 shows such a plot of $[C_2H_6]$ against $\tau I^{0.8}$ for $C_o = 12.6\%$ on a log-log graph with arbitrary multiplying factors on the ordinate and abscissa. The results are strikingly successful as the points fall on a straight line of slope 45° within the bounds of experimental error. We therefore require that the chemical mechanism should be one that explains the proportionality of $[C_2H_6]$ to $\tau\bar{n}_e$.

The concentrations of ethylene by itself did not show any simple dependence on τ and I . However, when the data were plotted as the ratio of acetylene to ethylene in the product stream, some interesting relationships became evident. Figure 54 shows that $[C_2H_2]/[C_2H_4]$ for $C_o = 12.6\%$ is also proportional to I^m with $m = 0.8 - 1.0$. Hence the ratio of these products varies as \bar{n}_e . The parameter

$\bar{\tau}n_e$ (equivalent to $\tau I^{0.8}$) was again tried to correlate all the data. Figure 56 for $C_0 = 12.6\%$ illustrates the 45° slope straight lines obtained. We thus arrive at a second requirement for any proposed mechanism--that it should explain linear dependence of $[C_2H_2]/[C_2H_4]$ on $\bar{\tau}n_e$.

In view of the promising success of the $\tau I^{0.8}$ parameter, it was decided to test the total CH_4 disappearance for first order dependence. As seen in Fig. 57, a standard plot of $\log(1 - x)$ vs. $\tau I^{0.8}$ (where x is the fraction methane converted to gaseous products, column j, Tables 21-36) yields a straight line within the bounds of experimental error. The chemical mechanism should therefore explain the approximate first order decay of CH_4 with respect to $\bar{\tau}n_e$, in addition to the behavior of $[C_2H_6]$ and $[C_2H_2]/[C_2H_4]$ already mentioned.

Chapter 9 offers a possible explanation of the d.c. discharge kinetic results in terms of a free radical mechanism. Some kinetic data have also been obtained in the flow reactor with the pulsed high-voltage source described in Section 6.4. The following Chapter 8 discusses the results of a pulsed d.c. discharge in CH_4 -Ar and CH_4 -He mixtures.

8. MEASUREMENTS IN CH₄-Ar AND CH₄-He WITH A
PULSED D.C. DISCHARGE FLOW SYSTEM

8.1 Aim of Experiments

The aim of the experiments reported in Chapter 8 was

- 1) to examine the detailed structure of the $i-t$ curve in pulsed discharges in pure He, Ar, CH₄ and CH₄-Ar and CH₄-He mixtures;
- 2) to obtain electron density as a function of time within the pulse;
- 3) to simultaneously measure the concentration of stable discharge products on the chromatograph, with residence time τ , initial concentration of methane C_0 , total pressure p_1 , pulse width τ_w and pulse interval τ_I as independent variables;
- 4) to investigate the effect of the two carrier gases Ar and He on the plasma chemical reaction of CH₄;
- 5) to reduce the data to a form that would permit comparison with the d.c. discharge data of Chapter 7, and hopefully lead to a consistent kinetic mechanism.

8.2 Description of Procedure Used

The system was evacuated and the flow of gases adjusted as described in Section 7.2 to give the desired values of τ , p_1 and C_0 . Pulse width τ_w and interval τ_I as seen on the oscilloscope traces of v_3 (Fig. 40) were set at the appropriate values. The d.c. power supply in the pulse generator circuit was now operated with its cathode side grounded. D.C. voltage was increased until breakdown occurred. After breakdown, the height of the current pulse would increase with

voltage and finally saturate at a peak value of 3-6 mA, depending on the gas. Stable pulse shapes were obtained under these saturation conditions. In the pre-saturation period, the current pulse was unstable to small changes in V . The pulsed discharge was invisible except for a violet glow which could be seen when all the laboratory lights were switched off. Orifice plugging and the necessity to control p_2 were not at all critical in the pulsed discharge experiments, making them more convenient to work with as compared to d.c. discharges in hydrocarbon mixtures.

The oscilloscope was triggered by voltage v_3 (Fig. 42) and the current pulses displayed on Channel Y-2 with vertical sensitivity 50 mV/cm. Photographs of the current pulses (i - t curves) were taken with sweep rates of 100 μ sec/cm to 10 msec/cm. The v_3 pulse also triggered the sawtooth voltage that externally swept the microwave sweeper at either 100 μ sec/cm or 200 μ sec/cm in the "recurrent" mode. Resonance curve of the cavity (Fig. 44) was seen on Channel 1 with a vertical sensitivity of 1-5 mV/cm. The vernier setting required to center the resonance curve on a particular position in the sweep was measured before and after the discharge was on. Difference between the vernier readings at a given position in the pulse was the shift in resonant frequency δf_o . Width $(\Delta f)_{1/2}$ was simultaneously measured in cm and converted to MHz knowing the total width of the sweep in frequency units. $(n_e)_o$ (and v_{en}) were calculated as in Sections 2.3a and 7.2.

Steady state composition measurements of the product stream were made by the procedure followed for the d.c. discharge measurements,

(see Section 7.2).

8.3 Fine Structure of the Pulsed D.C. Discharge and Its Variation with Gas Composition

Figures 58-64 show the i_m - t traces obtained in pulsed discharges of various compositions. In general, the measured current i_m builds up to a maximum within the first 100 μ sec of the initiation of the pulse voltage, and then decays to its zero value between pulses. There is a transient at the tail end of the i_m pulse that takes it about 0.5 mA in the negative direction before it decays to zero. In pure Ar, and to some extent in CH_4 -Ar mixtures, secondary maxima are seen in the i_m - t curve. The secondary maxima are attenuated out within 600 μ sec, so that no more than 3-4 peaks are observed. As % CH_4 increases, the curves become somewhat unreproducible from pulse to pulse (Figs. 60, 63 and 64). In addition, higher frequency oscillations (~ 20 KHz) were seen within the pulses. These were especially noticeable in pure He (Fig. 61) but were suppressed in CH_4 -He mixtures (Figs. 62, 63). Another feature in He is that peak current never exceeded 3 mA for $V < 5000\text{V}$ because of the broad maximum.

A qualitative explanation of the gross features of the i_m - t curves is illustrated in Fig. 65. The independent variable in the sequence of events to be described is the grid voltage of tube T_3 , which essentially controls the conduction current i_s through T_3 . As T_3 starts conducting at (a), v_c falls to a near ground value, so that the gas in the discharge tube breaks down and begins to conduct. i is the discharge current that adds negligibly to the current i_s .

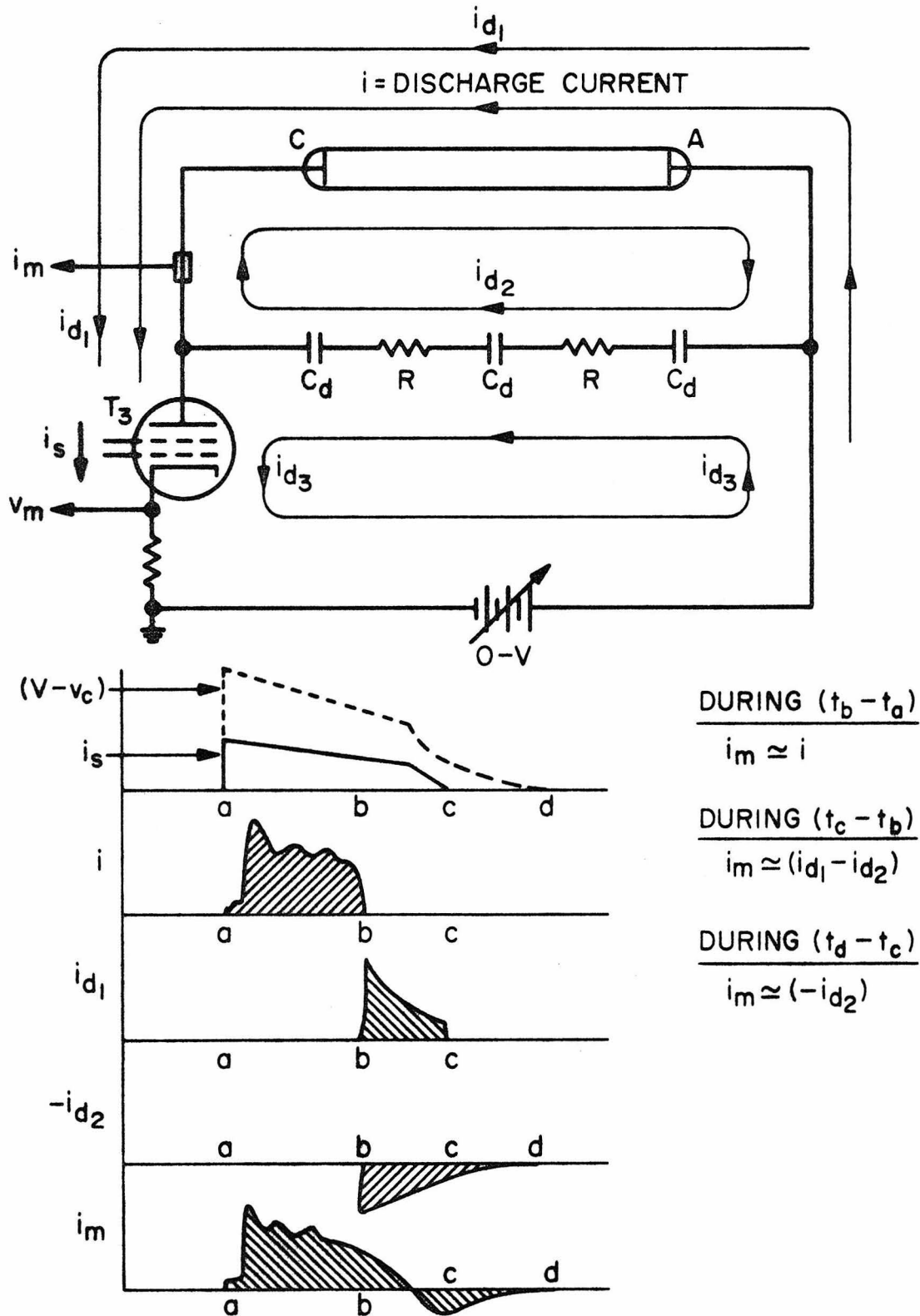


Fig. 65. Qualitative explanation of the measured current i_m in pulsed discharge circuit

As i_s falls, $(V - v_c)$ falls with it and at a certain point (b) is too small to sustain the ionization in the discharge tube. (b) is therefore the point where the discharge is "off". The afterglow plasma decays by recombination and diffusion to the walls (see Appendix A-5) and sustains current i_{d1} in the interval (b) - (c). i_{d1} is a displacement current if the afterglow plasma is looked upon as a dielectric and a conduction current if it is considered to be a conductor. Meanwhile, another displacement current i_{d2} is set off by the effect of distributed capacitances, and it tends to bring v_c back to the high voltage V . i_{d2} continues even after the tube T_3 has stopped conducting at point (c). The sum of i , i_{d1} and $(-i_{d2})$ is the measured current i_m . Current i_{d3} does not affect i_m and is neglected.

8.4 Electron Density as a Function of Time within the Pulse

$(n_e)_0$ as a function of time from the initiation of the pulse was obtained quite easily in pure Ar (Fig. 66). In pure He and CH_4 oscillations distorted the resonance curve enough to make microwave measurements practically impossible. However, one set of readings was possible in CH_4 at $p_1 = 1.5$ torr. This set is shown in Fig. 66 for comparison. $(n_e)_0$ is seen to fall with time, rapidly in the initial stages, and later more slowly. Since electron attachment is unlikely in both Ar and CH_4 ,⁽¹⁰⁵⁾ the results have to be interpreted in terms of electron-ion recombination and ambipolar diffusion to the tube walls (Appendix A-5).

The $(n_e)_0$ vs. t curves in CH_4 -Ar and CH_4 -He mixtures (Figs. 67-70) showed less regular behavior. Often, sharp drops and kinks,

which cannot be explained away as experimental error, would appear in the curves. The irregularities could be a result of the complexity of the ionic mixture in these systems. In addition to the atomic and molecular rare gas ions (Ar^+ or He^+ , Ar_2^+ or He_2^+), there can be present ions like CH_4^+ , CH_5^+ , CH_3^+ and CH_2^+ , leading to a large number of possible charge transfer reactions. Different segments of the $(n_e)_0$ -t curve would then represent the recombination or diffusion of different positive ions. Electron attachment and negative ions would further complicate the picture, but this is unlikely in CH_4 -Ar and CH_4 -He mixtures (by analogy with the corresponding pure components).

The effect of increasing percent methane C_0 in CH_4 -Ar and CH_4 -He mixtures is to lower $(n_e)_0$ (Figs. 67,68). Pulse width reduction (Fig. 69) tends to increase peak $(n_e)_0$ to compensate for the lower base τ_w . The n_e -t curves in Figs. 67-70 were measured under saturation current conditions (see Section 8.3). Varying total pressure in the range 3.0 to 7.0 torr is seen to have little effect on $(n_e)_0$ vs. t in a 0.97% CH_4 in Ar mixture (Fig. 70), thus making diffusion control unlikely. Variation of τ and τ_I had no perceptible effect on $(n_e)_0$, as expected. In view of the complicated time variation of $(n_e)_0$ in reacting mixtures, only the value of $(n_e)_0$ at $t = 300 \mu\text{sec}$ is reported with the composition measurements (Tables 38-42).

8.5 Composition Measurements of the Effluent Stream

Preliminary runs (Tables 19,20) with a low-frequency a.c. voltage source indicated that over 75% of the carbon in the converted methane may be accounted for in a pulsed discharge if total conversion is kept below about 3%. The disadvantage of an a.c. discharge is that

there is no independent control on the peak current i_{\max} and the pulse width τ_w , as both increase with applied voltage. Hence the main sequence of pulsed discharge experiments was conducted with the pulse generator described in Section 6.4, wherein τ_w , τ_I and i_{\max} can be independently controlled. Tables 38-43 summarize the results of composition measurements of the effluent stream from a pulsed d.c. discharge in CH_4 -Ar and CH_4 -He mixtures. Tables 38-42 contain, in addition, part of the microwave data, reported here as the value of $(n_e)_0$ 300 μsec after the initiation of the pulse. 300 μsec was, in general, the closest one could get to the start of the pulse without distorting the resonance curve (see Fig. 44).

% CH_4 in the feed stream varied between 0.8 and 17.7, with one run (#26) using pure methane feed. Total pressure p_1 was 3.0 - 7.0 torr, pulse width τ_w was in the range 0.2 - 1.6 msec, pulse interval τ_I was 22-52 msec, and mean gas residence time τ was 93.5 - 655 msec. Peak current i_{\max} , which was the stable saturation current (see Section 8.3) in all runs except #16, was 2.5 - 6.0 mA.

The most notable feature of the pulsed discharge experiments was the fact that there were, for all practical purposes, only two hydrocarbon products, i.e., ethane and ethylene. Some C_2H_2 and traces of C_3H_8 were observed at the highest conversions, e.g., run #4, but even there C_2H_6 and C_2H_4 accounted for over 85% of the gaseous hydrocarbon products. The selectivity is best in runs like 1, 5, 11 and 15 where the ratio of τ to τ_I is the smallest. This trend suggests that for good selectivity the pulse interval τ_I must be of the same order as the residence time τ (also $\tau_w \ll \tau_I$). Due to the

extremely low total conversions (0.043% to 3.22%), no accurate carbon balance could be performed in the pulsed discharge experiments. However, from the trend visible in the d.c. discharge runs, it is very likely that the gaseous products accounted for over 90% of the converted methane in runs 1-30 (Tables 38-43), a fact supported by the total absence of any solid or liquid deposits even in the reactive orifice region.

Both C_2H_6 and C_2H_4 are seen to increase with τ and decrease with τ_I for constant values of the other parameters. The effect of increasing total pressure p_1 (Table 40) is analogous to increasing C_o at constant p_1 ; percent conversion to the two products taken separately is reduced, as is the total percent conversion. Reducing τ_w (Table 42) reduces the amounts of products, although the relationship may not be linear. As C_o increases, $[C_2H_6]/[C_2H_4]$ increases in CH_4 -Ar as well as CH_4 -He mixtures (Fig. 78). In the concentration range 0.8 - 17.7%, the carrier gas does not affect the $[C_2H_6]$ to $[C_2H_4]$ ratio appreciably. The value of the ratio plotted in Fig. 78 is the smallest that can be realized for any C_o , and corresponds to the d.c. discharge runs with the lowest τ and I , which are shown for comparison. The agreement is reasonable despite the fact that more ethylene could be degrading to side products in the d.c. discharge as compared to a pulsed d.c. discharge.

Further treatment of the data of Tables 38-43 is discussed in Section 8.6.

8.6 Treatment of Data and Discussion of Results

The first step in the treatment of pulsed discharge data is to find a single parameter to account for the chemical effect of τ , τ_I , τ_w and the time-varying $(n_e)_0$. It has already been shown (Section 7.6) that $\tau \bar{n}_e$ is a useful group for correlating d.c. discharge kinetic data at a given value of C_0 and p_1 . By analogy, the parameter for pulsed discharges under the plug flow approximation should involve $\tau \bar{n}_e$ where \bar{n}_e is a time averaged value of the electron density.

$$\bar{n}_e = \frac{\int_0^{\tau_x} \bar{n}_e dt}{\tau_x}, \quad \text{where } \tau_x \leq \tau_w \quad (30)$$

We shall also have to incorporate a weighting factor τ_x/τ_I to account for the fact that the discharge is chemically "active" only for a period τ_x within the pulse and is completely inactive between pulses. Hence we arrive at the parameter

$$\xi = \tau \frac{\int_0^{\tau_x} \bar{n}_e dt}{\tau_x} \frac{\tau_x}{\tau_I} = \frac{\tau}{\tau_I} \int_0^{\tau_x} \bar{n}_e dt \quad (31)$$

τ/τ_I may be identified as the "pulse number" of Brown, Howarth, and Thornton.⁽¹⁰⁰⁾ When $\tau_x = \tau_I$ and \bar{n}_e is constant, ξ reduces to its d.c. value of $\tau \bar{n}_e$.

Two simplifications must be effected before ξ defined in equation (31) can be used in practice. First, since we are in a range where \bar{n}_e is generally proportional to the instantaneous current i ,

we can use $\int_0^{\tau_x} i dt$ instead of $\int_0^{\tau_x} \bar{n}_e dt$. This avoids the necessity of considering irregularities in the behavior of $(n_e)_0$ (see Section 8.4) and enables us to work with the convenient precisely measurable i . Second, some assumption has to be made about the electron temperature within the pulse. If T_e relaxes in a few μsec or less after the ionizing collisions have ceased (point (b) of Fig. 65), then $\tau_x < \tau_w$ and we are left with the problem of determining τ_x . However, as may be surmised from the voltage pulses (Fig. 40), the applied electric field in our case does not cut off instantaneously. Consequently, there is a possibility that the electrons remain hot during the afterglow period. In such an event, it would be more nearly correct to take $\tau_x = \tau_w$. Both the hypotheses ($\tau_x < \tau_w$ and $\tau_x = \tau_w$) were tried on the pulsed discharge data.

Figure 71 shows the percentage of reactant converted to ethane in the pulsed discharge runs in CH_4 -Ar mixtures with $C_0 = 4.2\%$. An approximately linear relationship is obtained with respect to $\frac{\tau}{\tau_I} \int_0^{\tau_x} i dt$, both with $\tau_x = \tau_w$ and $\tau_x = 150$ sec (arbitrary). Hence both hypotheses regarding T_e might appear equally tenable. However, the d.c. discharge data for $C_0 = 4.0\%$ lie closer to the former line, indicating the possibility of close correspondence between the pulsed data and the d.c. data if we take $\tau_x = \tau_w$. Figure 72 shows a similar curve for % CH_4 converted to C_2H_4 with $C_0 = 4.2\%$. An approximately linear relationship prevails at lower values of conversion, with saturation setting in as C_2H_4 is converted to byproducts, presumably acetylene (see Chapter 9). The d.c. data for $C_0 = 4.0\%$ fall

within 10% of the linear section. Correspondence of the pulsed and d.c. data indicates that the pulse width here was not small enough to result in increased T_e within the pulse as suggested by Brown, Howarth and Thornton.⁽¹⁰⁰⁾

Figures 73 and 74 illustrate further tests of the usefulness of the parameter $\frac{\tau}{\tau_I} \int_0^{\tau_w} idt$ in correlating the data. The first set of points is for $C_o = 1.75\%$ and represents the effect of varying τ_I in the range 22-52 msec. The second group of points is for $C_o = 2.05\%$ and shows the success of the parameter in handling situations where τ_w varies in the range 0.2 - 1.6 msec. In this group there are also points from runs 19 and 20 where τ , τ_I and τ_w were all varied. As seen in Figs. 73 and 74, all these variations can be handled within the proposed framework.

Figure 76 shows the slope of the lines such as those in Figs. 71 and 73 plotted against C_o . The slope falls with C_o in the range 1.0 - 4.2% indicating that there is less conversion to C_2H_6 at higher values of C_o . The lower reactivity of mixtures with high percent CH_4 is also visible in Fig. 77, which is a plot of the total % CH_4 converted vs. C_o . Varying the carrier gas is seen to have a measurable effect. Over most of the range, the conversion is higher in CH_4 -He than in CH_4 -Ar mixtures, e.g., at $C_o = 10\%$, the conversion is 67% higher with He than with Ar. For $C_o > 15\%$, both curves seem to be reaching a limiting value which ultimately has to be 0.075, the total percent conversion with pure CH_4 feed. The effect of increasing pressure (Fig. 75) is analogous to that of increasing C_o . Both total conversion and percent conversion to C_2H_6 fall as p_1 increases. The

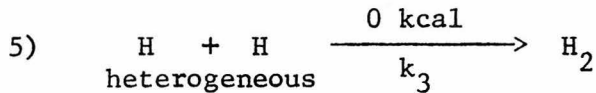
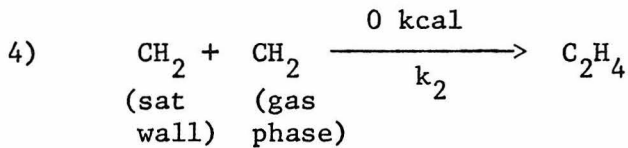
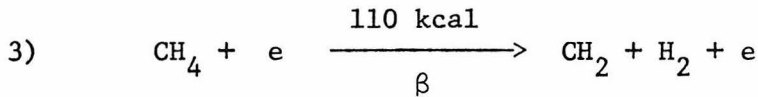
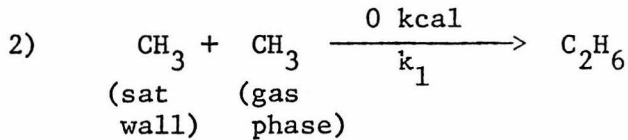
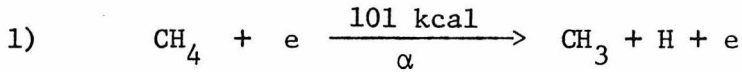
data for Figs. 75-77 have been made comparable by reduction to arbitrarily chosen values of τ and $\int idt$.

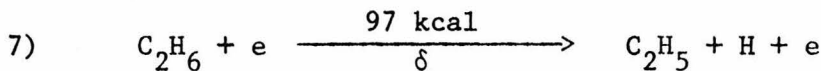
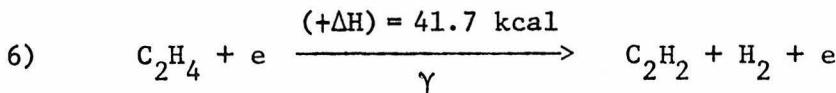
Chapter 9, which follows, is devoted to a discussion of a possible chemical mechanism to explain the kinetic data presented in Chapters 7 and 8.

9. A PROPOSED CHEMICAL MECHANISM TO EXPLAIN
THE KINETIC DATA

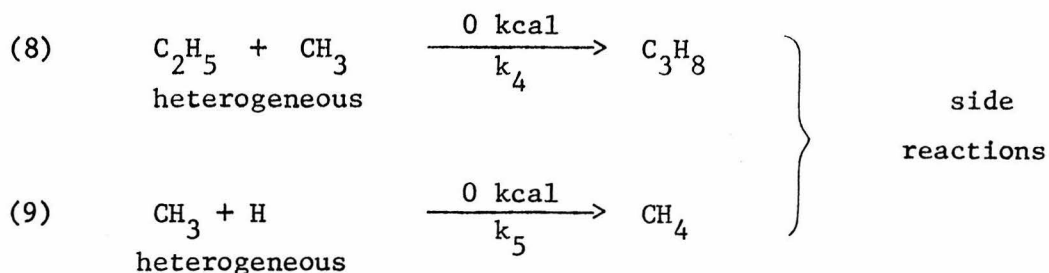
9.1 The Mechanism

The following free radical mechanism is proposed to explain qualitatively and quantitatively the reactions of methane in a low pressure non-equilibrium plasma:





} side
reactions



The figures in kcal/mole are the activation energies of the respective reactions. For reactions (1) and (7), the source of information is electron-impact data.⁽¹⁰⁶⁾ In reaction (3), Chupka and Lifshitz's recent value of 91.9 ± 1.0 kcal/mole⁽¹⁰⁷⁾ has been used for the heat of formation of CH_2 . Heats of formation of CH_4 , C_2H_4 and C_2H_2 have been obtained from standard thermochemical sources.⁽⁴⁵⁾ The activation energy of free radical recombination reactions is known to be close to zero.

Under conditions where the side reactions (7), (8) and (9) may be neglected, the overall kinetics takes the following form:

$$\frac{d[\text{CH}_3]}{dt} = \alpha n_e [\text{CH}_4] - k_1 [\text{CH}_3] \quad (32)$$

$$\frac{d[\text{CH}_2]}{dt} = \beta n_e [\text{CH}_4] - k_2 [\text{CH}_2] \quad (33)$$

$$\frac{d[\text{C}_2\text{H}_6]}{dt} = k_1 [\text{CH}_3] \quad (34)$$

$$\frac{d[\text{C}_2\text{H}_4]}{dt} = k_2 [\text{CH}_2] - \gamma n_e [\text{C}_2\text{H}_4] \quad (35)$$

$$\frac{d[\text{C}_2\text{H}_2]}{dt} = \gamma n_e [\text{C}_2\text{H}_4] \quad (36)$$

$$\frac{d[\text{CH}_4]}{dt} = -\alpha n_e [\text{CH}_4] - \beta n_e [\text{CH}_4] \quad (37)$$

Under the pseudo-steady state hypothesis, the net rate of formation of free radicals in the gas phase may be equated to zero.

Therefore

$$\frac{d[\text{CH}_3]}{dt} = \frac{d[\text{CH}_2]}{dt} = 0$$

With the initial conditions $[\text{CH}_4] = [\text{CH}_4]_0$, $[\text{C}_2\text{H}_6] = [\text{C}_2\text{H}_4] = [\text{C}_2\text{H}_2] = [\text{H}_2] = 0$, the integrated forms of the kinetic equations are:

$$[\text{CH}_4] = [\text{CH}_4]_0 \exp\{-(\alpha + \beta)\bar{n}_e \tau\} \quad (38)$$

$$[\text{C}_2\text{H}_6] = \alpha \bar{n}_e \tau [\text{CH}_4]_0 \quad (39)$$

$$[\text{C}_2\text{H}_4] = \frac{\beta}{\gamma} [\text{CH}_4]_0 \{1 - e^{-\gamma \bar{n}_e \tau}\} \quad (40)$$

$$[\text{C}_2\text{H}_2] = \beta \bar{n}_e \tau [\text{CH}_4]_0 \{1 - e^{-\gamma \bar{n}_e \tau}\} \quad (41)$$

Equations (39), (40) and (41) are for low total conversions, i.e., approximately constant $[\text{CH}_4]$. For small values of $\gamma \bar{n}_e \tau$, i.e., negligible acetylene formation, the concentration of ethylene in the effluent is

$$[\text{C}_2\text{H}_4]_{\text{lim}} = \beta \bar{n}_e \tau [\text{CH}_4]_0 \quad (42)$$

The expressions (38) - (42) will be tested on the kinetic data of Chapters 7 and 8.

9.2 Agreement with Fundamental Work in Free Radical Chemistry

The presence of atoms and free radicals in non-equilibrium electrical discharges is well known.⁽⁵³⁾ In fact, Wood's tube⁽⁴⁸⁾ is often used as a source of atomic species such as H, O, N, and Cl. For free radicals, it is more usual to employ specific sources, e.g., photolysis and thermal decomposition. Free radical mechanisms have been invoked, for example, to explain the results of vacuum ultraviolet photolysis of methane.^(99,108) Jen et al⁽¹⁰⁹⁾ have, however, condensed out the CH₃ radical from a 8 MHz electrodeless discharge in CH₄, and used esr spectroscopy to study the trapped radical. Borisova and Eremin⁽⁶¹⁾ postulated a free radical mechanism to explain methane conversion in a d.c. glow discharge; but their mechanism could not be quantitatively tested because the reaction had not been made selective as in the present work.

In view of the fact that electrons in a non-equilibrium plasma have mean energies of the order of 1 eV (Section 5.2), the most likely mechanism for forming free radicals is by electron-impact dissociation of the parent molecule. CH₃ and CH₂ are easily produced from CH₄ by the elementary reactions (1) and (3) for electron energies exceeding $101 \frac{\text{kcal}}{\text{mole}}$ (4.40 eV/molecule) and $110 \frac{\text{kcal}}{\text{mole}}$ (4.76 eV/molecule), respectively. The formation of CH by the elementary reaction $\text{CH}_4 + e \xrightarrow{210 \text{ kcal}} \text{CH} + \text{H}_2 + \text{H} + e$ appears unlikely because there are comparatively very few electrons in the system possessing the energies of more than 9 eV that would be required. On the other hand, the secondary reactions (6) and (7) appear quite probable, considering the

low energies involved. CH_2 may be formed from CH_3 by electron impact, and CH from either CH_3 or CH_2 , but this is not supported by the present kinetic evidence (Section 9.3).

Given the fact that CH_3 , CH_2 and H are present in the system, one can examine different ways in which the stable products can be formed. At $p_1 = 1-10$ torr, homogeneous recombination of radicals seems less likely compared to that at the walls. Only homogeneous recombination of CH_3 has been extensively studied. Shepp⁽¹¹⁰⁾ measured a bimolecular rate constant of $2.2 \times 10^{13} \text{ cm}^3/(\text{mole sec})$ in the range 125°C to 175°C . Dodd and Steacie⁽¹¹¹⁾ suggest that this constant may be a decreasing function of pressure. Norrish and Porter⁽¹¹²⁾ have compared the homogeneous recombination of CH_2 with that of CH_3 . The reaction (8) has not been extensively studied but Steacie believes that it "probably has a collision efficiency not far from unity."

According to Porter,⁽¹¹³⁾ reaction (2) can be pseudo-first order with respect to gas phase concentration of CH_3 if this is high enough. By analogy, we suggest the heterogeneous recombination reaction (4) which is also postulated to be first order with respect to $[\text{CH}_2]$. Reactions such as $\text{CH}_3 + \text{CH}_4 \xrightarrow{48 \text{ kcal}} \text{C}_2\text{H}_6 + \text{H}$ and $\text{CH}_2 + \text{CH}_4 \xrightarrow{(-\Delta\text{H}) = 61.5 \text{ kcal}} \text{C}_2\text{H}_4 + \text{H}_2$ appear unlikely because the neutral species at room temperature are not energetic enough to supply the required activation energy. They would also lead to an increase of rate of reaction with increasing $[\text{CH}_4]$ to a greater extent than is supported by our kinetic data. The data can also be explained satisfactorily without considering reaction (9) which would tend to re-form CH_4 . Hence (9) was neglected, although it is theoretically as likely

as (2), (4) and (5).

9.3 Tests of the Proposed Mechanism Using the D.C. Discharge Data

The concentration of ethane in the effluent stream $[C_2H_6]$ was found in Section 7.6 (Fig. 55) to be linearly proportional to $\tau I^{0.8}$ (or $\bar{\tau n}_e$) for a given value of C_0 . From equation (39) we find that the slope

$$\frac{d}{d(\bar{\tau n}_e)} \{ [C_2H_6] / [CH_4] \}$$

is nothing but α , under conditions where $[CH_4]$ is approximately constant. α differs from the usual chemical rate constants in that it is a function of the electron energy distribution function $f_e(\epsilon)$, which can vary with C_0 and p_1 . Section 9.5 gives an interpretation of α as the integrated cross-section for the electron impact dissociation step $CH_4 + e \rightarrow CH_3 + H + e$. Although α is a decreasing function of C_0 (Fig. 79), it appears unlikely that it can decrease even more rapidly to accommodate recombination steps involving the CH_4 molecule such as $CH_3 + CH_4 \rightarrow C_2H_6 + H$. In other words, the order of dependence of $[C_2H_6]$ on $[CH_4]$ is not likely to be greater than the postulated unity.

The d.c. discharge results can be explained only by considering acetylene formation in addition to ethylene. Hence equations (40) and (41) must be used rather than the simpler equation (42). This leads to an exponential dependence of $[C_2H_4]$ on $\bar{\tau n}_e$. Since equation (40) involves the two unknown parameters β and γ , a direct plot of $[C_2H_4]$ data is inconvenient for testing the model. However, when equation (41) is divided by (40), we get

$$\frac{[C_2H_2]}{[C_2H_4]} = \bar{\gamma} n_e \tau \quad (43)$$

which is a very convenient form for evaluating γ . As seen in Fig. 56, this particular prediction of the model is borne out to a remarkable degree. Formation of C_2H_2 in any other manner than through C_2H_4 is thus precluded. In particular, the sequence $CH_3 \xrightarrow{e} CH + H_2 \longrightarrow C_2H_2$ appears ruled out. The slope $\frac{d}{d(\bar{\tau} n_e)} \left\{ \frac{[C_2H_2]}{[C_2H_4]} \right\}$ is the constant γ , which varies only with C_0 and p_1 . Knowing γ for any C_0 , the $[C_2H_4]$ data may be used to evaluate β . The results are shown in Table 44 and Fig. 79. The data strongly suggest that only one electron-impact step is involved in C_2H_4 molecule formation, ruling out the sequence $CH_3 \xrightarrow{e} CH_2 + H \longrightarrow C_2H_4$.

Although the value of $\bar{\gamma} n_e \tau$ in the d.c. discharge experiments was not low enough to permit use of equation (42), it appears that it was sufficiently small to lead to an approximate $(\bar{\tau} n_e)^2$ dependence of $[C_2H_2]$. For small $\bar{\gamma} n_e \tau$, equation (41) is approximated as

$$\begin{aligned} [C_2H_2] &= \beta \bar{n}_e \tau [CH_4]_0 \{1 - (1 - \bar{\gamma} n_e \tau + \text{higher order terms})\} \\ &\approx \beta \gamma (\bar{\tau} n_e)^2 [CH_4]_0 \end{aligned} \quad (44)$$

which fits the $[C_2H_2]$ data (Tables 21-36) within the bounds of experimental error.

As $[C_2H_2]$ is small and has a broader peak, any deviation from equation (44) could have been masked by the error. The same %

deviation from $[C_2H_4]$ predicted by equation (42) is more easily detectable as $[C_2H_4]$ is measured more precisely than $[C_2H_2]$.

As a final test of the d.c. data, the total conversion of CH_4 was tested for the first order dependence on $\bar{\tau n}_e$ predicted by equation (38). As seen for example in Fig. 57, the fit is reasonable with the slope interpretable as $(\alpha + \beta)$.

9.4 Tests of the Proposed Mechanism on the Pulsed Discharge Data

The pulsed discharge data of Chapter 8 may be explained within the framework of equations (38), (39) and (42) with

$$\xi = \frac{\tau}{\tau_I} \int_0^{\tau_x} \bar{n}_e dt$$

being substituted for $\bar{\tau n}_e$. As seen in Section 8.6, successful correlations are possible with the equivalent parameter

$$\xi^* = \frac{\tau}{\tau_I} \int_0^{\tau_w} i dt$$

where $i \propto \bar{n}_e$ and $\tau_x = \tau_w$. The predictions of the model are that for a given C_0 , $[C_2H_6] / [CH_4]_0$ and $[C_2H_4] / [CH_4]_0$ should be proportional to ξ^* , with slopes equal to $q\alpha$ and $q\beta$ respectively, q being the value of i / \bar{n}_e . The $[C_2H_6]$ data (e.g., Fig. 71) do, in fact, show linear behavior throughout the range investigated ($\xi^* = 0 - 23.5$ mA msec), whereas the $[C_2H_4]$ data (e.g., Fig. 72) are linear only for $\xi^* < 8$. The saturation of $[C_2H_4]$ for higher values of ξ^* is explained by the model as due to the conversion to C_2H_2 . Figure 76 illustrates the behavior of the slopes of the two straight lines with respect to C_0 for $p_1 = 5.0$ torr. The agreement of the

α and β values in a pulsed discharge with those in a d.c. discharge at $C_0 = 4.0 - 4.2\%$ suggests that there is no additional effect on these parameters attributable to pulsing the voltage. This conclusion may only be true for high τ_w (~ 1 msec) as T_e may be significantly higher when τ_w is in the range of $10 \mu\text{sec}$.⁽¹⁰⁰⁾

The model also permits a qualitative explanation of the behavior of $\{[C_2H_6] / [C_2H_4]\}_{\min}$ shown in Fig. 78. To explain lower total conversions of CH_4 as C_0 increases (Fig. 77), it is necessary to postulate that the mean electron energy $\bar{\epsilon}$ falls with C_0 both in CH_4 -Ar and CH_4 -He mixtures. Assuming Maxwellian $f_e(\epsilon)$, this means that T_e is a decreasing function of C_0 . It is now necessary to verify that as T_e decreases, $[C_2H_6] / [C_2H_4]$ should increase.

Although the precise form of the cross-sections for the processes 1 and 3 is not known, we can calculate the ratio of particles with energy above $101 \frac{\text{kcal}}{\text{mole}}$ to those with energy above $110 \frac{\text{kcal}}{\text{mole}}$, and check if the ratio increases as T_e decreases. $101 \frac{\text{kcal}}{\text{mole}}$ ($4.40 \frac{\text{eV}}{\text{molecule}}$) and $110 \frac{\text{kcal}}{\text{mole}}$ ($4.76 \frac{\text{eV}}{\text{molecule}}$) are, of course, the threshold energies for reactions 1 and 3 respectively.

The Maxwellian distribution of particle energies is given by⁽²⁾

$$f_e(\epsilon) = \frac{2}{\sqrt{\pi}} \left(\frac{1}{k_B T_e}\right)^{3/2} \epsilon^{1/2} \exp\left(-\frac{\epsilon}{k_B T_e}\right) d\epsilon \quad (45)$$

$$\bar{\epsilon} = \frac{3}{2} k_B T_e \quad (46)$$

The fraction of particles $(1 - \theta)$ possessing energies above ϵ_θ is therefore

$$(1 - \theta) = 1 - P\left(\frac{3}{2}, \frac{3}{2} \frac{\epsilon_\theta}{\bar{\epsilon}}\right) \quad (47)$$

where

$$P(a,x) = \frac{1}{\Gamma(a)} \int_0^x e^{-t} t^{a-1} dt \quad (48)$$

$P(a,x)$ has been tabulated in Ref. (114). The calculations are shown in Table 45 below for $\bar{\epsilon} = 1$ eV and $\bar{\epsilon} = 0.75$ eV which are typical values to be expected in d.c. glow discharges at $p_1 = 1-10$ torr. The ratio

$$\frac{(1-\theta)_{\epsilon_{\theta} = 4.40 \text{ eV}}}{(1-\theta)_{\epsilon_{\theta} = 4.76 \text{ eV}}}$$

increases from 1.66 to 2.01 as $\bar{\epsilon}$ falls from 1.0 eV to 0.75 eV, which is in qualitative accord with the observed increase of

$\left\{ \frac{[C_2H_6]}{[C_2H_4]} \right\}_{\min}$ with C_0 . With Langer et al's older value⁽¹¹⁵⁾ of 66.4

$\frac{\text{kcal}}{\text{mole}}$ for heat of formation of CH_2 (activation energy for reaction 3 84.3 $\frac{\text{kcal}}{\text{mole}}$ instead of the correct 110 $\frac{\text{kcal}}{\text{mole}}$), this would no longer be true. The pulsed data therefore provide circumstantial evidence in favor of the new value of 91.9 $\frac{\text{kcal}}{\text{mole}}$ for $(\Delta H_f)_{CH_2}$ as measured by Chupka and Lifshitz.⁽¹⁰⁷⁾

	$\bar{\epsilon} = 1.0$ eV	$\bar{\epsilon} = 0.75$ eV
$(1-\theta)_{\epsilon_{\theta} = 4.40}$	(a) 0.00428	(d) 0.000544
$(1-\theta)_{\epsilon_{\theta} = 4.76}$	(b) 0.00258	(e) 0.00027
Ratio (b)/(a)	(c) 1.66	--
Ratio (d)/(e)	--	(f) 2.01

Table 45: Values of $(1-\theta)$ in the Maxwellian Energy Distribution

9.5 Integrated Cross-Sections for Electron-Impact Reactions (1), (3) and (6)

Sample calculations are now presented to evaluate α , β and γ from the d.c. discharge data in CH_4 -Ar mixtures with $C_o = 12.6\%$ at $p_1 = 5.0$ torr. From Fig. 55, $[\text{C}_2\text{H}_6] = 8.68 \times 10^{-4} \tau I^{0.8} \%$ and from Fig. 52, $(n_e)_o = 3.5 \times 10^9 \left(\frac{I}{0.75}\right)^{0.8}$ per cm^3 . The radially averaged electron density $\bar{n}_e = 0.433 (n_e)_o$ if a Bessel function profile (equation 16) is assumed. Therefore

$$\begin{aligned} \frac{d}{d\tau} [\text{C}_2\text{H}_6] &= 8.68 \times 10^{-1} \times \frac{0.75^{0.8}}{3.5 \times 10^9} \times \frac{\bar{n}_e}{0.433} \\ &= 12.6 \bar{n}_e \alpha \end{aligned} \quad \text{(from eqn.(39))}$$

which leads to

$$\alpha = 3.55 \times 10^{-11} \text{sec}^{-1} \text{cm}^3 \quad (49)$$

The slope of the straight line in Fig. 57 is evaluated as $0.18 \text{ sec}^{-1} (\text{mA})^{-0.8}$, from which is obtained

$$\begin{aligned} (\alpha + \beta) &= 0.18 \times \frac{(0.75)^{0.8}}{0.433 \times 3.5 \times 10^9} \\ &= 9.32 \times 10^{-11} \text{sec}^{-1} \text{cm}^3 \end{aligned} \quad (50)$$

Subtracting (49) from (50) gives a β value of $5.77 \times 10^{-11} \text{sec}^{-1} \text{cm}^3$.

γ is evaluated from the slope of the straight line of Fig. 56 and equation 43. From Fig. 56

$$\frac{[C_2H_2]}{[C_2H_4]} = 3.75 \times 10^{-3} \tau_I^{0.8\%}$$

Therefore

$$\begin{aligned} \gamma &= 3.75 \times 10^{-6} \times \frac{0.75^{0.8}}{0.433 \times 3.5 \times 10^9} \\ &= 9.65 \times 10^{-10} \text{sec}^{-1} \text{cm}^3 \end{aligned} \quad (51)$$

This value of γ was used with equation (40) and the $[C_2H_4]$ data of Tables 21-36 to calculate β as $4.5 \times 10^{-11} \text{sec}^{-1} \text{cm}^3$, which checks reasonably with the independently calculated value of $5.8 \times 10^{-11} \text{sec}^{-1} \text{cm}^3$.

Similar calculations were performed for other values of C_O . The results are shown in Table 44 and Fig. 79. α and β are seen to decrease with C_O , which is consistent with the hypothesis that the mean electron energy is also falling with C_O . γ values are an order of magnitude larger than the α and β values, which explains why the side reaction (6) leading to acetylene formation is so noticeable. In terms of a radially averaged version of equation (19), α , β and γ represent the quantity

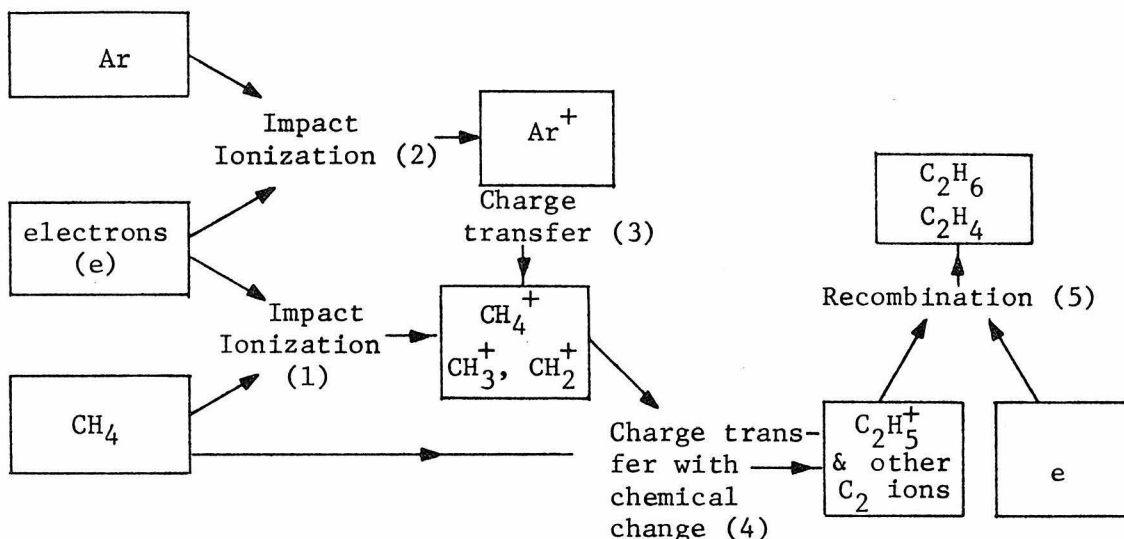
$$\int_{\epsilon=0}^{\infty} \sqrt{\frac{2\epsilon}{m_e}} \phi(\epsilon) \bar{f}_e(\epsilon) \cdot d\epsilon$$

If reliable measurement or calculation of $f_e(\epsilon)$ is possible in such systems (see Chapter 10), it may be possible to back out the cross-sections $\phi(\epsilon)$ for electron-impact dissociation steps of reactions (1), (3) and (6). This is not being proposed as a method of measuring cross-sections, which will have to come ultimately from low energy

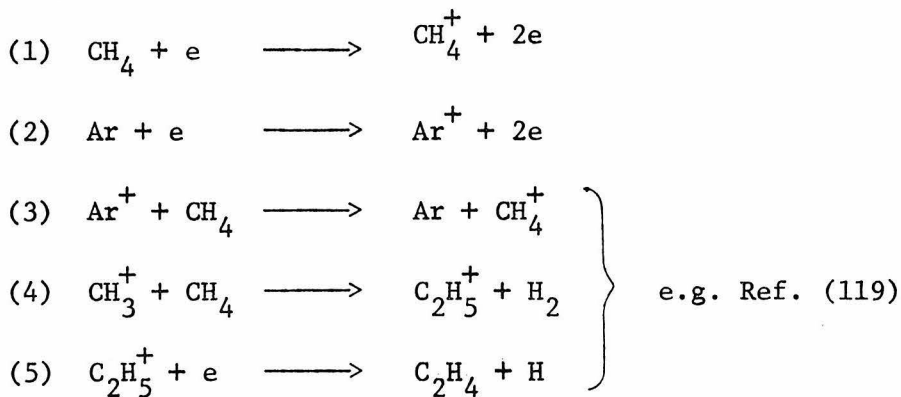
beam or from electron swarm experiments. No cross-sections for electron impact dissociation of hydrocarbons were available at the time of writing, although dissociative ionization (91,116,117) and "total" scattering cross-sections⁽¹¹⁸⁾ have been investigated for CH₄. However, when the fundamental data do become available, experiments such as the present one could act as a valuable check. In addition, reduction of the data to the form of energy dependent cross-sections will enable extrapolation of the results, with the aid of equation (19), to systems where \bar{n}_e and $f_e(\epsilon)$ are very different from the present experiments.

9.6 Order of Magnitude Calculations to Rule Out Ionic and Photo-chemical Mechanisms

It is possible to conceive of an ionic mechanism of the following type in order to account for the observed formation of C_2H_6 and C_2H_4 from CH_4 in the discharge.



One may give as examples of the reactions that may be involved:



A wide variety of reactions is possible under each of the five categories⁽¹²⁰⁾ which would make an ionic scheme possible in principle.

Only endothermic ion-molecule reactions are excluded from consideration because the ions, which have temperatures $\sim 4 \times 10^2$ °K, do not have sufficient kinetic energy to overcome the activation energy barrier that would be involved.

The rates of ion-molecule reactions have bimolecular constants $\sim 10^{-9}$ cc/(molecule \times sec)⁽¹¹⁰⁾ and are therefore comparatively high. The rate limiting step in an ionic mechanism is therefore likely to be the rate at which ions are being created. Ionization potentials for Ar⁺ and CH₄⁺ are 15.77 eV and 13.12 eV respectively⁽¹²¹⁾ and are generally > 10 eV for C₂ hydrocarbons. On the other hand, dissociation threshold energies for CH₃ and CH₂ formation from CH₄ (Section 9.1) are 4.40 and 4.76 eV respectively. A simple calculation with the Maxwellian distribution (equations 45-48) reveals

$$\frac{(1-\theta)_{\epsilon_{\theta}=10 \text{ eV}}}{(1-\theta)_{\epsilon_{\theta}=4.40 \text{ eV}}} = \frac{10^{-6}}{4.28 \times 10^{-3}} = 2.3 \times 10^{-4}$$

for $\bar{\epsilon} = 1.0$ eV. Thus the rate at which free radicals are being formed in the discharge exceeds the rate of ion formation by a factor of $\sim 10^4$. A free radical mechanism is therefore far more plausible than an ionic one in a CH₄-Ar system. Spectroscopic evidence could provide confirmation that the mechanism does indeed proceed through radicals.

Another possibility that may be suggested is that the CH₃ and CH₂ radicals are formed by a photochemical mechanism^(99,108). The existence of argon resonance lines in the vacuum ultraviolet (1048Å and 1067Å) would make such a scheme theoretically possible. Apart from

the improbability of being able to explain the observed dependencies on $\tau \bar{n}_e$ (Sections 9.3-9.5) with such a mechanism, the following upper bound calculation would appear to rule it out in our system.

Lane and Kupperman⁽¹²²⁾ constructed an Ar resonance lamp which took 85 W of microwave power to produce a vacuum uv. photon flux of 10^{14} per sec through a 4.9 cm^2 window. Assuming the same flux per unit area for the whole lamp, this corresponds to a rate of production of 3.4×10^{13} photons/sec in each cm^3 of the 147 cm^3 tube. If the discharge tube in our experiments had the same rate for a corresponding power density, it would be producing 1.2×10^{14} photons/sec in the vacuum uv. for a typical input of 2W. Since 1 quantum at 1048\AA has 1.9×10^{-18} joules, the power going into vacuum uv. in our discharge is $1.9 \times 10^{-18} \times 1.2 \times 10^{14} = 2.2 \times 10^{-4}$ watts. For a typical residence time of 60 msec, the maximum available photon energy is therefore $0.06 \times 2.2 \times 10^{-4} = 1.3 \times 10^{-5}$ joule. Since 1048\AA photons have an energy corresponding to $270 \frac{\text{kcal}}{\text{mole}}$, the maximum utilizable energy for CH_3 production is approximately $\frac{101}{270} \times 1.3 \times 10^{-5} = 4.9 \times 10^{-6}$ joule. Since photochemical free radical production in such systems has a quantum yield near unity, this corresponds to 1.2×10^{-5} μmoles . The observed rate of CH_4 decomposition in our discharge is $\sim 3\%$ for $\tau = 60 \text{ msec}$, $p_1 = 5 \text{ torr}$, $C_0 = 10\%$, for a power input of $\sim 2\text{W}$ into the positive column, which is equivalent to 2.4×10^{-2} μmoles . Hence the observed rate exceeds the maximum allowed photochemical rate of reaction by a factor of $\frac{2.4 \times 10^{-2}}{1.2 \times 10^{-5}} = 2000$.

The above calculation assumes that all the Ar resonance radiation is utilized for the chemical reaction. Since CH_4 has a decadic

absorption coefficient of $20.4 \text{ cm}^{-1} \text{ atm}^{-1}$ in the range being considered, (108) it can be shown that for a path length of 0.5 cm and a CH_4 partial pressure of 0.5 torr, less than 3% of the radiation is absorbed, with the remainder getting through to the walls of the discharge tube. This would make the available photon energy too low by an extra factor of 33 over the 2×10^3 factor calculated before.

10. THE ROLE OF THE ELECTRON ENERGY DISTRIBUTION

FUNCTION $f_e(\epsilon)$

10.1 Calculations on H_2 Dissociation with Maxwellian and Druyvesteyn Distributions

In order to evaluate the sensitivity of the expression of equation (19) to the exact form of the electron energy distribution function $f_e(\epsilon)$, calculations have been made for the reaction $H_2 + e \rightarrow H + H + e$. This is a chemical reaction for which cross-section data are available. The data of Engelhardt and Phelps⁽⁹⁰⁾ show that $\phi(\epsilon)$ rises steeply from a threshold value of about 9 eV and then falls in an approximately exponential manner from a peak of $4 \times 10^{-17} \text{ cm}^2$. The two distribution functions evaluated are the Maxwellian and the Druyvesteyn, the latter corresponding to a case in which E is high and elastic collisions predominate. Equations (52) and (53) are the expressions for the two functions.⁽²⁾

Maxwellian:

$$f_e(\epsilon) d\epsilon = \frac{2}{\sqrt{\pi}} \left(\frac{1}{k_B T_e} \right)^{3/2} \epsilon^{1/2} \exp\left[-\frac{\bar{\epsilon}}{k_B T_e}\right] d\epsilon$$

with $\bar{\epsilon} = \frac{3}{2} kT_e$ (52)

Druyvesteyn:

$$f_e(\epsilon) d\epsilon = 1.04 \left(\frac{\epsilon}{\bar{\epsilon}} \right)^{1/2} \exp\left(-0.55 \frac{\epsilon^2}{\bar{\epsilon}^2}\right) \frac{d\epsilon}{\bar{\epsilon}} \quad (53)$$

10.1a) Frequency of inelastic collision processes involving electrons with a Maxwellian distribution of energy. As a first approximation, let us consider the inelastic collision cross-section

to be given by

$$\begin{aligned} \phi(\epsilon) &= 0, & \epsilon < \epsilon_{\theta} \\ \phi(\epsilon) &= C' \exp[-B(\epsilon - \epsilon_{\theta})], & \epsilon \geq \epsilon_{\theta} \end{aligned} \quad (54)$$

Considering electron impact dissociation as an inelastic collision process, the rate per electron is

$$v = \int_{\epsilon=0}^{\infty} g \phi(\epsilon) N f_e(\epsilon) d\epsilon \quad (55)$$

where g is the relative velocity of the electrons with respect to the other body taking part in the collision. If the other body is considered to be at rest, g is the electron velocity $\sqrt{2\epsilon/m_e}$. Hence,

$$v = \int_{\epsilon_i}^{\infty} \sqrt{\frac{2}{m_e}} \epsilon^{1/2} C' \exp[-B(\epsilon - \epsilon_{\theta})] N A \epsilon^{1/2} \exp[-\frac{3}{2} \frac{\epsilon}{\epsilon}] d\epsilon \quad (56)$$

where $A = \frac{2}{\sqrt{\pi}} \left(\frac{1}{kT_e}\right)^{3/2}$

or

$$v = N C' A \sqrt{\frac{2}{m_e}} \exp(B\epsilon_{\theta}) \int_{\epsilon_i}^{\infty} \epsilon \exp[-(B + \frac{3}{2\epsilon})\epsilon] d\epsilon \quad (57)$$

Let

$$(B + \frac{3}{2\epsilon}) = D' \quad (\text{Units of reciprocal energy}) \quad (58)$$

Then, integrating by parts,

$$v = N C' A \sqrt{\frac{2}{m_e}} \frac{1}{D'} (\epsilon_{\theta} + \frac{1}{D'}) \exp(-\frac{3}{2} \frac{\epsilon_{\theta}}{\epsilon}) \quad (59)$$

Substituting for A and simplifying,

$$\begin{aligned} \nu &= \frac{3^{1.5}}{\sqrt{\pi}} \frac{NC'}{\sqrt{m_e}} \frac{(\bar{\epsilon})^{-3/2}}{D'} \left(\epsilon_\theta + \frac{1}{D'}\right) \exp\left(-\frac{3}{2} \frac{\epsilon_\theta}{\bar{\epsilon}}\right) \\ &= 2.94 \frac{NC'}{\sqrt{m_e}} \frac{(\bar{\epsilon})^{-1.5}}{D'} \left(\epsilon_\theta + \frac{1}{D'}\right) \exp\left(-1.5 \frac{\epsilon_\theta}{\bar{\epsilon}}\right) \end{aligned} \quad (60)$$

10.1b) Frequency of inelastic collision processes involving electrons with a Druyvesteyn distribution of electron energy. With the Druyvesteyn distribution of equation (53), the rate of dissociation per electron (equation (55)) is given by

$$\nu = \int_{\epsilon_i}^{\infty} \sqrt{\frac{2\epsilon}{m_e}} C' \exp[-B(\epsilon - \epsilon_\theta)] 1.04N \left(\frac{\epsilon}{\bar{\epsilon}}\right)^{1/2} \exp\left(-0.55 \frac{\epsilon^2}{\bar{\epsilon}^2}\right) \frac{d\epsilon}{\bar{\epsilon}} \quad (61)$$

or

$$\nu = \frac{1.04}{\sqrt{m_e}} \sqrt{2} \frac{C'N}{\bar{\epsilon}^{3/2}} \int_{\epsilon_i}^{\infty} \epsilon \exp\left[B\epsilon_\theta - B\epsilon - \frac{0.55\epsilon^2}{\bar{\epsilon}^2}\right] d\epsilon \quad (62)$$

Putting $B\epsilon_\theta - B\epsilon - \frac{0.55\epsilon^2}{\bar{\epsilon}^2} = -t$,

$$\nu = \sqrt{\frac{2}{m_e}} \frac{1.04 C'N}{\bar{\epsilon}^{3/2}} \int_{\frac{0.55\epsilon_\theta^2}{\bar{\epsilon}^2}}^{\infty} \frac{-\epsilon \exp(-t) \bar{\epsilon} dt}{\pm(\bar{\epsilon}^{-2} B^2 + 2.2B\epsilon_\theta + 2.2t)^{1/2}} \quad (63)$$

which on simplification yields

$$\begin{aligned} \nu &= \frac{1.04\sqrt{2}}{\sqrt{m_e}} \frac{C'N\bar{\epsilon}^{-1/2}}{1.10} \exp\left(-0.55 \frac{\epsilon_\theta^2}{\bar{\epsilon}^2}\right) \\ &\pm \sqrt{\frac{2}{m_e}} \frac{1.04C'BN\bar{\epsilon}^{-3/2}}{1.10 \sqrt{2.2}} \int_x^{\infty} e^{-\zeta} \zeta^{-1/2} d\zeta \exp\left(B\epsilon_\theta + \frac{\bar{\epsilon}^{-2} B^2}{2.2}\right) \end{aligned}$$

where

$$\zeta = \frac{\bar{\epsilon}^{-2} B^2}{2.2} + B\epsilon_{\theta} + t \quad x = \frac{\bar{\epsilon}^{-2} B^2}{2.2} + B\epsilon_{\theta} + \frac{0.55\epsilon_{\theta}^2}{\bar{\epsilon}^{-2}} \quad (64)$$

Taking only the + sign as physically meaningful,

$$v = \frac{NC'}{\sqrt{m_e}} [1.34\bar{\epsilon}^{-1/2} \exp(-\frac{0.55\epsilon_{\theta}^2}{\bar{\epsilon}^{-2}}) + 0.905 B\bar{\epsilon}^{-3/2} \exp(B\epsilon_{\theta} + \frac{\bar{\epsilon}^{-2} B^2}{2.2}) \bar{I}] \quad (65)$$

The evaluation of the integral \bar{I} is discussed in Appendix A-6.

$$\bar{I} = \int_x^{\infty} e^{-\zeta} \zeta^{-1/2} d\zeta \quad (66)$$

10.1c) A comparison of the rate of dissociation of H₂ using i) Maxwellian and ii) Druyvesteyn Distributions. Consider a typical inelastic collision cross-section, i.e., the dissociation of hydrogen as reported by Engelhardt and Phelps.⁽⁹⁰⁾ As shown in Fig. 80, the choice of the constants $B = 0.23(\text{eV})^{-1}$, $\epsilon_{\theta} = 10 \text{ eV}$ and $C' = 4 \times 10^{-17} \text{ cm}^2$, gives an approximate fit to the data. The rates of dissociation of H₂ can now be calculated for various values of the mean electron energy, assuming in turn the two types of distributions for the electron energy.

For example, when $\bar{\epsilon} = 1 \text{ eV}$, with the Maxwellian distribution we have from equation (60)

$$D' = B + \frac{1.5}{\bar{\epsilon}} = 1.73$$

$$\epsilon_{\theta} + \frac{1}{D'} = 10.6$$

$$\frac{v\sqrt{m}}{NC^1} e^{-x} = 5.7 \times 10^{-7} \quad \text{Dimensionless} \quad (67)$$

For the Druyvesteyn distribution equation (65) yields

$$\bar{I} \approx \frac{e^{-x}}{\sqrt{x}} = \frac{e^{-57.3}}{7.57}, \quad \text{as } x = 57.3$$

Hence,

$$\frac{v\sqrt{m}}{NC^1} e^{-x} = 1.37 \times 10^{-24} \quad \text{Dimensionless} \quad (68)$$

Therefore, from (67) and (68), $v_{\text{Max}} / v_{\text{Dru}} = 4 \times 10^{17}$

Table 46 presents the results of these calculations.

It is seen that for low values of $\bar{\epsilon}$ e.g., 1 eV, there is a large difference in the rates (a ratio of 10^{17} !). As $\bar{\epsilon}$ rises to about 5 eV, the rates become nearly equal for the two distributions. From Figs. 81 and 82, it is difficult to see why there should be such a great difference. However, Fig. 83 shows the behavior of these distributions for high values of energy (the "tails"). It is seen that in the high energy range, the behavior of the Maxwellian and the Druyvesteyn distributions is completely different. This explains the widely different reaction rates that were obtained.

In contrast to chemical reaction rates, transport properties such as conductivity are less dependent on the precise form of $f_e(\epsilon)$. Cross-sections for elastic scattering⁽³⁾ generally peak at low ϵ 's e.g., 2-3 eV, so that elastic collision frequency is negligibly affected by the behavior of the tail end of the energy distribution.

Taking the particular case of H_2 , where the scattering occurs as a result of ρ^{-4} polarization forces, the electron-neutral collision frequency is given by $\nu_{en}(\epsilon) = 5.93 \times 10^9 p_0$, where p_0 is the pressure in torr reduced to 273°K. Since the collision frequency is independent of ϵ , its average value is easily found to be $\nu_{en} = 5.93 \times 10^9 p_0 \int_0 f_e(\epsilon) d\epsilon = 5.93 \times 10^9 p_0$ independent of the form of $f_e(\epsilon)$, and certainly independent of the tail end of $f_e(\epsilon)$. This particularly simple result is also valid for He, where $\nu_{en}(\epsilon) = 2.37 \times 10^9 p_0$, which agrees with the measured values of Fig. 16 to within 50%. Ar and CH_4 elastic scattering cross-sections are not amenable to the simple ρ^{-4} modeling approach. However, numerical integration of these cross-sections with respect to $f_e(\epsilon)$ is expected to reveal only a weak dependence on the tail end of $f_e(\epsilon)$.

10.2) Difficulties in experimentally measuring $f_e(\epsilon)$. A

well-explored experimental technique for obtaining information on $f_e(\epsilon)$ is the use of conducting probes in contact with the plasma. Langmuir⁽¹²³⁾ first used such probes to measure T_e in mercury discharges, assuming a Maxwellian energy distribution. Druyvesteyn⁽¹²⁴⁾ pointed out that double differentiation of accurate probe data can be used, in principle, to calculate $f_e(\epsilon)$ from the expression

$$f\left(\frac{2eV_p}{m_e}\right)^{1/2} = \frac{4m_e V_p}{e^2 A} \frac{\partial^2 I_-}{\partial V^2} \quad (69)$$

Electronic circuits to perform the differentiation have been used, for example, by Garscadden.⁽¹²⁵⁾ A literature review of probe techniques may be found in Bond.⁽¹²⁶⁾

Double (floating) probes were first employed in outer space applications to get around the necessity of having a grounded electrode. They are also useful in reducing the bias voltage required when the space potential is too high above ground. Boyd and Twiddy⁽¹²⁷⁾ used the technique in H_2 and Ar plasmas at $p = 0.04$ torr to obtain decidedly non-Maxwellian energy distributions. Analysis of double probe data has been discussed at length by Chen in Ref. (17).

The simple circuit of Fig. 84 was used along with the tungsten probes previously used to measure E (Sec. 2.2), to explore the feasibility of the double probe method in the present d.c. discharges.

Figure 85 shows a typical characteristic in Ar at 1.5 torr. i_{1+} and i_{2+} were calculated graphically by extrapolation of the tangents to the saturation currents.⁽¹⁷⁾ As shown in Fig. 85, a linear plot of $\log\left(\frac{I + i_{1+}}{i_{2+} - I}\right)$ vs. bias voltage V_p was obtained, indicating a Maxwellian distribution. However, T_e calculated from equation (70) below had the unreasonably high value of 1.4×10^5 °K.

$$T_e = \frac{e}{k_B} \frac{dV_p}{d\left[\log \frac{I + i_{1+}}{i_{2+} - I}\right]} \quad (70)$$

It is believed that the probes were not in full contact with the plasma. Sheaths of un-ionized gas around the probes could have introduced additional resistance into the circuit, leading to abnormally high values of T_e .

Although the floating double probe seems to be a feasible technique in our system, several improvements over the basic circuit of Fig. 64 will have to be made before $f_e(\epsilon)$ can be reliably measured.

Noise suppressing circuits⁽⁸⁸⁾ are certainly necessary, especially in hydrocarbon systems where point by point measurements proved to be impossible. Electronic circuits will have to be developed to display $\frac{\partial^2 I}{\partial V^2}$ directly, and to adapt the system to a pulsed d.c. discharge. These sophisticated approaches were beyond the scope of the present work, but are capable of being used to measure $f_e(\epsilon)$. Brockmeier⁽¹²⁸⁾ has been working on probe techniques in reacting microwave discharges.

Measurements of microwave noise from a discharge have been used to calculate T_e .⁽¹²⁹⁾ The advantage of this technique is that there are no errors due to disturbance of the plasma, as in probe methods.

10.3 Difficulties in Solving Boltzmann's Equation for $f_e(\epsilon)$

Boltzmann's equation (17) for the electrons has been successfully solved in situations where only elastic collisions need be considered. The form of the solution is a series expansion of f_e in terms of spherical functions^(85,130)

$$f_e = \alpha_{00}(w,t) + \sum [\alpha_{\ell m}(w,t) C_{\ell m} + \beta_{\ell m}(w,t) S_{\ell m}] \quad (71)$$

where $w = |v_i|$ and the gas is homogeneous and infinite. α_{00} is the isotropic part of the distribution function, which may or may not be Maxwellian. Each order of anisotropy is characterized by a relaxation frequency ν_ℓ , with ν_1 corresponding to the electron-neutral collision frequency for momentum transfer. Solutions of (71) are obtained for the so-called modified Lorentzian model of the plasma, in which collisions between charged particles are neglected, and a central force is assumed for the binary e-n collisions. m_e/m_0 is permitted to be

finite to allow for an electron cooling mechanism. The Druyvesteyn distribution function (equation (53)) is a particular case of this type of solution of the Boltzmann equation, and is valid for strong electric field E .

In order to get an accurate picture of the tail end of the distribution, it is necessary to consider the effect of inelastic collisions. Apart from making analytical solutions impossible, the biggest difficulty in doing this is the fact that cross-sections for the various possible inelastic processes are often not known. In the simplest molecules, e.g., H_2 , D_2 , N_2 , O_2 and the rare gases, the iterative approach of Engelhardt and Phelps⁽⁹⁰⁾ may be used. Cross-sections are determined concurrently with $f_e(\epsilon)$, and successive adjustments to the initial estimates are made until theoretical and experimental values of the transport coefficients D and μ , and Townsend's primary ionization coefficient α_1 are brought into good agreement. The approach is capable of being extended to reacting systems, with the rate constant k joining the list of experimental parameters that must be successfully predicted. However, CH_4 -Ar and CH_4 -He mixtures appear too complex to be analyzed in any great detail by the Engelhardt and Phelps method.⁽⁹⁰⁾

It is also important in theoretical studies to consider the effect of recombination processes on $f_e(\epsilon)$. Lindgren and Gavalas⁽¹³¹⁾ have recently published a theory of the positive column including electron-ion recombination.

At the present state of understanding of reacting nonequilibrium plasmas, e.g., those in CH_4 -Ar or CH_4 -He mixtures, it is our judgment

that experimental measurement of $f_e(\epsilon)$ (Sec. 10.2) is likely to be more reliable than theoretical solution of Boltzmann's equation. The practical problems involved, although formidable, are capable of being overcome by proper design of the electronic circuitry for a floating double probe measurement of $f_e(\epsilon)$.

11. SUGGESTIONS FOR FUTURE WORK IN REACTING

NON-EQUILIBRIUM PLASMAS

- 1) The electron energy distribution function $f_e(\epsilon)$ must be measured accurately, especially in the energy range $\epsilon > 4$ eV where chemical reactions in the plasma start becoming important. Double Langmuir probe techniques with electronic differentiation and noise suppressing circuitry may be used.
- 2) Spectral studies of the discharge could provide direct evidence of the existence of free radical intermediates postulated in Chapter 9.
- 3) Mass spectroscopic analysis of the products would be more sensitive than the gas chromatography used in the present work. Also, some of the ionic intermediates, e.g., CH_4^+ , can be identified by this means.
- 4) The kinetic data, if reduced to the form of energy dependent cross-sections for electron-impact dissociation, can be extended to discharge systems where n_e and $f_e(\epsilon)$ are different from present values. Low-energy beam measurements of cross-sections for processes like $\text{CH}_4^+ + e \xrightarrow{\alpha} \text{CH}_3 + \text{H} + e$ and $\text{CH}_4^+ + e \xrightarrow{\beta} \text{CH}_2 + \text{H}_2 + e$ would be very valuable as a check.
- 5) Commercial development of a non-equilibrium plasma reactor could proceed as outlined in Appendix A-8. The main requirements are a well-designed flow system to get low residence time τ , use of a pulsed discharge to effectively reduce τ even further, and

extension to pressures of the order of 1 atm. An important parameter for optimization would be the energy efficiency of the process.

12. SUMMARIZED CONCLUSIONS OF PARTS I AND II

Part I:

- 1) The complex microwave conductivity of d.c. glow discharges in pure He, Ne and Ar at $p = 1-10$ torr is even more sensitive to small amounts of impurities than the electric field E .
- 2) Electronic drift velocities v_d calculated from the average electron density \bar{n}_e measured by microwave techniques in He and Ne fall well below the drift tube values of Bradbury and Nielsen.⁽³⁴⁾ In He, for example, the discrepancy is a factor of 4 at $E/p = 4.0$ volts/(cm × torr), and in Ne at $E/p = 2.5$ volts/(cm × torr) the discrepancy is a factor of 2. In Ar, v_d values generally agree with the drift tube values. The cause of the discrepancy in He and Ne could be metastable ionization of the type $\text{He}^* + \text{He} \rightarrow \text{He}_2^+ + e$ and $\text{Ne}^* + \text{Ne} \rightarrow \text{Ne}_2^+ + e$.
- 3) Electric field values measured in pure rare gas d.c. discharges without oscillations agreed with measurements of previous workers if the similarity rule $E = f(pR)$ was used. However, n_e , v_{en} and v_d at $p = 1-10$ torr violate the similarity rule based on pR only.
- 4) $\langle n_e \rangle$ and v_{en} in He-Ar and He-Ne mixtures at $p = 2-5$ torr and $I = 15$ mA exhibit time and space dependent values due to the effect of cataphoresis. The steady state results can be used to back calculate impurity (Ar or Ne) concentrations as a function of z .

- 5) The model of Shair and Remer⁽⁸⁾ which assumes constant α is a reasonable description of the phenomenon of cataphoresis in the two end bulb discharge tube when impurity (Ar or Ne) concentrations are in the range 2-20%.

Part II:

- 1) CH_4 can be converted selectively to C_2H_6 , C_2H_4 , C_2H_2 and H_2 in a d.c. discharge flow system at $p_1 = 5$ torr with low residence times (~ 50 - 100 msec), low currents (~ 0.5 - 2.0 mA) and high concentration of methane C_0 ($> 4\%$) in the feed, of which the other component is a rare gas such as Ar.
- 2) Simultaneous measurements of the electron density $(n_e)_0$ shows that it is a function of I with an approximate $I^{0.8}$ dependence in the range 0.5 - 2.0 mA.
- 3) Kinetic measurements show that $[\text{C}_2\text{H}_6]$ is proportional to $\bar{\tau} n_e$, as is $\frac{[\text{C}_2\text{H}_2]}{[\text{C}_2\text{H}_4]}$. $[\text{CH}_4]$ exhibits a first order decay with respect to $\bar{\tau} n_e$. The results can be explained in terms of a free radical mechanism involving CH_3 and CH_2 . Derived values of the integrated cross-section for $\text{CH}_4 + e \xrightarrow{\alpha} \text{CH}_3 + \text{H} + e$ and $\text{CH}_4 + e \xrightarrow{\beta} \text{CH}_2 + \text{H}_2 + e$ are in the range $3.6 - 15.5 \times 10^{-11} \text{ cm}^3 \text{ sec}^{-1}$ and that for $\text{C}_2\text{H}_4 + e \xrightarrow{\gamma} \text{C}_2\text{H}_2 + \text{H}_2 + e$ is $\sim 9 \times 10^{-10} \text{ cm}^3 \text{ sec}^{-1}$. α and β fall with C_0 in the range 4.0 - 12.6% .
- 4) With pulsed discharges in which pulse interval τ_I is of the same order as τ , the selectivity is improved even further, with C_2H_6 , C_2H_4 and H_2 as the only significant products.

- 5) Pulsed discharge kinetic data can be correlated by means of the similarity parameter $\xi^* = \frac{\tau}{\tau_I} \int_0^{\tau} w \, dt$ which corresponds to $\tau \bar{n}_e$ of the d.c. case for equal values of C_0 .
- 6) Transient values of \bar{n}_e measured with the microwave cavity fall with time in the afterglow. In the case of Ar, the results were interpreted in terms of the recombination $\text{Ar}_2^+ + e \rightarrow 2\text{Ar} + e$ with a recombination coefficient of $3.4 \pm 0.6 \times 10^{-7} \text{ cm}^3/\text{sec}$ independent of pressure.
- 7) Calculations for H_2 dissociation show that the form of the tail end of $f_e(\epsilon)$ has a large influence on the reaction rate. A feasible measurement of $f_e(\epsilon)$ is with double Langmuir probes.

TABLES 1 - 46
(except 5, 6, 8, 45 in text)

Table 1

Calibration of the TM₀₁₁ Mode

Helium 2.7 mm Hg

1.05 mA

$$n_e = (n_e)_o J_o \left(\frac{2.4r}{R} \right)$$

<u>Mode</u>	<u>f_o MHz</u>	<u>Δf_o MHz</u>	<u>(f₂ - f₁)_{empty} MHz</u>	<u>(f₂ - f₁)_{with plasma} MHz</u>	<u>v_{en} = $\frac{\Delta f_o / f_o}{\Delta f_c / f_c} \frac{\omega^2}{2}$</u>
TM ₀₁₀	2360	3.18	1.43	8.15	8.2 × 10 ⁹
TM ₀₁₁	3043	6.1	6.70	9.1	7.2 × 10 ⁹

$$\eta_{011} = \frac{(\Delta f_o)_{011} / (f_o)_{011}}{(\Delta f_o)_{010} / (f_o)_{010}} \frac{[2\pi(f_o)_{011}]^2 + v_{en}^2}{[2\pi(f_o)_{010}]^2 + v_{en}^2} \eta_{010}$$

$$= 0.59 \eta_{010}$$

Table 2

Dielectric Constants of Organic Liquids Determined with TM_{010} Mode

$$f_o = 2360 \text{ MHz}$$

$$(f_2 - f_1)_{\text{empty}} = 1.40 \text{ MHz}$$

<u>Liquid</u>	<u>Δf_o MHz</u>	<u>$(f_2 - f_1)_{\text{with liquid}}$ MHz</u>	<u>η from (23)</u>	<u>$K_R = 1 + \frac{2\Delta f_o}{f_o \eta}$</u>
Benzene	61.0	1.40	0.04	2.292
m-Xylene	64.6	1.40	0.04	2.370
Ethyl Ether	159.5	12.05	0.04	4.38

Literature values of K_R at 24°C (27)

Benzene $K_R = 2.275$

m-Xylene $K_R = 2.366$

Ethyl Ether $K_R = 4.26$

Table 3

Measurements in Helium-Argon Mixtures

Initial Composition % Ar	Total Pressure Torr	Position of Cavity $\eta \pm 0.06$	$(n_e)_o$ per $\text{cm}^3 \times 10^{-11}$	v_{en} per $\text{sec} \times 10^{-9}$	E volts/cm	$i = \frac{\langle n_e \rangle}{\langle n_o \rangle} \times 10^5$	$J = \frac{\langle n_+ \rangle}{\langle n_e \rangle}$	$\frac{\frac{\mu EL}{D} \langle n_+ \rangle}{\langle n_o \rangle}$	$\theta(\eta, \infty)$
2.4	2.0	0.30	3.28	7.8	14.1	12.21	0.85	3.08	0.63
		0.49	3.20	10.5	-	8.52	0.55	1.98	0.57
		0.72	1.82	7.6	11.5	6.32	0.68	1.33	0.54
	2.45	0.30	4.49	8.6	16.2	10.11	0.66	2.91	0.66
		0.49	4.89	11.0	-	7.46	0.40	1.89	0.59
		0.72	3.23	14.5	11.9	5.84	0.45	1.27	0.56
	3.0	0.30	3.84	10.1	16.9	10.36	0.91	3.14	0.62
		0.49	3.25	13.2	-	7.24	0.69	1.98	0.57
		0.72	2.94	11.0	13.2	5.50	0.55	1.33	0.54
3.5	0.30	4.34	11.7	18.2	9.30	0.87	3.02	0.64	
	0.49	4.05	15.4	-	6.60	0.61	1.90	0.59	
	0.72	3.39	13.2	13.6	3.65	0.41	0.89	0.60	
4.6	2.0	0.30	4.03	7.4	12.5	5.99	1.00	1.03	0.97
		0.49	4.21	7.3	-	6.18	1.00	0.94	0.98
		0.72	4.67	9.1	9.65	8.47	0.68	1.33	0.54

Table 3 (continued)

Initial Composition % Ar	Total Pressure Torr	Position of Cavity $\eta \pm 0.06$	$(n_e)_0$ per $\text{cm}^3 \times 10^{-11}$	v_{en} per $\text{sec} \times 10^{-9}$	E volts/cm	$i = \frac{\langle n_e \rangle}{\langle n_o \rangle} \times 10^5$	$J = \frac{\langle n_+ \rangle}{\langle n_e \rangle}$	$\frac{\frac{\mu EL}{D}}{\frac{\langle n_+ \rangle}{\langle n_o \rangle + \langle n_+ \rangle}}$	$\theta(\eta, \infty)$	
4.6	2.5	0.30	4.89	8.2	13.25	5.80	1.00	1.06	0.97	
		0.49	5.51	9.5	-	9.36	0.90	1.81	0.61	
		0.72	5.09	13.2	11.25	7.26	0.67	1.33	0.54	
	3.0	0.30	5.31	9.5	17.0	3.86	1.00	0.90	0.99	
		0.49	5.03	17.25	-	7.46	0.96	1.77	0.62	
		0.72	4.45	16.3	13.25	6.16	0.78	1.33	0.54	
	9.4	1.95	0.30	4.30	7.4	12.25	3.08	1.00	0.37	1.01
			0.49	4.17	10.4	-	3.20	1.00	0.37	0.96
			0.72	3.06	11.6	10.3	2.42	1.00	0.26	0.91
2.5		0.30	3.98	10.85	15.9	2.21	1.00	0.35	1.01	
		0.49	3.10	13.1	-	1.82	1.00	0.26	0.96	
		0.72	3.19	11.3	11.9	1.97	1.00	0.24	0.91	
3.0		0.30	2.90	10.8	18.2	1.35	1.00	0.24	1.01	
		0.49	3.22	11.45	-	1.57	1.00	0.26	0.96	
		0.72	2.82	10.1	13.9	1.42	1.00	0.20	0.93	

Table 3 (continued)

Initial Composition % Ar	Total Pressure Torr	Position of Cavity $\eta \pm 0.06$	$(n_e)_0$ per $\text{cm}^3 \times 10^{-11}$	v_{en} per $\text{sec} \times 10^{-9}$	E volts/cm	$i = \frac{\langle n_e \rangle}{\langle n_o \rangle} \times 10^5$	$J = \frac{\langle n_+ \rangle}{\langle n_e \rangle}$	$\alpha = \frac{\langle n_+ \rangle \mu EL}{\langle n_o \rangle + \langle n_+ \rangle D}$	$\theta(\eta, \infty)$
9.4	3.4	0.30	3.30	12.9	18.9	1.35	1.00	0.25	1.01
		0.49	3.28	13.4	-	1.40	1.00	0.23	0.97
		0.72	3.18	12.4	13.9	1.41	1.00	0.20	0.93

Table 4

Measurements in Helium-Neon Mixtures

Initial Composition % Ne	Total Pressure Torr	Position of Cavity $\eta \pm 0.06$	I = 15 mA Steady State		$\delta = 30.7$	$\epsilon = 19.2$	$L = 66.3$	$\alpha = \frac{\langle n_+ \rangle}{\langle n_0 \rangle + \langle n_+ \rangle} \frac{\mu EL}{D}$	$\theta(\eta, \infty)$
			$(n_e)_0$ per cm $\times 10^{-11}$	v_{en} per sec $\times 10^{-9}$	E volts/cm	$i = \frac{\langle n_e \rangle}{\langle n_0 \rangle} \times 10^5$	$J = \frac{\langle n_+ \rangle}{\langle n_e \rangle}$		
2.65	2.5	0.30	4.37	13.0	14.0	11.51	0.83	3.08	0.63
		0.49	3.56	12.0	-	7.73	0.63	1.93	0.58
		0.72	3.64	12.6	12.0	5.45	0.42	1.26	0.56
	3.4	0.30	4.88	15.0	14.65	10.62	0.96	2.96	0.65
		0.49	4.20	14.2	-	8.76	0.78	2.07	0.55
		0.72	4.44	13.9	10.0	7.00	0.57	1.36	0.53
	4.6	0.30	4.29	15.6	18.65	5.54	1.00	1.91	0.84
		0.49	3.24	16.2	-	5.97	1.00	1.86	0.59
		0.72	3.91	15.7	14.35	4.88	0.61	1.36	0.53
4.7	2.45	0.30	4.17	12.7	13.1	4.94	1.00	1.06	0.97
		0.49	3.15	11.1	-	4.36	1.00	0.90	0.83
		0.72	3.26	10.9	12.25	5.96	0.86	1.33	0.54
	2.95	0.30	4.34	12.6	13.9	4.23	1.00	0.96	0.98
		0.49	3.43	11.5	-	3.89	1.00	0.86	0.84
		0.72	3.60	11.2	12.2	5.98	0.94	1.33	0.54

Table 4 (continued)

Initial Composition % Ne	Total Pressure Torr	Position of Cavity $\eta \pm 0.06$	$(n_e)_0$ per $\text{cm}^3 \times 10^{-11}$	v_{en} per $\text{sec} \times 10^{-9}$	E volts/cm	$i = \frac{\langle n_e \rangle}{\langle n_o \rangle} \times 10^5$	$J = \frac{\langle n_+ \rangle}{\langle n_e \rangle}$	$\alpha = \frac{\langle n_+ \rangle \frac{\mu EL}{D}}{\langle n_o \rangle + \langle n_+ \rangle}$	$\theta(\eta, \infty)$	
4.7	3.5	0.30	2.11	9.0	18.5	1.68	1.00	0.50	1.01	
		0.49	2.07	9.9	-	1.81	1.00	0.50	0.92	
		0.72	1.86	9.7	15.2	1.78	1.00	0.46	0.84	
	4.45	0.30	4.25	14.4	18.2	2.71	1.00	0.80	0.99	
		0.49	3.11	14.8	-	2.18	1.00	0.59	0.90	
		0.72	3.62	15.1	14.5	3.22	1.00	0.81	0.71	
	19.65	2.5	0.30	3.34	9.4	16.3	0.90	1.00	0.136	1.00
			0.49	2.09	10.9	-	0.57	1.00	0.077	0.99
			0.72	2.14	9.4	12.7	0.59	1.00	0.071	0.97
3.3		0.30	3.02	10.1	18.0	0.62	1.00	0.103	1.00	
		0.49	2.28	9.5	-	0.47	1.00	0.070	0.99	
		0.72	2.20	11.3	14.0	0.46	1.00	0.061	0.97	
4.55		0.30	2.40	12.4	23.3	0.36	1.00	0.044	1.00	
		0.49	2.44	12.3	-	0.36	1.00	0.064	0.99	
		0.72	2.39	11.8	20.7	0.36	1.00	0.071	0.97	

Table 7

Reynolds Number for Flow in the Reactor

$T_g = 300^\circ\text{K}$ $C_o = 12\% \text{ in Ar}$ $\mu' = 0.0216 \text{ cp}$ $p_1 = 5.0 \text{ torr}$
 $\rho_m = 1.0 \times 10^{-5} \text{ gm/cm}^3$

τ msec	\bar{u} cm/sec	$Re = \frac{D_R \bar{u} \rho_m}{\mu'}$
50	600	27.7
75	400	18.5
100	300	13.4
125	240	11.1

Table 9

Calculated Pressure Drop in Flow Reactor with Pure Argon
at 295°K

Equation (25) was used with $D_R = 1.0$ cm, $L = 30.0$ cm,
 $\mu' = 2.28 \times 10^{-4}$ poise

\dot{V}_f cm ³ /sec at atm.pr.	P_4 torr	P_4 gm _f /cm ²	P_1 gm _f /cm ²	P_1 torr	Δp torr	Δp as % of P_4
9.1	10.0	13.6	11.45	8.4	1.6	16
5.0	8.0	10.9	9.55	7.0	1.0	12.5
2.7	6.0	8.15	7.1	5.2	0.8	13.3
1.05	4.0	5.45	4.85	3.6	0.4	10
0.28	2.0	2.72	2.4	1.8	0.2	10

Table 10

Retention Times of C₁-C₃ Hydrocarbons on Silica
Gel Column at Various Column Temperatures

Carrier gas flow rate: 25 cm³/min

<u>Substance</u>	<u>Retention time min.</u>		
	49°C	64°C	70°C
Methane	0.6	0.6	0.55
Ethane	0.75	0.75	0.75
Ethylene	1.1	1.05	1.0
Propane	1.4	1.3	1.15
Acetylene	2.5	1.9	1.4
Cyclopropane	2.8	2.2	1.9
Propylene	3.7	2.8	2.3

Table 11

Relative Response Factors of C₁-C₃ Hydrocarbons on
Silica Gel Column

Methane	1.0	} Based on equal number of moles injected
Ethane	1.9	
Ethylene	1.85	
Propane	2.8	
Acetylene	1.8	
Cyclopropane	2.75	
Propylene	2.75	

Table 12

Preliminary runs #1-8

Carrier gas was He

Residence time $\tau = 220$ msec% CH₄ in feed stream, C₀ = 0.05

Type of discharge: d.c. glow

p₁ = 4.6 torr , p₂ = 1.8 torr

#	V Volts (a)	I ma (b)	E volts/cm (c)	(n _e) ₀ per cm ³ (d)	v _{en} per sec (e)	% Conversion			% Total Conversion (i)	% of (i) Accounted for (j)
						to C ₂ H ₆ (f)	to C ₂ H ₄ (g)	to C ₂ H ₂ (h)		
1	3700	0.40	30	8.0 × 10 ⁹	10.4 × 10 ⁹	4.7	3.6	n.a.	46	18
2	3900	0.45	27	8.8 × 10 ⁹	9.3 × 10 ⁹	4.5	3.2	n.a.	53	14.5
3	4200	0.50	14	9.6 × 10 ⁹	11.5 × 10 ⁹	3.9	2.6	n.a.	59	11.0
4	4350	0.55	14	1.11 × 10 ¹⁰	10.5 × 10 ⁹	3.9	2.5	n.a.	67	9.5
5	4500	0.60	15	1.21 × 10 ¹⁰	9.4 × 10 ⁹	3.6	2.2	n.a.	69	8.4
6	4700	0.70	17	1.32 × 10 ¹⁰	10.2 × 10 ⁹	3.1	1.9	n.a.	73	6.9
7	4800	0.80	20	1.57 × 10 ¹⁰	10.5 × 10 ⁹	2.5	1.8	n.a.	84	5.1
8	5000	0.90	25	1.81 × 10 ¹⁰	9.8 × 10 ⁹	2.1	1.3	n.a.	87	3.9

Table 13

Preliminary runs #9-11

Carrier gas was He

Residence time $\tau = 180$ msec

% CH₄ in feed stream, C₀ = 1.7

Type of discharge: d.c. glow

p₁ = 5.3 torr, p₂ = 1.5 torr

#	V Volts (a)	I ma (b)	E volts/cm (c)	% Conversion to C ₂ H ₆ (f)	% Conversion to C ₂ H ₄ (g)	% Conversion to C ₂ H ₂ (h)	% Total Conversion (i)	% of (i) Accounted For (j)
9	3600	0.3	32	2.2	1.1	n.a.	7.4	44.5
10	4200	0.5	28	3.9	1.5	n.a.	10.3	52.5
11	4500	0.65	30	4.7	1.6	n.a.	13.3	47.5

Table 14

Preliminary runs #12-15

Carrier gas was Ar

Residence time $\tau = 210$ msec

% CH₄ in feed stream, C₀ = 0.35

Type of discharge: d.c. glow

p₁ = 5.5 torr , p₂ = 1.3 torr

#	V Volts (a)	I ma (b)	E volts/cm (c)	% Conversion to C ₂ H ₆ (f)	% Conversion to C ₂ H ₄ (g)	% Conversion to C ₂ H ₂ (h)	% Total Conversion (i)	% of (i) Accounted For (j)
12	1550	0.85	8.0	7.4	2.8	4.3	57.1	28.0
13	1550	1.5	8.0	6.2	1.8	3.6	77.2	17.0
14	1600	2.0	8.0	5.3	1.5	3.3	83.5	13.9
15	1800	2.55	4.0	3.9	1.1	2.7	88.2	11.4

Table 15

Preliminary runs #16-20

Carrier gas was Ar

Residence time $\tau = 150$ msec

% CH₄ in feed stream, C₀ = 3.9

Type of discharge: d.c. glow

p₁ = 8.1 torr , p₂ = 1.5 torr → 0.4 torr

#	V Volts (a)	I ma (b)	E volts/cm (c)	% Conversion to C ₂ H ₆ (f)	% Conversion to C ₂ H ₄ (g)	% Conversion to C ₂ H ₂ (h)	% Total Conversion (i)	% of (i) Accounted For (j)
16	4700	0.25	n.a.	2.4	1.5	0.3	6.3	69
17	3800	0.5	40	4.1	1.8	1.0	11.3	69
18	3500	1.0	37	5.9	1.8	1.8	16.7	59
19	3000	1.45	35	7.6	1.8	2.5	18.6	67
20	3150	2.0	30	9.0	1.8	3.0	24.5	59

Table 16

Preliminary runs #21-23

Carrier gas was Ar

Residence time $\tau = 750$ msec

% CH₄ in feed stream, C₀ = 3.6

Type of discharge: d.c. glow

p₁ = 8.3 torr , p₂ = 0.3 torr

#	V Volts (a)	I ma (b)	E volts/cm (c)	% Conversion to C ₂ H ₆ (f)	% Conversion to C ₂ H ₄ (g)	% Conversion to C ₂ H ₂ (h)	% Total Conversion (i)	% of (i) Accounted For (j)
21	4200	0.5	33	12.6	1.2	2.4	27.7	66
22	4800	0.75	30	14.2	1.3	3.0	34.5	61
23	5000	1.0	27	15.2	1.3	3.2	37.8	60

Table 17

Preliminary runs #24-28

Carrier gas was Ar

Residence time $\tau = 75$ msec

% CH₄ in feed stream, C₀ = 8

Type of discharge: d.c. glow

p₁ = 4.5 torr , p₂ = 1.5 torr

#	V Volts (a)	I ma (b)	% Conversion to C ₂ H ₆ (f)	% Conversion to C ₂ H ₄ (g)	% Conversion to C ₂ H ₂ (h)	% Total Conversion (i)	% of (i) Accounted For (j)
24	4800	0.075	0.13	0.04	0	0.17	100
25	5000	0.15	0.25	0.11	0.03	0.39	100
26	4200	0.5	0.7	0.3	0.06	1.1	96
27	5000	0.7	2.1	0.6	0.23	3.3	89
28	3500	1.5	3.6	0.8	0.52	6.1	80

Table 18

Preliminary runs #29-35

Carrier gas was Ar

Residence time $\tau = 75$ msec

% CH₄ in feed stream, C₀ = 2.0

Type of discharge: d.c. glow

p₁ = 4.5 torr , p₂ = 1.0 torr → 0.2

#	V Volts (a)	I ma (b)	% Conversion to C ₂ H ₆ (f)	% Conversion to C ₂ H ₄ (g)	% Conversion to C ₂ H ₂ (h)	% Total Conversion (i)	% of (i) Accounted For (j)
29	3800	0.075	0.33	0.31	0	0.85	75
30	3800	0.15	0.72	0.7	0	1.7	84
31	4000	0.25	1.2	1.1	0	4.2	55
32	4000	0.5	2.1	1.6	0.4	8.4	50
33	4200	0.75	2.8	1.8	0.84	10.8	52
34	3000	1.0	5.6	1.9	1.9	16.7	59
35	3000	2.0	7.7	1.6	2.7	25.0	50

Table 19

Preliminary runs #36-40

Carrier gas was Ar

Residence time $\tau = 41$ msec

% CH₄ in feed stream, C_o = 7.1

Type of discharge: a.c. glow, 60 cps

p₁ = 10.75 torr , p₂ = 0.5 torr

#	V Arbitrary Units (a)	% Conversion to C ₂ H ₆ (f)	% Conversion to C ₂ H ₄ (g)	% Conversion to C ₂ H ₂ (h)	% Total Conversion (i)	% of (i) Accounted For (j)
36	1.9	0.07	0.02	0	0.09	n.a.
37	2.1	0.10	0.04	0	0.14	n.a.
38	2.3	0.22	0.14	0.03	0.40	n.a.
39	2.5	0.64	0.43	0.11	1.23	100
40	2.75	2.2	1.03	0.52	5.2	76

Table 20

Preliminary runs #41-43

Carrier gas was Ar

Residence time $\tau = 41$ msec

% CH₄ in feed stream, C₀ = 7.1

Type of discharge: a.c. glow, 30 cps

p₁ = 10.75 torr , p₂ = 0.5 torr

#	V Arbitrary Units (a)	% Conversion to C ₂ H ₆ (f)	% Conversion to C ₂ H ₄ (g)	% Conversion to C ₂ H ₂ (h)	% Total Conversion (i)	% of (i) Accounted For (j)
41	2.4	0.21	0.13	0.01	0.36	n.a.
42	2.7	1.44	0.81	0.22	3.5	73
43	3.0	3.5	1.3	0.9	10.0	61

Table 21

Kinetic runs #1-4

Carrier gas was Ar

Residence time $\tau = 70$ msec

% CH₄ in feed stream, C₀ = 6.7 Type of discharge: d.c. glow

p₁ = 5.0 torr , p₂ = 0.7 - 1.0 torr

#	V Volts (a)	I ma (b)	E volts/cm (c)	10 ⁻⁹ × (n _e) ₀ per cm ³ (d)	10 ⁻⁹ × v _{en} per sec (e)	2 × % C ₂ H ₆ in Product Stream (f)	2 × % C ₂ H ₄ in Product Stream (g)	2 × % C ₂ H ₂ in Product Stream (h)	3 × % C ₃ H ₈ in Product Stream (i)	% CH ₄ Converted to Gaseous Products (j)
1	3600	0.75	30	3.5	3.9	0.080	0.025	0.0064	0.0025	1.7
2	3600	1.0	34	4.7	5.2	0.094	0.029	0.0092	0.0030	2.0
3	3700	1.5	35	5.8	6.9	0.143	0.047	0.018	0.0056	3.2
4	3900	2.0	35	7.5	9.5	0.193	0.053	0.034	0.0075	4.3

Table 22

Kinetic runs #5-9

Carrier gas was Ar

Residence time $\tau = 80.5$ msec

% CH₄ in feed stream, C₀ = 6.7

Type of discharge: d.c. glow

p₁ = 5.0 torr , p₂ = 0.7-1.0 torr

#	V Volts (a)	I ma (b)	E volts/cm (c)	10 ⁻⁹ × (n _e) ₀ per cm ³ (d)	10 ⁻⁹ × v _{en} per sec (e)	2 × % C ₂ H ₆ in Product Stream (f)	2 × % C ₂ H ₄ in Product Stream (g)	2 × % C ₂ H ₂ in Product Stream (h)	3 × % C ₃ H ₈ in Product Stream (i)	% CH ₄ Converted to Gaseous Products (j)
5	3800	0.5	n.a.	1.3	16.8	0.074	0.028	0.0059	0.0026	1.6
6	3800	0.75	32	2.4	8.7	0.112	0.037	0.011	0.0039	2.5
7	3600	1.0	32	4.5	5.5	0.138	0.037	0.015	0.0051	3.9
8	3600	1.5	37	5.6	8.0	0.197	0.044	0.028	0.0086	4.2
9	3800	2.0	37	8.1	12.6	0.248	0.057	0.041	0.011	5.4

Table 23

Kinetic runs #10-16

Carrier gas was Ar

Residence time $\tau = 93$ msec

% CH₄ in feed stream, C_o = 6.7

Type of discharge: d.c. glow

p₁ = 5.0 torr , p₂ = 0.7 - 1.0 torr

#	V Volts (a)	I ma (b)	E volts/cm (c)	10 ⁻⁹ × (n _e) _o per cm ³ (d)	10 ⁻⁹ × v _{en} per sec (e)	2 × % C ₂ H ₆ in Product Stream (f)	2 × % C ₂ H ₄ in Product Stream (g)	2 × % C ₂ H ₂ in Product Stream (h)	3 × % C ₃ H ₈ in Product Stream (i)	% CH ₄ Converted to Gaseous Products (j)
10	4500	0.5	n.a.	3.0	3.0	0.086	0.030	0.0021	0.0058	1.9
11	4400	0.75	35	3.4	4.6	0.122	0.041	0.0037	0.012	2.7
12	3700	1.0	40	4.4	5.2	0.156	0.043	0.0047	0.019	3.3
13	4100	1.5	40	6.5	6.4	0.219	0.057	0.0086	0.034	4.8
14	3800	2.0	45	7.7	7.7	0.275	0.070	0.012	0.055	6.2

Table 24

Kinetic runs #15-19

Carrier gas was Ar

Residence time $\tau = 116$ msec

% CH₄ in feed stream, C₀ = 6.7

Type of discharge: d.c. glow

p₁ = 5.0 torr , p₂ = 0.7 - 1.0 torr

#	V Volts (a)	I ma (b)	E volts/cm (c)	10 ⁻⁹ × (n _e) ₀ per cm ³ (d)	10 ⁻⁹ × v _{en} per sec (e)	2 × % C ₂ H ₆ in Product Stream (f)	2 × % C ₂ H ₄ in Product Stream (g)	2 × % C ₂ H ₂ in Product Stream (h)	3 × % C ₃ H ₈ in Product Stream (i)	% CH ₄ Converted to Gaseous Products (j)
15	4000	0.5	n.a.	2.4	3.6	0.113	0.039	0.0084	0.0035	2.5
16	3750	0.75	35	4.2	3.9	0.146	0.046	0.014	0.0049	3.2
17	3600	1.0	35	4.9	4.8	0.196	0.053	0.024	0.0081	4.2
18	3800	1.5	40	6.3	7.1	0.268	0.067	0.049	0.012	5.9
19	3700	2.0	40	6.7	6.5	0.333	0.084	0.078	0.015	7.7

Table 25

Kinetic runs #20-24

Carrier gas was Ar

Residence time $\tau = 74.6$ msec

% CH₄ in feed stream, C_o = 4.0

Type of discharge: d.c. glow

p₁ = 5.0 torr , p₂ = 0.7 - 1.0 torr

#	V Volts (a)	I ma (b)	E volts/cm (c)	10 ⁻⁹ × (n _e) _o per cm ³ (d)	10 ⁻⁹ × v _{en} per sec (e)	2 × % C ₂ H ₆ in Product Stream (f)	2 × % C ₂ H ₄ in Product Stream (g)	2 × % C ₂ H ₂ in Product Stream (h)	3 × % C ₃ H ₈ in Product Stream (i)	% CH ₄ Converted to Gaseous Products (j)
20	4300	0.5	n.a.	1.6	7.9	0.044	0.021	0.0054	0.0015	3.2
21	4300	0.75	25	3.1	7.7	0.075	0.030	0.0096	0.0024	5.2
22	4000	1.0	30	5.0	6.2	0.096	0.038	0.016	0.0038	6.9
23	4400	1.5	35	6.8	8.7	0.134	0.046	0.031	0.0056	9.7
24	4500	2.0	40	8.4	10.1	0.164	0.054	0.045	0.0066	12.1

Table 26

Kinetic runs #25-29

Carrier gas was Ar

Residence time $\tau = 85.5$ msec

% CH₄ in feed stream, C₀ = 4.0

Type of discharge: d.c. glow

p₀ = 5.0 torr , p₂ = 0.7 - 1.0 torr

#	V Volts (a)	I ma (b)	E volts/cm (c)	10 ⁻⁹ × (n _e) ₀ per cm ³ (d)	10 ⁻⁹ × v _{en} per sec (e)	2 × % C ₂ H ₆ in Product Stream (f)	2 × % C ₂ H ₄ in Product Stream (g)	2 × % C ₂ H ₂ in Product Stream (h)	3 × % C ₃ H ₈ in Product Stream (i)	% CH ₄ Converted to Gaseous Products (j)
25	4200	0.5	40	2.7	2.7	0.051	0.024	0.0066	0.0029	3.8
26	4000	0.75	35	3.6	6.5	0.101	0.039	0.016	0.0040	7.2
27	3800	1.0	25	5.5	5.9	0.125	0.044	0.025	0.0058	8.9
28	3800	1.5	40	7.2	8.2	0.168	0.051	0.043	0.0081	12.1
29	3600	2.0	45	8.9	10.6	0.206	0.058	0.060	0.010	14.9

Table 27

Kinetic runs #30-34

Carrier gas was Ar

Residence time $\tau = 98.0$ msec

% CH₄ in feed stream, C₀ = 4.0

Type of discharge: d.c. glow

p₁ = 5.0 torr , p₂ = 0.7 - 1.0 torr

#	V Volts (a)	I ma (b)	E volts/cm (c)	10 ⁻⁹ × (n _e) ₀ per cm ³ (d)	10 ⁻⁹ × v _{en} per sec (e)	2 × % C ₂ H ₆ in Product Stream (f)	2 × % C ₂ H ₄ in Product Stream (g)	2 × % C ₂ H ₂ in Product Stream (h)	3 × % C ₃ H ₈ in Product Stream (i)	% CH ₄ Converted to Gaseous Products (j)
30	4400	0.5	n.a.	1.7	4.1	0.060	0.033	0.0075	0.0018	4.6
31	4300	0.75	35	4.0	5.3	0.116	0.042	0.022	0.0022	8.3
32	4000	1.0	25	5.4	5.9	0.148	0.047	0.032	0.0074	10.5
33	4400	1.5	30	7.1	8.1	0.197	0.053	0.048	0.011	13.8
34	4400	2.0	30	9.8	12.1	0.231	0.062	0.066	0.013	16.6

Table 28

Kinetic runs #35-39

Carrier gas was Ar

Residence time $\tau = 106$ msec

% CH₄ in feed stream, C_o = 4.0

Type of discharge: d.c. glow

p₁ = 5.0 torr , p₂ = 0.7 - 1.0 torr

#	V Volts (a)	I ma (b)	E volts/cm (c)	10 ⁻⁹ × (n _e) _o per cm ³ (d)	10 ⁻⁹ × v _{en} per sec (e)	2 × % C ₂ H ₆ in Product Stream (f)	2 × % C ₂ H ₄ in Product Stream (g)	2 × % C ₂ H ₂ in Product Stream (h)	3 × % C ₃ H ₈ in Product Stream (i)	% CH ₄ Converted to Gaseous Products (j)
35	4000	0.5	35	1.7	3.7	0.064	0.032	0.010	0.0027	4.9
36	3600	0.75	45	3.4	7.4	0.131	0.045	0.026	0.0062	9.3
37	3800	1.0	40	5.2	6.2	0.156	0.048	0.034	0.0085	11.0
38	4000	1.5	42	7.2	8.7	0.205	0.053	0.052	0.012	14.4
39	4500	2.0	35	9.7	12.3	0.247	0.062	0.059	0.013	17.5

Table 29

Kinetic runs #40-43

Carrier gas was Ar

Residence time $\tau = 59.1$ msec

% CH₄ in feed stream, C₀ = 10.4

Type of discharge: d.c. glow

p₁ = 5.0 torr , p₂ = 0.7 - 1.0 torr

#	V Volts (a)	I ma (b)	E volts/cm (c)	10 ⁻⁹ × (n _e) ₀ per cm ³ (d)	10 ⁻⁹ × v _{en} per sec (e)	2 × % C ₂ H ₆ in Product Stream (f)	2 × % C ₂ H ₄ in Product Stream (g)	2 × % C ₂ H ₂ in Product Stream (h)	3 × % C ₃ H ₈ in Product Stream (i)	% CH ₄ Converted to Gaseous Products (j)
40	4600	0.75	50	2.8	4.9	0.078	0.022	0.0038	0.0019	1.8
41	4600	1.0	50	4.4	4.4	0.099	0.026	0.0056	0.0024	2.3
42	4700	1.5	45	5.8	6.1	0.134	0.036	0.0099	0.0036	3.2
43	4500	2.0	50	6.9	7.4	0.177	0.046	0.015	0.0047	4.2

Table 30

Kinetic runs #44-47

Carrier gas was Ar

Residence time $\tau = 71.5$ msec

% CH₄ in feed stream, C₀ = 10.4

Type of discharge: d.c. glow

p₁ = 5.0 torr , p₂ = 0.7 - 1.0 torr

#	V Volts (a)	I ma (b)	E volts/cm (c)	10 ⁻⁹ × (n _e) ₀ per cm ³ (d)	10 ⁻⁹ × v _{en} per sec (e)	2 × % C ₂ H ₆ in Product Stream (f)	2 × % C ₂ H ₄ in Product Stream (g)	2 × % C ₂ H ₂ in Product Stream (h)	3 × % C ₃ H ₈ in Product Stream (i)	% CH ₄ Converted to Gaseous Products (j)
44	5000	0.75	45	1.9	7.8	0.096	0.025	0.0056	0.0023	2.2
45	4800	1.0	42	4.9	4.3	0.129	0.035	0.0086	0.0036	3.1
46	4800	1.5	45	6.0	6.5	0.187	0.044	0.016	0.0056	4.4
47	4600	2.0	42	7.6	8.1	0.229	0.050	0.023	0.0073	5.4

Table 31

Kinetic runs #48-51

Carrier gas was Ar

Residence time $\tau = 85.5$ msec

% CH₄ in feed stream, C_o = 10.4

Type of discharge: d.c. glow

p₁ = 5.0 torr , p₂ = 0.7 - 1.0 torr

#	V Volts (a)	I ma (b)	E volts/cm (c)	10 ⁻⁹ × (n _e) _o per cm ³ (d)	10 ⁻⁹ × v _{en} per sec (e)	2 × % C ₂ H ₆ in Product Stream (f)	2 × % C ₂ H ₄ in Product Stream (g)	2 × % C ₂ H ₂ in Product Stream (h)	3 × % C ₃ H ₈ in Product Stream (i)	% CH ₄ Converted to Gaseous Products (j)
48	4500	0.75	45	3.4	4.1	0.116	0.028	0.0073	0.0031	2.7
49	4600	1.0	45	4.4	5.2	0.146	0.039	0.010	0.0043	3.5
50	4700	1.5	45	5.6	7.3	0.204	0.045	0.018	0.0066	4.7
51	4200	2.0	40	7.0	8.4	0.259	0.056	0.025	0.0086	6.1

Table 32

Kinetic runs #52-55

Carrier gas was Ar

Residence time $\tau = 98.0$ msec

% CH₄ in feed stream, C₀ = 10.4

Type of discharge: d.c. glow

p₁ = 5.0 torr , p₂ = 0.7 -1.0 torr

#	V Volts (a)	I ma (b)	E volts/cm (c)	10 ⁻⁹ × (n _e) ₀ per cm ³ (d)	10 ⁻⁹ × v _{en} per sec (e)	2 × % C ₂ H ₆ in Product Stream (f)	2 × % C ₂ H ₄ in Product Stream (g)	2 × % C ₂ H ₂ in Product Stream (h)	3 × % C ₃ H ₈ in Product Stream (i)	% CH ₄ Converted to Gaseous Products (j)
52	4900	0.75	n.a.	2.7	5.7	0.135	0.034	0.0084	0.0038	3.1
53	4300	1.0	45	4.1	5.8	0.167	0.039	0.012	0.0051	3.9
54	4800	1.5	45	5.7	6.8	0.244	0.049	0.022	0.0080	5.6
55	4800	2.0	45	7.7	7.2	0.303	0.060	0.034	0.012	7.1

Table 33

Kinetic runs #56-59

Carrier gas was Ar

Residence time $\tau = 57.5$ msec

% CH₄ in feed stream, C₀ = 12.6

Type of discharge: d.c. glow

p₁ = 5.0 torr , p₂ = 0.7 -1.0 torr

#	V volts (a)	I ma (b)	E volts/cm (c)	10 ⁻⁹ × (n _e) ₀ per cm ³ (d)	10 ⁻⁹ × v _{en} per sec (e)	2 × % C ₂ H ₆ in Product Stream (f)	2 × % C ₂ H ₄ in Product Stream (g)	2 × % C ₂ H ₂ in Product Stream (h)	3 × % C ₃ H ₈ in Product Stream (i)	% CH ₄ Converted to Gaseous Products (j)
56	5000	0.75	47	2.8	4.7	0.080	0.026	0.0043	0.0019	1.6
57	4700	1.0	52	4.2	4.2	0.103	0.031	0.0064	0.0026	2.0
58	4700	1.5	60	5.8	6.2	0.139	0.033	0.0096	0.0035	2.7
59	4700	2.0	45	6.8	7.3	0.188	0.047	0.017	0.0056	3.7

Table 34

Kinetic runs #60-63

Carrier gas was Ar

Residence time $\tau = 65.3$ msec

% CH₄ in feed stream, C₀ = 12.6

Type of discharge: d.c. glow

p₁ = 5.0 torr , p₂ = 0.7 -1.0 torr

#	V volts (a)	I ma (b)	E volts/cm (c)	10 ⁻⁹ × (n _e) ₀ per cm ³ (d)	10 ⁻⁹ × v _{en} per sec (e)	2 × % C ₂ H ₆ in Product Stream (f)	2 × % C ₂ H ₄ in Product Stream (g)	2 × % C ₂ H ₂ in Product Stream (h)	3 × % C ₃ H ₈ in Product Stream (i)	% CH ₄ Converted to Gaseous Products (j)
60	4700	0.75	45	3.2	4.4	0.101	0.027	0.0052	0.0023	1.9
61	4200	1.0	45	4.6	4.6	0.127	0.034	0.0077	0.0032	2.5
62	4500	1.5	40	5.9	6.4	0.183	0.045	0.015	0.0054	3.6
63	4800	2.0	40	7.1	7.8	0.228	0.053	0.021	0.0072	4.4

Table 35

Kinetic runs #64-67

Carrier gas was Ar

Residence time $\tau = 81.0$ msec

% CH₄ in feed stream, C₀ = 12.6

Type of discharge: d.c. glow

p₁ = 5.0 torr , p₂ = 0.7 -1.0 torr

#	V volts (a)	I ma (b)	E volts/cm (c)	10 ⁻⁹ × (n _e) ₀ per cm ³ (d)	10 ⁻⁹ × v _{en} per sec (e)	2 × % C ₂ H ₆ in Product Stream (f)	2 × % C ₂ H ₄ in Product Stream (g)	2 × % C ₂ H ₂ in Product Stream (h)	3 × % C ₃ H ₈ in Product Stream (i)	% CH ₄ Converted to Gaseous Products (j)
64	4700	0.75	50	3.5	4.8	0.133	0.036	0.0085	0.0039	2.6
65	4500	1.0	45	4.6	4.5	0.164	0.041	0.011	0.0046	3.2
66	4800	1.5	45	5.9	6.6	0.236	0.053	0.020	0.0074	4.5
67	4500	2.0	45	7.2	8.2	0.292	0.064	0.028	0.0096	5.6

Table 36

Kinetic runs #68-71

Carrier gas was Ar

Residence time $\tau = 88.7$ msec

% CH₄ in feed stream, C₀ = 12.6

Type of discharge: d.c. glow

p₁ = 5.0 torr , p₂ = 0.7 - 1.0 torr

#	V volts (a)	I ma (b)	E volts/cm (c)	10 ⁻⁹ × (n _e) ₀ per cm ³ (d)	10 ⁻⁹ × v _{en} per sec (d)	2 × % C ₂ H ₆ in Product Stream (f)	2 × % C ₂ H ₄ in Product Stream (g)	2 × % C ₂ H ₂ in Product Stream (h)	3 × % C ₃ H ₈ in Product Stream (i)	% CH ₄ Converted to Gaseous Stream (j)
68	4700	0.75	55	3.4	4.5	0.152	0.040	0.010	0.0047	3.0
69	4700	1.0	50	4.5	4.7	0.196	0.047	0.015	0.0061	3.8
70	4800	1.5	45	5.9	6.5	0.270	0.058	0.024	0.0093	5.2
71	4900	2.0	42	7.1	7.5	0.336	0.070	0.035	0.012	6.5

Table 37

Effects of Radial and Longitudinal Diffusion in the
Experimental Reactor

$$D = 32.8 \text{ cm}^2/\text{sec}$$

$$p = 5 \text{ torr}$$

$$R = 0.5 \text{ cm}$$

$$L = 30 \text{ cm}$$

τ msec	$D\tau/2R^2$	$D\tau/L^2$
50	3.3	1.8×10^{-3}
75	4.9	2.7×10^{-3}
100	6.5	3.6×10^{-3}
125	8.2	4.6×10^{-3}

Table 38

Pulsed discharge runs 1-4

Effect of varying gas residence time:

Carrier gas was Ar

% CH₄ in feed stream, C_o = 1.0 ± 0.05

p₁ = 5.0 torr, p₂ = 2.5 torr

Type of discharge: pulsed d.c. glow

τ_w = 1.6 msec, τ_I = 52 msec

#	τ msec (a)	V volts (b)	i _{max} mA (c)	$\frac{\tau}{\tau_I} \int_0^{\tau_w} i dt$ mA msec (d)	(n _e) _o per cm ³ at t = 300 μsec (e)	% Conversion to C ₂ H ₆ (f)	% Conversion to C ₂ H ₄ (g)	% Conversion to all Products (h)
1	109	3700	4.0	3.08	1.24 × 10 ¹⁰	0.262	0.316	0.578
2	156	3500	6.0	6.20	1.24 × 10 ¹⁰	0.425	0.475	1.000
3	241	3500	6.0	8.22	1.08 × 10 ¹⁰	0.674	0.665	1.496
4	655	3500	6.0	23.50	1.08 × 10 ¹⁰	1.715	1.010	3.215

Table 39

Pulsed discharge runs 5-8

Effect of varying gas residence time:

Carrier gas was Ar

% CH₄ in feed stream, C_O = 4.2 ± 0.1%

p_O = 5.0 torr, p₂ = 2.5 torr

Type of discharge: pulsed d.c. glow

τ_w = 1.6 msec, τ_I = 52 msec

#	τ msec (a)	V volts (b)	i _{max} mA (c)	$\frac{\tau}{\tau_I} \int_0^{\tau_w} i dt$ mA msec (d)	(n _e) ₀ per cm ³ at t = 300 μsec (e)	% Conversion to C ₂ H ₆ (f)	% Conversion to C ₂ H ₄ (g)	% Conversion to all Products (h)
5	93.5	4400	5.0	2.73	6.44 × 10 ⁹	0.0925	0.0404	0.133
6	166.5	4100	5.0	4.60	6.21 × 10 ⁹	0.146	0.0655	0.212
7	327	4500	5.0	8.74	1.13 × 10 ¹⁰	0.304	0.100	0.423
8	467	4300	4.0	12.16	1.00 × 10 ¹⁰	0.380	0.114	0.511

Table 40

Pulsed discharge runs 2,9,10

Effect of varying total pressure:

Carrier gas was Ar

$p_1 = 3.0 - 7.0$ torr, $p_2 = 1.8 - 3.2$ torr

% CH₄ in feed stream, $C_o = 1.0 \pm 0.05$

$\tau = 153 \pm 7$ msec

Type of discharge: pulsed d.c. glow

$\tau_w = 1.6$ msec, $\tau_I = 52$ msec

#	p_1 torr (a)	V volts (b)	i_{max} mA (c)	$\frac{\tau}{\tau_I} \int_0^{\tau} w idt$ mA msec (d)	$(n_e)_o$ per cm ³ at $t = 300 \mu\text{sec}$	% Conversion to C ₂ H ₆	% Conversion to C ₂ H ₄	% Conversion to all Products
9	3.0	3300	6.0	5.64	1.25×10^{10}	0.529	0.670	1.289
2	5.0	3500	6.0	6.20	1.24×10^{10}	0.425	0.475	1.000
10	7.0	4500	6.0	4.94	1.58×10^{10}	0.326	0.386	0.773

Table 41

Pulsed discharge runs 11-14

Effect of varying pulse interval:

Carrier gas was Ar

$p_1 = 5.0$ torr, $p_2 = 2.5$ torr

% CH₄ in feed stream, $C_o = 1.75 \pm 0.05\%$

$\tau = 93.5$ msec

Type of discharge: pulsed d.c. glow

$\tau_w = 1.6$ msec

#	τ_I msec (a)	V volts (b)	i_{max} mA (c)	$\frac{\tau}{\tau_I} \int_0^{\tau} i dt$ mA msec (d)	$(n_e)_o$ per cm ³ at $t = 300 \mu sec$ (e)	% Conversion to C ₂ H ₆ (f)	% Conversion to C ₂ H ₄ (g)	% Conversion to all Products (h)
11	52	3700	5.0	2.79	1.00×10^{10}	0.1655	0.138	0.304
12	40	3800	5.0	3.48	9.02×10^9	0.195	0.164	0.359
13	30	3800	4.0	3.74	7.36×10^9	0.211	0.170	0.381
14	22	3800	4.0	3.91	5.37×10^9	0.250	0.190	0.440

Table 42

Pulsed discharge runs 15-20

Effect of varying pulse width τ_w , and τ , τ_I and τ_w simultaneously:

Carrier gas was Ar

% CH₄ in feed stream, C_o = 2.05 ± 0.1%

p₁ = 5.0 torr , p₂ = 2.5 torr

Type of discharge: pulsed d.c. glow

#	τ msec (a)	τ_I msec (b)	τ_w msec (c)	V volts (d)	i _{max} mA (e)	$\frac{\tau}{\tau_I} \int_0^{\tau} i dt$ mA msec (f)	(n _e) _o per cm ³ at t = 300 μsec (g)	% Conversion to C ₂ H ₆ (h)	% Conversion to C ₂ H ₄ (i)	% Conversion to all Products (j)
15	93.5	30	0.8	3900	5.0	3.92	1.31 × 10 ¹⁰	0.190	0.152	0.342
16	93.5	30	0.8	3500	4.0	3.49	n.a.	0.172	0.139	0.311
17	93.5	30	0.2	3400	4.0	1.31	n.a.	0.059	0.0435	0.102
18	93.5	30	0.6	3400	4.0	3.18	n.a.	0.131	0.114	0.245
19	142	52	1.6	3600	6.00	4.30	9.02 × 10 ⁹	0.214	0.153	0.367
20	281	52	1.6	3600	5.0	8.32	1.07 × 10 ¹⁰	0.392	0.232	0.671

Table 43

Pulsed discharge runs 21-30

Effect of varying rare gas carrier:

$p_1 = 3.0$ torr , $p_2 = 1.7$ torr ; Type of discharge: pulsed d.c. glow ;

$\tau_w = 1.6$ msec , $\tau_I = 52$ msec

#	Carrier Gas (a)	% CH ₄ in feed C _o (b)	τ msec (c)	Voltage V (d)	i_{max} mA (e)	τ_w $\int_0^{id_t} idt$ mA msec (f)	% Conversion to all Products (g)	Total Conversion for $\tau = 100$ (h)	Total Conversion for $\int idt = 1.76$ and $\tau = 100$ (i)	$\frac{C_2 H_6}{C_2 H_4}$ (j)
21	Ar	0.91	165	3200	5.0	1.67	1.082	0.656	0.694	0.92
22	Ar	1.5	165	3400	6.0	1.63	0.685	0.415	0.448	1.25
23	Ar	4.0	150	3900	5.0	1.76	0.274	0.183	0.183	2.00
24	Ar	9.3	135	4200	5.0	1.63	0.099	0.073	0.079	3.62
25	Ar	17.7	97	4800	5.0	1.59	0.043	0.044	0.049	5.45
26	--	100	300	5000	4.0	1.39	0.177	0.059	0.075	7.05
27	He	0.82	125	4200	2.5	1.11	0.479	0.383	0.606	1.17
28	He	2.2	120	4500	2.5	1.35	0.308	0.256	0.334	1.73
29	He	6.3	115	4500	3.0	0.99	0.116	0.101	0.180	2.35
30	He	16.4	105	4500	4.0	1.11	0.050	0.048	0.075	5.45

Table 44

Calculated Values of Electron-Impact Cross-Sections for
Reactions (1), (3) and (6)

C_o % in CH_4 -Ar	$10^{11} \alpha$ $sec^{-1} cm^3$ (a)	$10^{11} (\alpha + \beta)$ $sec^{-1} cm^3$ (b)	$10^{11} \beta$ Calculated as (b)-(a) (c)	$10^{11} \gamma$ $sec^{-1} cm^3$ (d)	$10^{11} \beta$ from (d) and Eqn. (9) (e)
7.25	9.25	24.7	15.45	-	-
12.0	6.13	19.4	13.27	-	-
18.7	4.32	9.32	5.00	93.0	4.4
22.7	3.55	9.32	5.77	96.5	4.5

Table 46

A Comparison of the Rate of Dissociation of H₂ Using
 i) Maxwellian and ii) Druyvesteyn Distributions

$\bar{\epsilon}$	Mean Energy of Electrons	$\nu_{\text{Maxwellian}}$	$\nu_{\text{Druyvesteyn}}$	$\frac{\nu_{\text{Max}}}{\nu_{\text{Dru}}}$
	1 eV	ν_{M_1}	ν_{D_1}	4×10^{17}
	2 eV	$1.15 \times 10^3 \nu_{M_1}$	$1.53 \times 10^{18} \nu_{D_1}$	3.1×10^3
	5 eV	$2.0 \times 10^5 \nu_{M_1}$	$3.0 \times 10^{24} \nu_{D_1}$	0.7

$$\nu_{M_1} = \nu_{\text{Maxwellian}} \quad \text{when } \bar{\epsilon} = 1 \text{ eV}$$

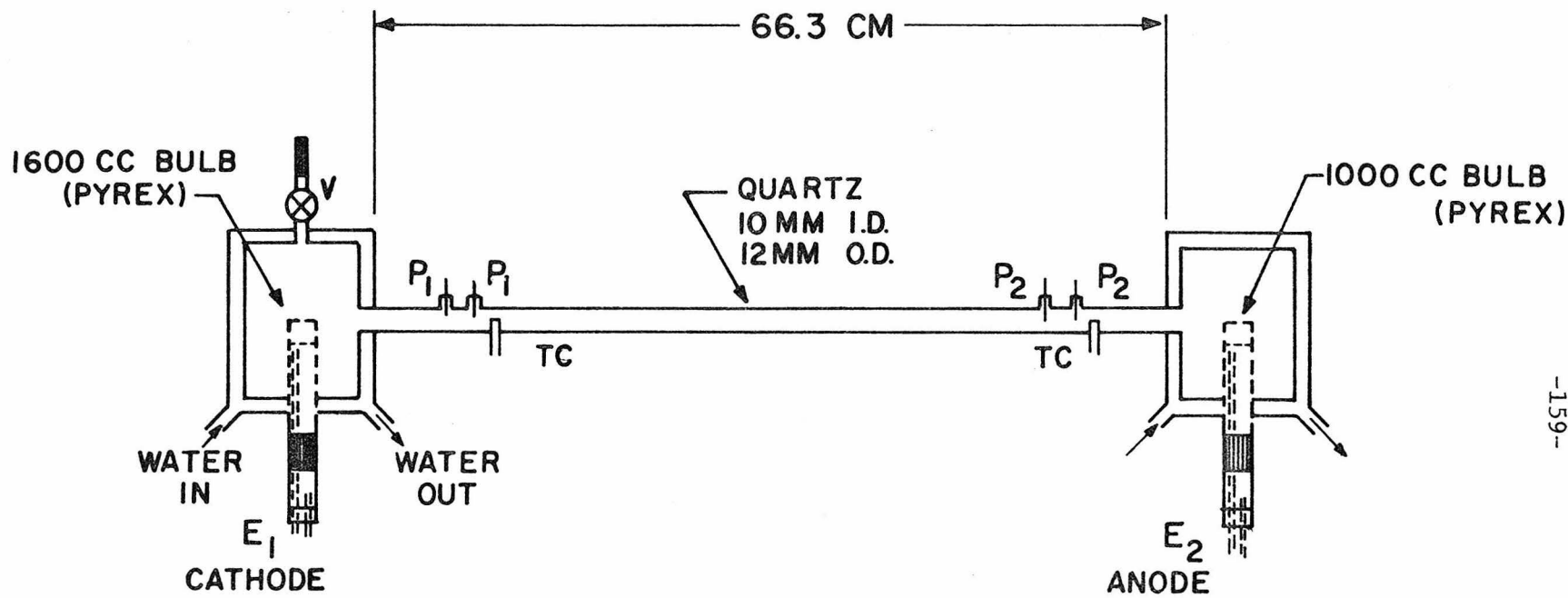
$$\nu_{D_1} = \nu_{\text{Druyvesteyn}} \quad \text{when } \bar{\epsilon} = 1 \text{ eV}$$

$$\nu_{M_1} = 9.65 \text{ per electron per sec for } N = 10^{17} \text{ per cm}^3$$

$$(\text{= } 9.65 \times 10^9 \text{ per cm}^3 \text{ per sec if } n_e = 10^9 \text{ per cm}^3)$$

FIGURES 1 - 85

(except 1, 2, 3, 24, 28, 41, 65 in text)



-159-

P — PROBE WIRES, 20 MIL TUNGSTEN
 TC — GLASS SHIELDED, 20 MIL Cu-CONSTANTAN
 THERMOCOUPLE WIRES
 E₁, E₂ — WATER-COOLED ELECTRODE ASSEMBLIES

Fig. 4. Glow discharge tube 1

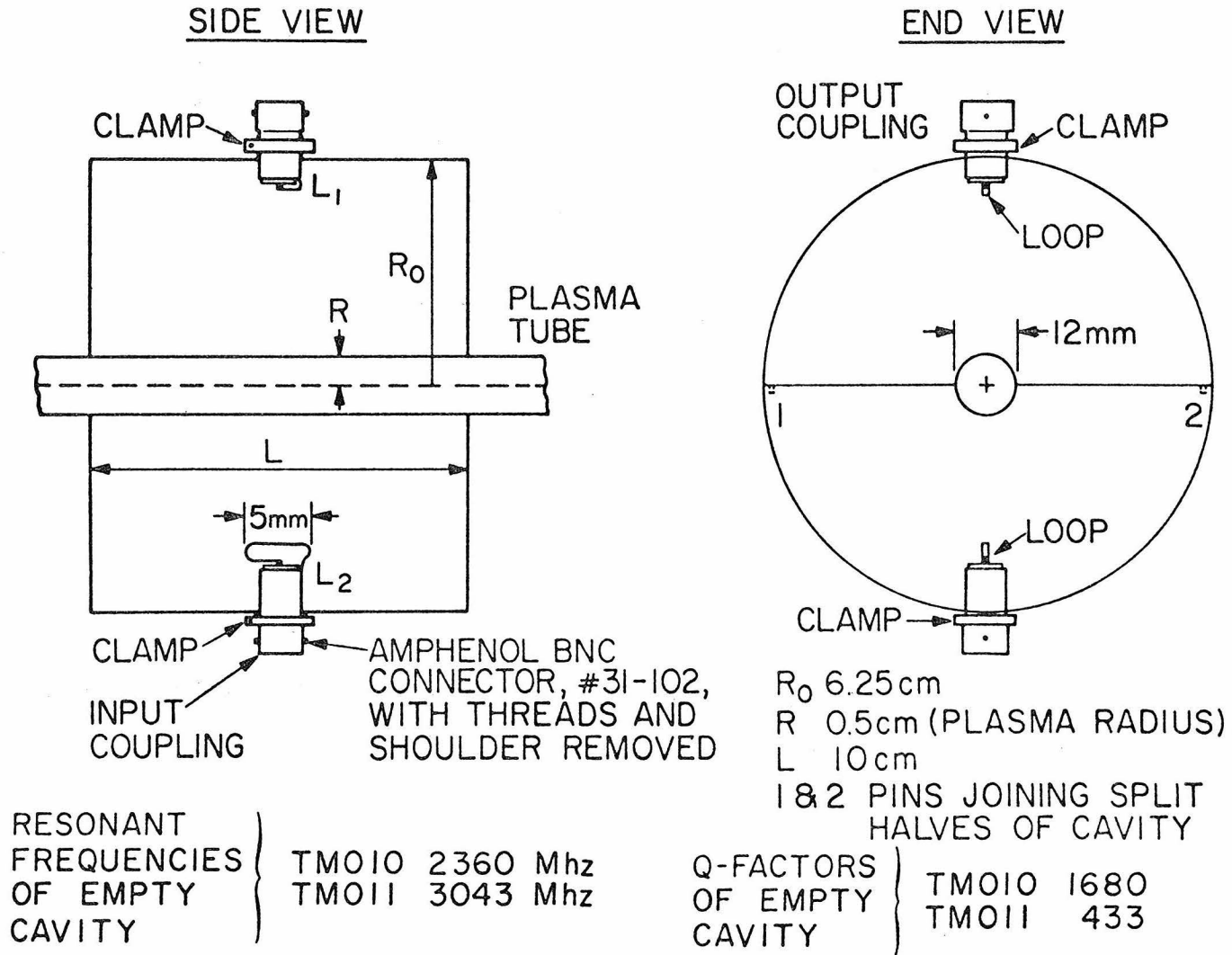


Fig. 5. The microwave cavity

COAXIAL CIRCUIT FOR AUTOMATIC PLOTTING OF TRANSMISSION
CHARACTERISTIC OF MICROWAVE CAVITY WITH GLOW DISCHARGE PLASMA

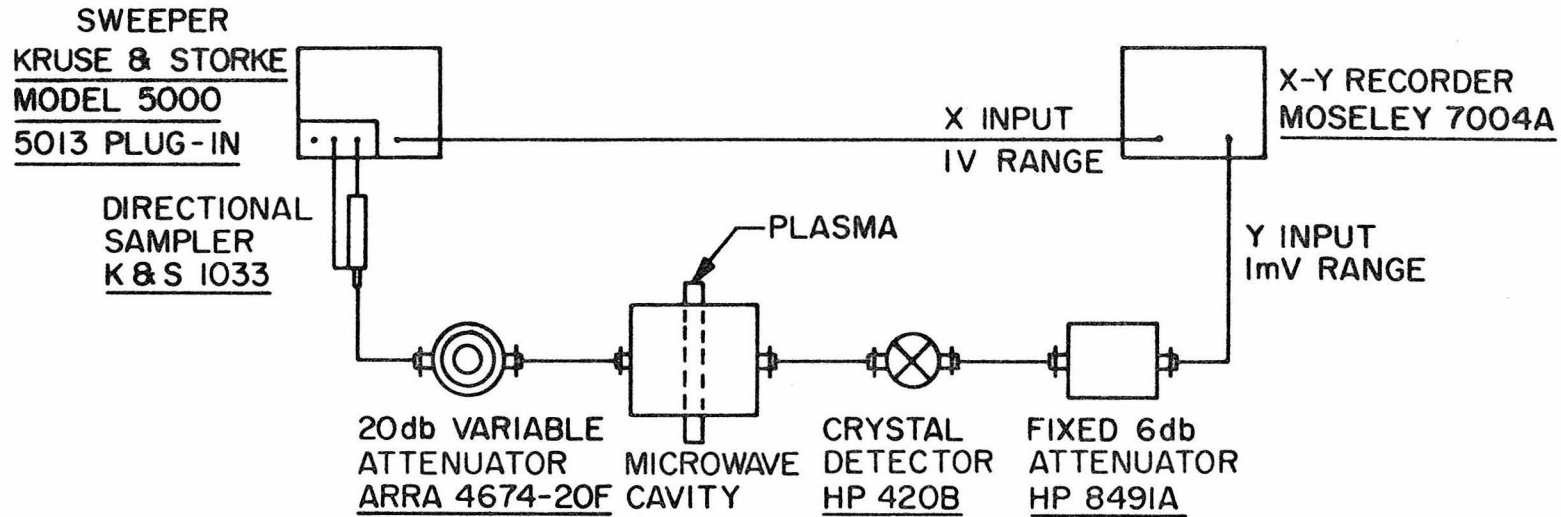


Fig. 6. Coaxial circuit for automatic plotting of transmission characteristic of microwave cavity with glow discharge plasma

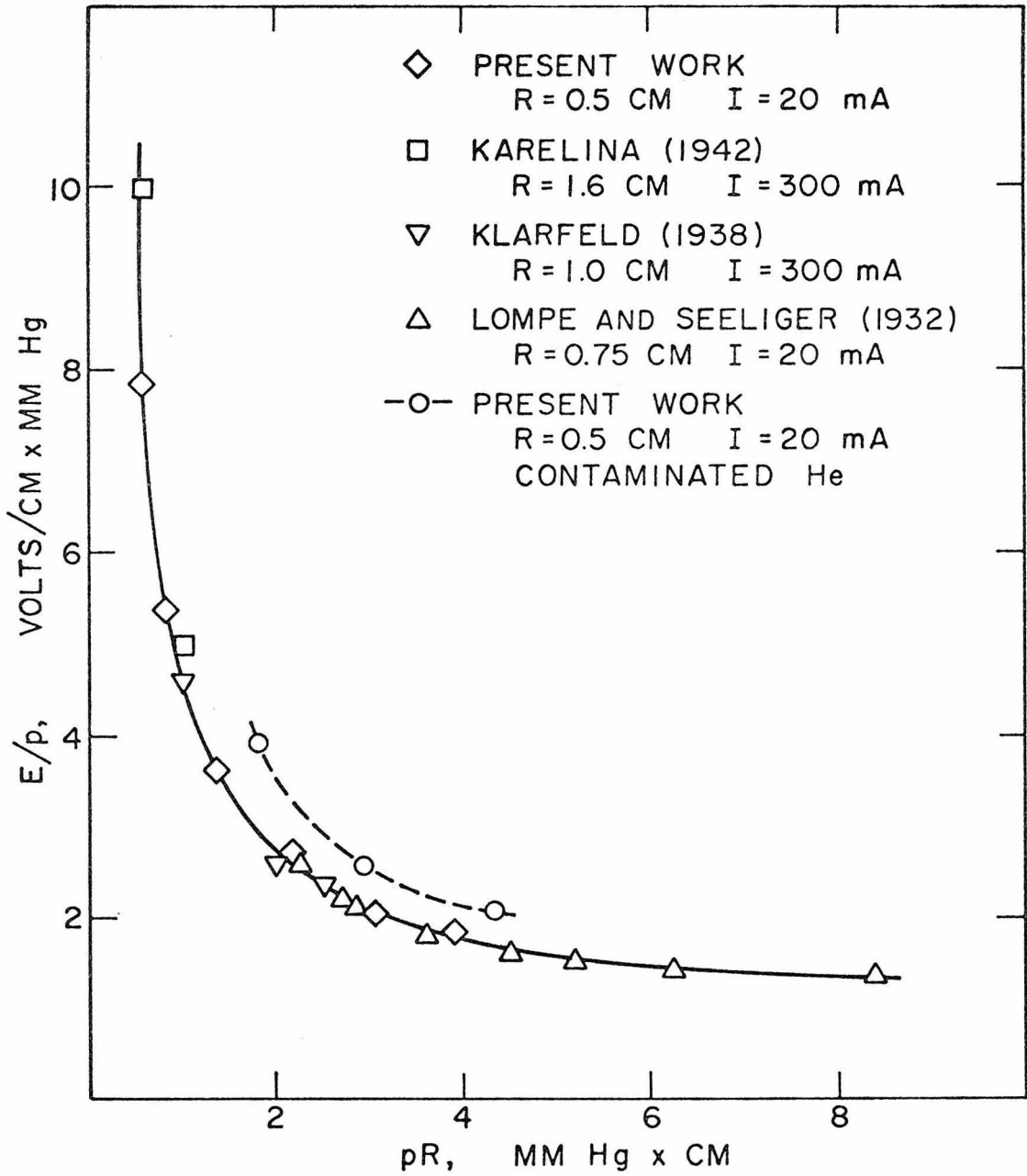


Fig. 7. Electric field in the positive column of helium

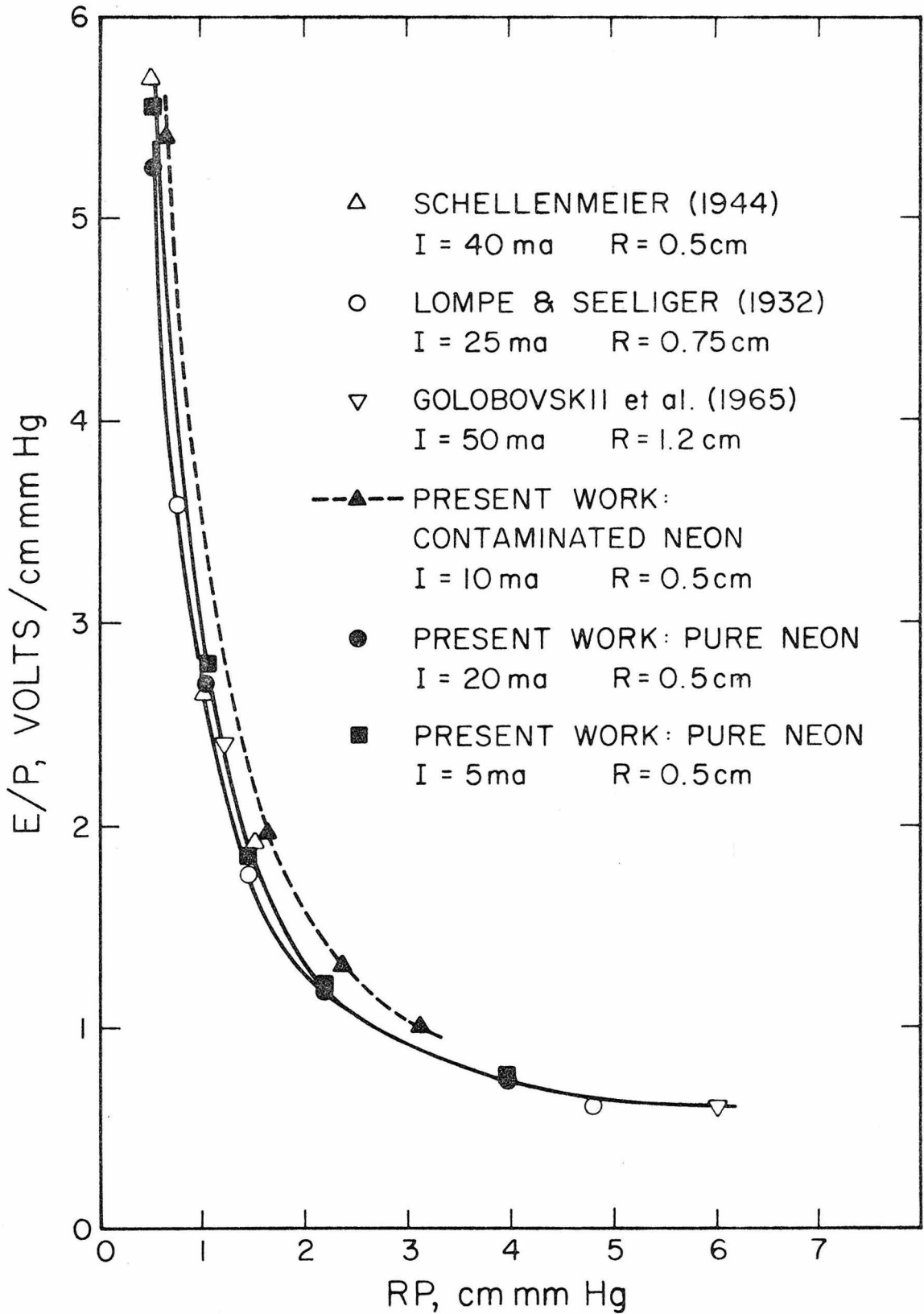


Fig. 8. Electric field in the positive column of neon

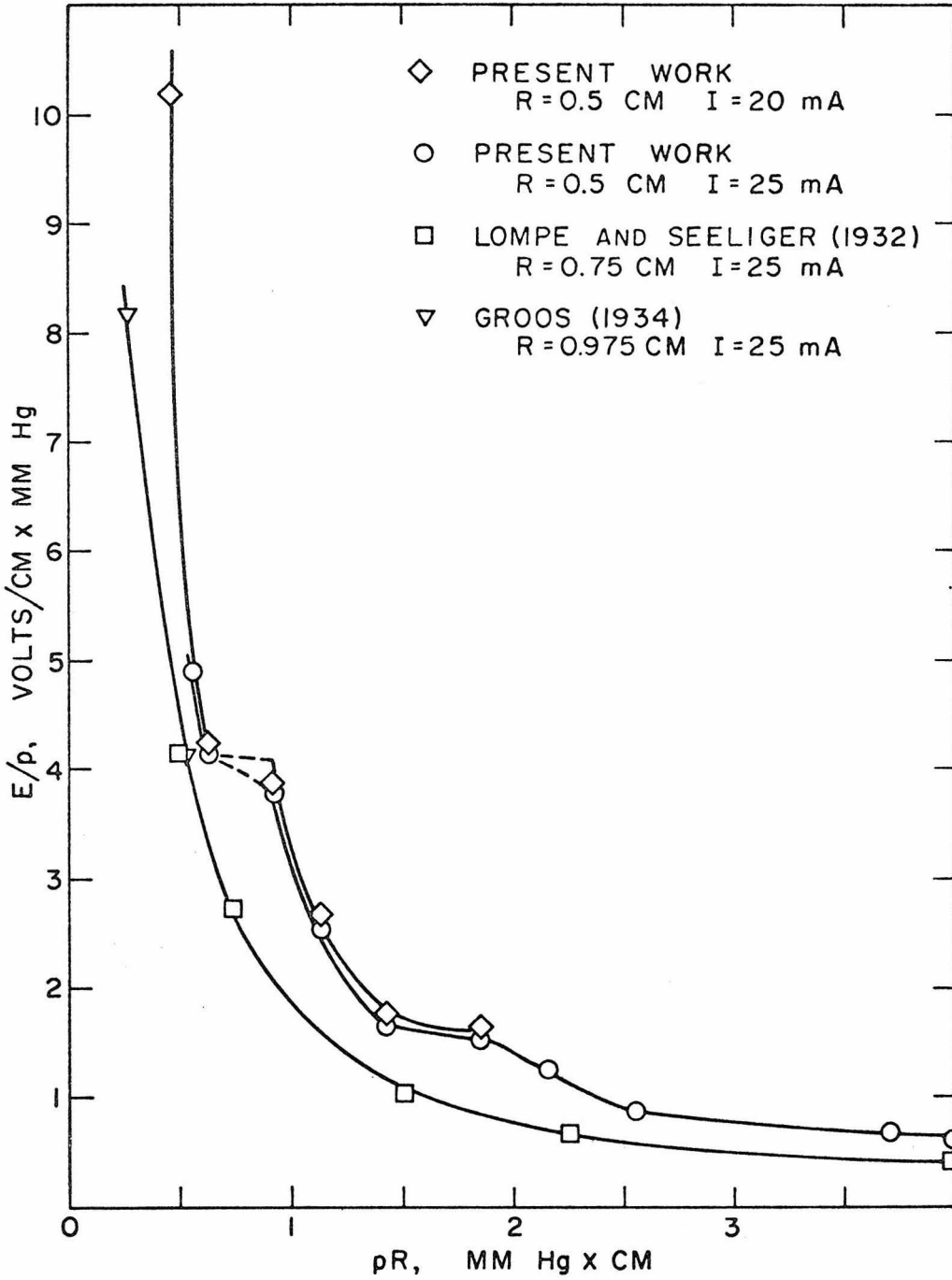


Fig. 9. Electric field in the positive column of argon

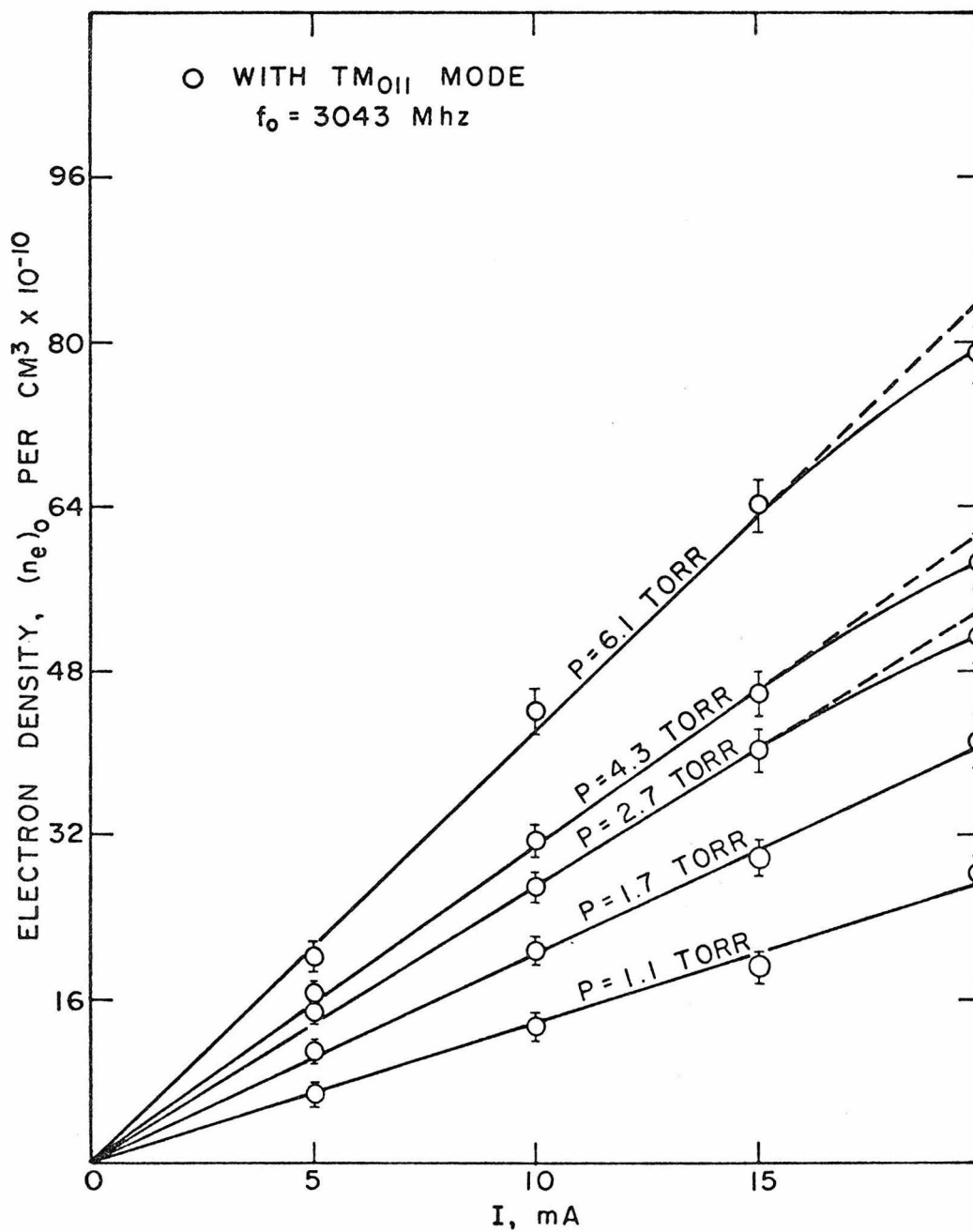


Fig. 10. Electron densities in the positive column of pure helium

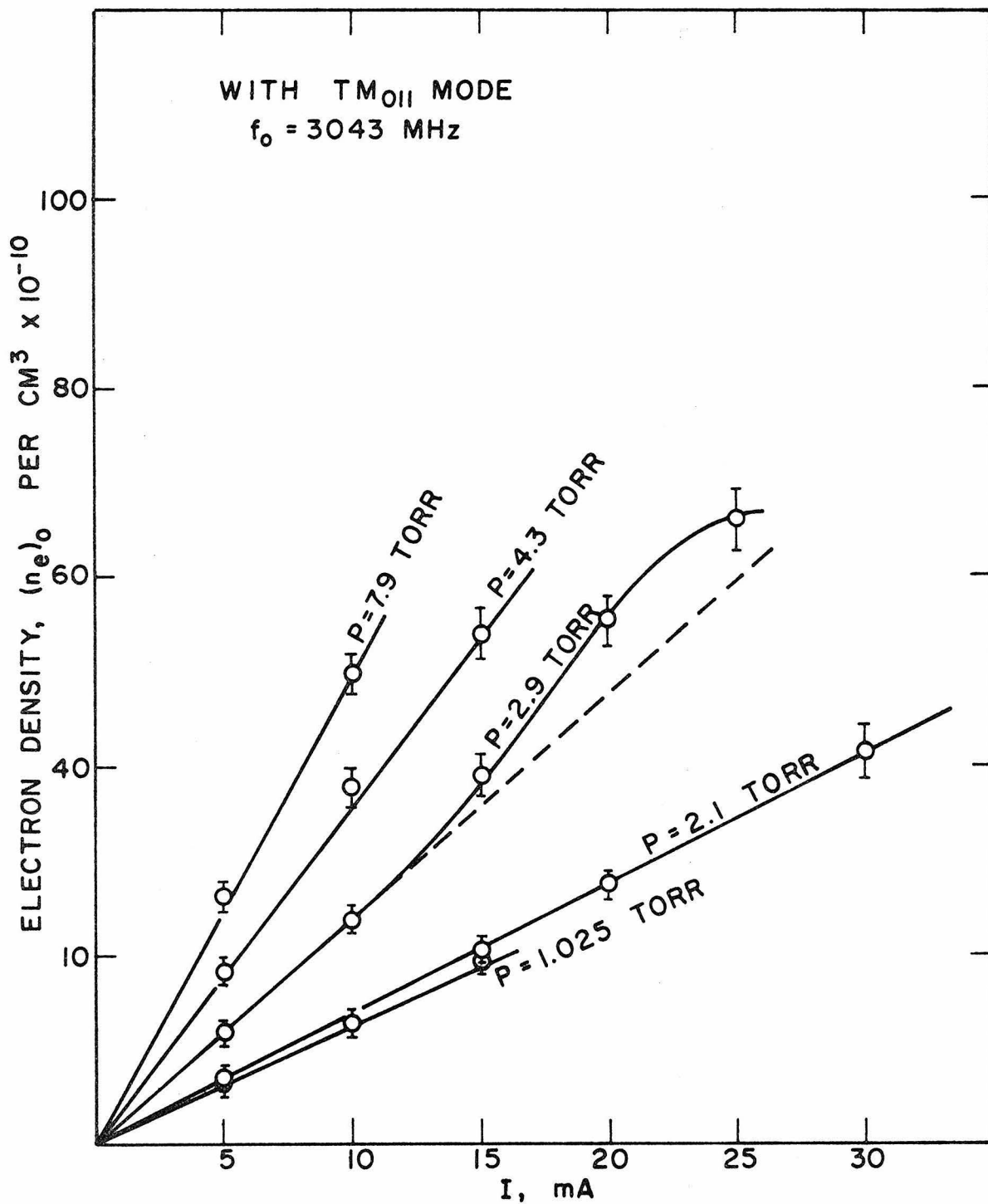


Fig. 11. Electron densities in the positive column of pure neon

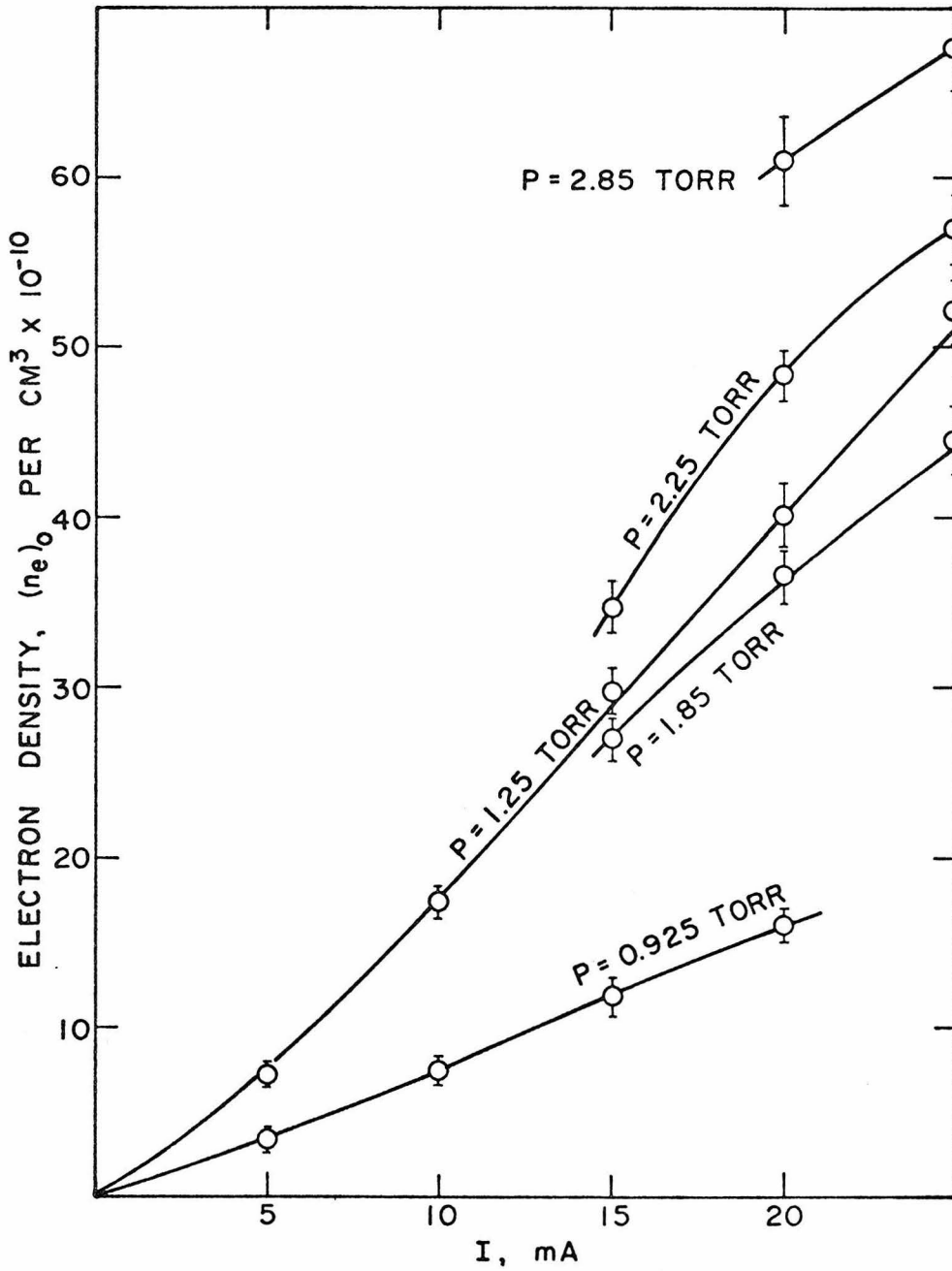


Fig. 12. Electron densities in the positive column of pure argon

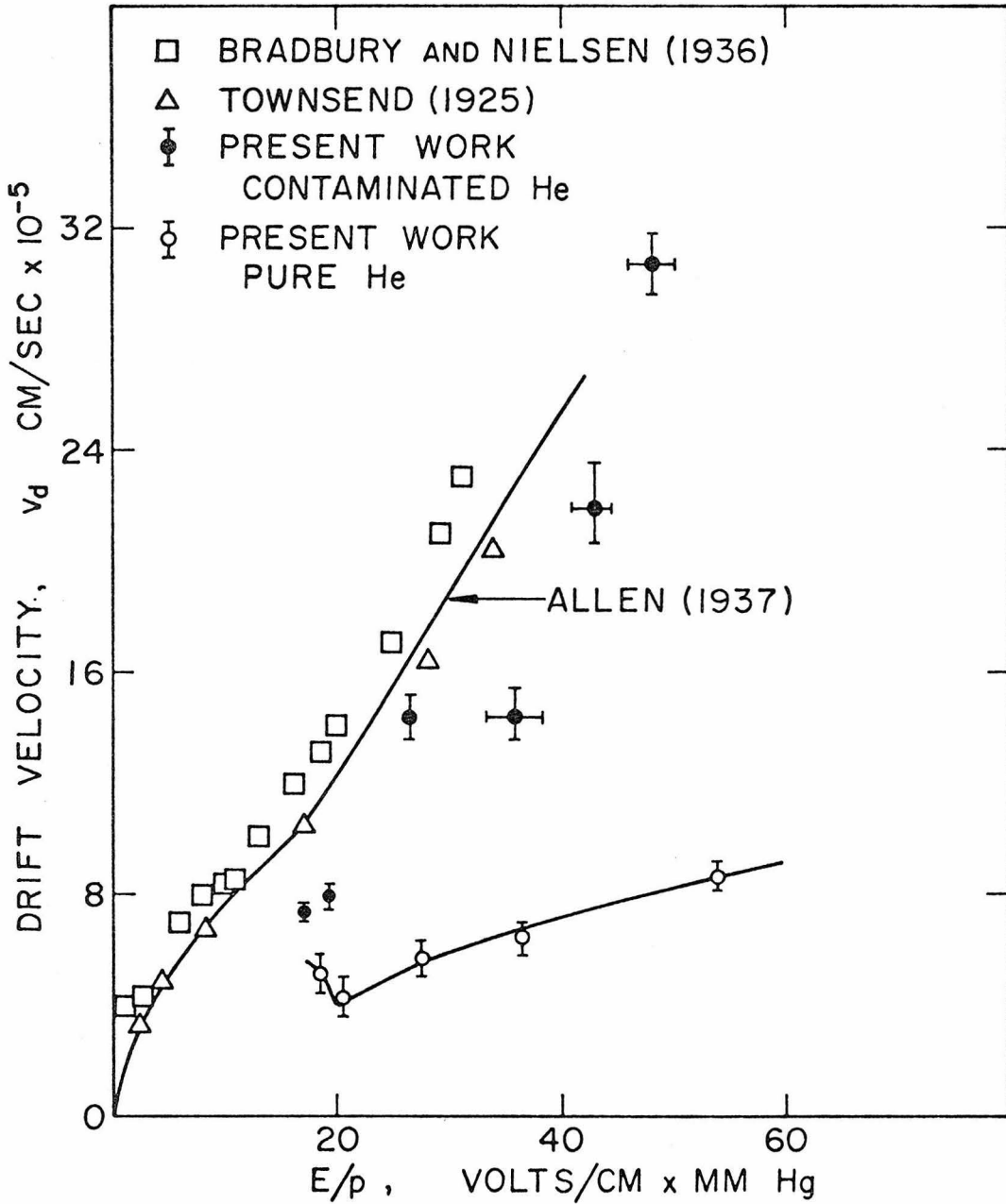


Fig. 13. Drift velocities of electrons in helium

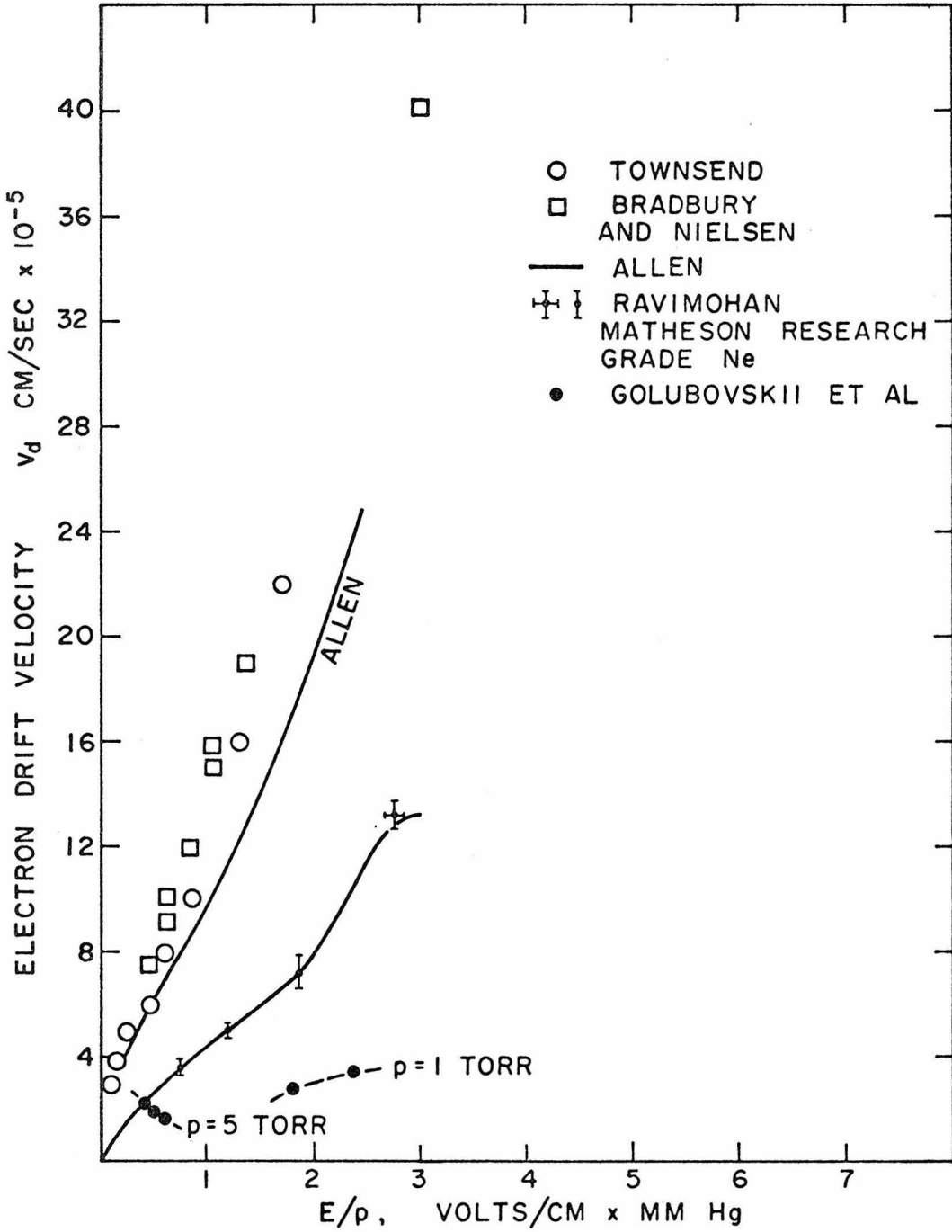


Fig. 14. Drift velocities of electrons in neon

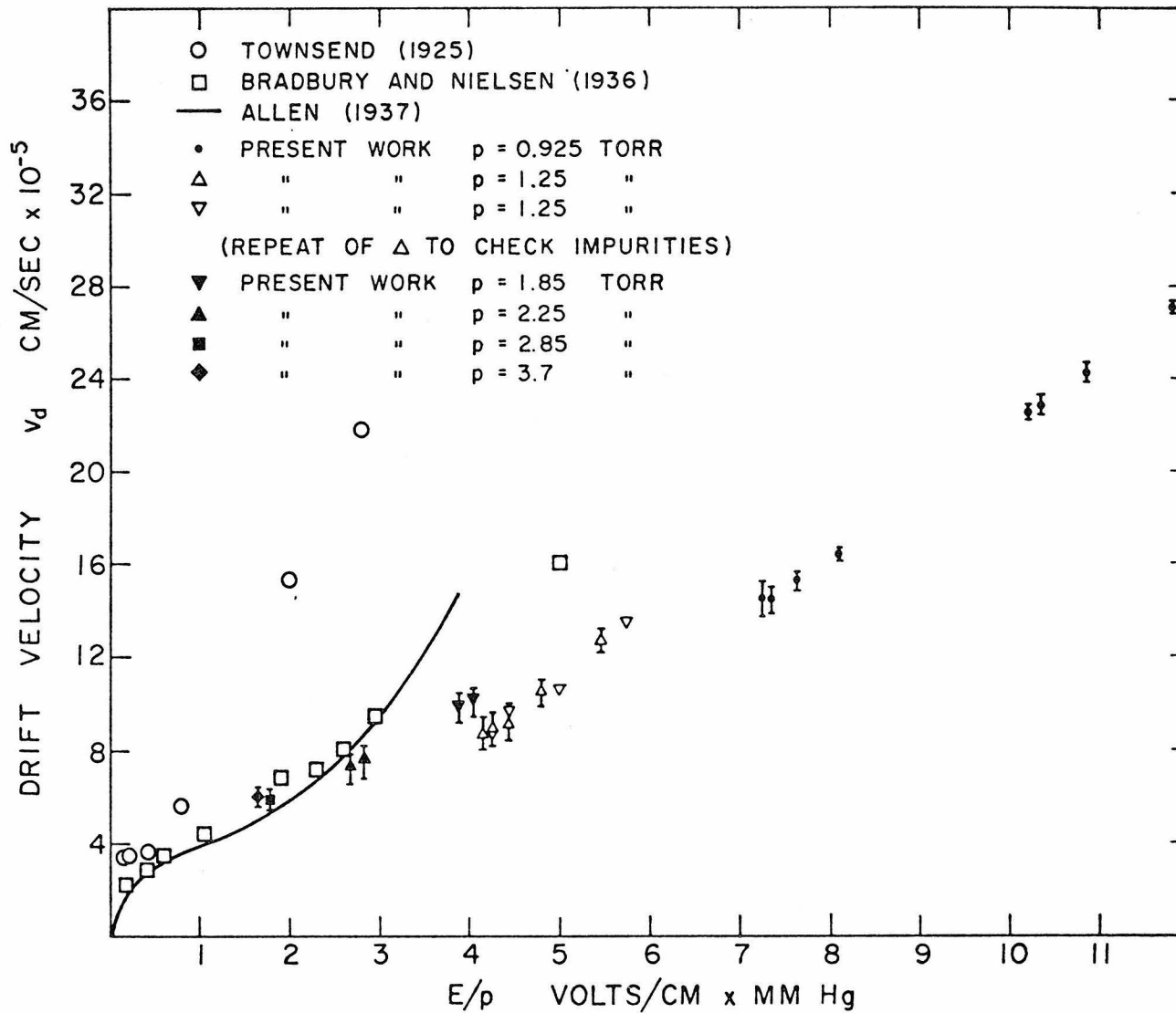


Fig. 15. Drift velocities of electrons in argon

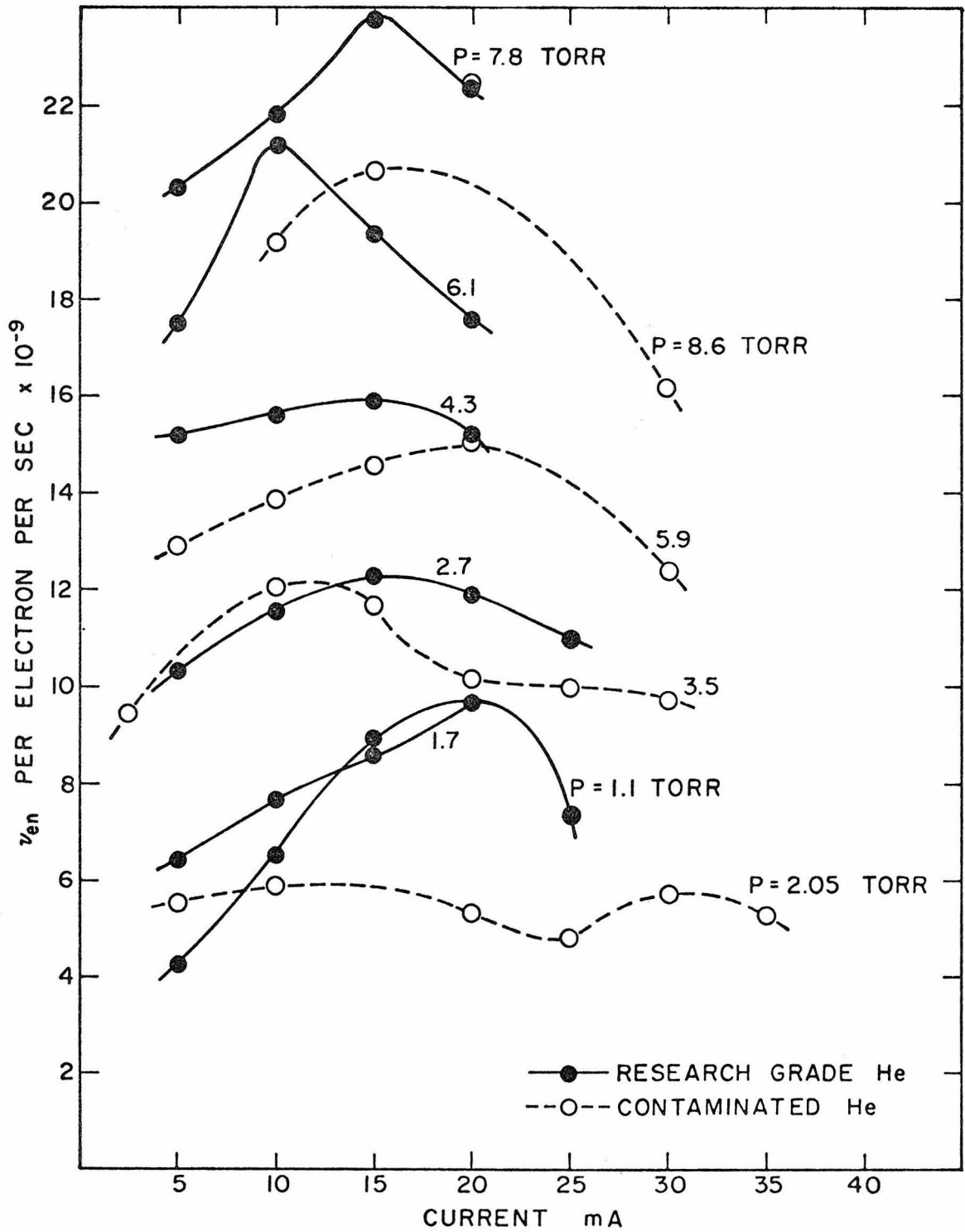


Fig. 16. Electron-neutral collision frequency in helium

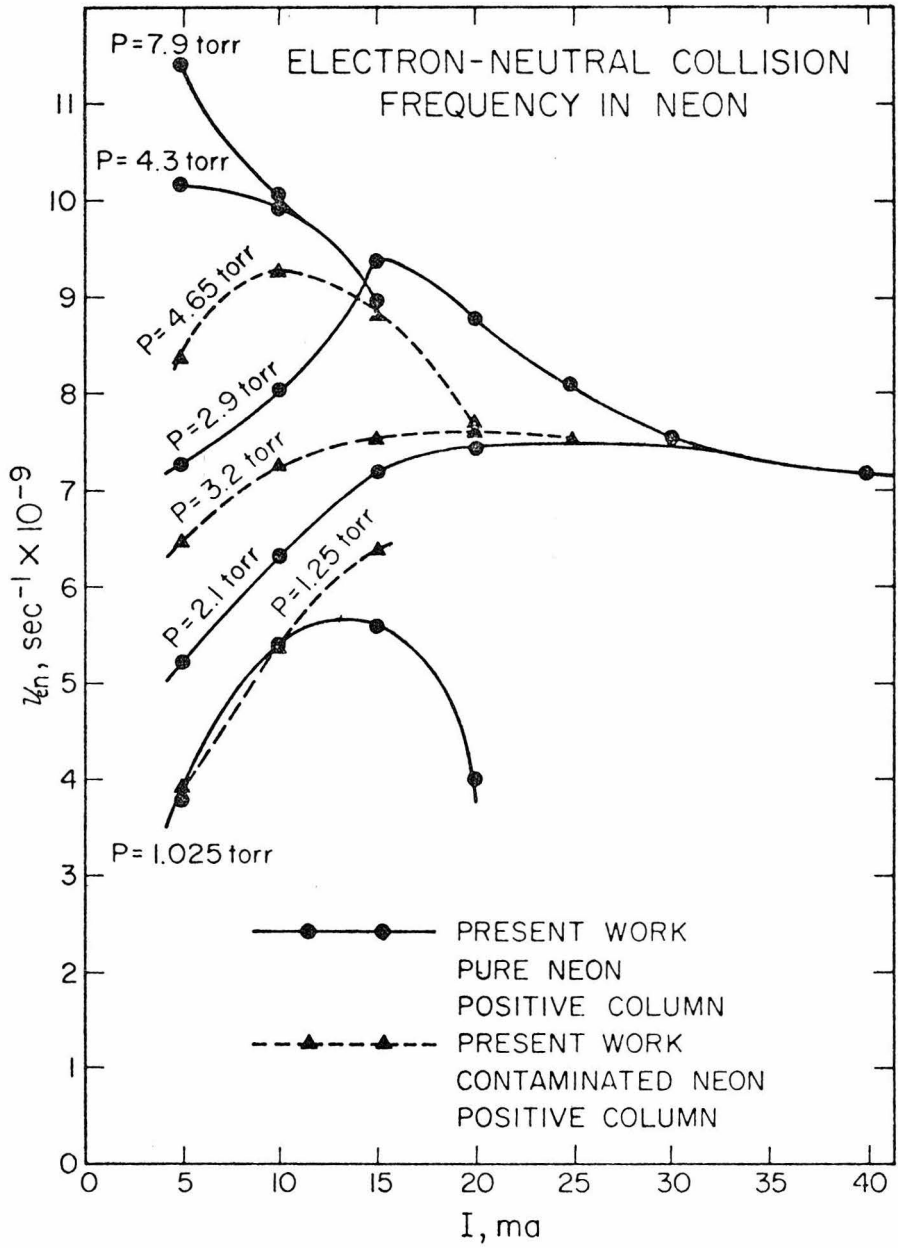


Fig. 17. Electron-neutral collision frequency in neon

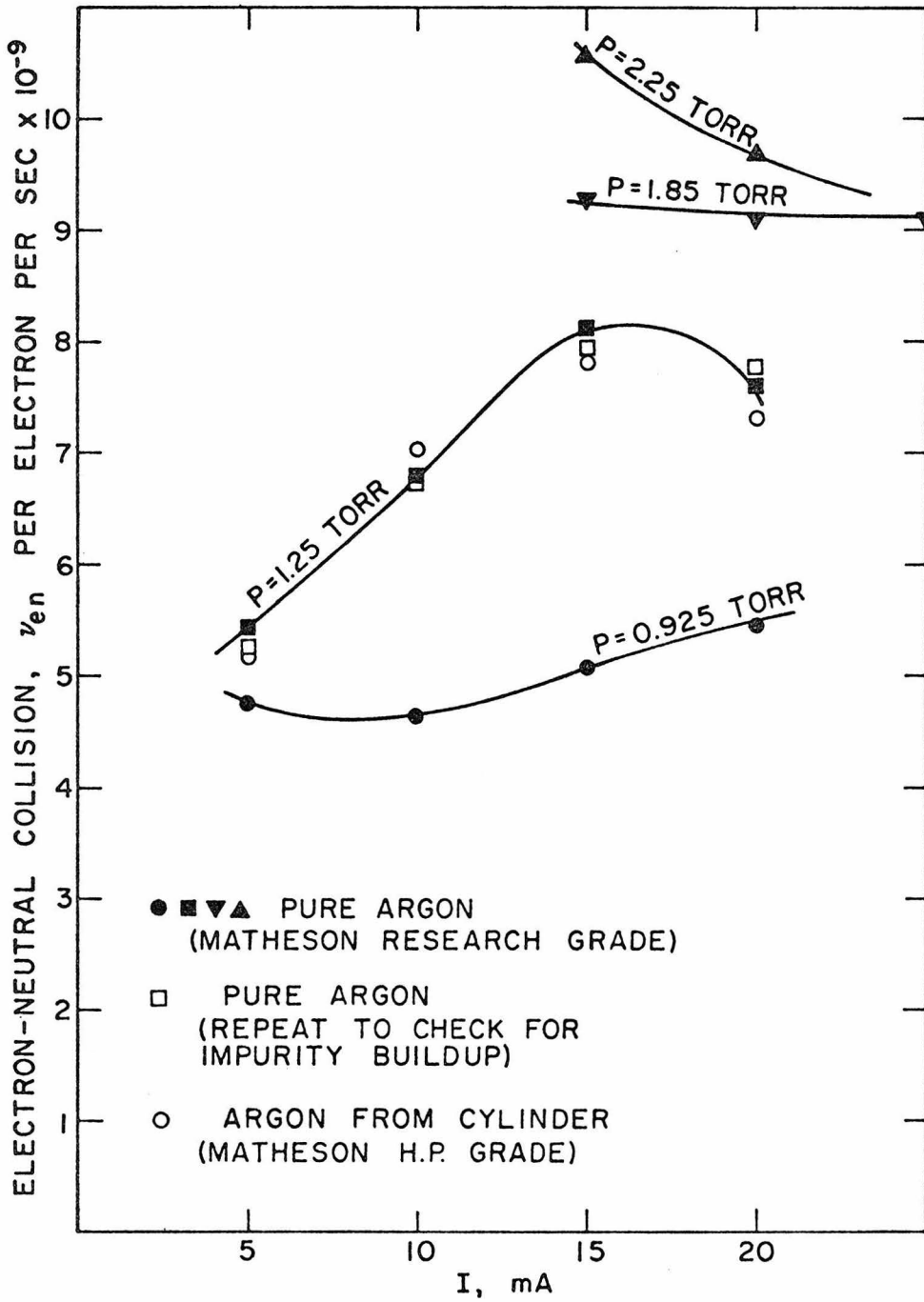


Fig. 18. Electron-neutral collision frequency in argon

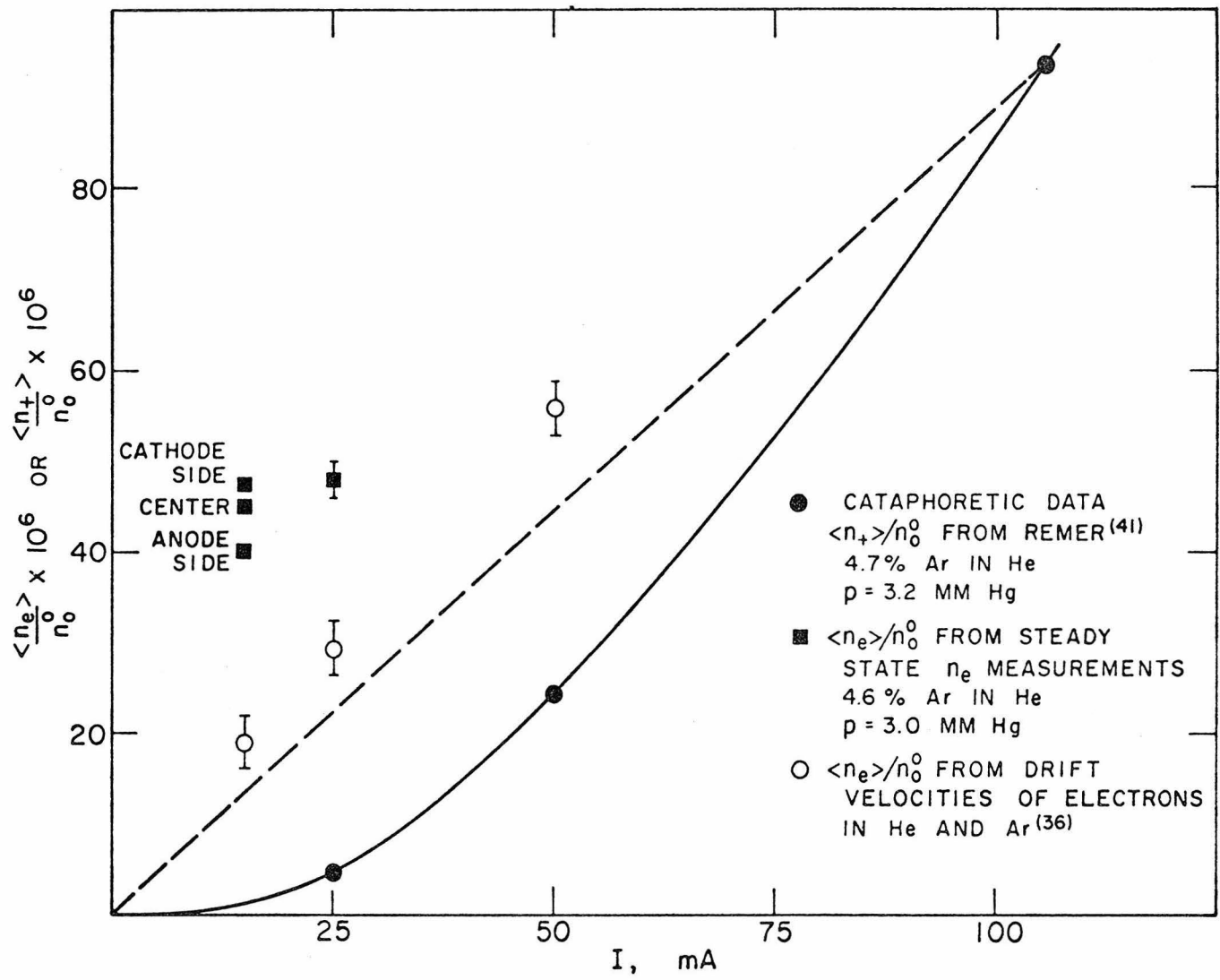


Fig. 19. Levels of ionization in a He-Ar mixture

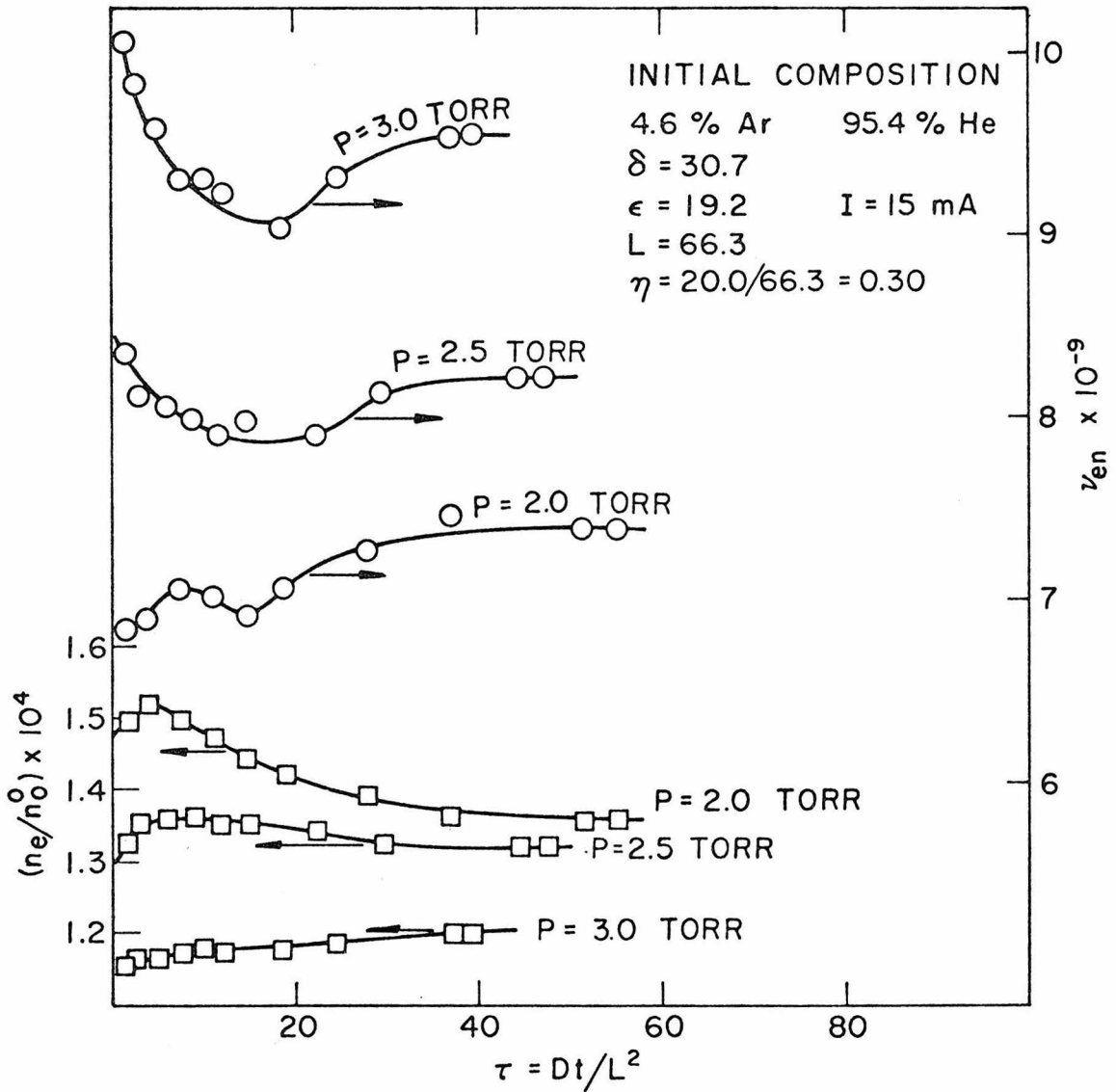


Fig. 20. Electron density and collision frequency vs. time in helium-argon mixtures at cathode end

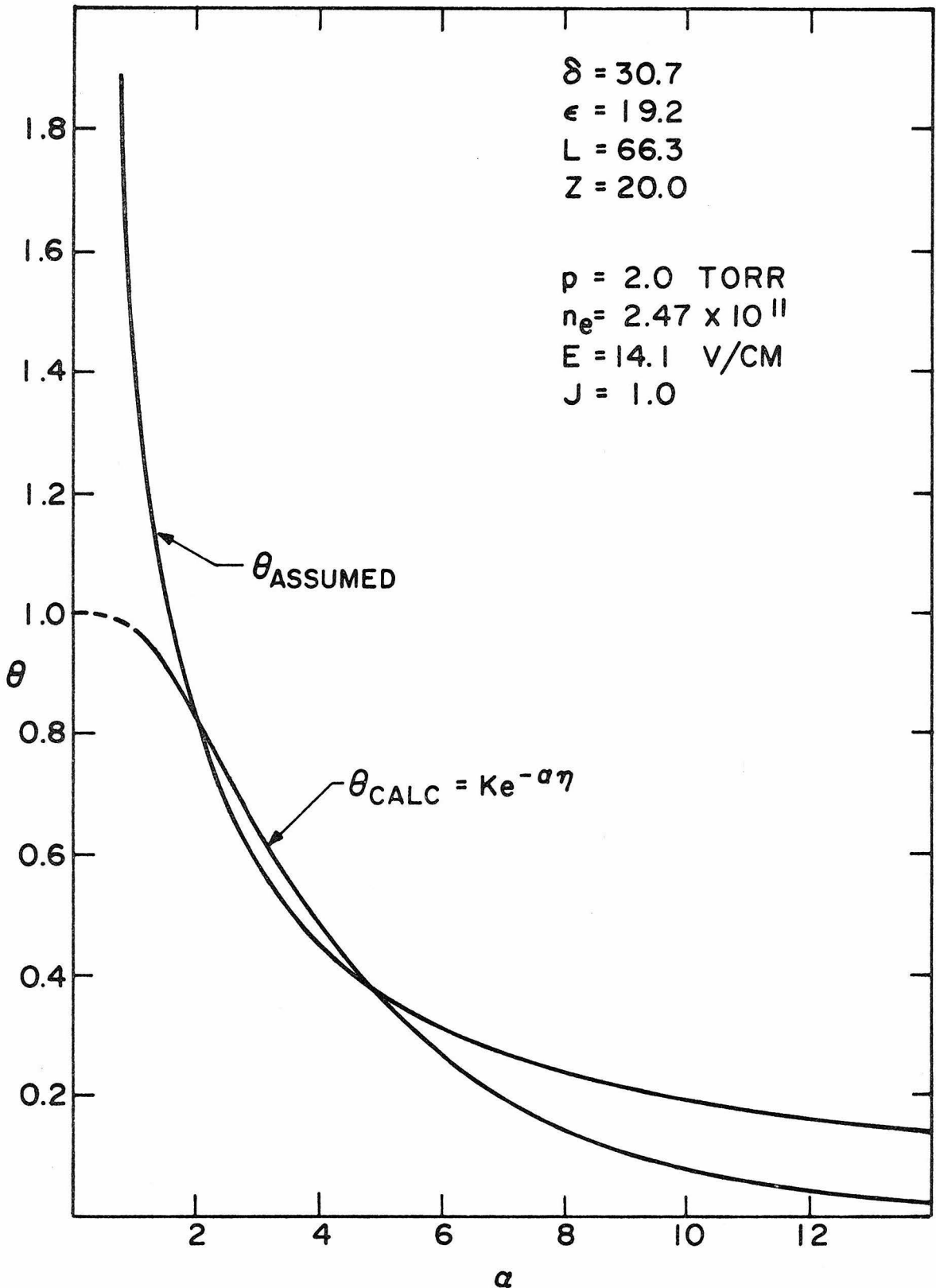


Fig. 21. Nature of solution to cataphoresis equations--normal case

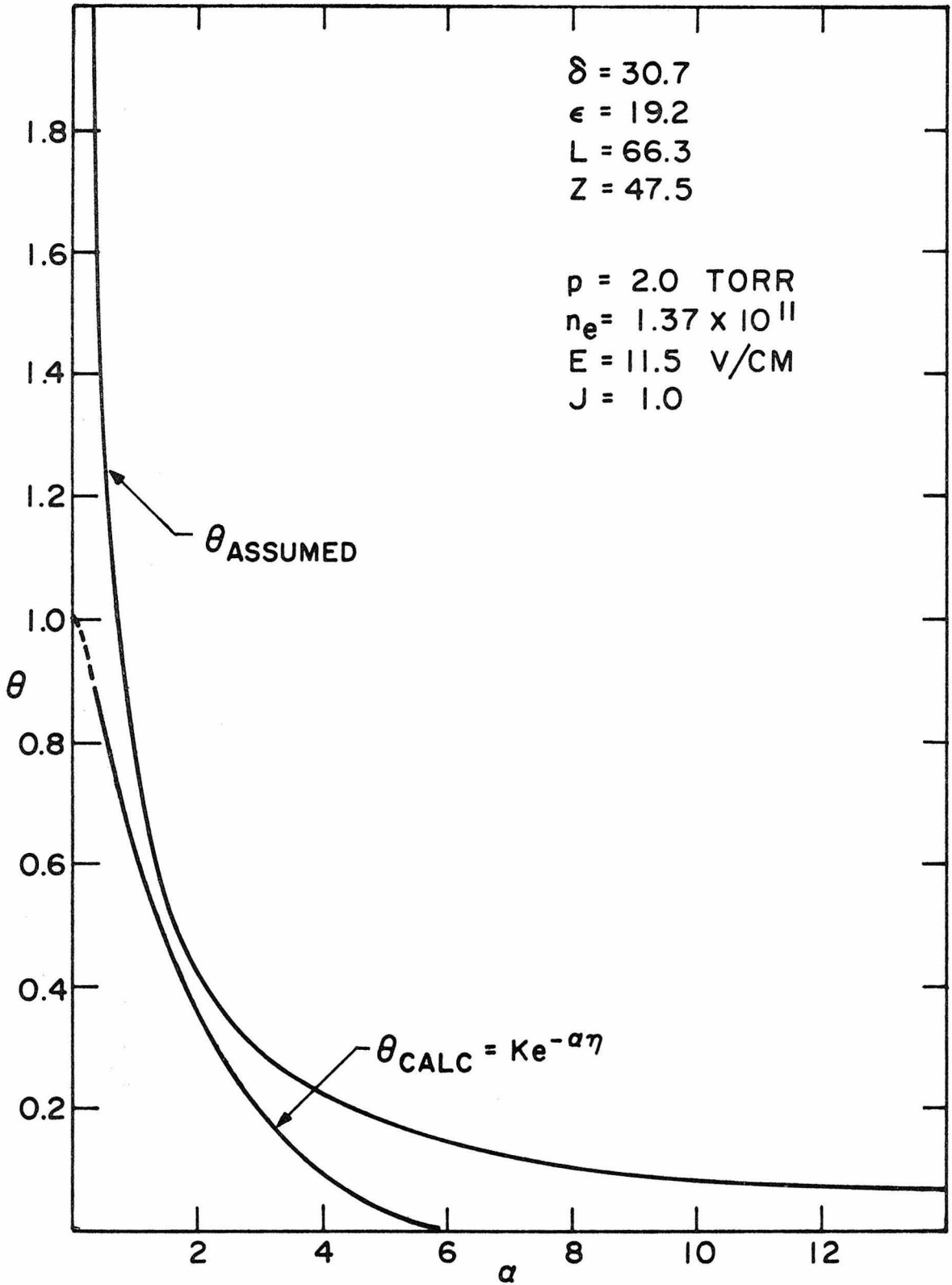


Fig. 22. Nature of solution to cataphoresis equations---anomalous case

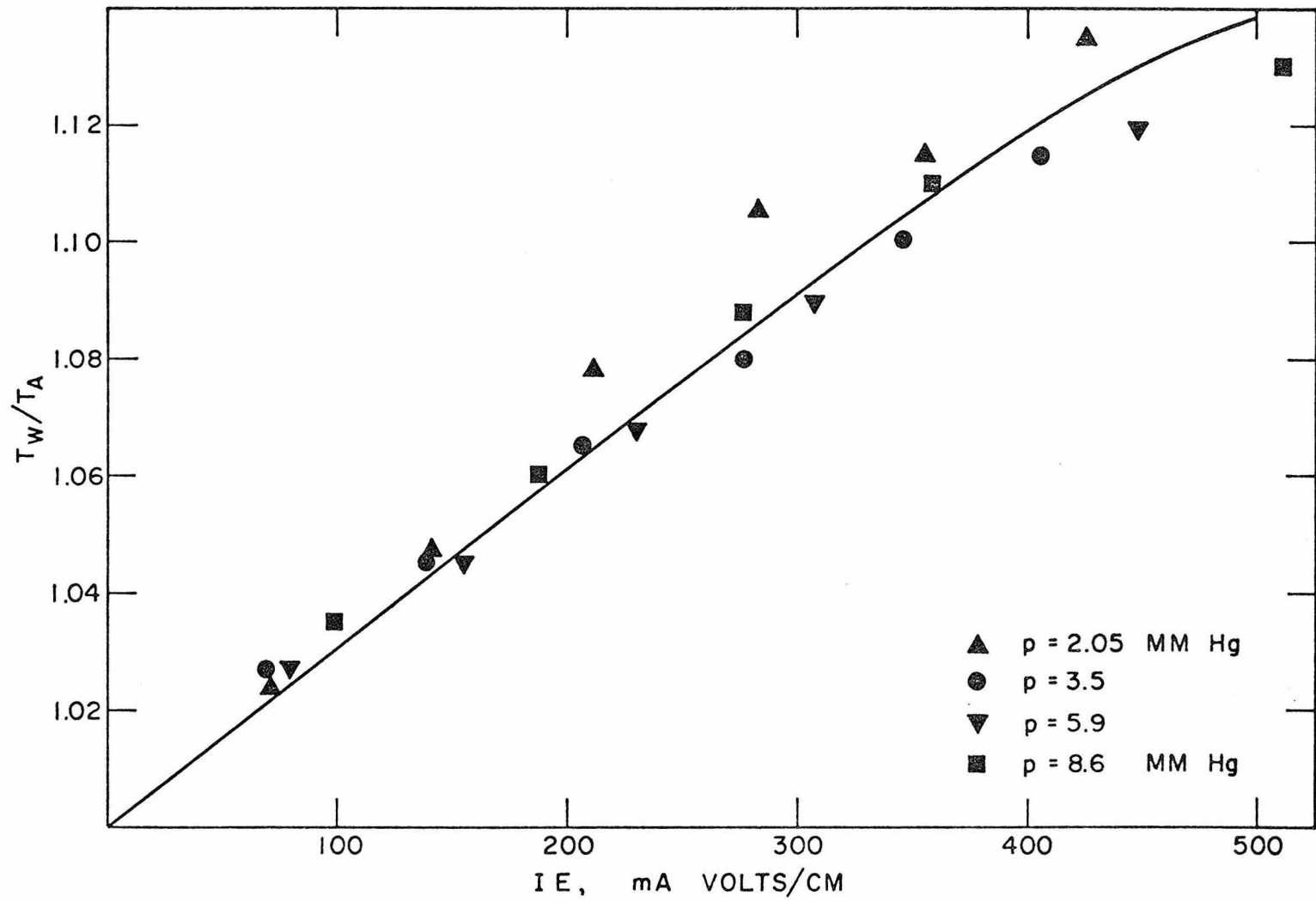


Fig. 23. Wall temperatures in He discharges

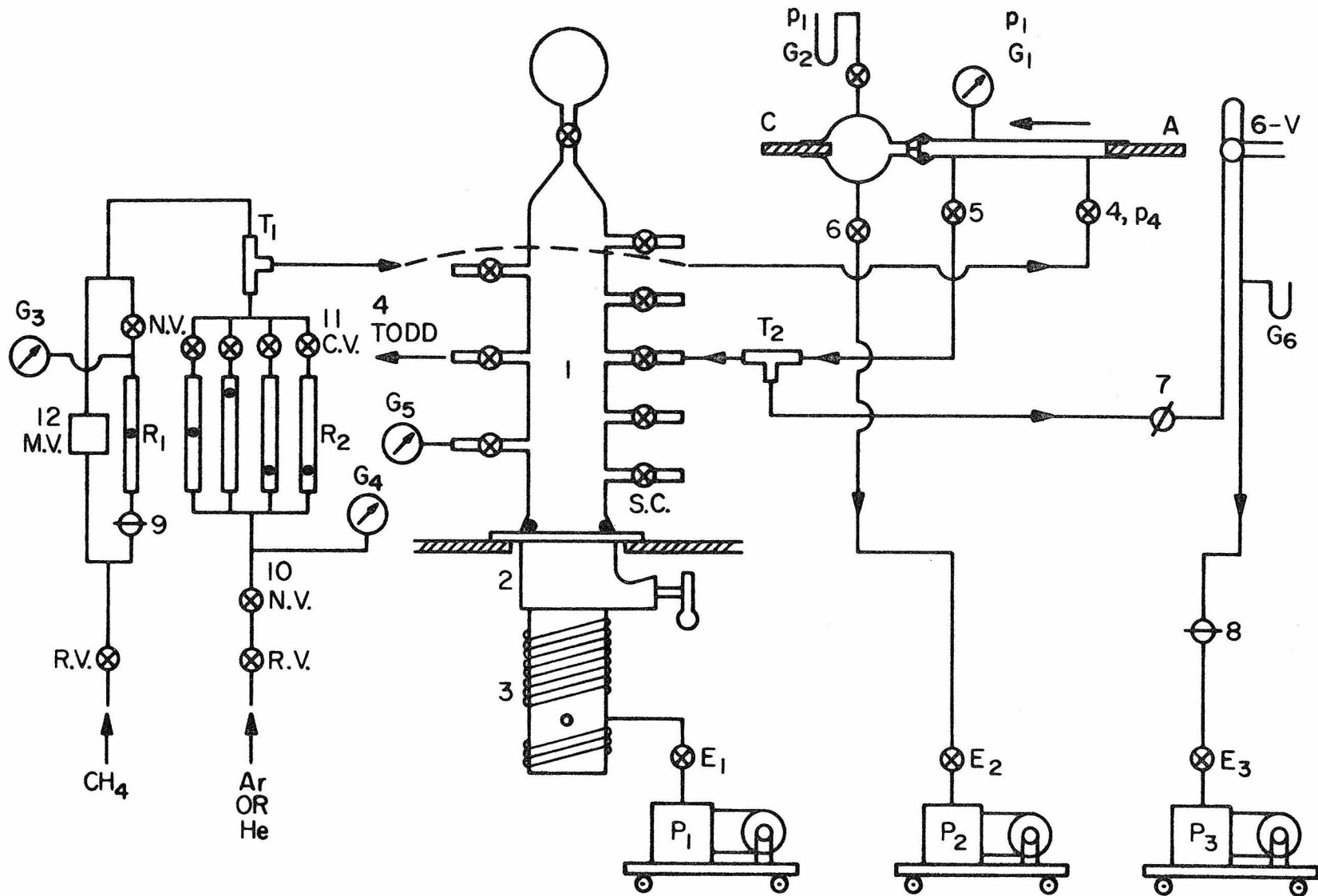
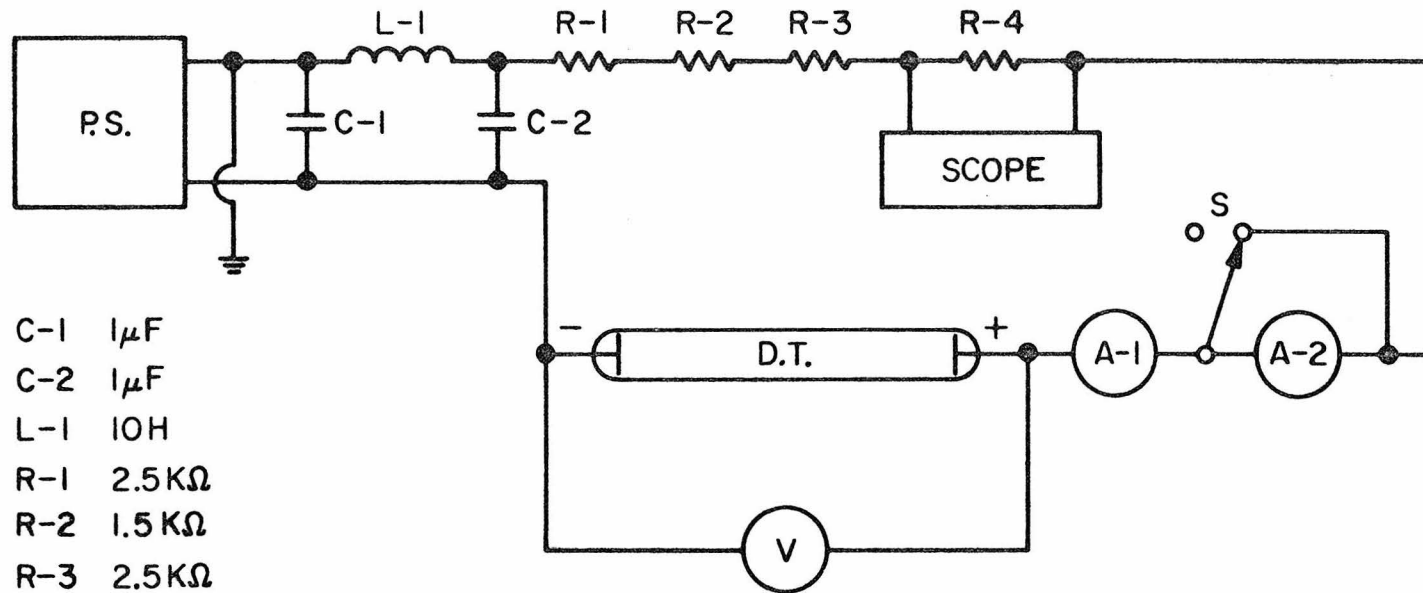


Fig. 25. The gas flow system

Fig. 25. Gas Flow System

A	5/16" dia. molybdenum anode
C	5/16" dia. molybdenum cathode
E ₁ - E ₃	Edwards valves
G ₁ , G ₃ , G ₄ , G ₅	0-50 torr Bourdon type absolute pressure gauges
G ₂ , G ₆	0-5 torr McLeod gauges
P ₁ - P ₃	Kinney rotary vacuum pumps
R ₁ , R ₂	Brooks R-2-15 rotameters
T ₁ , T ₂	1/4" Swagelock mixing tees
1	2" dia. 19" length glass manifold (mixing chamber)
2	CVC VSTM2 vacuum gate valve
3	CVC 2" diffusion pump
4,5	6 mm bore Eck and Krebs greased stopcocks
6	2 mm bore Eck and Krebs greased stopcock
7,8,9	Circle Seal 9533B-4CC miniaturized plug shut-off valves
R.V.	Whitey 1/4" roughing valves
N.V.	Nupro needle valves
M.V.	Circle Seal MV92T1-4CC micrometer valve
C.V.	Circle Seal M92T1-4CC flow control valves
S.C.	6 mm bore Eck and Krebs greased stopcocks
6.V.	Loenco 6-way valve (Fig. 36) for introducing sample into chromatograph



C-1 $1\mu\text{F}$
 C-2 $1\mu\text{F}$
 L-1 10H
 R-1 $2.5\text{K}\Omega$
 R-2 $1.5\text{K}\Omega$
 R-3 $2.5\text{K}\Omega$
 R-4 10.8Ω
 S SWITCH

P.S. - CVC-LC031 HIGH VOLTAGE
 POWER SUPPLY. 5000V, 750mA

D.T. - DISCHARGE TUBE

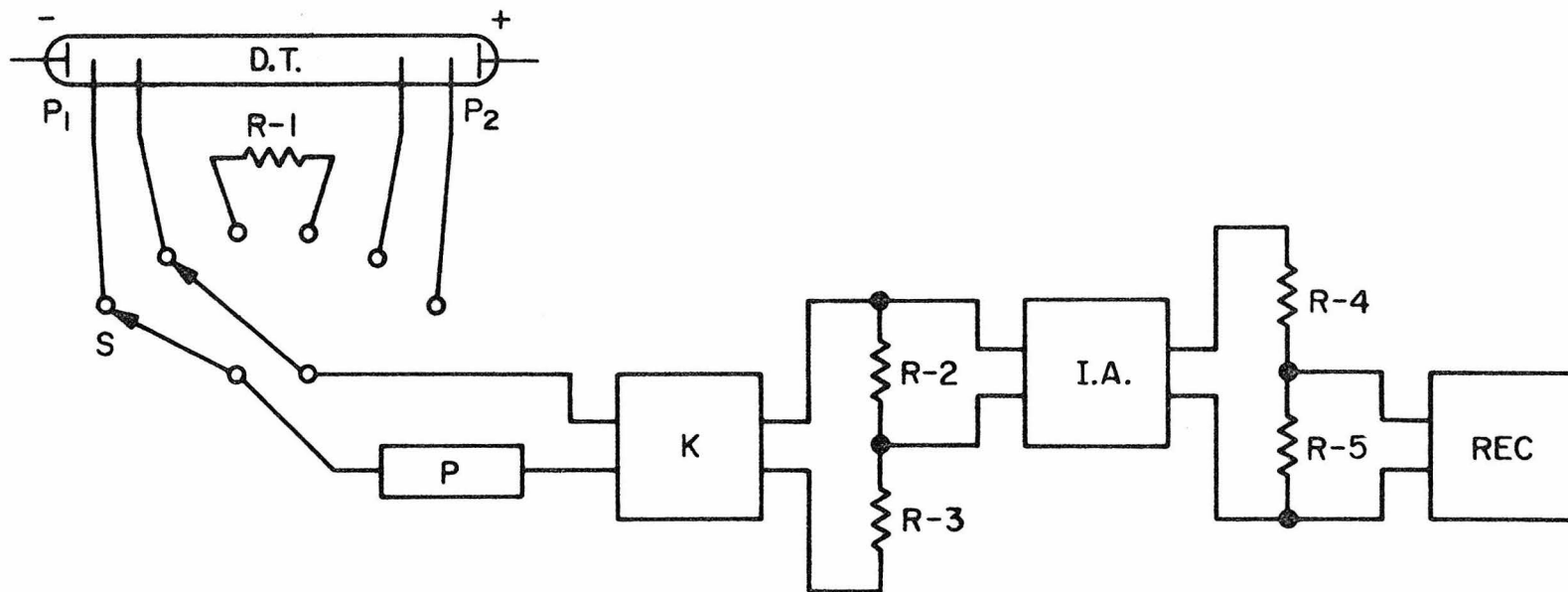
SCOPE - HP-122AR OSCILLOSCOPE

A-1 - TRIPLETT 420-G, 50 mA

A-2 - WESTON, 6mA

V - TRIPLETT 420, 5000V

Fig. 26. D.C. power supply and measuring circuit



R-1 100 K Ω
 R-2 2 Ω
 R-3 1400 Ω
 R-4 45 Ω
 R-5 1000 Ω

D.T. - DISCHARGE TUBE
 S - 2P3T SWITCH
 P - KEITHLEY 6103A
 1000:1 DIVIDER PROBE
 K - KEITHLEY 601 ELECTROMETER
 I.A. - FLUKE A88 ISOLATION AMPLIFIER
 REC - LEEDS & NORTHRUP SPEEDOMAX W

Fig. 27. Circuit for electric field measurement

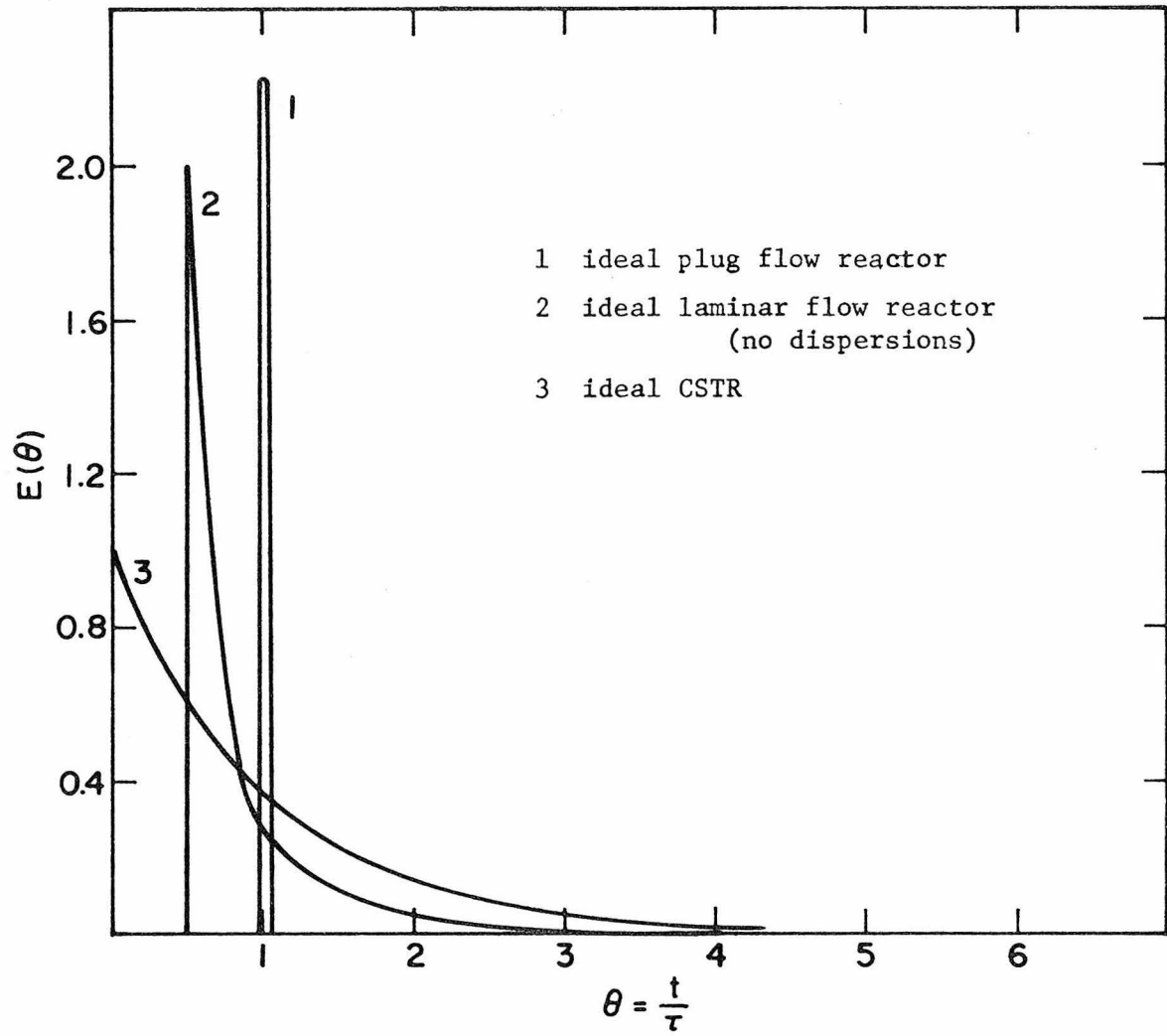


Fig. 29. Comparison of residence time distribution in idealized reactors

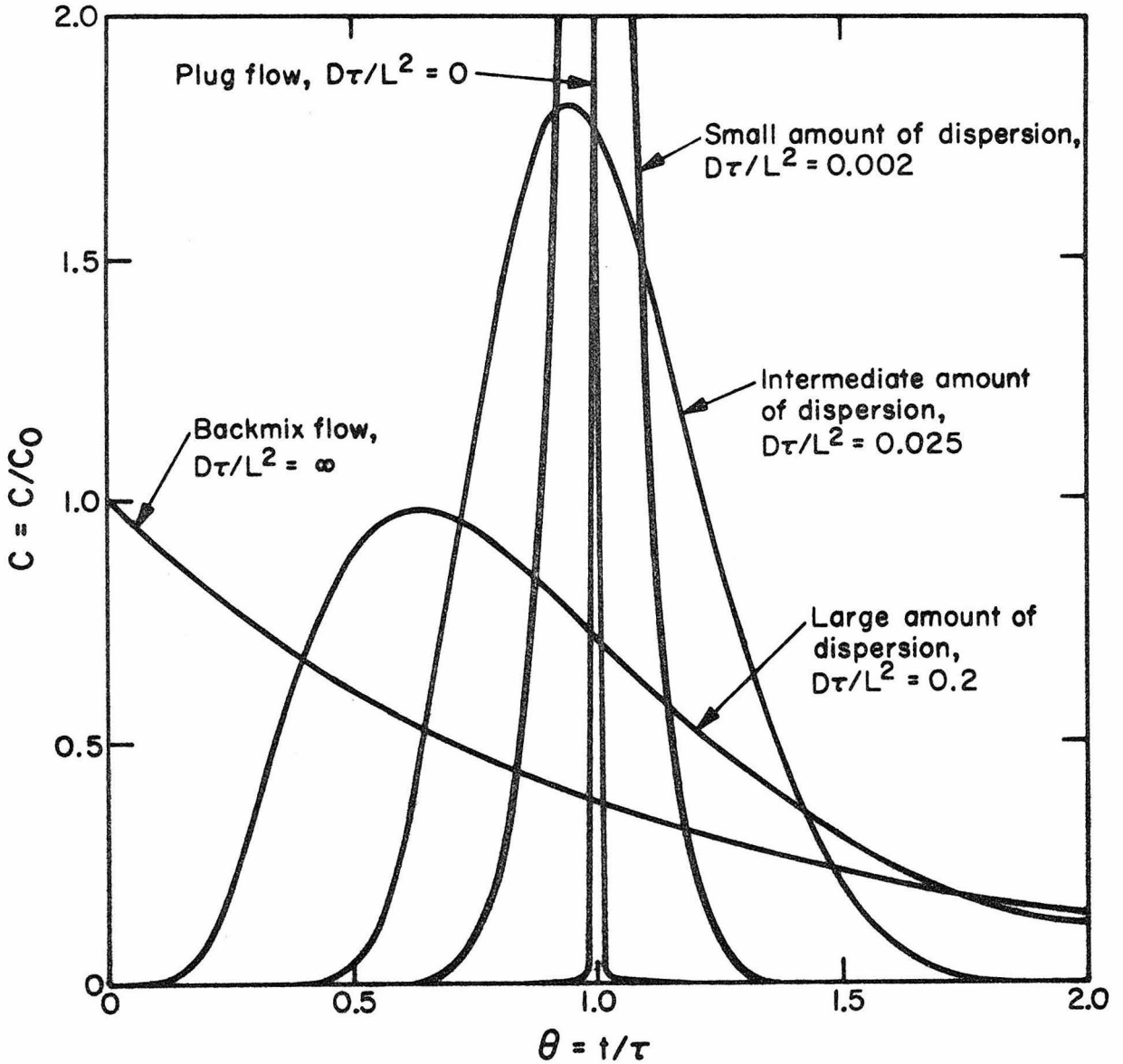


Fig. 30. Effect of varying amounts of longitudinal dispersion on the residence time distribution

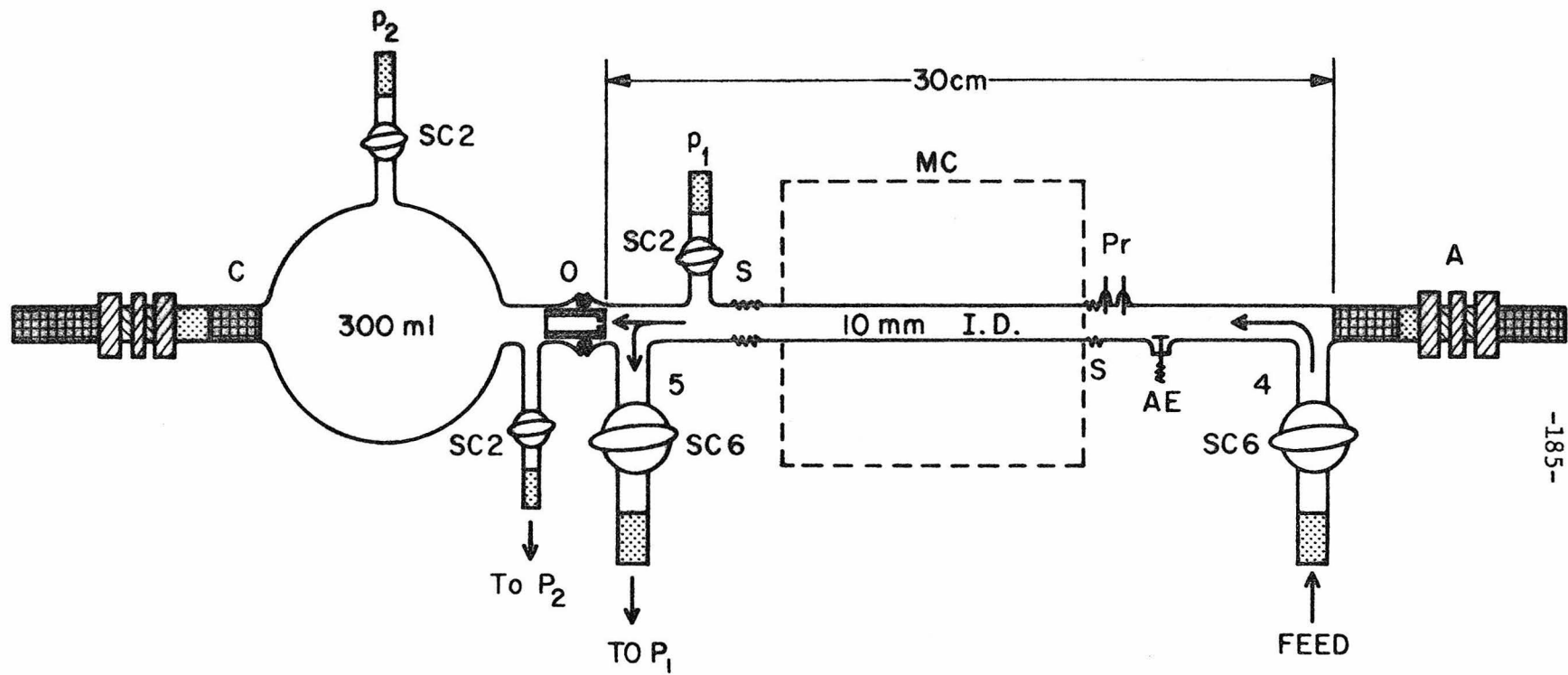


Fig. 31. Glow discharge tube 2

Fig. 31

A	5/16" molybdenum anode and Swagelock union
AE	Auxiliary Ni disc electrode 3/8" dia.
C	5/16" molybdenum cathode and Swagelock union
MC	Microwave cavity
O	Orifice and O-ring support (baked soapstone)
P ₁ , P ₂	Pressure gauges
P ₂	Vacuum pump
Pr	20 mil tungsten wires 1.0 cm apart for electric field measurement and double Langmuir probe
S	Quartz-pyrex seal
SC2	2 mm bore Eck and Krebs greased stopcock
SC6	6 mm bore Eck and Krebs greased stopcock
4	Gas inlet
5	Gas outlet

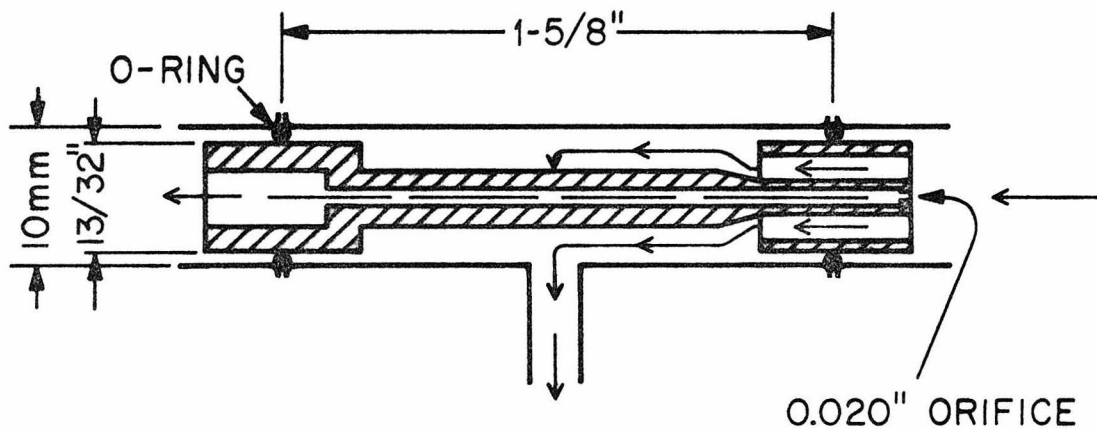


Fig. 32. Positive column isolation system

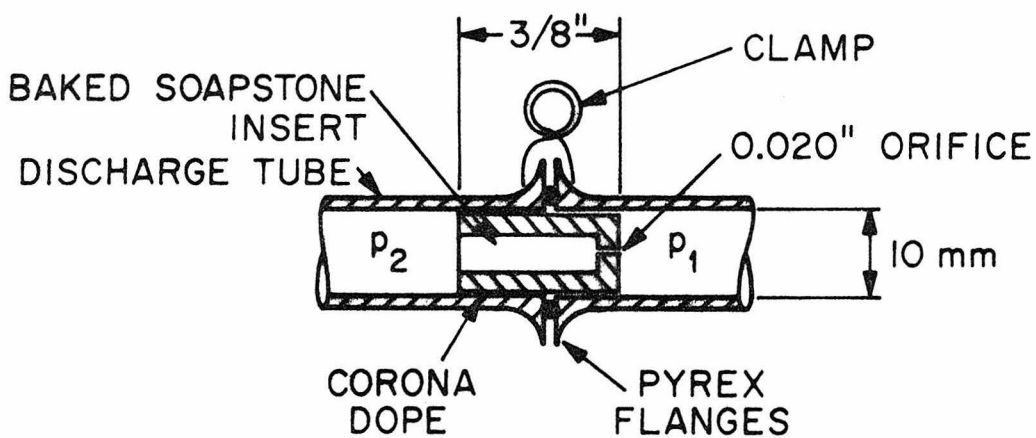


Fig. 33. Simple design of the orifice

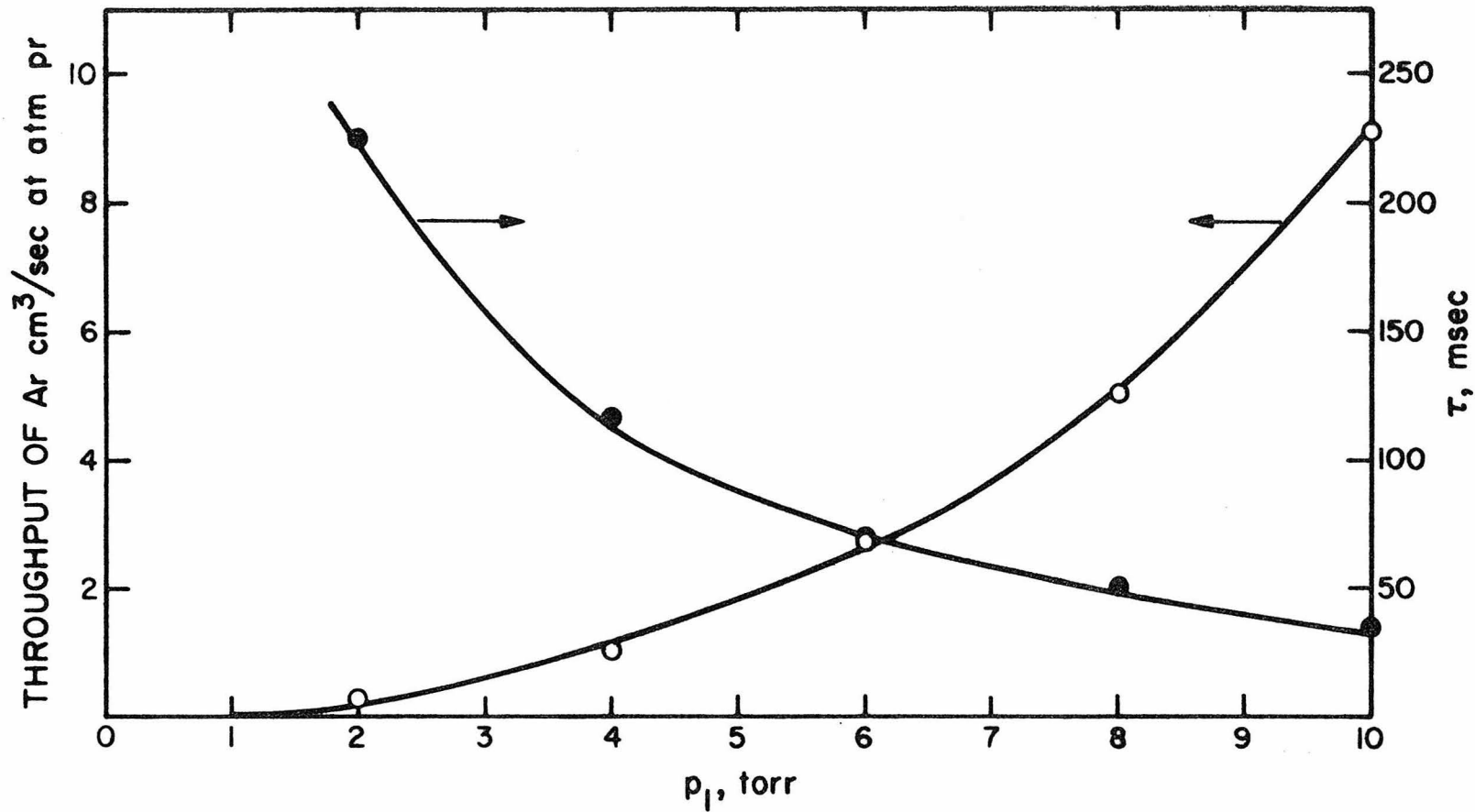


Fig. 34. Throughput of Ar and residence time vs. pressure p_1

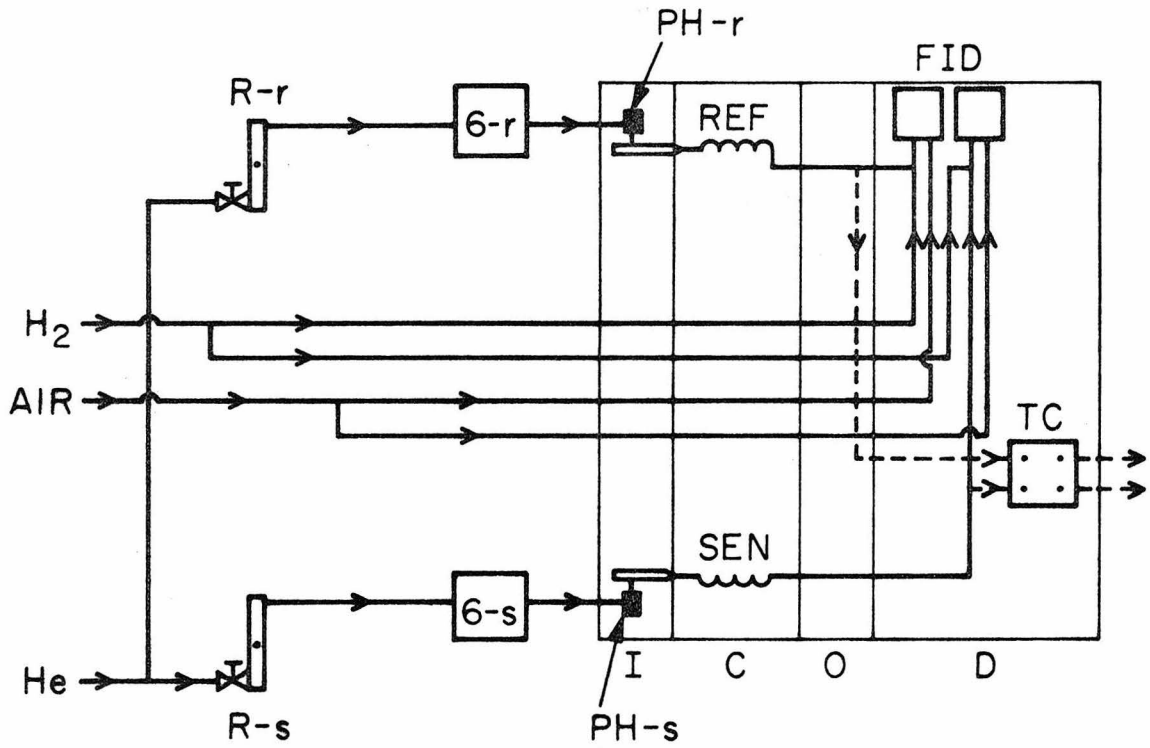
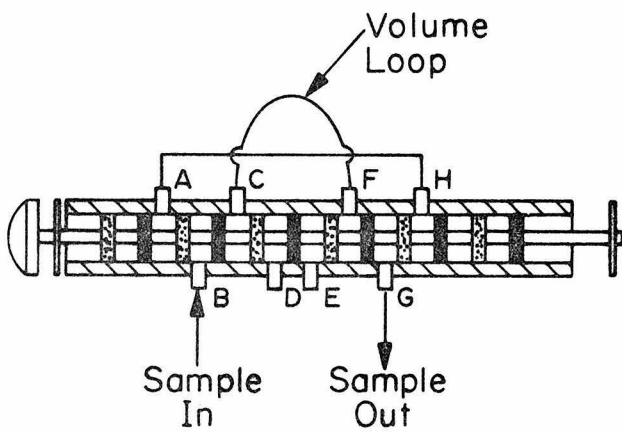


Fig. 35. Gas flow in the chromatographic system

Fig. 35. Gas Flow in the Chromatographic System

R-r, R-s	Rotameters for carrier gas 0-50 cm ³ /min
6-r, 6-s	Sample introduction valve (6-way)
PH-r, PH-s	Preheaters
REF	Reference column
SEN	"Sense" column
FID	Dual flame ionization detector
TC	Dual thermocouple detector
I	Injection oven
C	Temperature programmed column oven
O	Outlet oven
D	Detector oven



"O"-RING POSITIONS

- ▨ "Pick-Up" Position
- "Inject" Position

NORMAL CONNECTIONS

- B & G - Sample Gas
- D & E - Carrier Gas

Fig. 36. LOENCO 6-way valve for sample injection into chromatograph

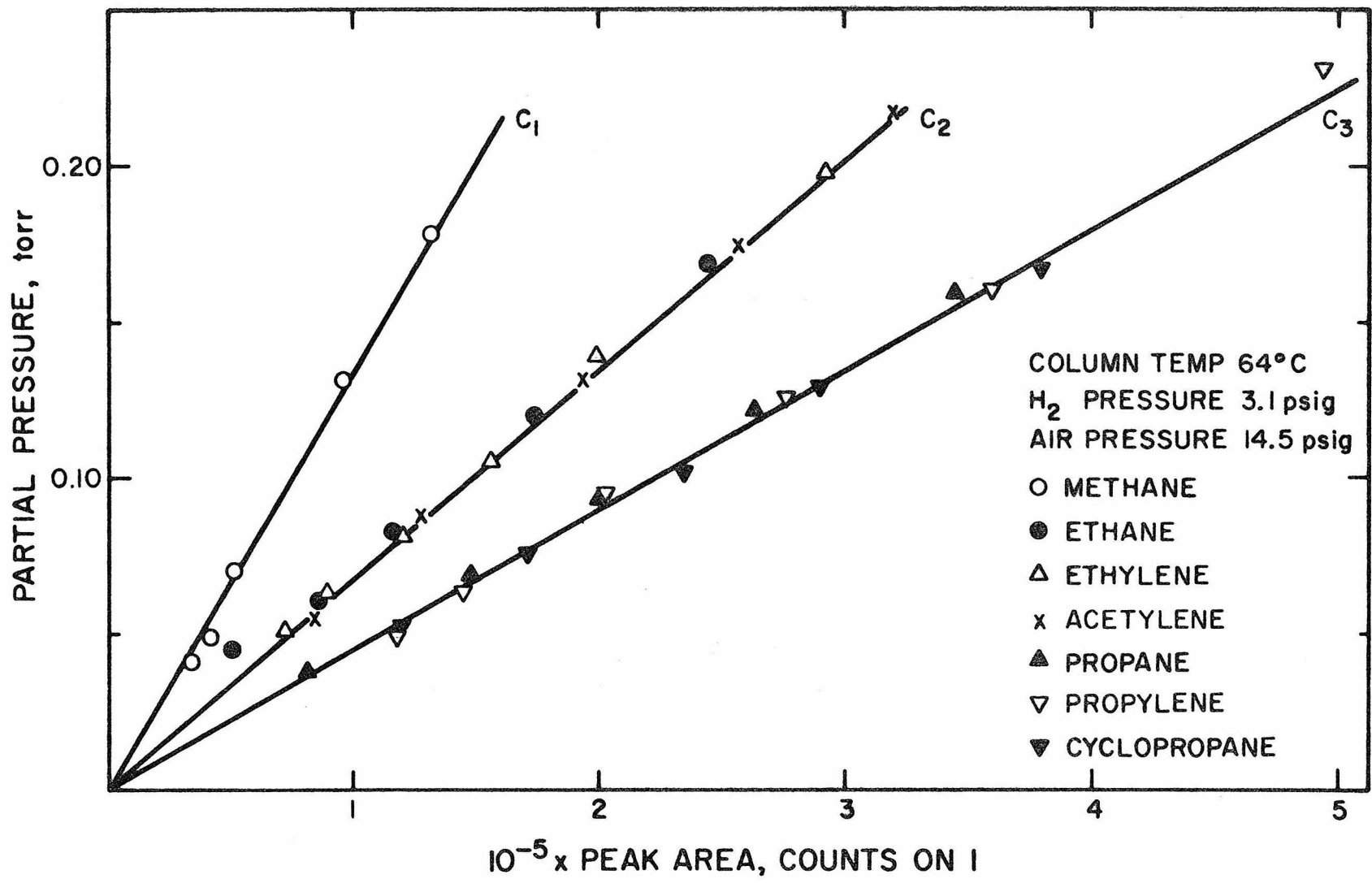


Fig. 37. Quantitative calibration of the flame ionization detector

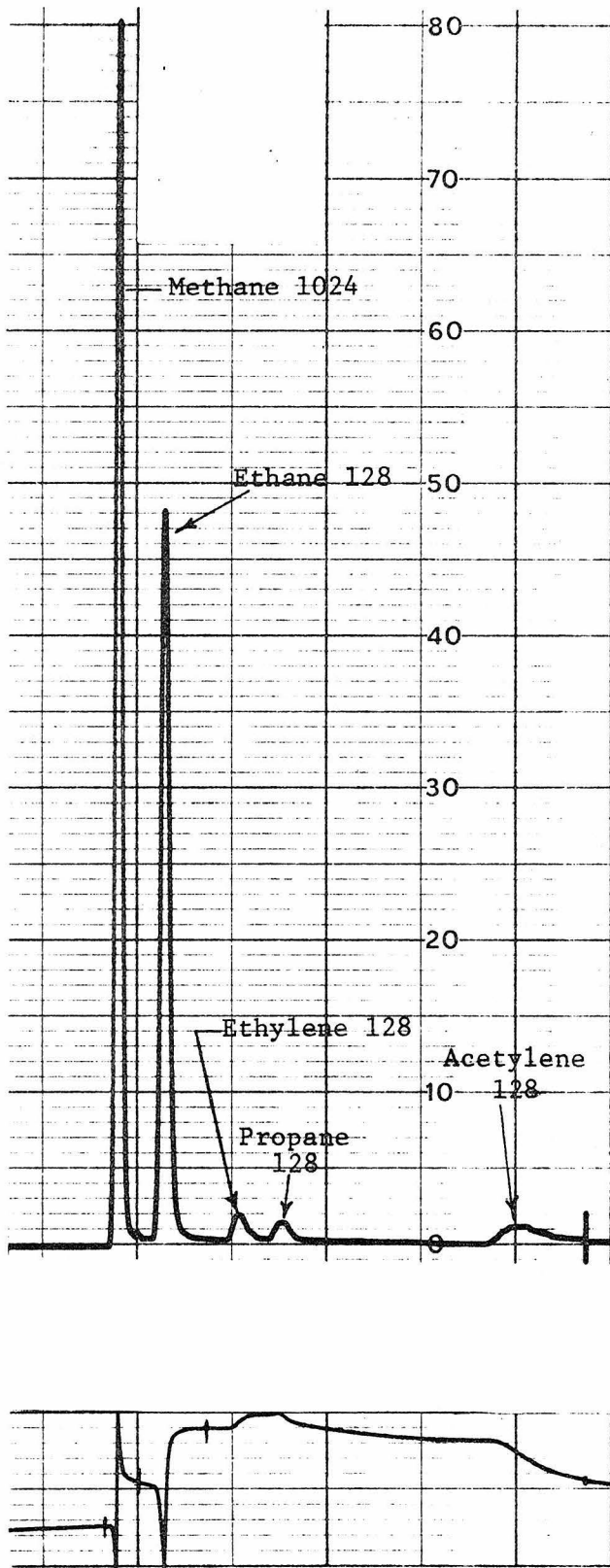


Fig. 38. Typical separation of lower hydrocarbons

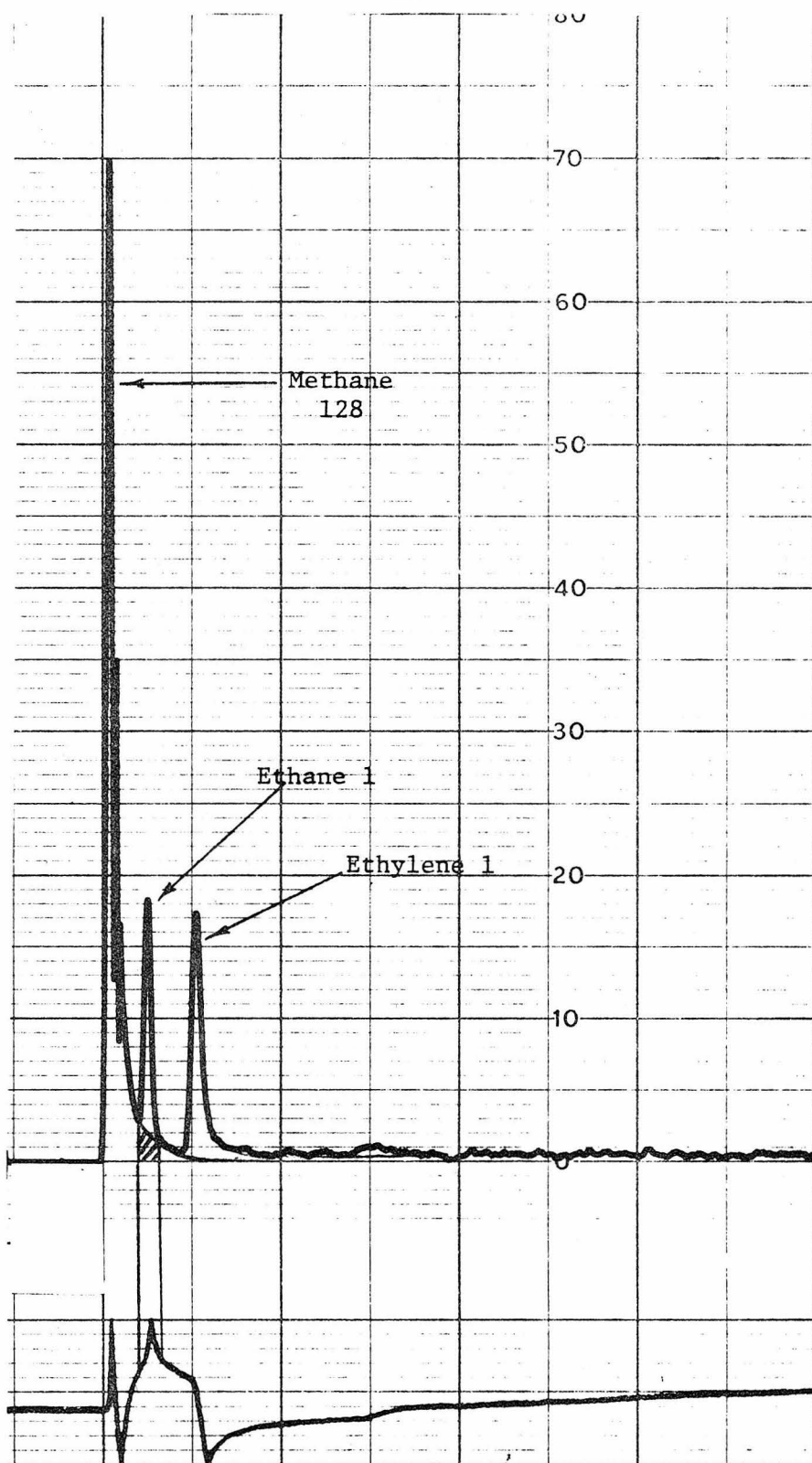


Fig. 39. Atypical separation of lower hydrocarbons

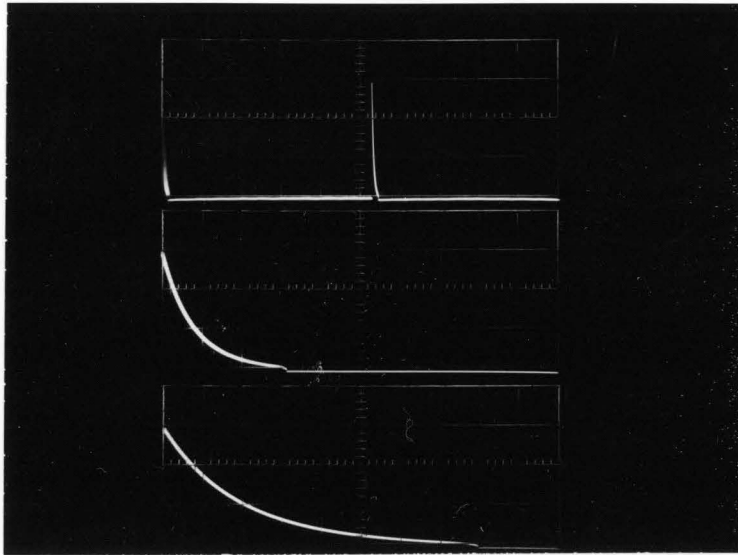


Fig. 40a Voltage v_3 10V/cm

Time Scale: i) 10 msec/cm, ii) 500 μ sec/cm,
iii) 200 μ sec/cm

$$\tau_I = 52 \text{ msec}$$

$$\tau_W = 1.6 \text{ msec}$$

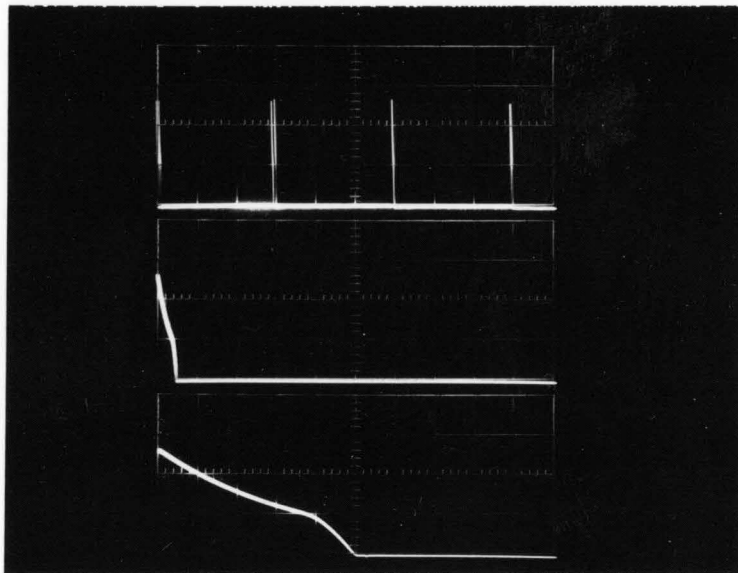


Fig. 40b Voltage v_3 10V/cm

Time Scale: i) 10 msec/cm, ii) 1 msec/cm,
iii) 100 μ sec/cm

$$\tau_I = 30 \text{ msec}$$

$$\tau_W = 0.5 \text{ msec}$$

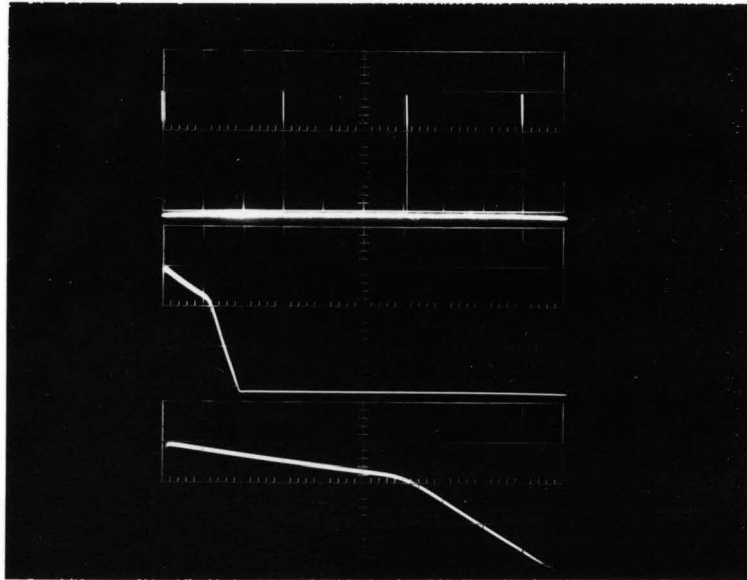


Fig. 40c Voltage v_3 10V/cm

Time Scale: i) 10 msec/cm, ii) 100 μ sec/cm,
iii) 20 μ sec/cm

$\tau_I = 30$ msec

$\tau_W = 200$ μ sec

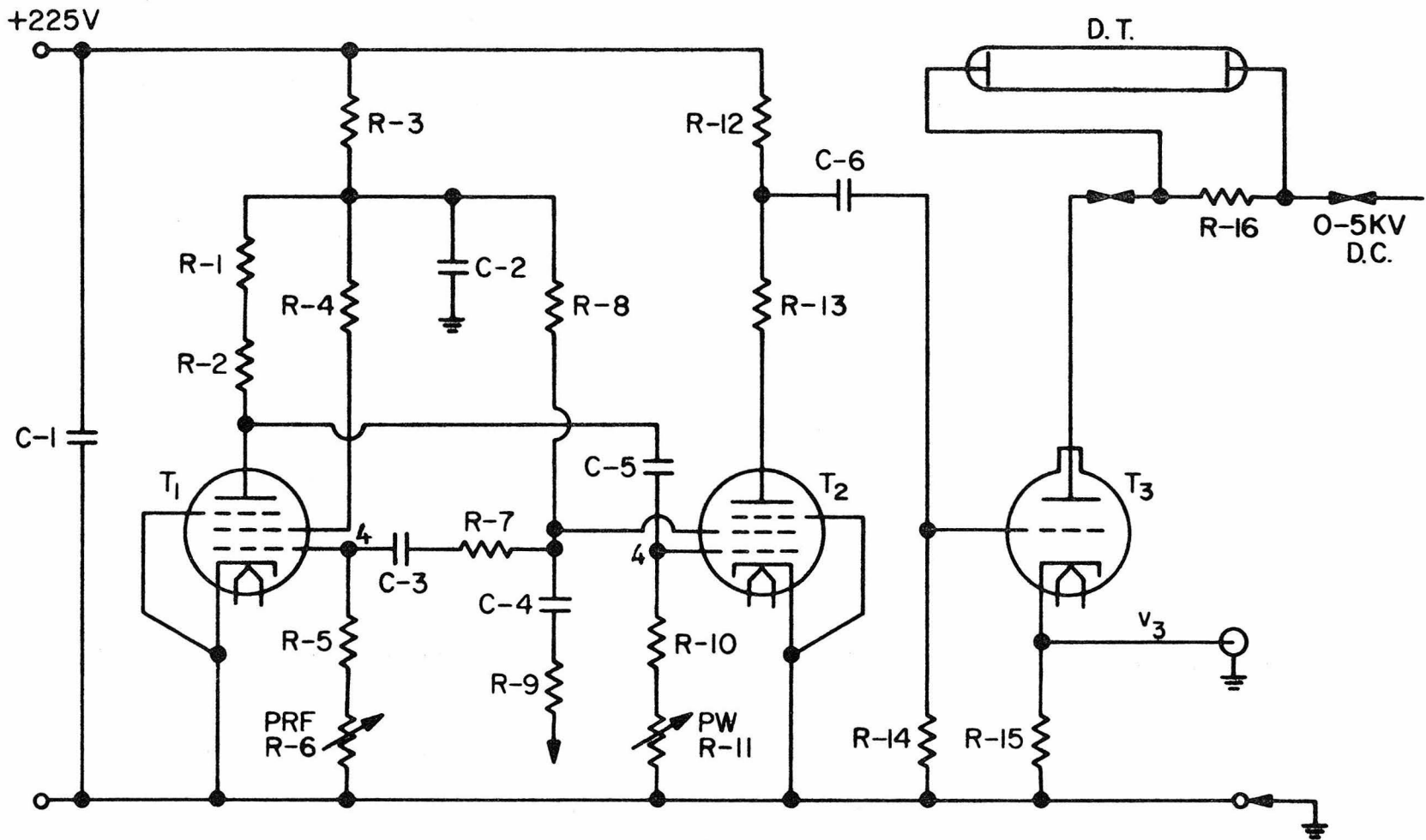


Fig. 42. Pulse generator circuit

Fig. 42. Pulse Generator

D.T.	Discharge tube
T ₁ , T ₂	6AG7 RCA tubes
T ₃	6BK4C/6EL4A RCA high voltage tube
C-1	8 mf capacitor, 450V
C-2	8 mf capacitor, 450V
C-3	0.05 mf capacitor
C-4	0.1 mf capacitor
C-5	1000 pf capacitor
C-6	0.05 mf capacitor
R-1	1 KΩ, 2W
R-2	1.3 KΩ, 2W
R-3	2 KΩ, 2W
R-4	5.6 KΩ, 2W
R-5	250 KΩ
R-6	500 KΩ
R-7	4.7 KΩ
R-8	5.6 KΩ, 2W
R-9	22 KΩ
R-10	16 KΩ
R-11	1 MΩ
R-12	2 KΩ, 10W
R-13	2 KΩ, 10W
R-14	470 KΩ
R-15	5 KΩ, 4W
R-16	10 MΩ

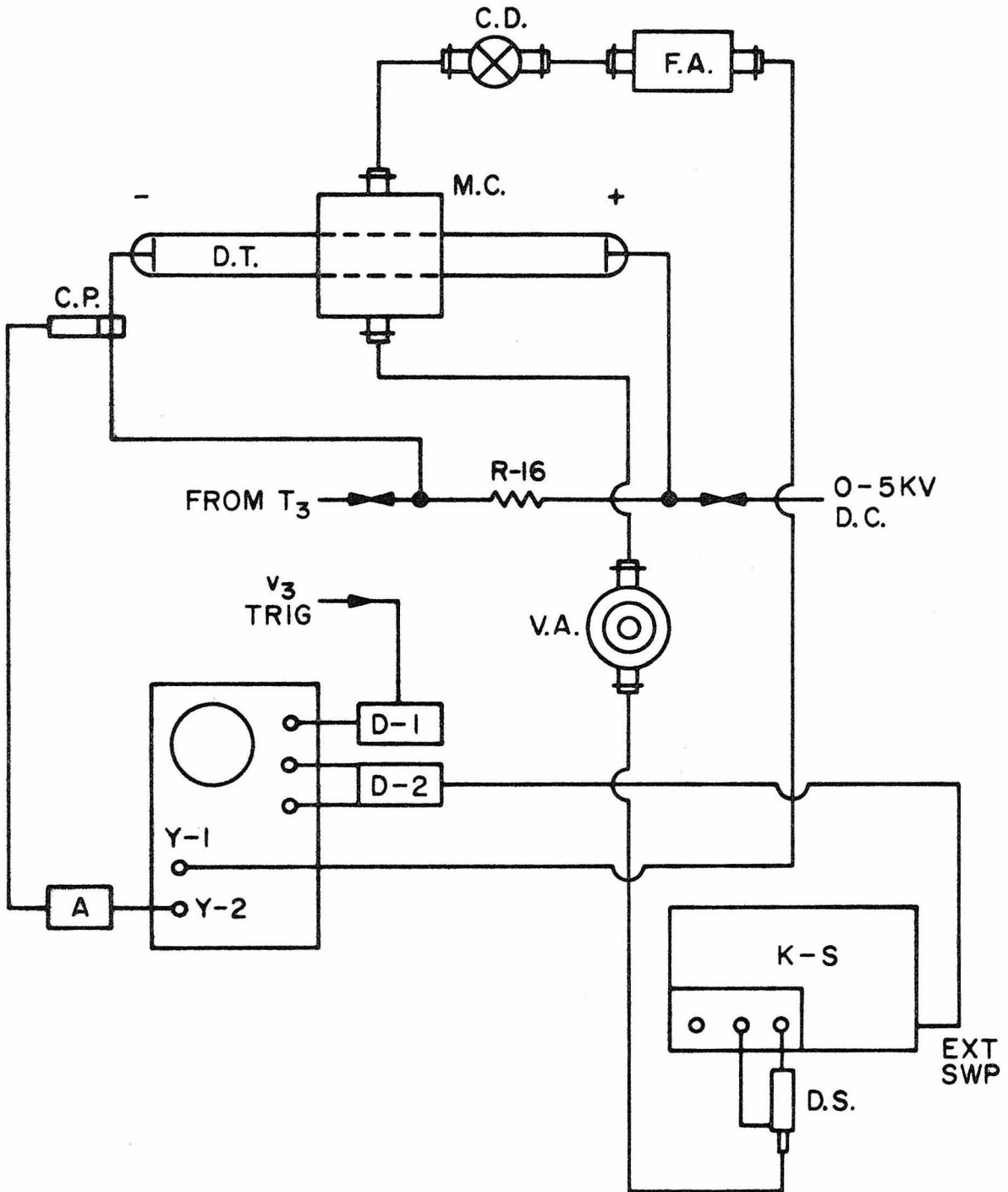


Fig. 43. Electrical measurements on pulsed discharge

Fig. 43. Electrical Measurements on Pulsed Discharge

A	Tektronix type 131 amplifier
C.P.	Tektronix P-6016 current probe
C.D.	Hewlett-Packard 420B crystal detector
D.T.	Discharge tube
D.S.	Kruse and Storke 1033 directional sampler
D-1,D-2	Voltage dividers
F.A.	Hewlett-Packard 8491A, 6 db fixed attenuator
K.S.	Kruse and Storke 5000 microwave sweeper with 5013 plug-in
M.C.	Microwave cavity
R-16	10 M Ω resistor
V.A.	ARRA 4674-20F 20 db variable attenuator
Y-1,Y-2	Vertical axes of Tektronix 541 oscilloscope

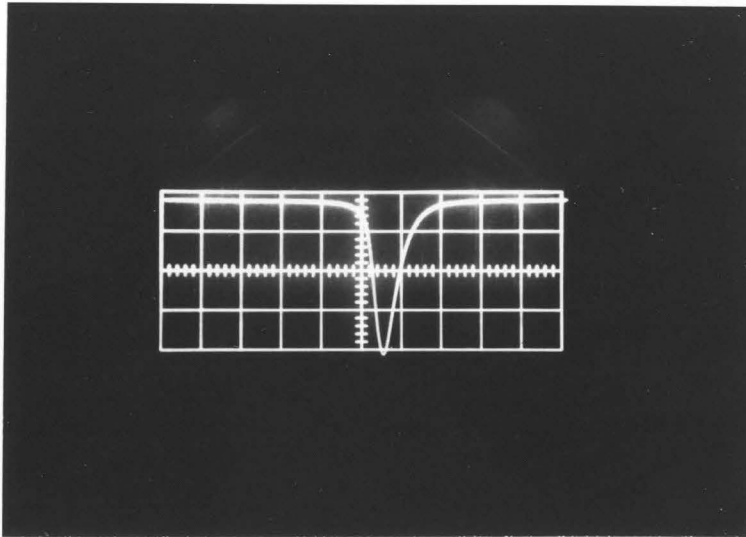


Fig. 44a Resonance curve of empty cavity
 Time Scale: 100 μ sec/cm \leftrightarrow 3 MHz/cm

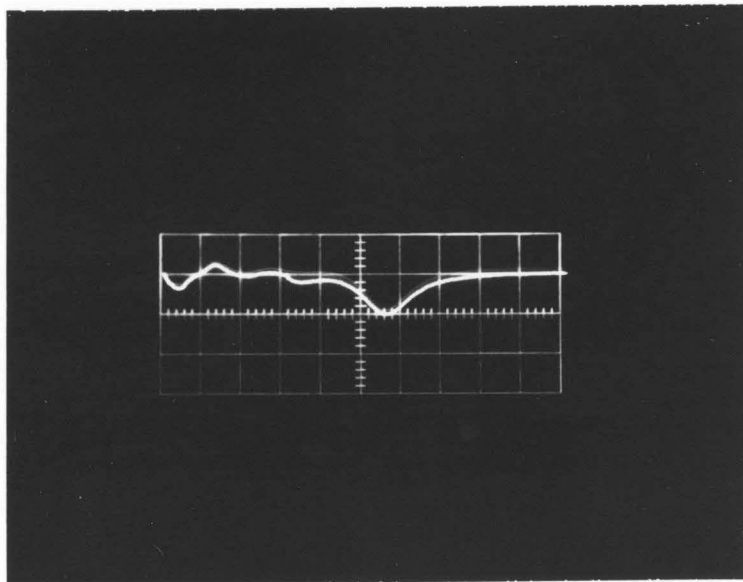


Fig. 44b Resonance curve in Ar pulsed discharge
 Time Scale: 100 μ sec/cm \leftrightarrow 3 MHz/cm
 $\tau_W = 1.6$ msec. Curve at arbitrary position.

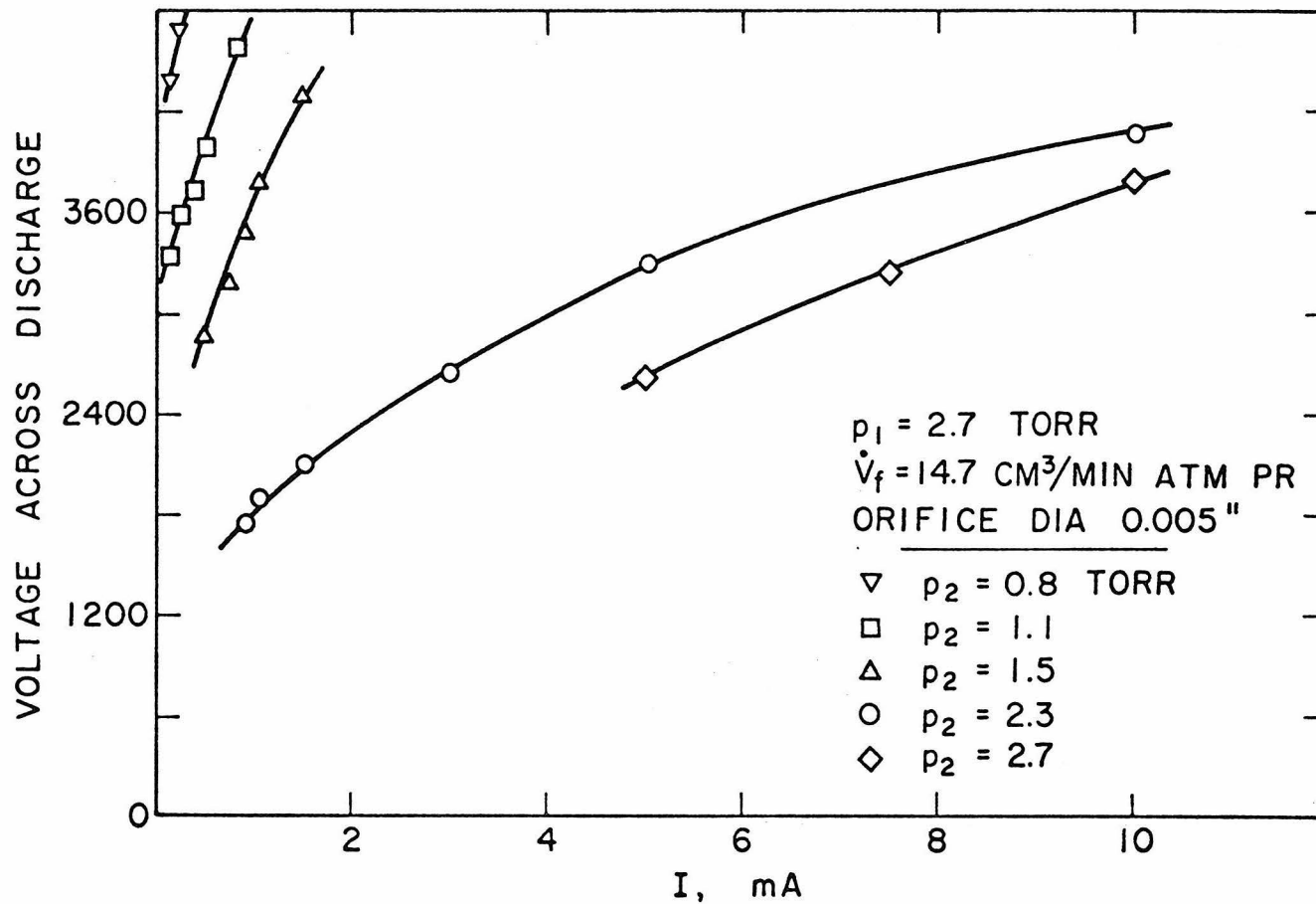


Fig. 45. V-I characteristics of He discharge in a choked flow orifice system

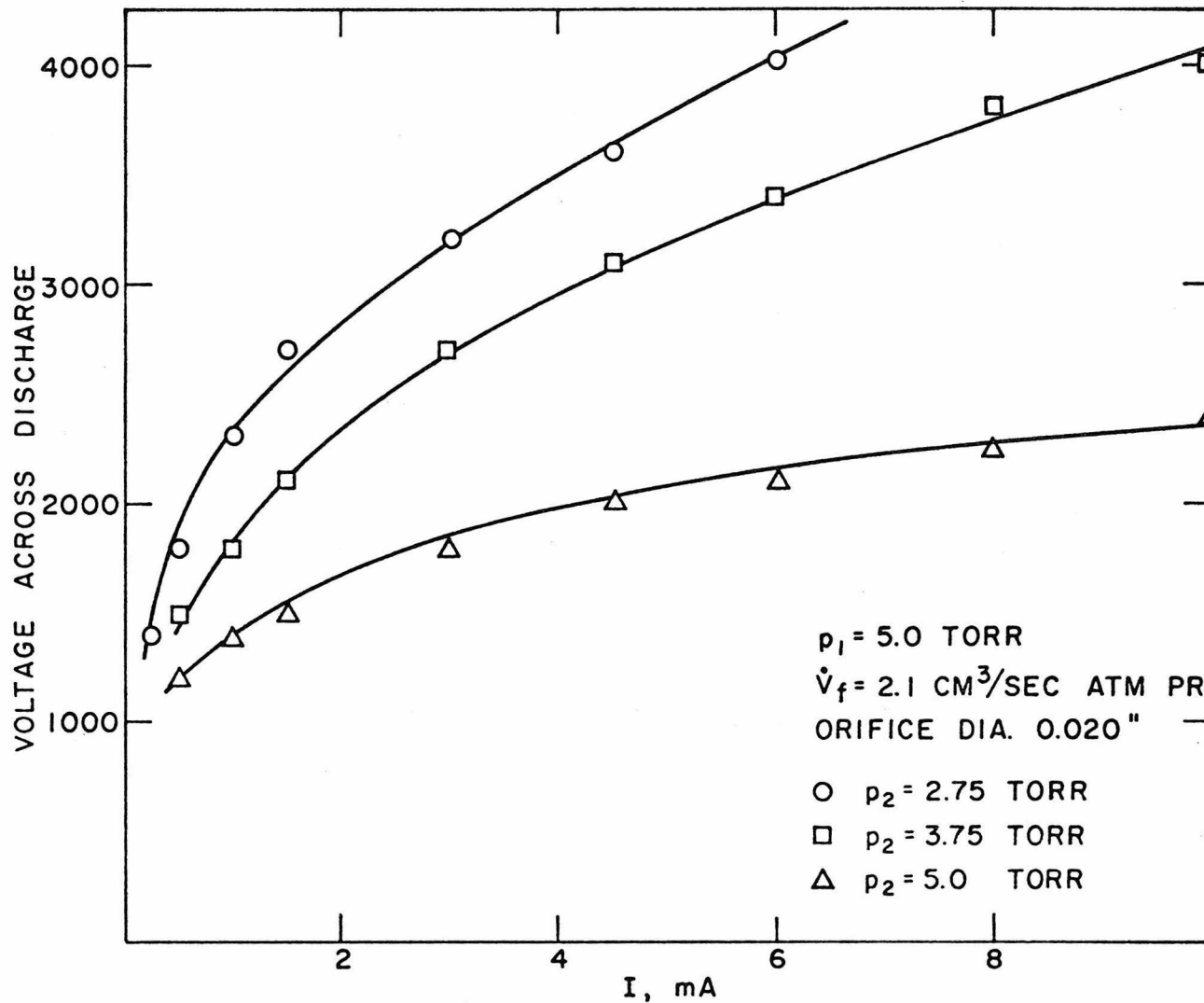


Fig. 46. V-I characteristics of Ar discharge in a choked flow orifice system

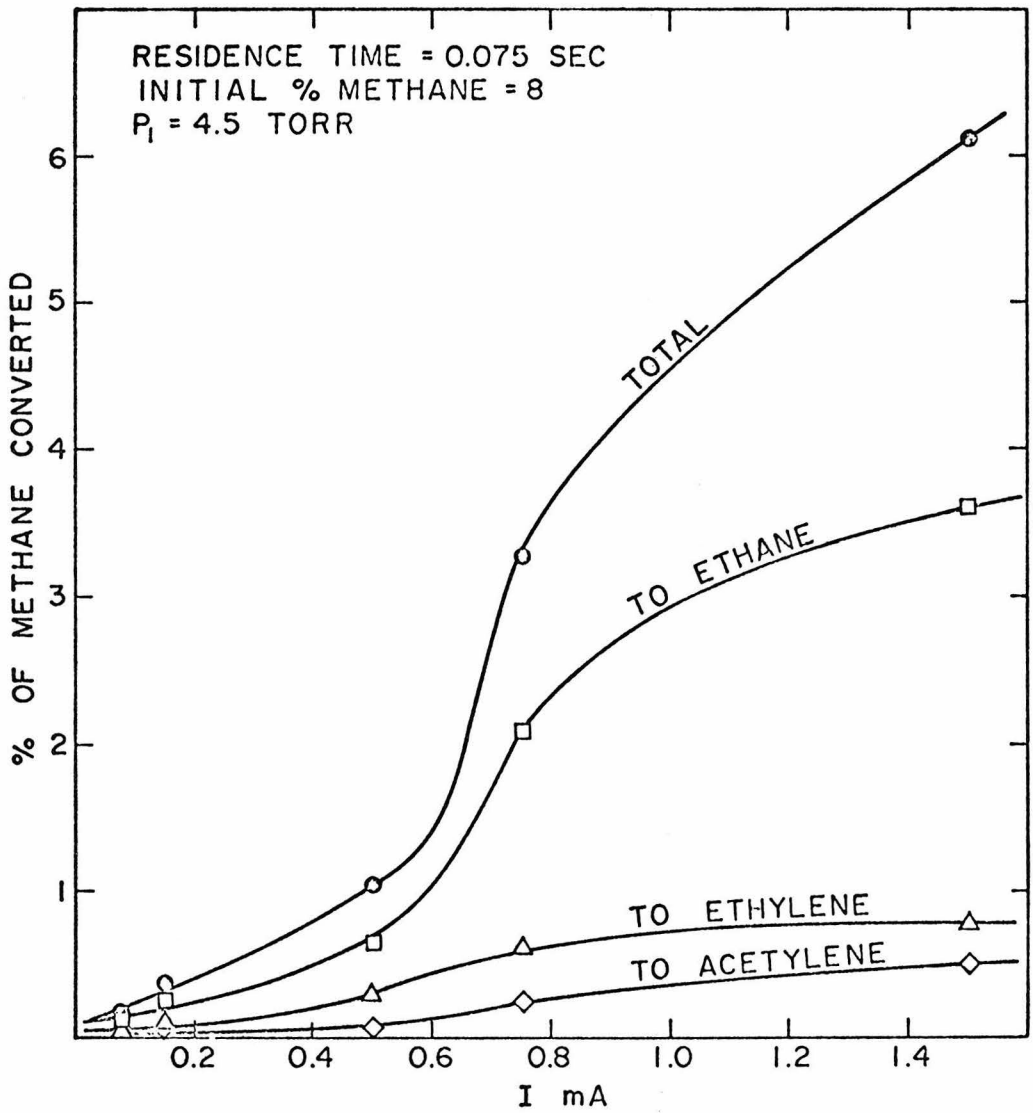


Fig. 47. % of methane converted vs. I --preliminary results

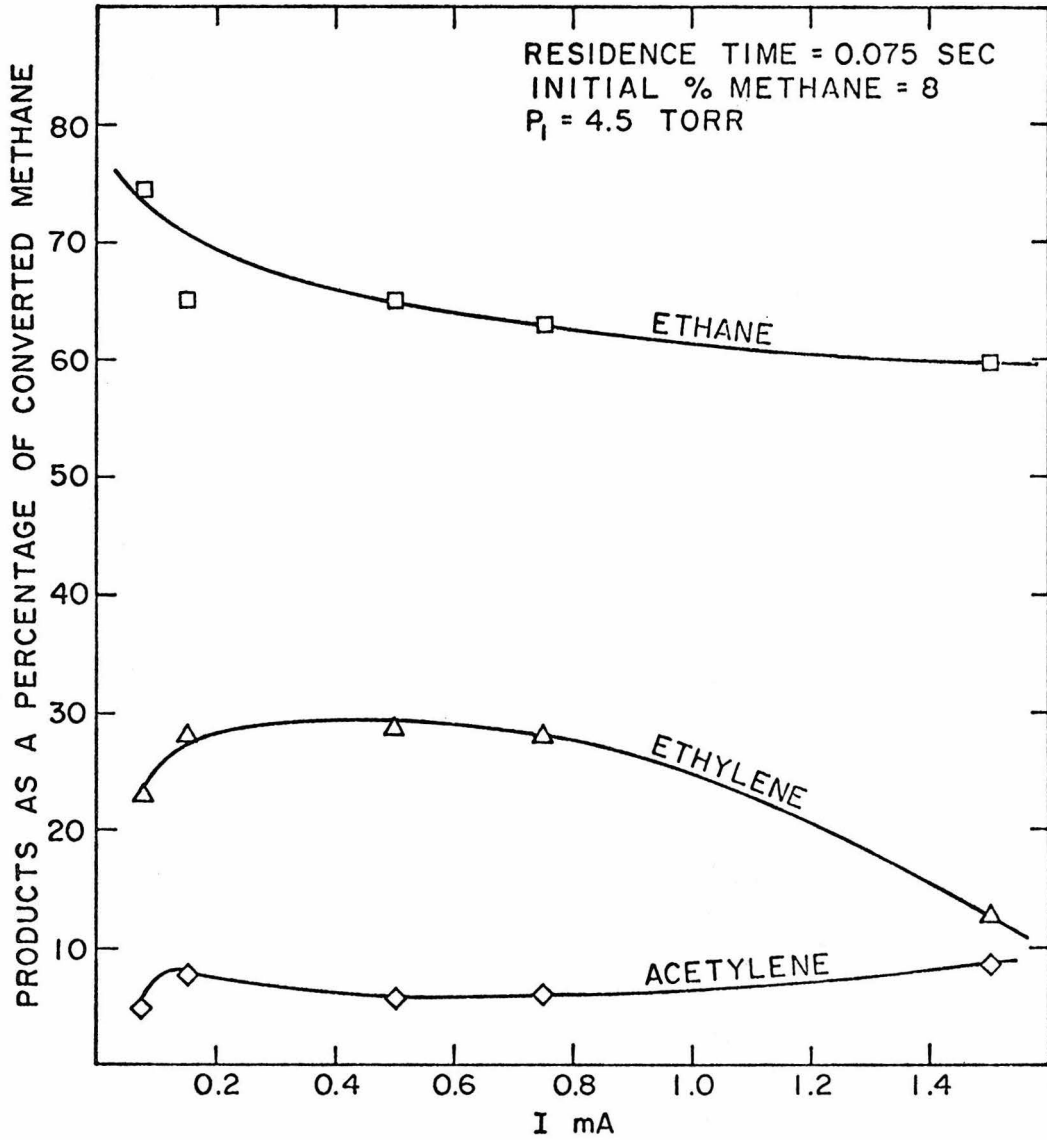


Fig. 48. Product distribution of converted methane--preliminary results

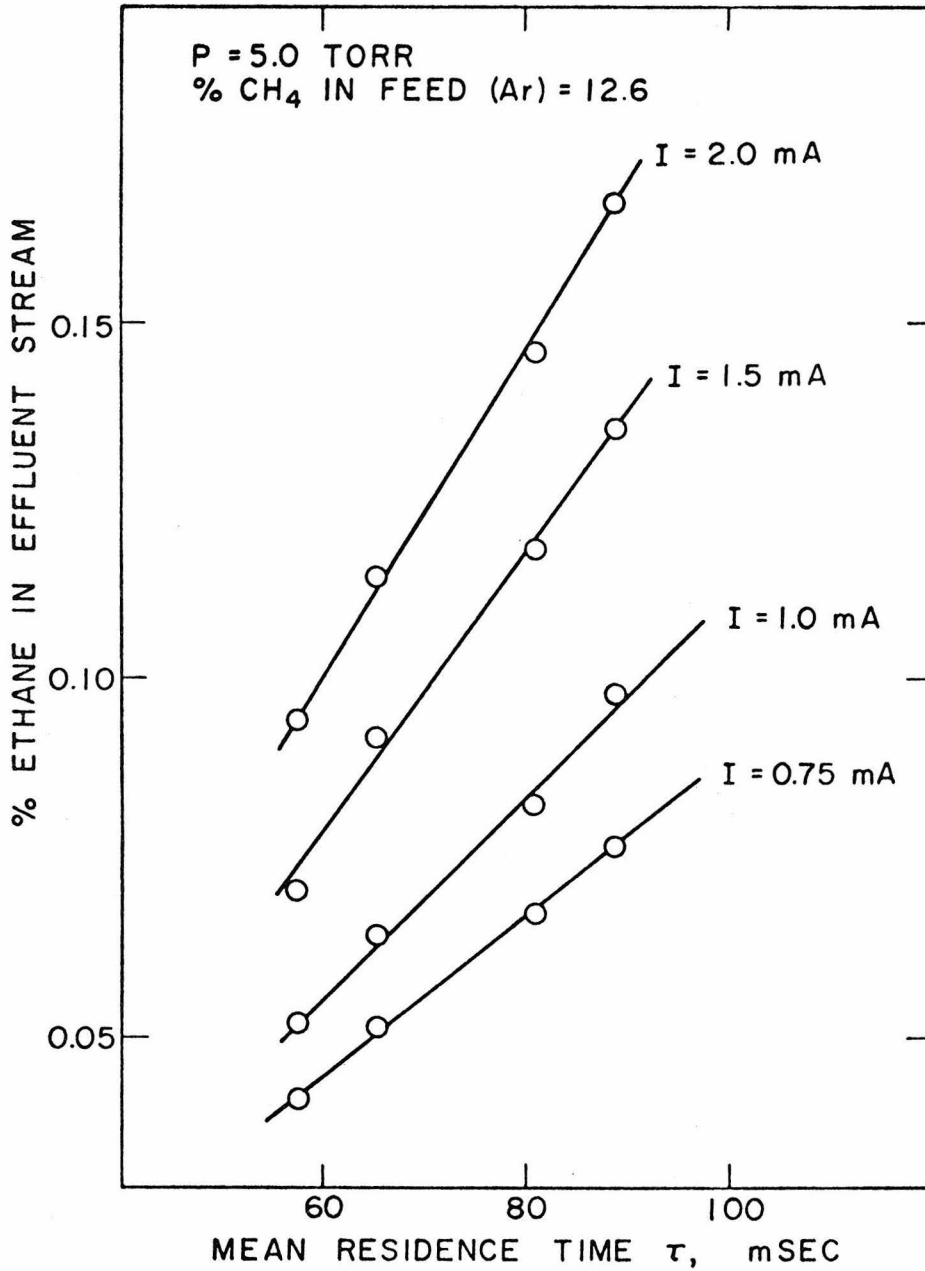


Fig. 49. % ethane in effluent stream vs. mean residence time τ

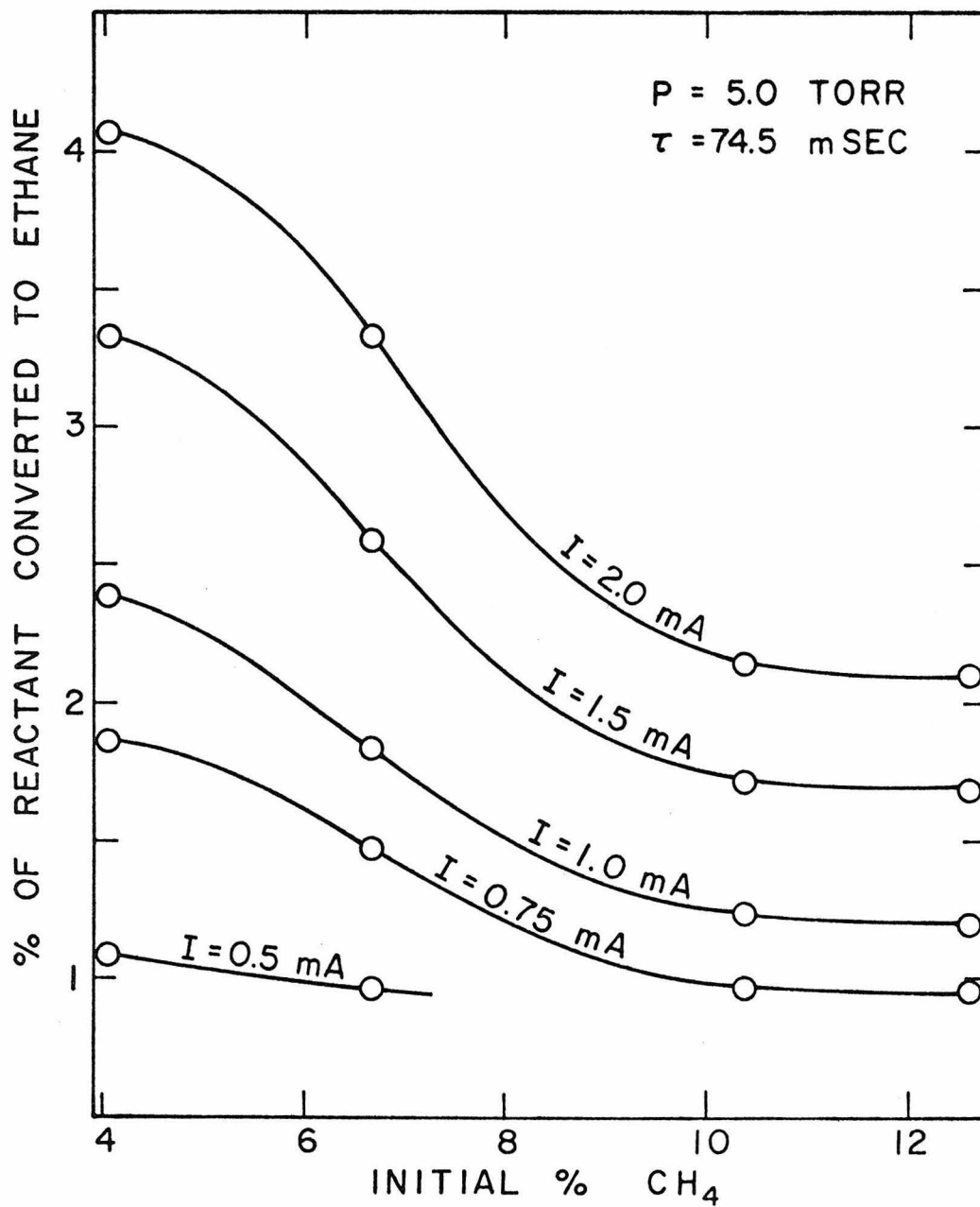


Fig. 50. % of reactant converted to ethane vs. initial % CH₄ (C₀)

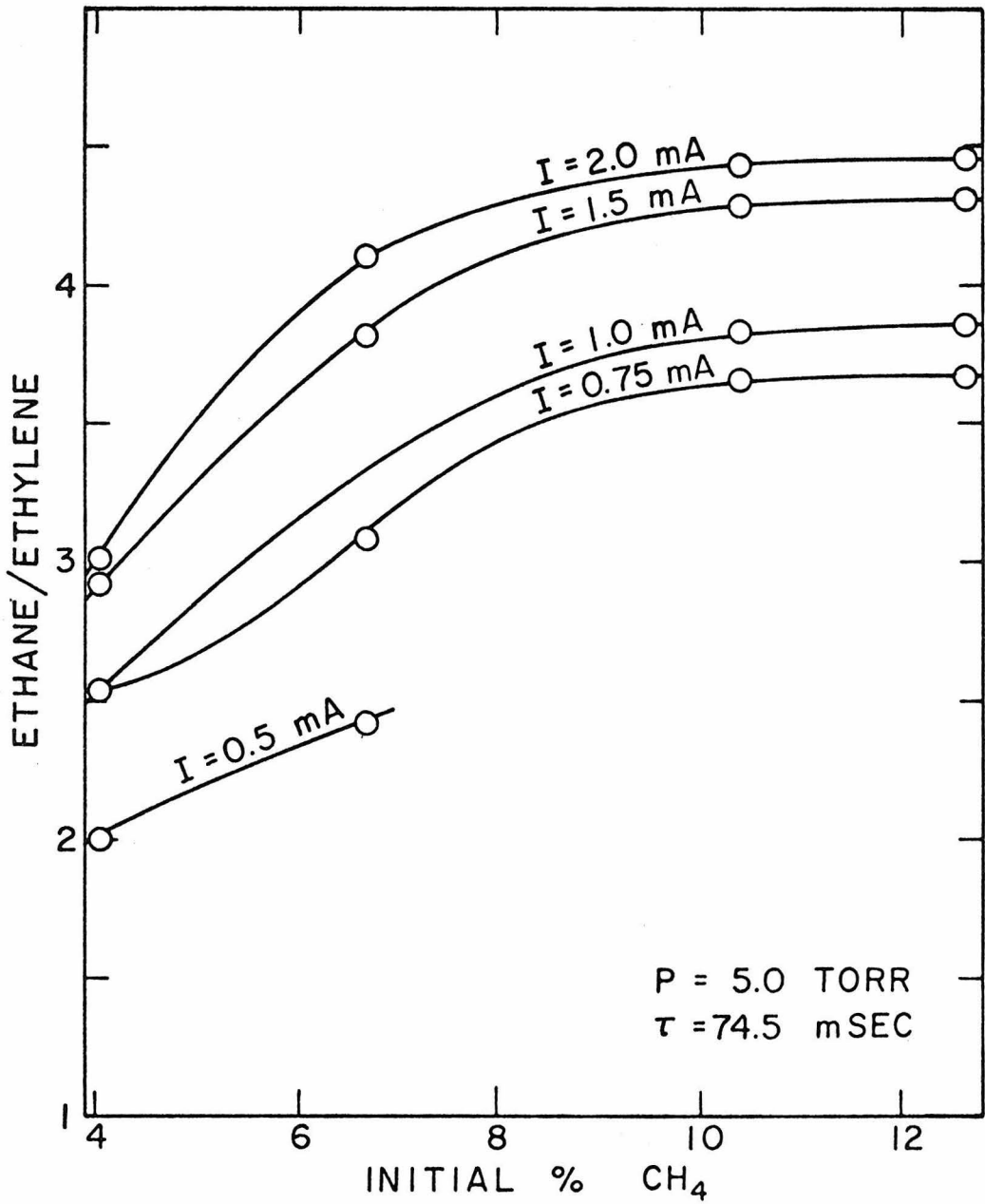


Fig. 51. Ethane/Ethylene vs. initial % CH₄ (C₀)

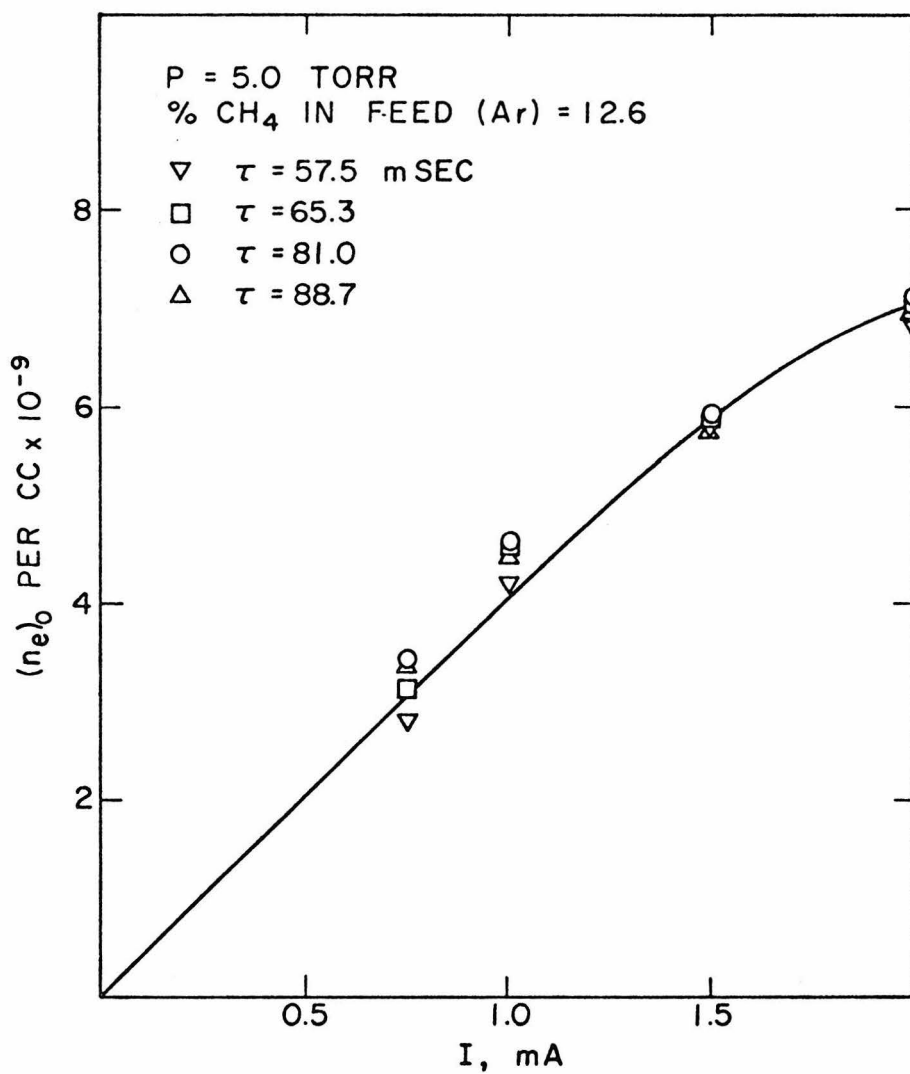


Fig. 52. Electron density in reacting CH₄-Ar d.c. glow vs. discharge current I

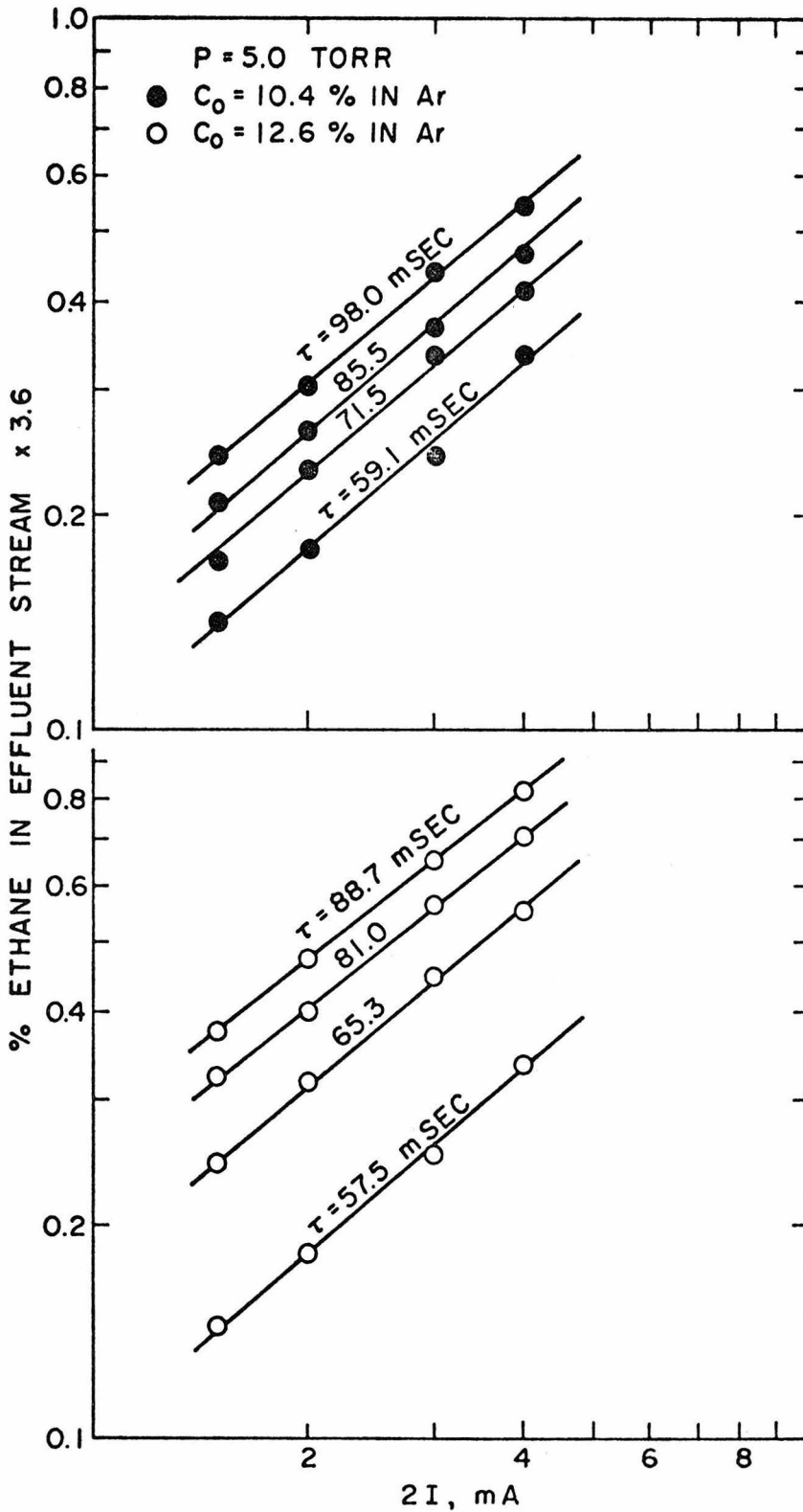


Fig. 53. % ethane in effluent stream vs. discharge current I

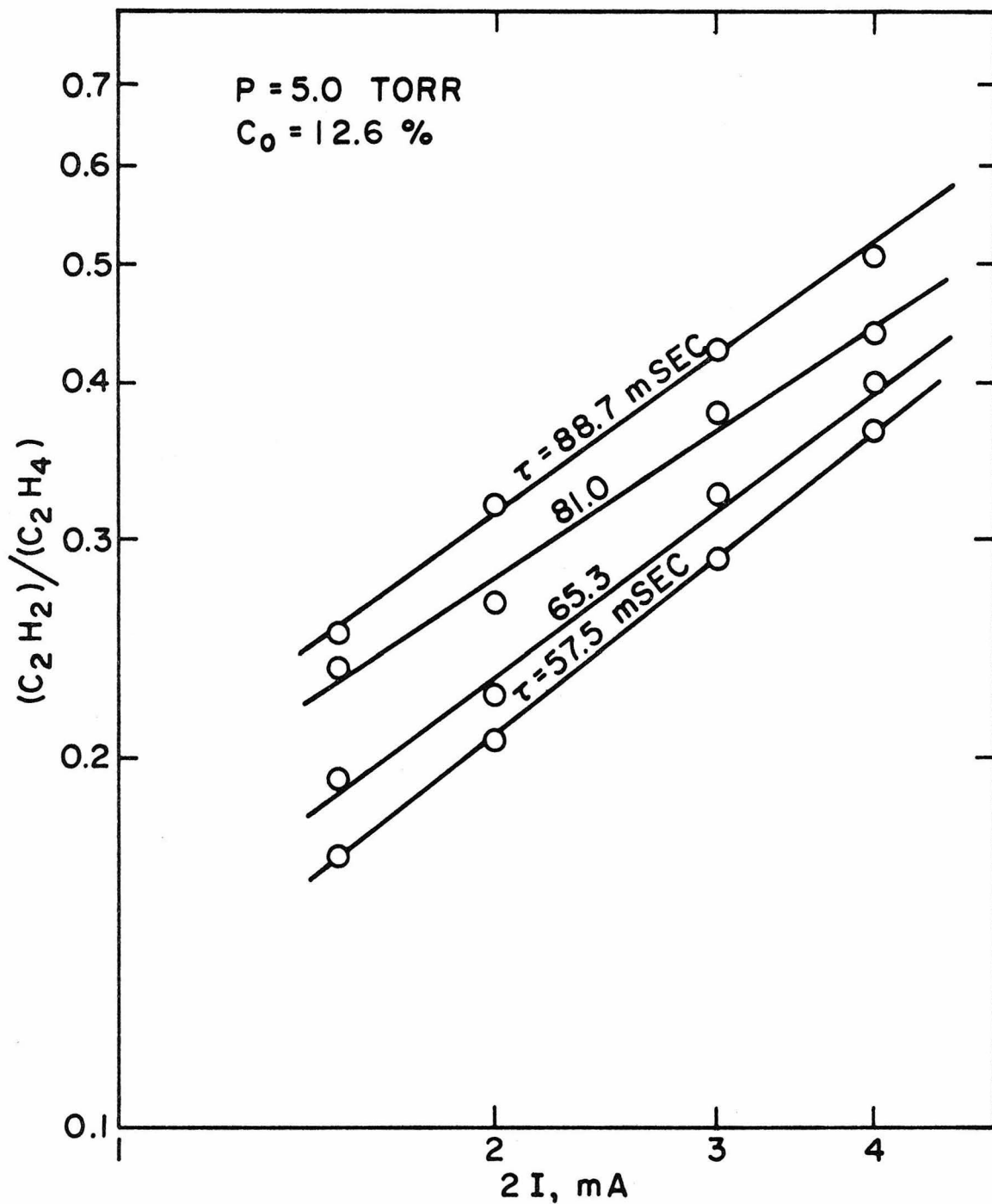


Fig. 54. $(C_2H_2)/(C_2H_4)$ vs. discharge current I

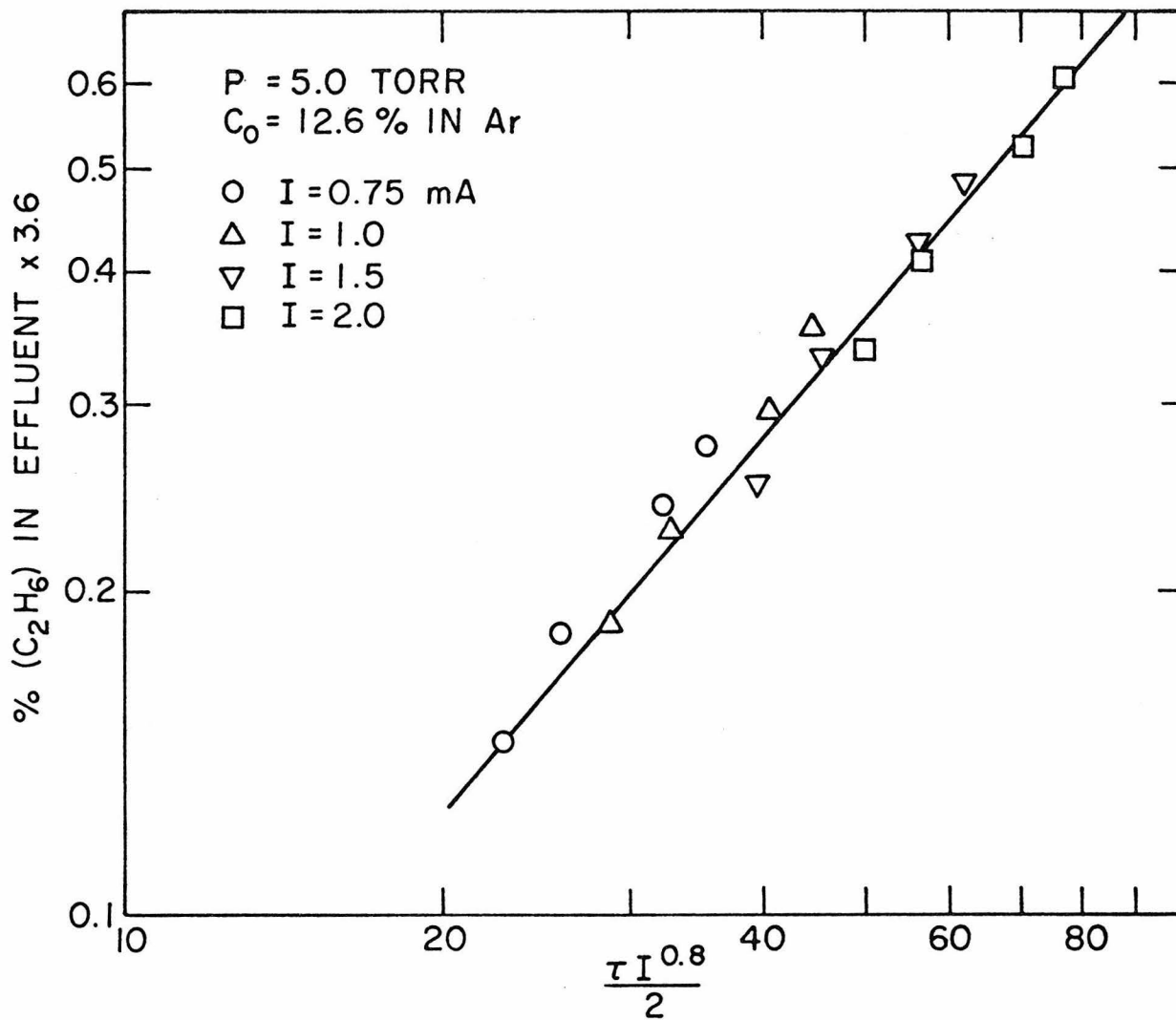


Fig. 55. % C₂H₆ in effluent vs. $\tau I^{0.8}$

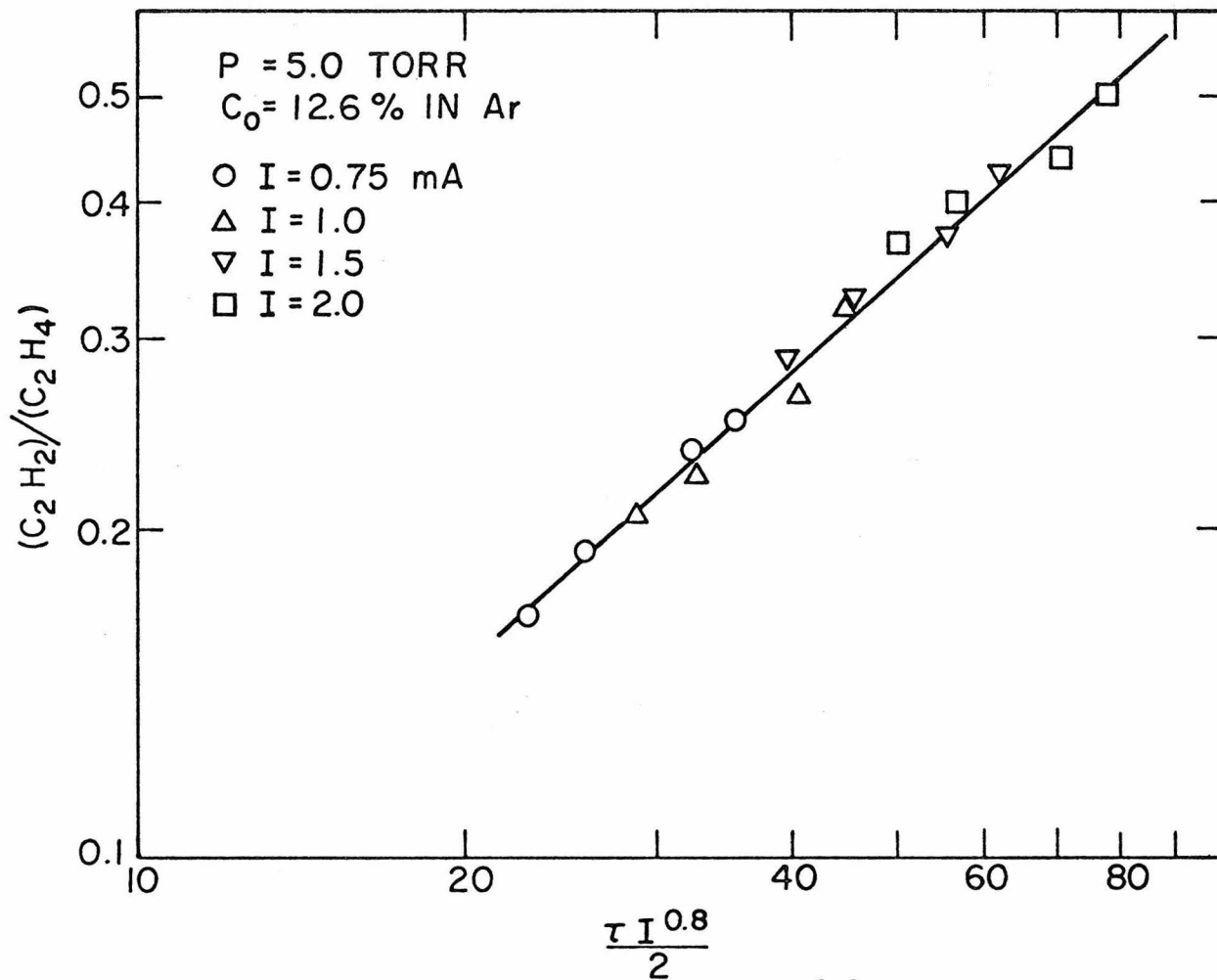


Fig. 56. $(C_2H_2)/(C_2H_4)$ vs. $\tau I^{0.8}$

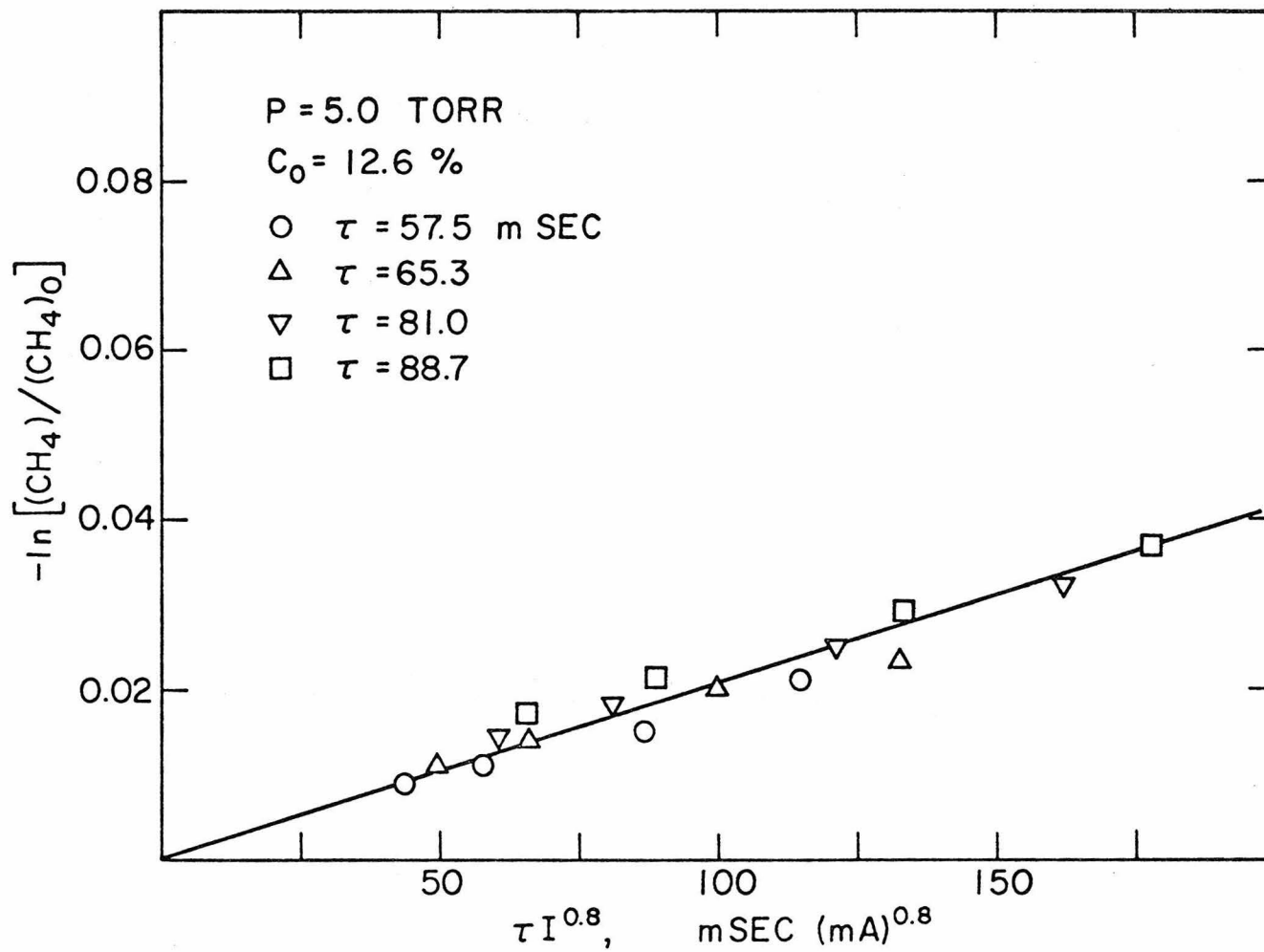


Fig. 57. Test of first order decay of reacting CH_4

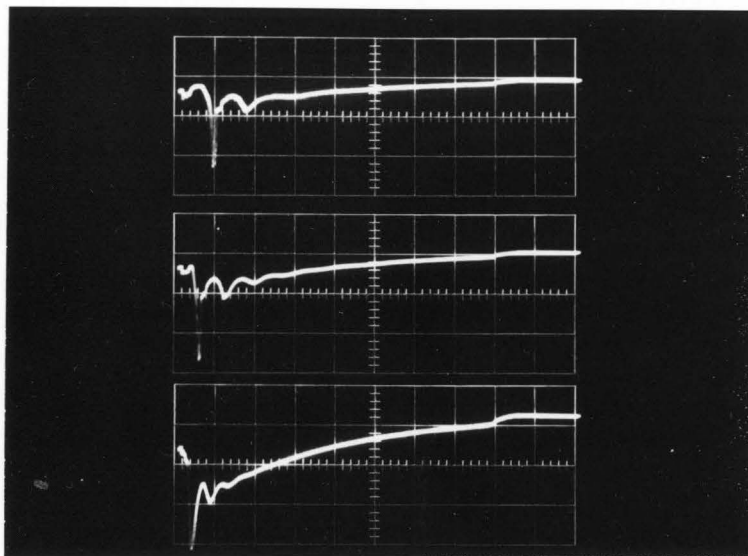


Fig. 58 i_m vs. t in pure Ar, i) $p = 9.0$ torr, ii) $p = 6.0$ torr,
iii) $p = 3.0$ torr.

Time Scale: $200 \mu\text{sec}/\text{cm}$

Current Scale: i) $5 \text{ mA}/\text{cm}$, ii) $2 \text{ mA}/\text{cm}$, iii) $2 \text{ mA}/\text{cm}$

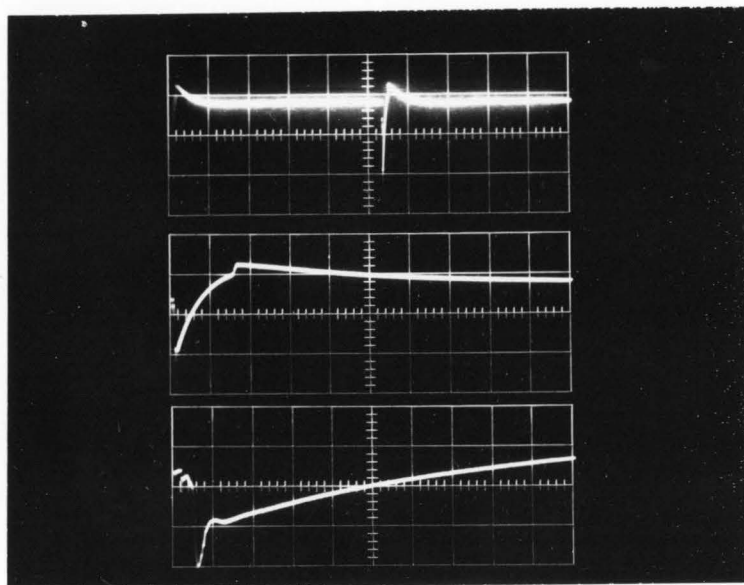


Fig. 59 i_m vs. t for $0.91\% \text{ CH}_4$ in Ar, $p = 3.0$ torr

Time Scale: i) $10 \text{ msec}/\text{cm}$, ii) $1 \text{ msec}/\text{cm}$,
iii) $100 \mu\text{sec}/\text{cm}$

Current Scale: $2 \text{ mA}/\text{cm}$

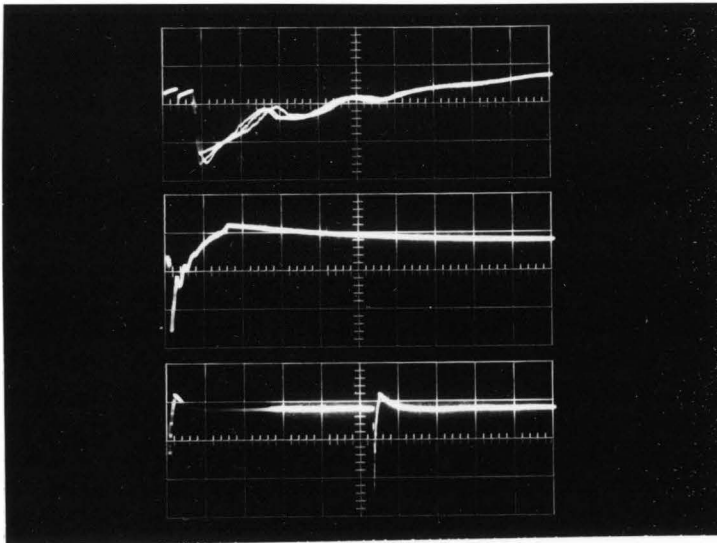


Fig. 60 i_m vs. t for 17.7% CH_4 in Ar, $p = 3.0$ torr
 Time Scale: i) 100 $\mu\text{sec}/\text{cm}$, ii) 1 msec/cm, iii) 10 msec/cm
 Current Scale: 2 mA/cm

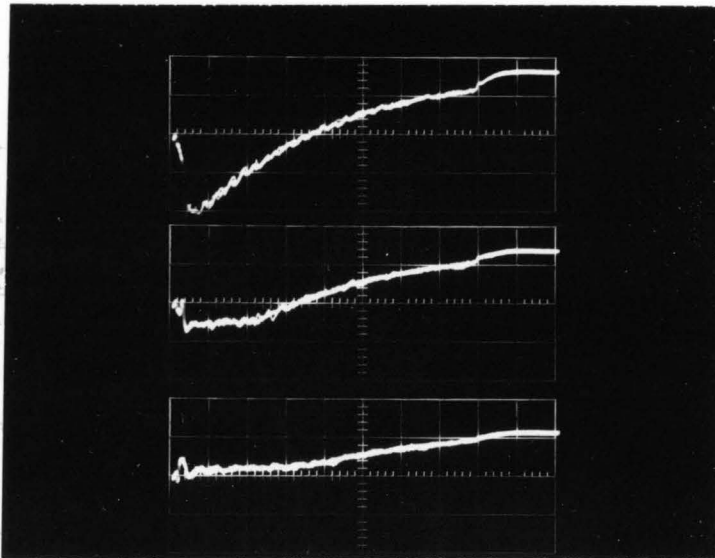


Fig. 61 i_m vs. t for pure He, $p = 7.0$ torr
 Time Scale: 200 $\mu\text{sec}/\text{cm}$
 Current Scale: 1 ma/cm, i) $i_{\text{max}} = 3\text{mA}$, ii) $i_{\text{max}} = 1 \text{ mA}$,
 iii) $i_{\text{max}} = 0.5 \text{ mA}$

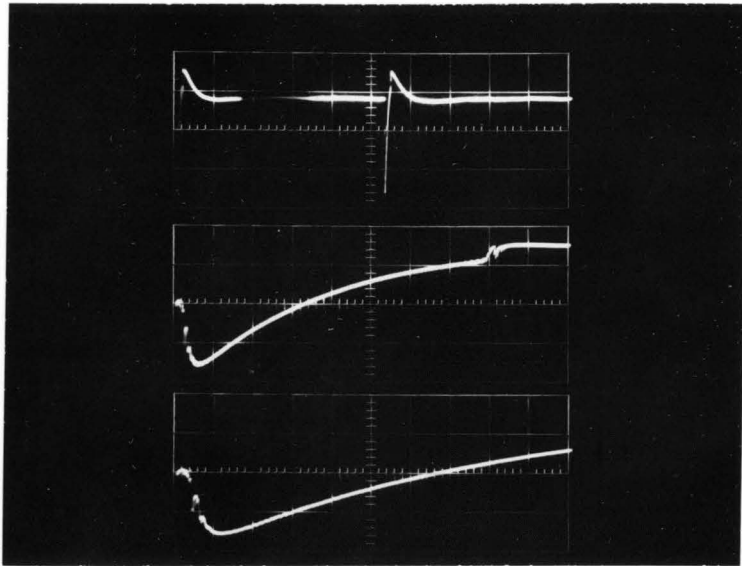


Fig. 62 i_m vs. t for 0.82% CH_4 in He, $p = 3.0$ torr
 Time Scale: i) 10 msec/cm, ii) 200 $\mu\text{sec/cm}$,
 iii) 100 $\mu\text{sec/cm}$
 Current Scale: 1 mA/cm

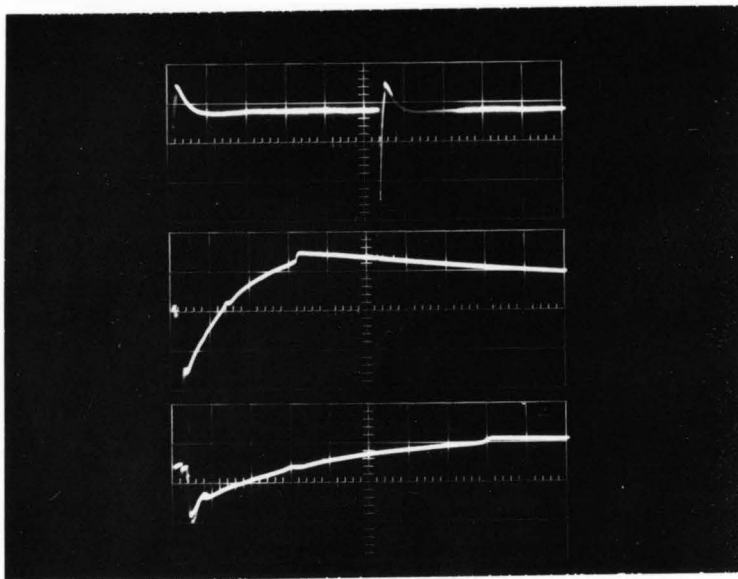


Fig. 63 i_m vs. t for 16.4% CH_4 in He, $p = 3.0$ torr
 Time Scale: i) 10 msec/cm, ii) 500 $\mu\text{sec/cm}$,
 iii) 200 $\mu\text{sec/cm}$
 Current Scale: i) 1 mA/cm, ii) 1 mA/cm, iii) 2mA/cm

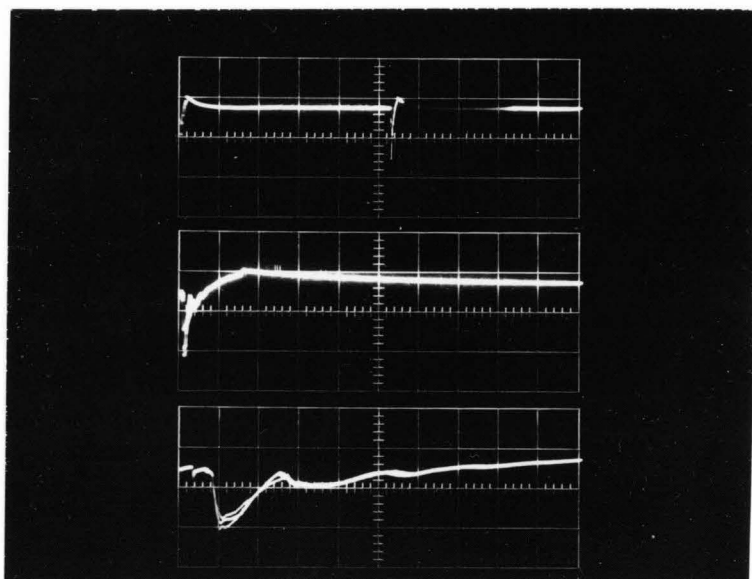


Fig. 64 i_m vs. t for pure CH_4 , $p = 3.0$ torr
Time Scale: i) 10 msec/cm, ii) 1 msec/cm,
iii) 100 $\mu\text{sec/cm}$
Current Scale: 2 mA/cm

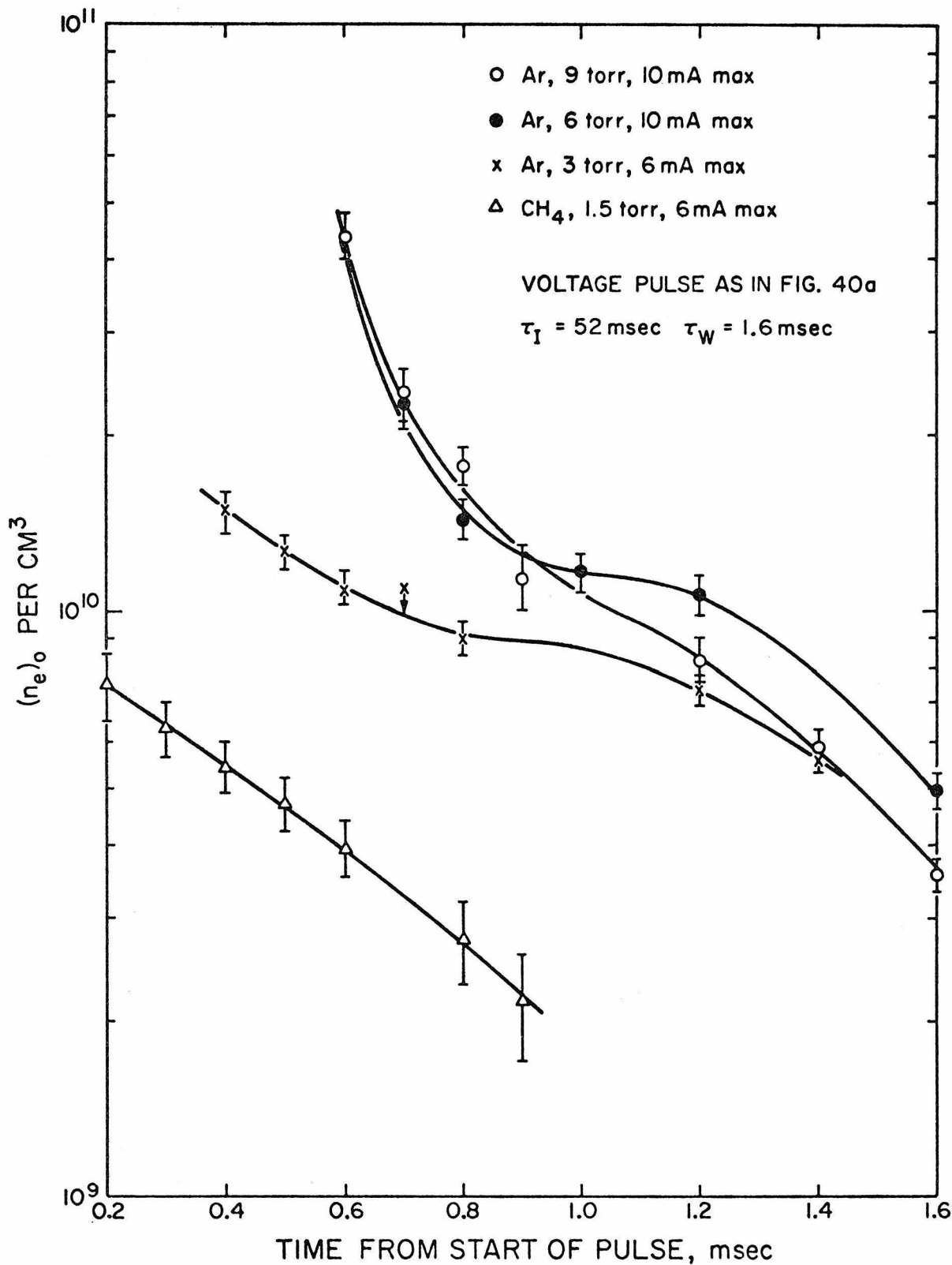


Fig. 66. Electron density as a function of time in the afterglow of CH₄ and Ar

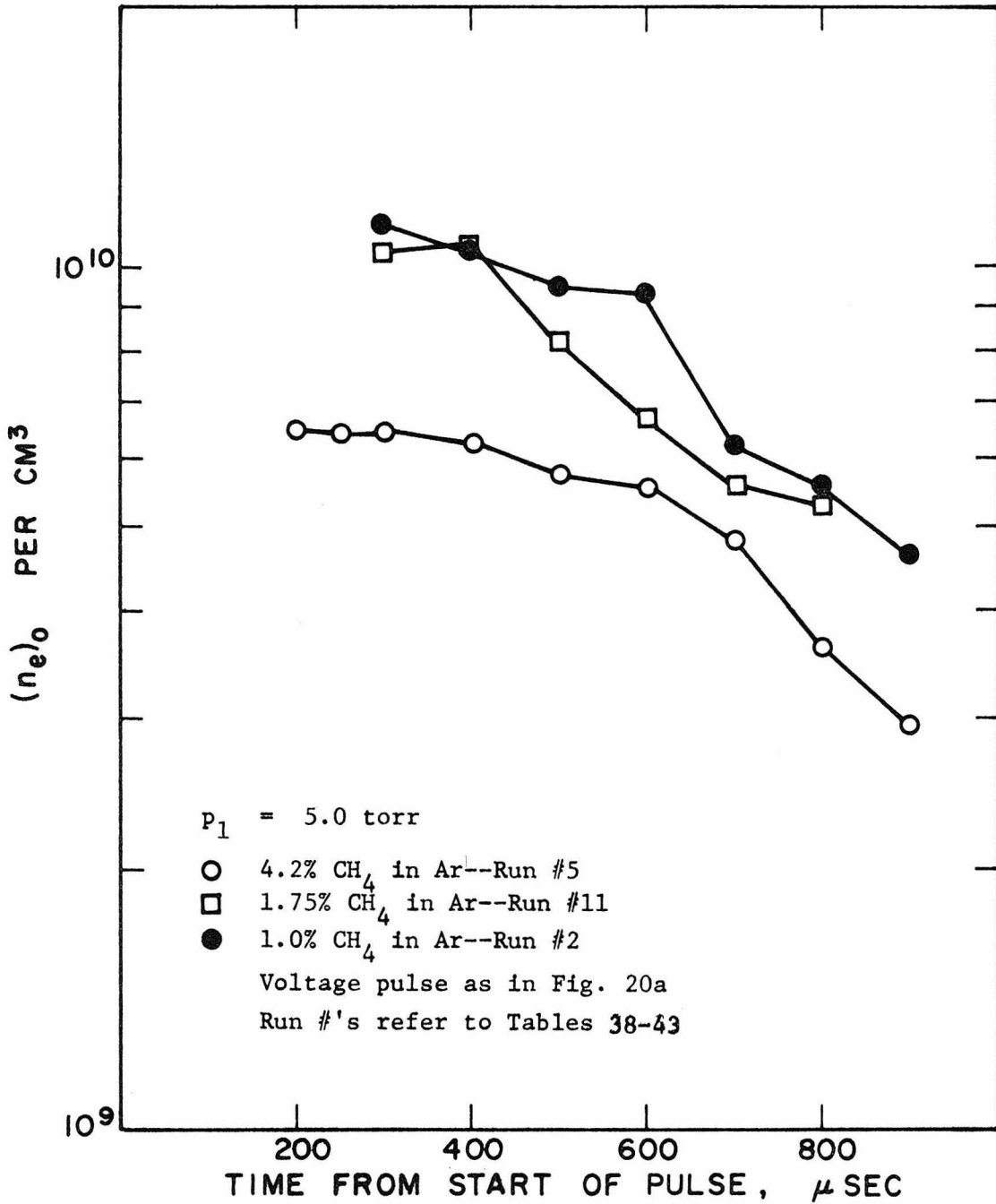


Fig. 67. Effect of C_o on $(n_e)_o$ vs. t in CH_4 -Ar mixtures

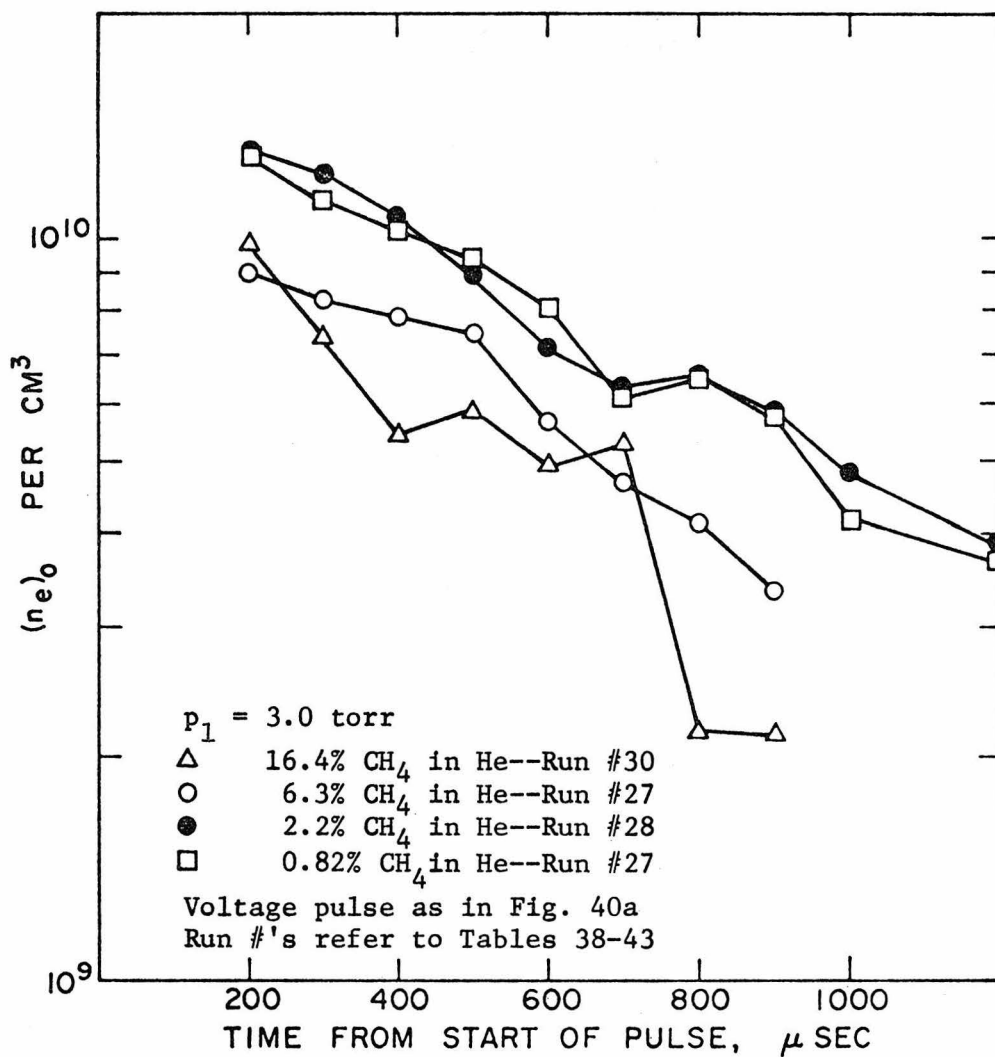


Fig. 68. Effect of C_o on $(n_e)_o$ vs. t in CH_4 -He mixtures

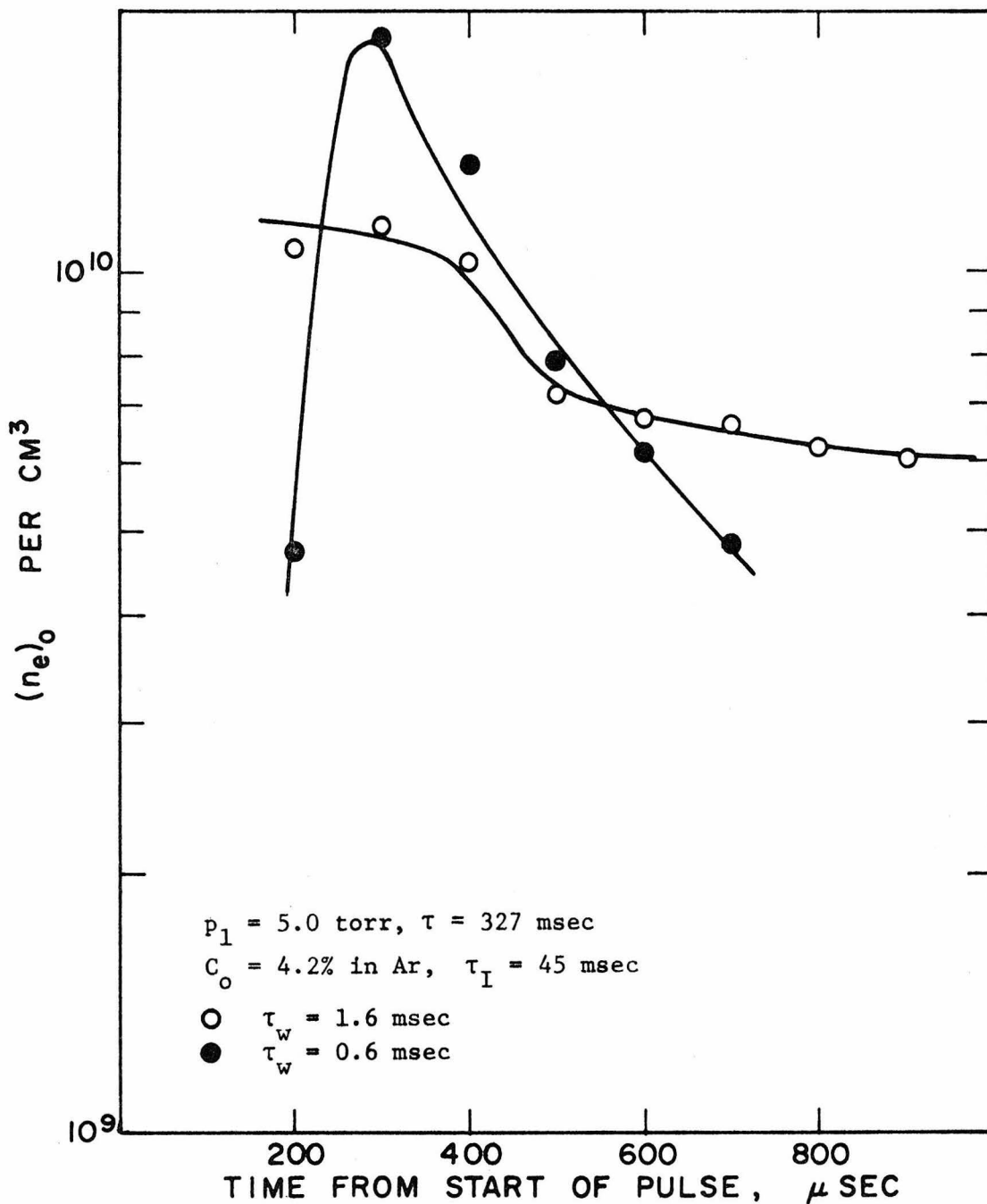


Fig. 69. Effect of pulse width τ_w on $(n_e)_0$ vs. t in CH_4 -Ar mixtures

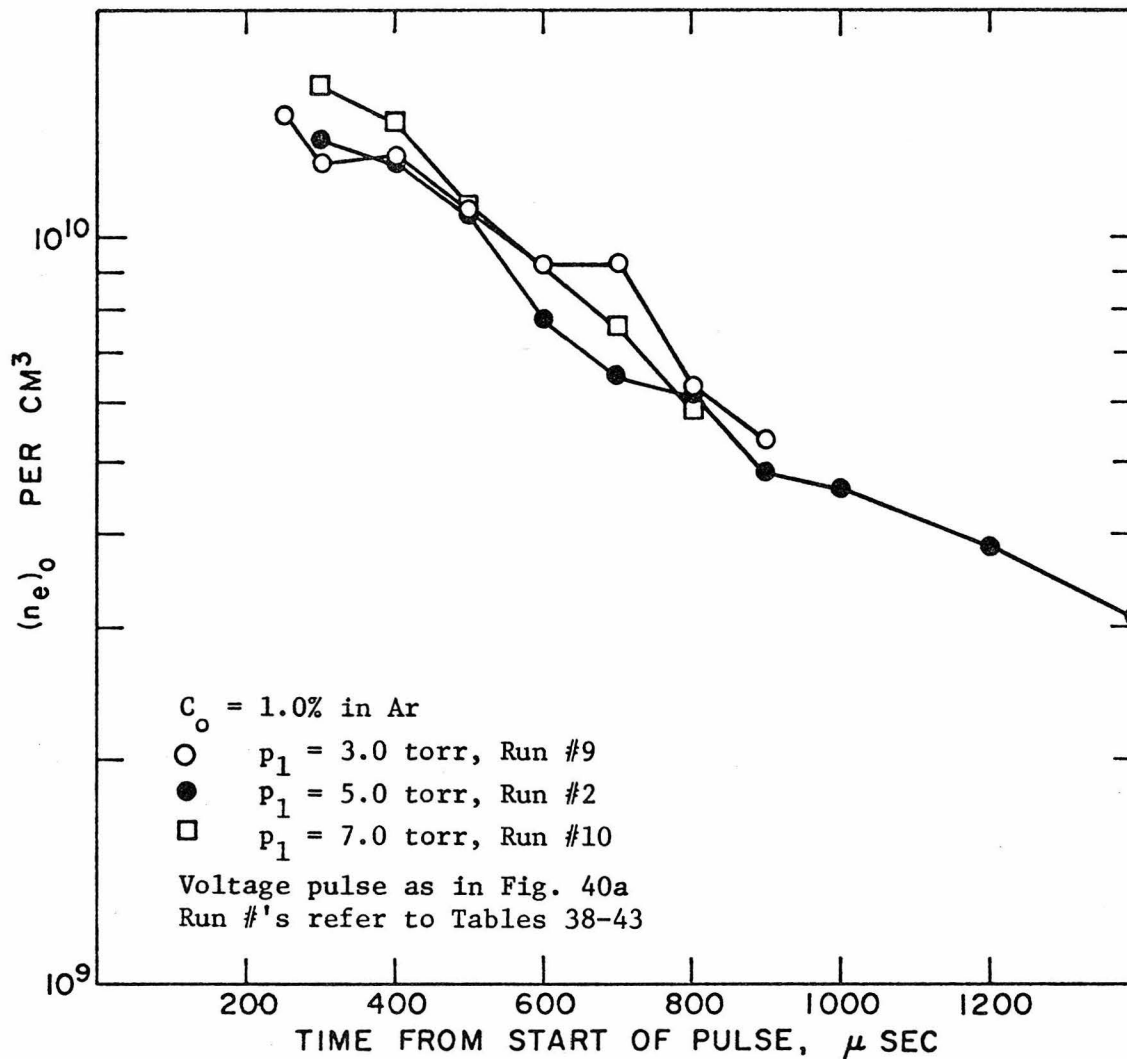


Fig. 70. Effect of total pressure p_1 on (n_{e_0}) vs. t in CH_4 -Ar mixtures

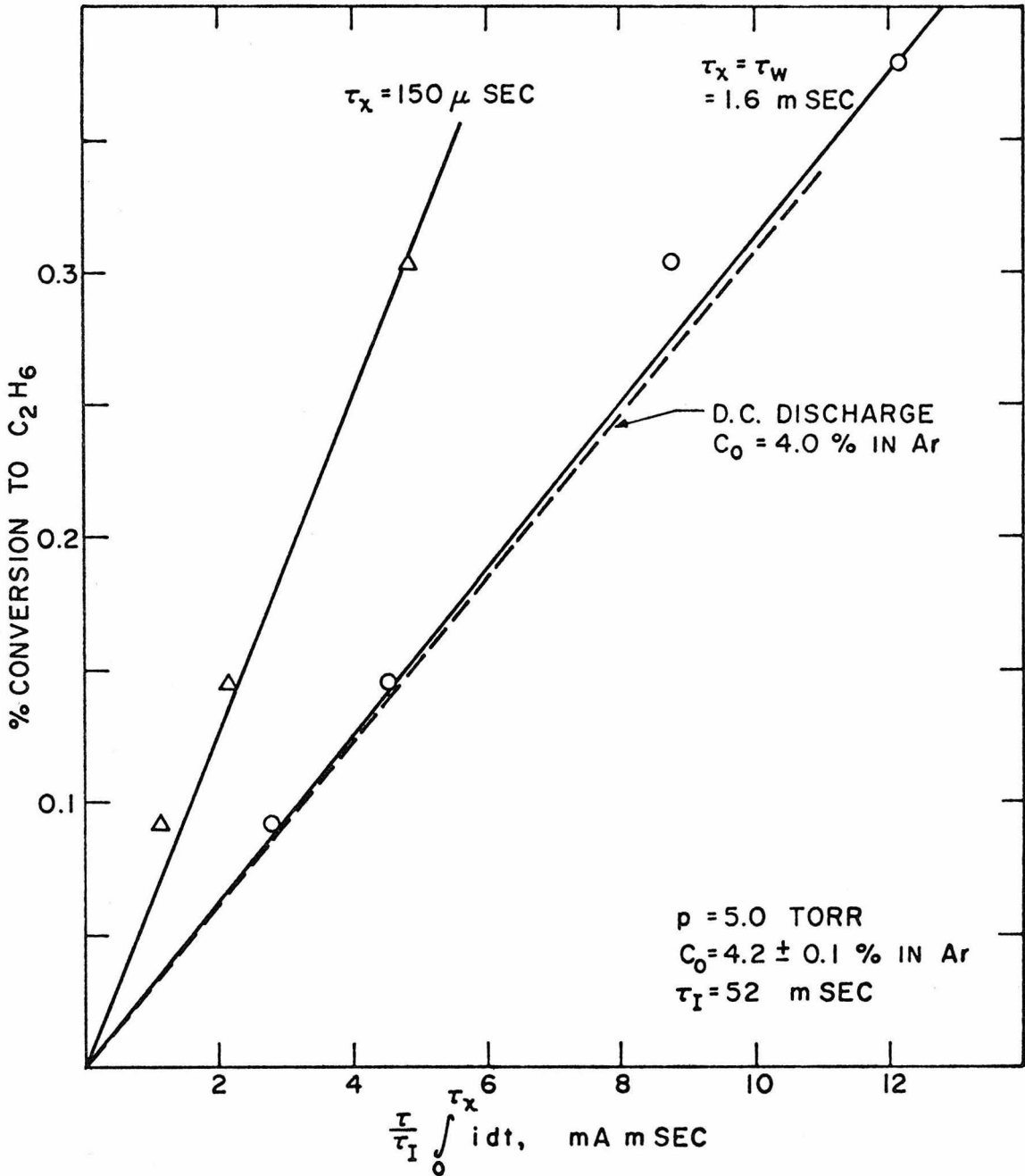


Fig. 71. % conversion to C_2H_6 vs. ξ^* in pulsed discharge

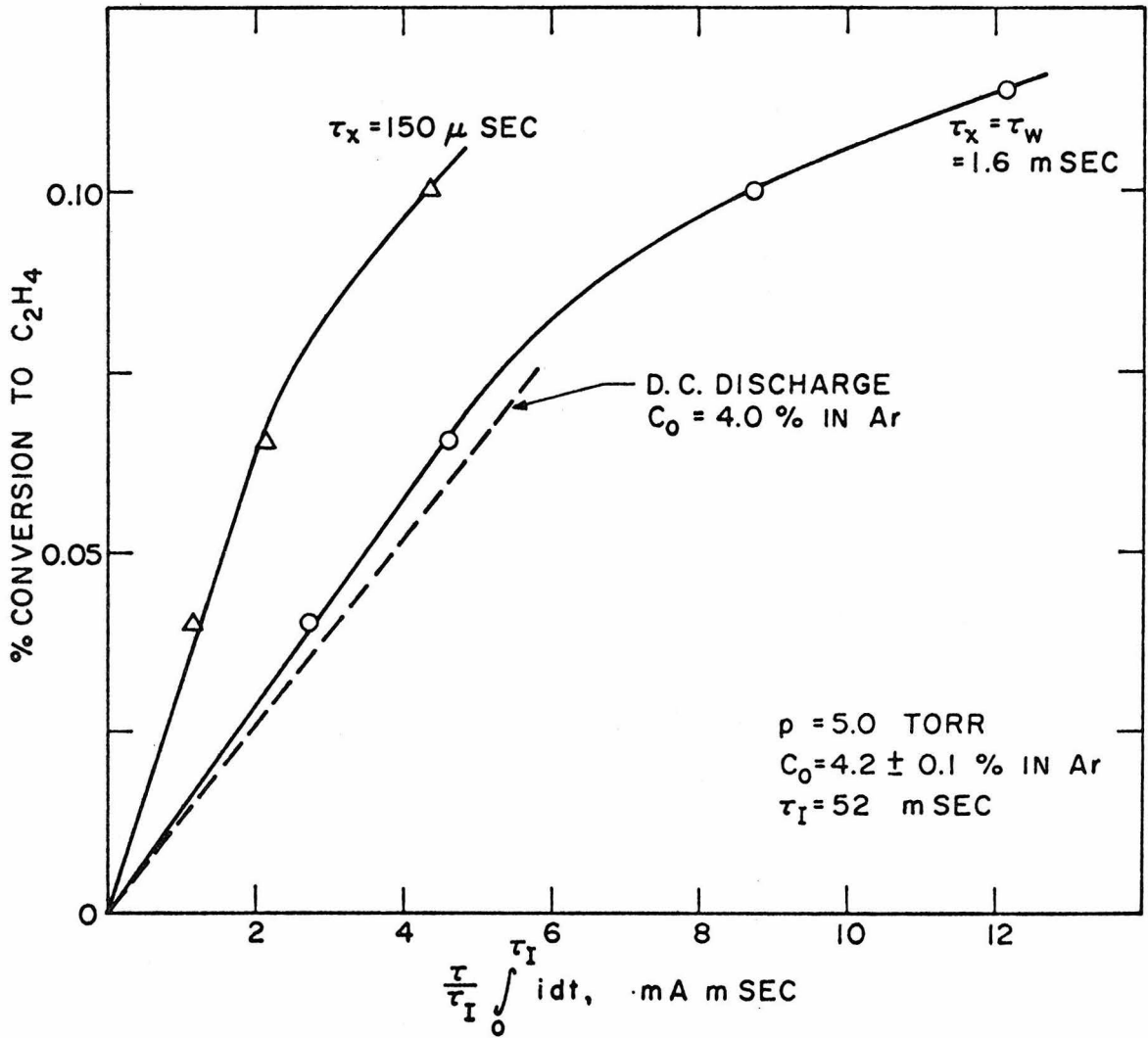


Fig. 72. % Conversion to C_2H_4 vs. ξ^* in pulsed discharge

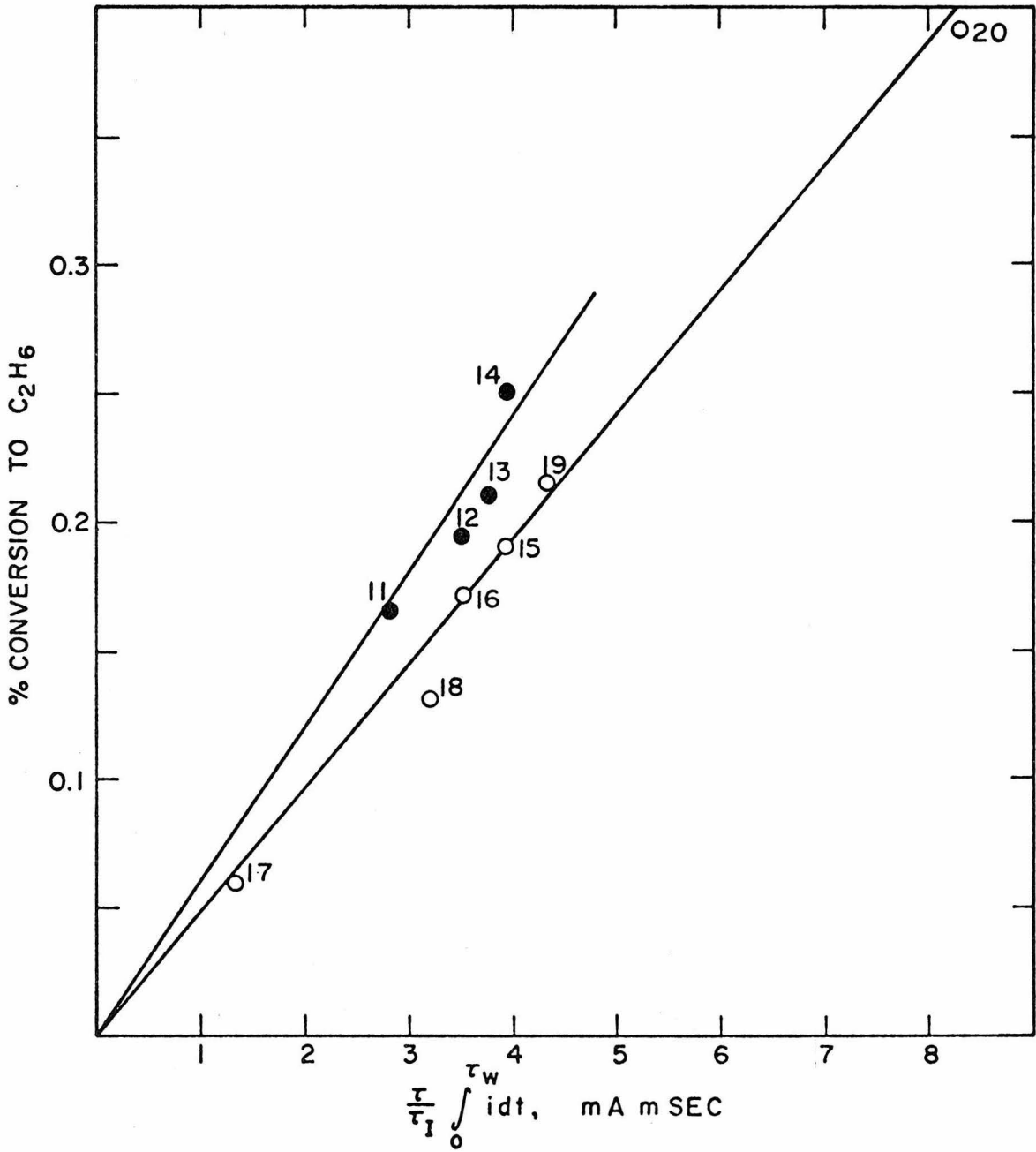


Fig. 73. Effect of τ , τ_w , τ_I variation on % conversion to C_2H_6 vs. ξ^*

Figure 73.

$p_1 = 5.0$ torr

#	τ msec	τ_I msec	τ_w msec	C_o % in Ar
11	93.5	52	1.6	1.75
12	93.5	40	1.6	1.75
13	93.5	30	1.6	1.75
14	93.5	22	1.6	1.75
15	93.5	30	0.8	2.05
16	93.5	30	0.8	2.05
17	93.5	30	0.2	2.05
18	93.5	30	0.6	2.05
19	142	52	1.6	2.05
20	281	52	1.6	2.05

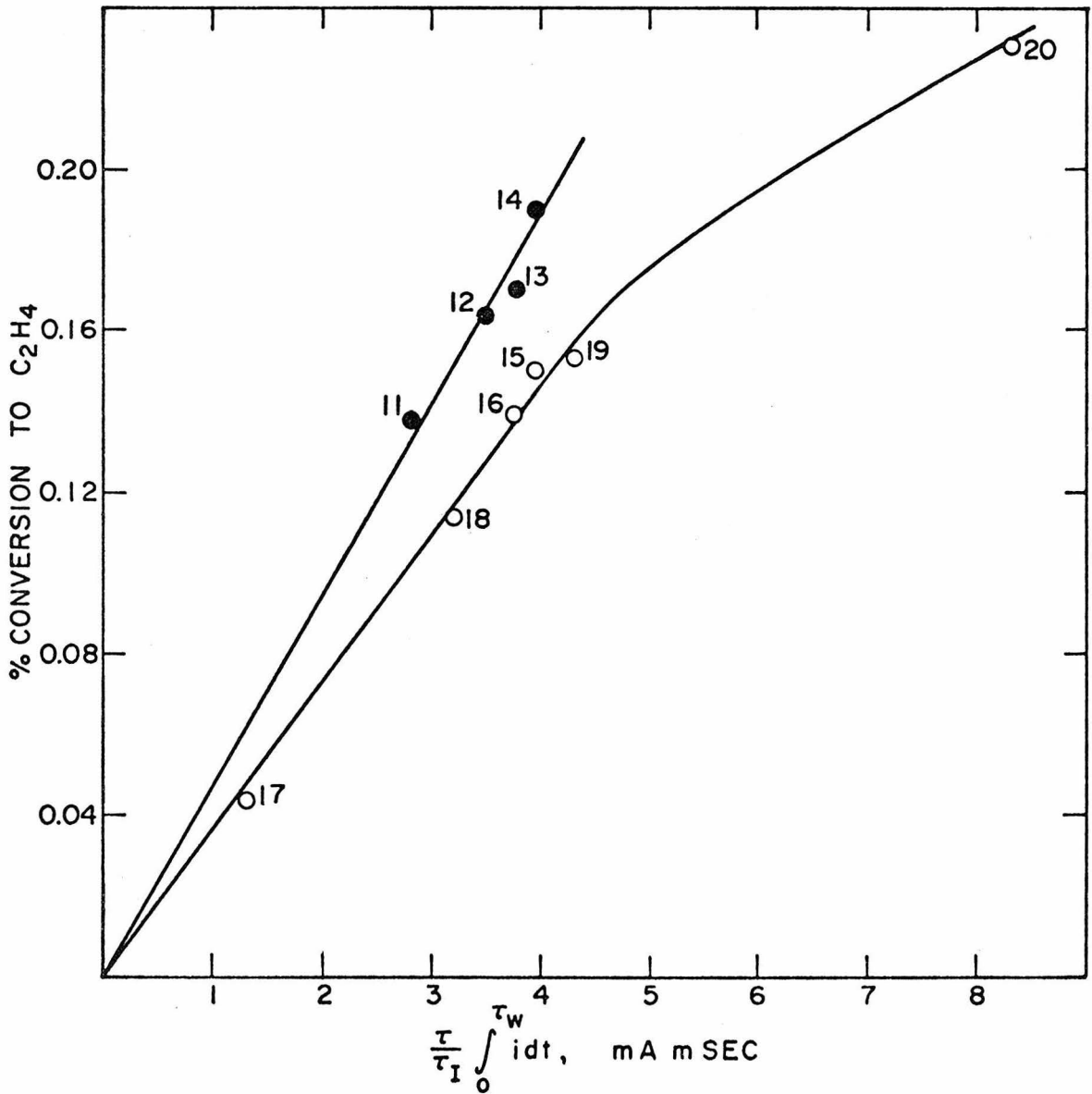


Fig. 74. Effect of τ , τ_w , τ_I variation on % conversion to C₂H₄ vs. ξ^*

Figure 74

$p_1 = 5.0$ torr

#	τ msec	τ_I msec	τ_w msec	C_o % in Ar
11	93.5	52	1.6	1.75
12	93.5	40	1.6	1.75
13	93.5	30	1.6	1.75
14	93.5	22	1.6	1.75
15	93.5	30	0.8	2.05
16	93.5	30	0.8	2.05
17	93.5	30	0.2	2.05
18	93.5	30	0.6	2.05
19	142	52	1.6	2.05
20	281	52	1.6	2.05

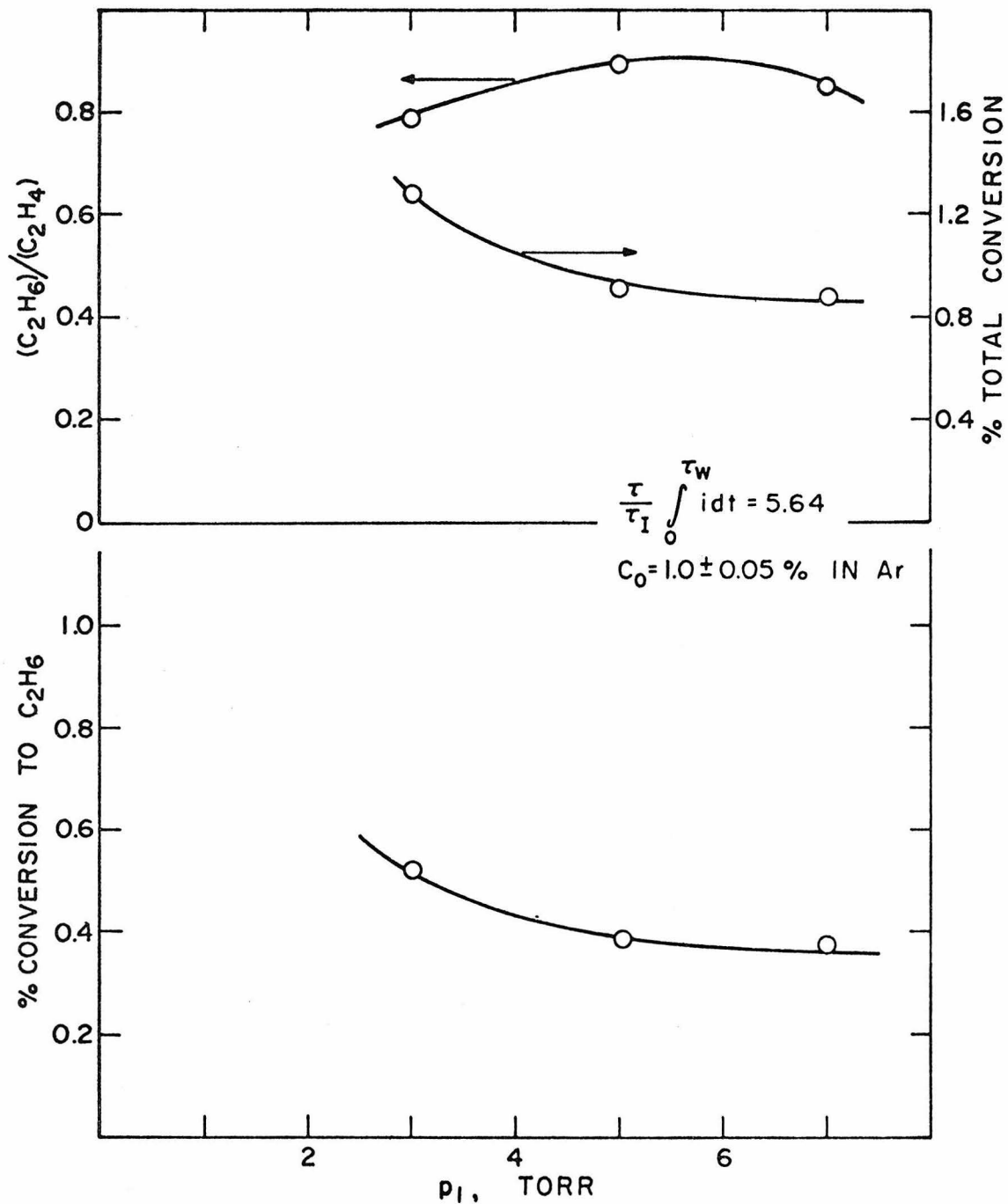


Fig. 75. Effect of total pressure p_1 on pulsed discharge reaction of CH_4

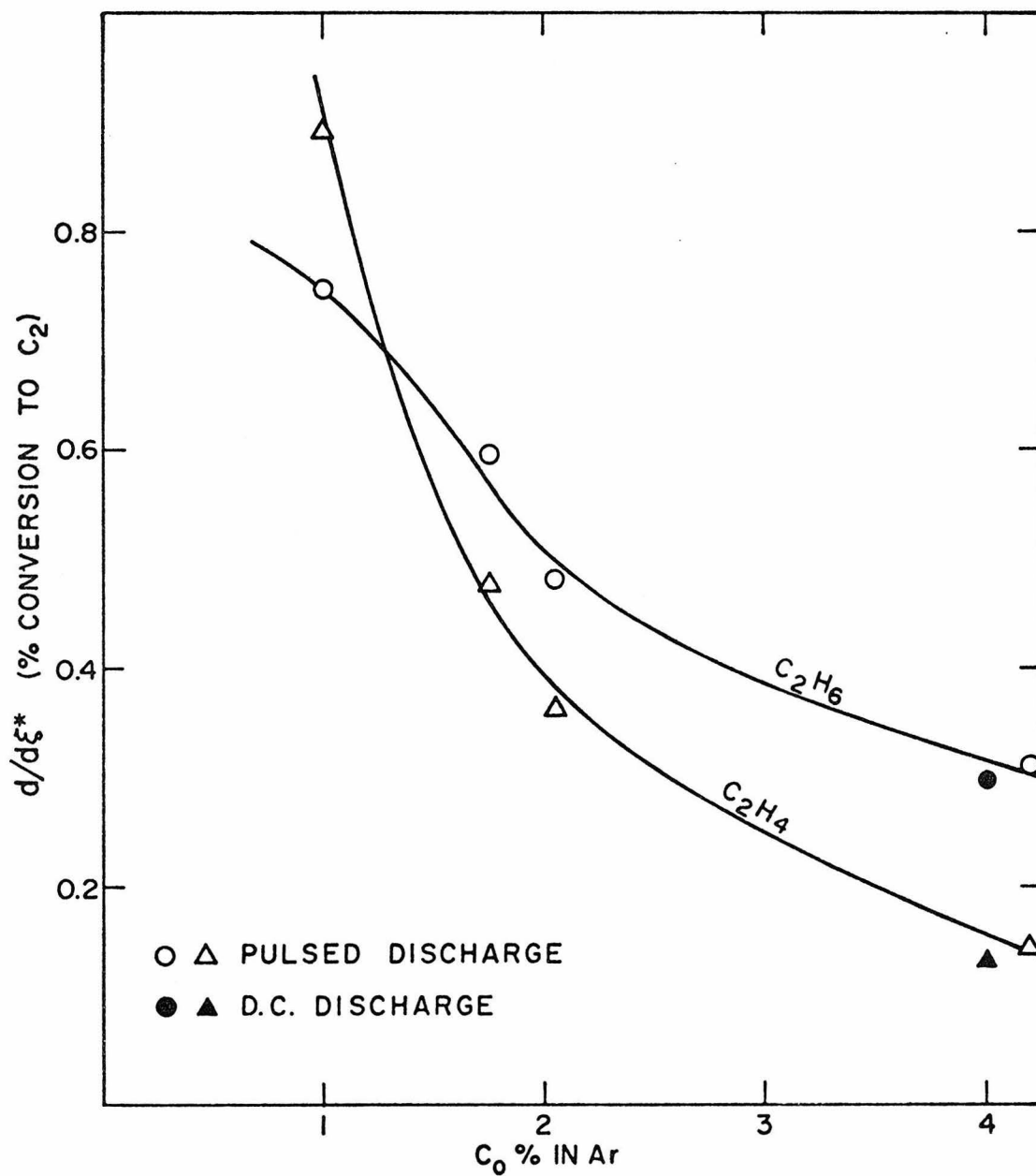
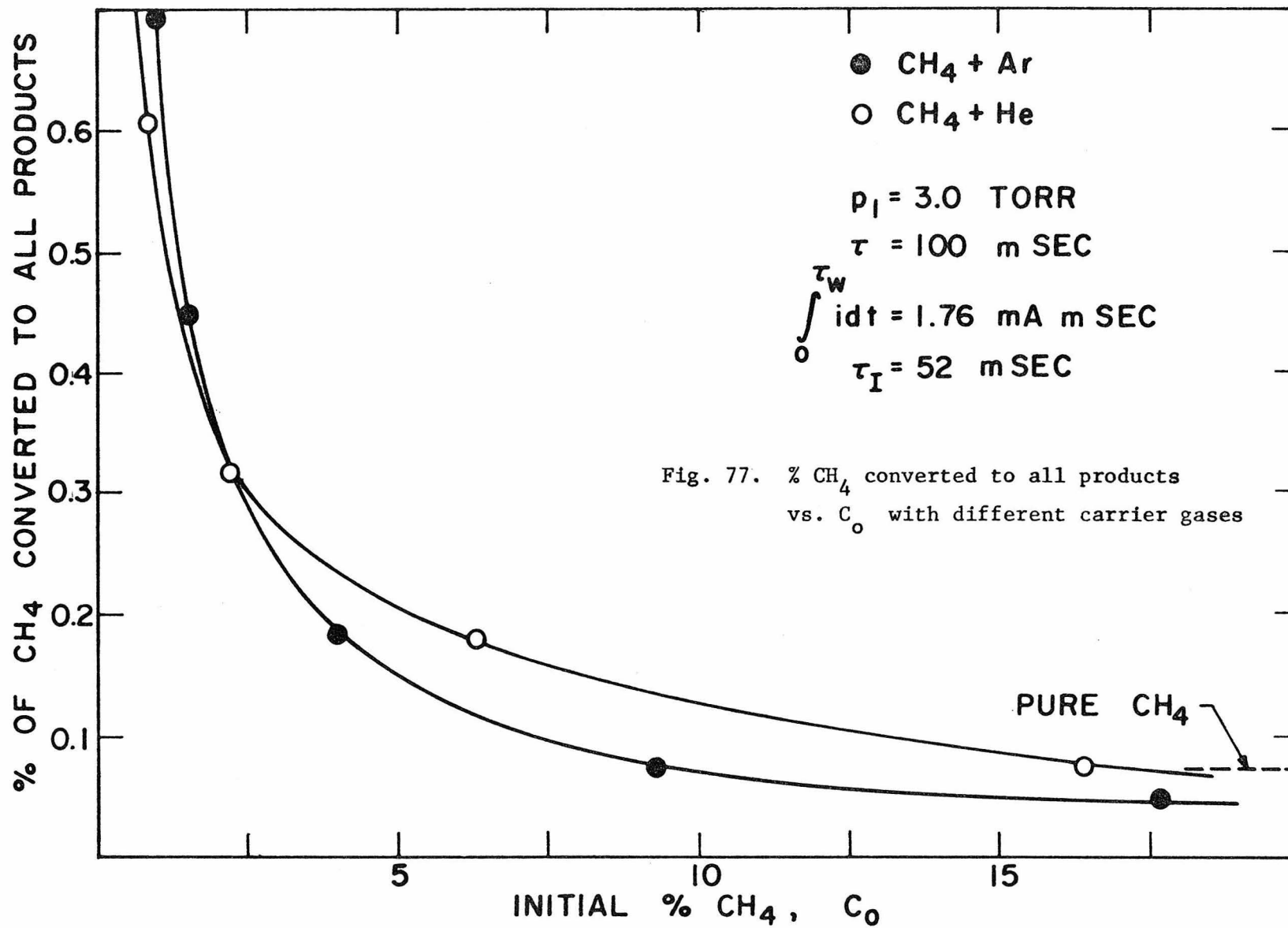


Fig. 76. Slopes of ethane and ethylene conversion curves in pulsed discharge vs. C_0



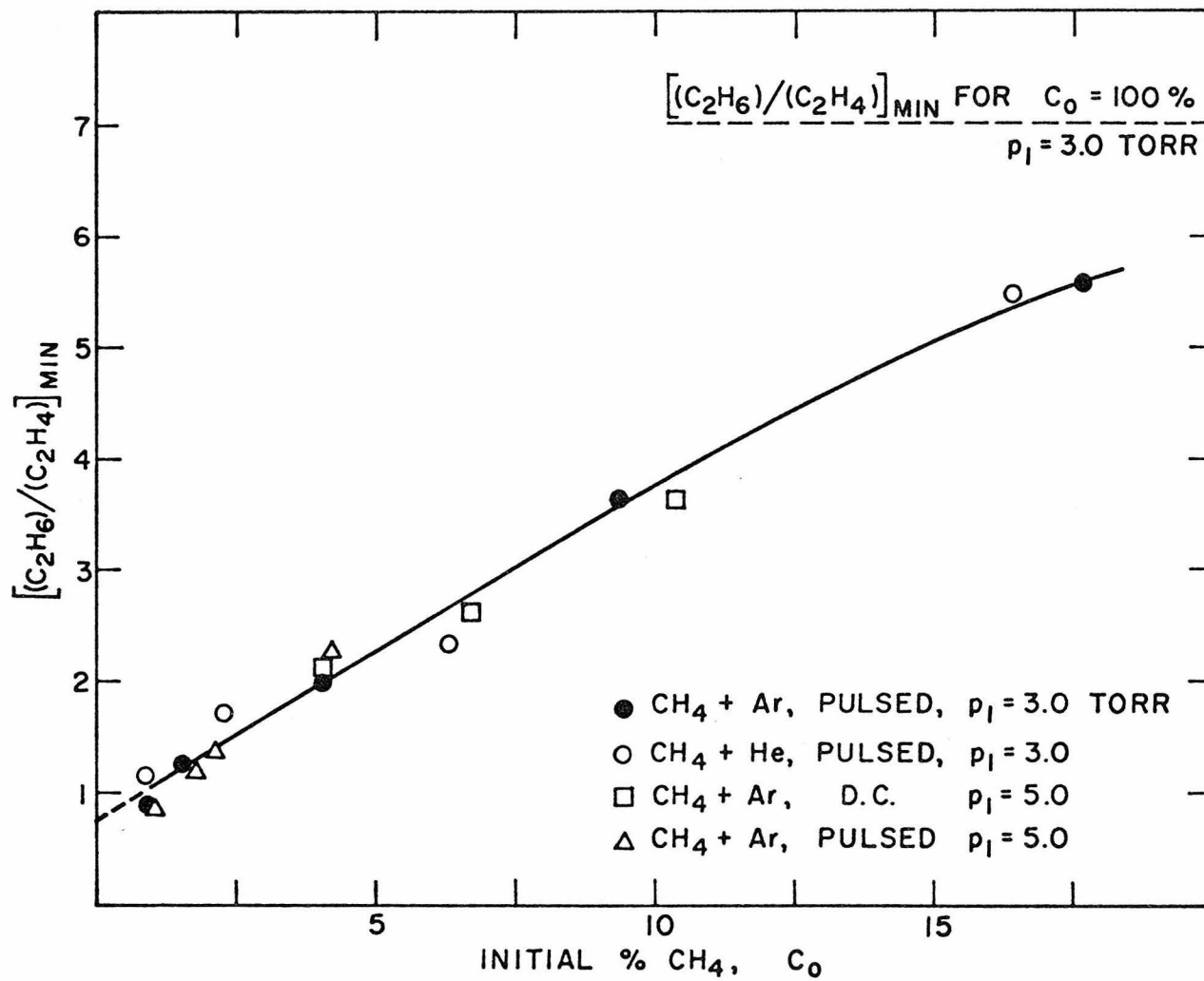


Fig. 78. Minimum ethane/ethylene ratio vs. C₀ with different carrier gases

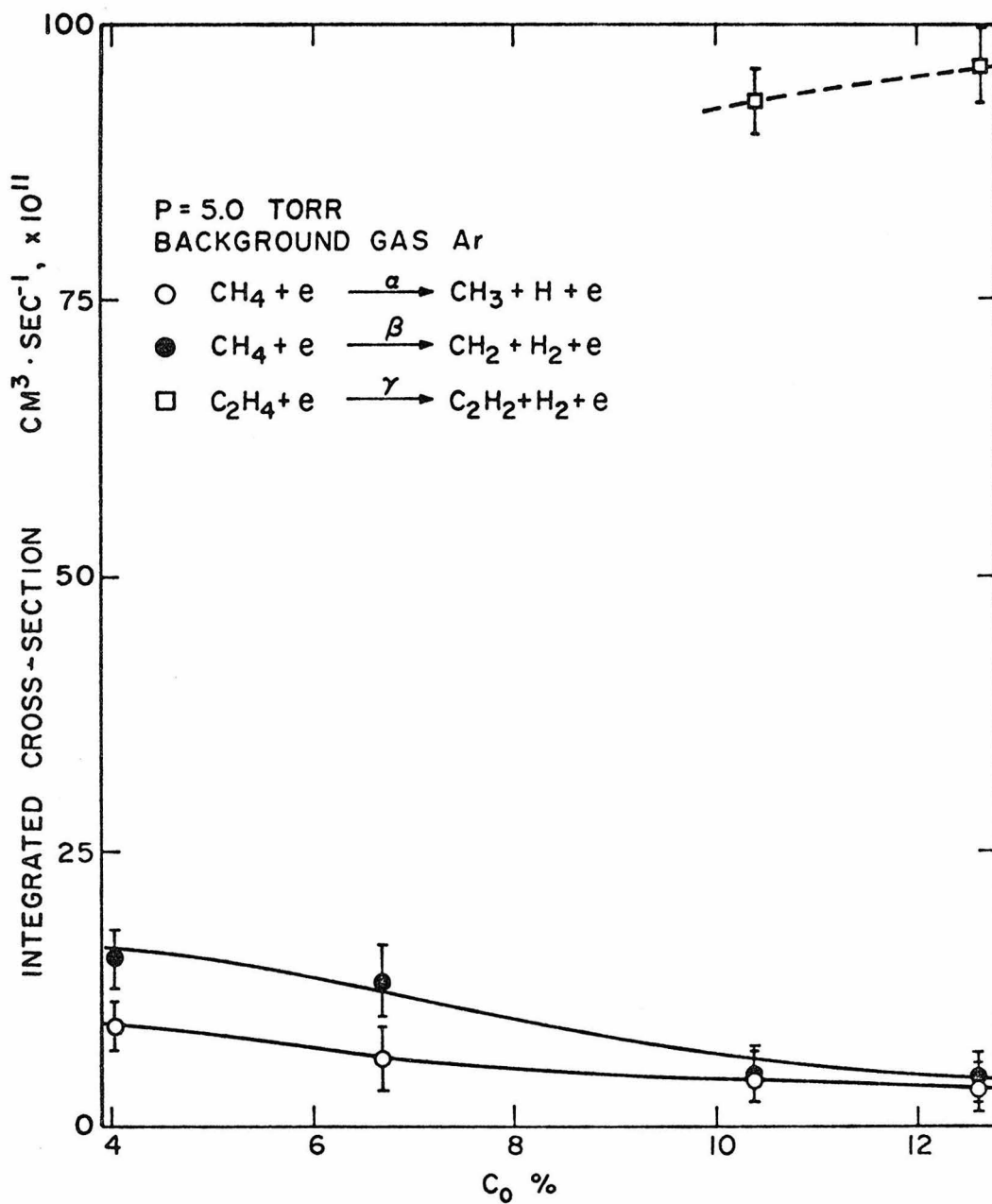


Fig. 79. Integrated cross-sections for electron-impact dissociation reactions

Fig. 80. INELASTIC COLLISION CROSS-SECTION
FOR H₂ DISSOCIATION
(PHYS. REV. VOL. 131, 5, 2115)

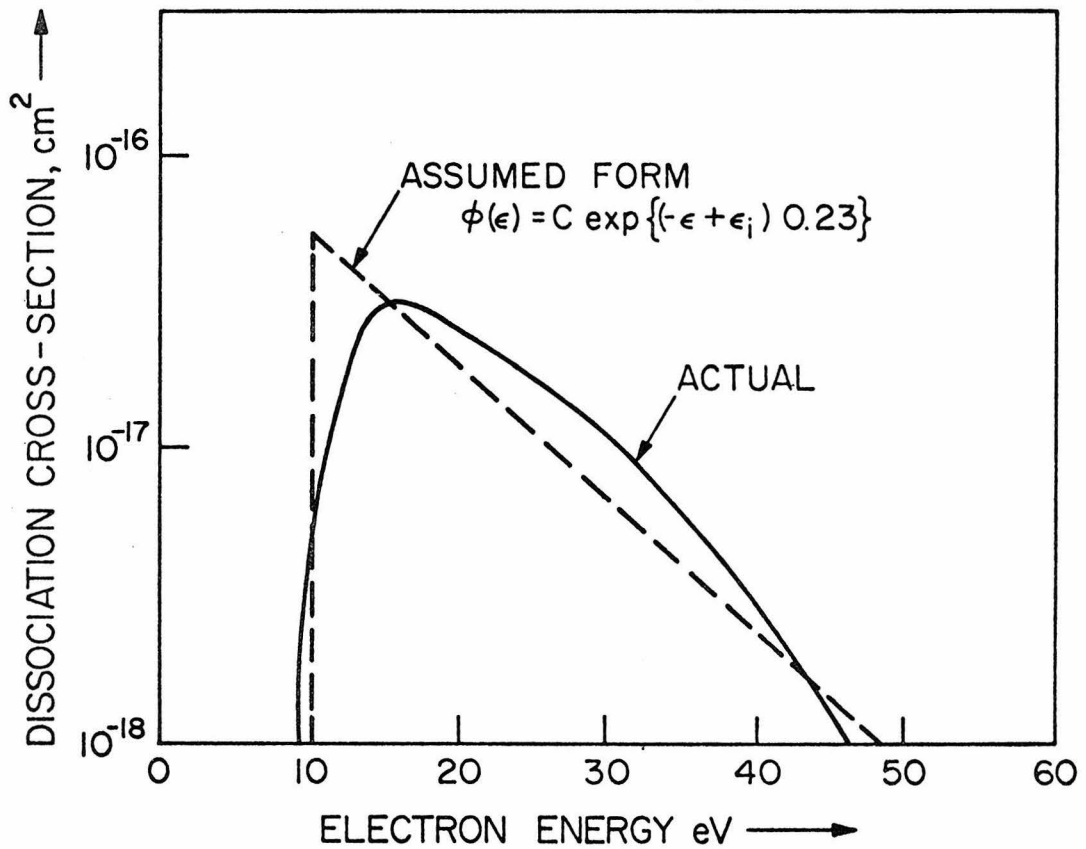


Fig. 81

THE MAXWELLIAN DISTRIBUTION OF ELECTRON ENERGIES

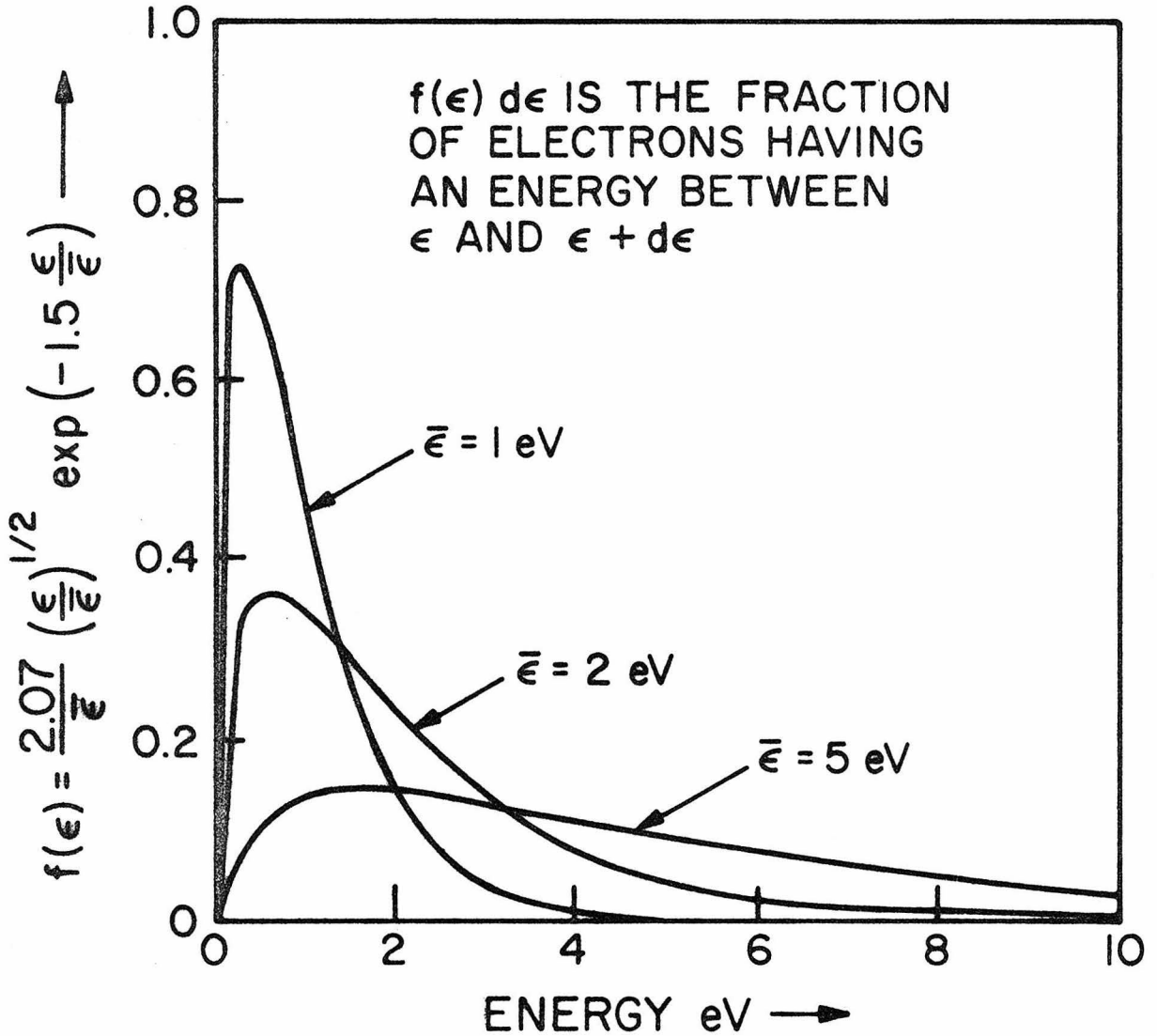


Fig. 82

THE DRUYVESTEYN DISTRIBUTION OF ELECTRON ENERGIES

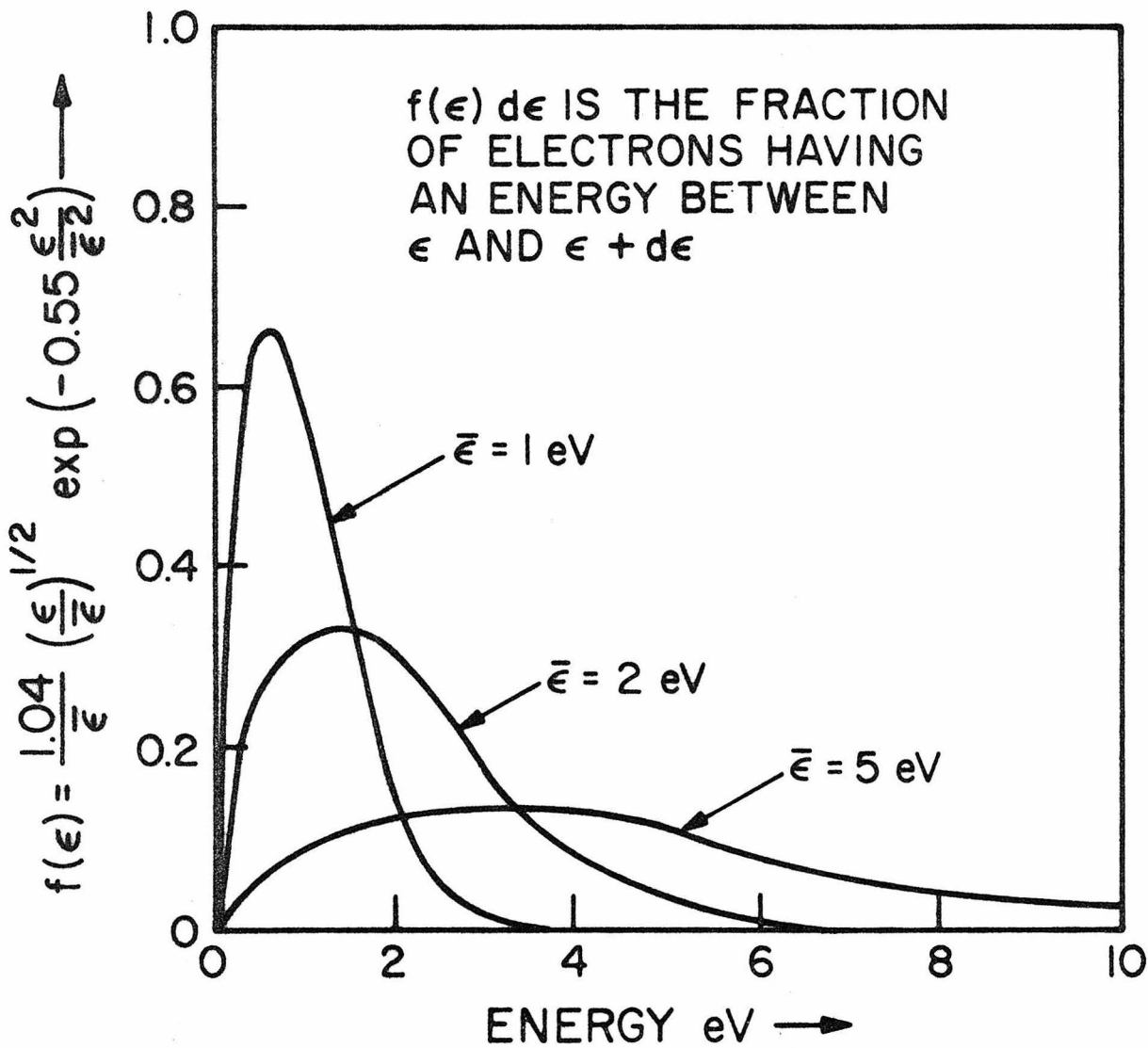
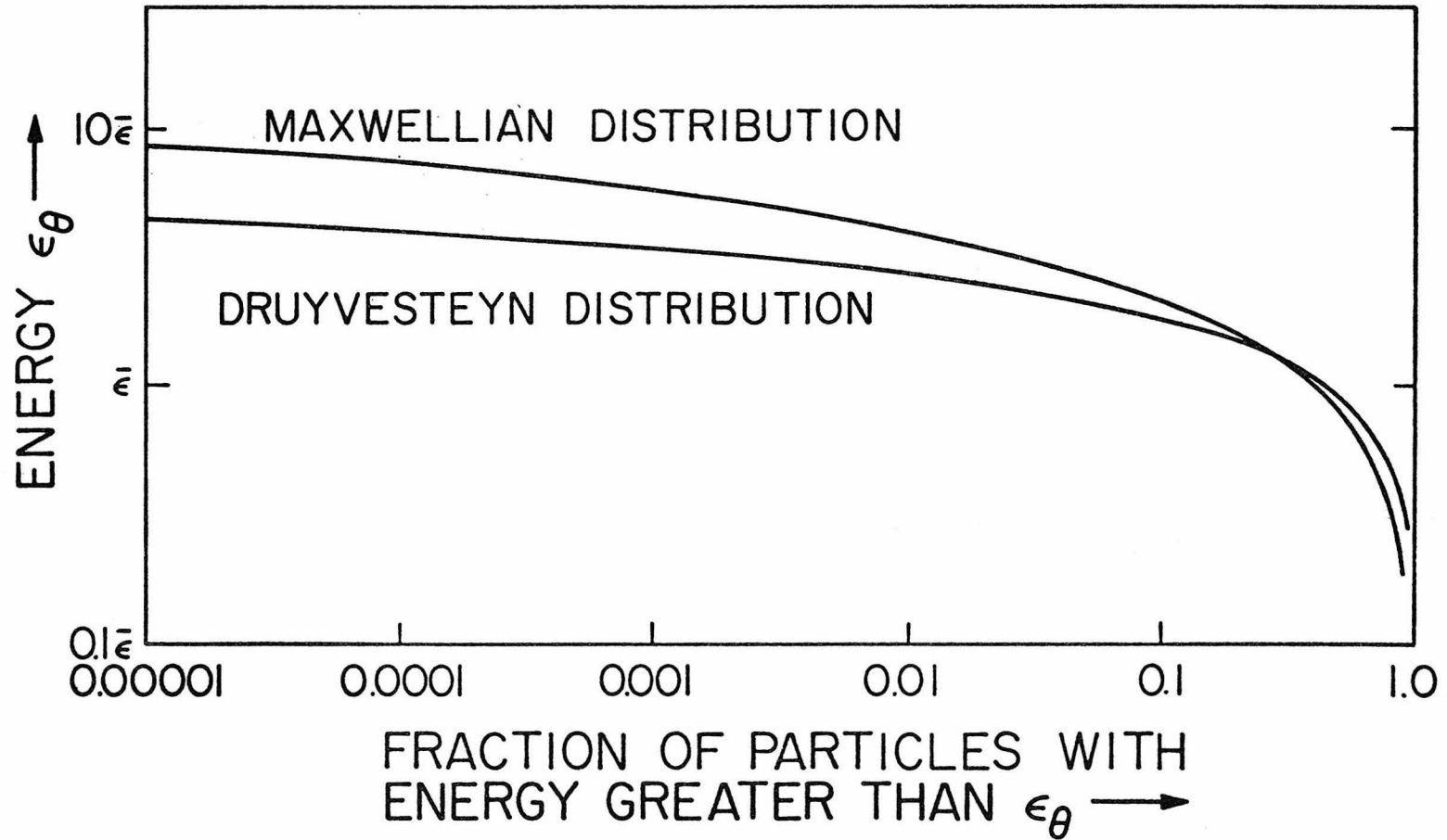


Fig. 83

A COMPARISON OF THE "TAILS" OF
THE MAXWELLIAN AND DRUYVESTEYN DISTRIBUTIONS



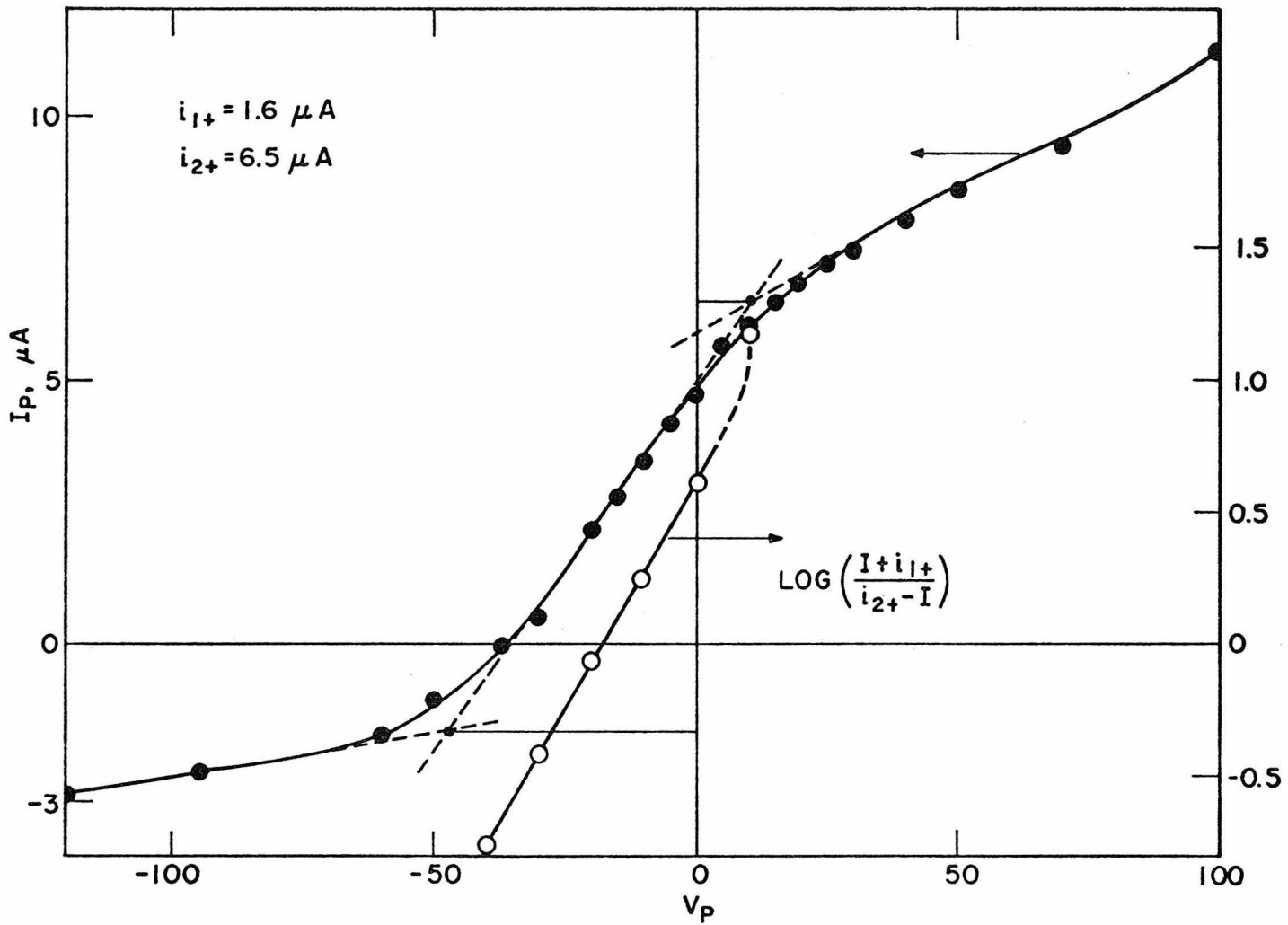


Fig. 85. Measured double probe characteristic in Ar at $p = 5.0$ torr , $I = 1.5$ mA

APPENDICES A-1 to A-9

Appendix A-1

ERROR ANALYSIS

The estimated errors of the directly measured quantities in the respective ranges in which observations were taken are summarized below.

<u>Variable</u>	<u>Range</u>	<u>% Error</u>
1) Pressure p (Todd gauge of Fig.25)	0.1 torr- 25 torr	±1%
2) Pressure p_1	3-9 torr	±2%
3) Pressure p_2	0.7 - 2.5 torr	±5%
4) Pressure p_6	0.9 - 2.0 torr	±5%
5) Electric Field E	5-60 V/cm	±5%
6) Voltage V	1000-5000V	±2%
7) Current I	0.5 - 20 mA	±2.5%
8) Resonant Frequency Shift δf_o	2-20 MHz ($\Delta f \times 1$)	±0.20 MHz
9) Change in half power width $\delta \Delta f_{1/2}$	2-20 MHz ($\Delta f \times 1$)	±0.20 MHz
10) Length L	30-66 cm	±2%
11) Residence time τ	57.5 - 655 msec	±5%
12) Pulse width τ_w	0.2 - 1.6 msec	±2%
13) Pulse interval τ_I	22-52 msec	±2%
14) Pulse current i	0.5-10 mA	±2%

	<u>Variable</u>	<u>Range</u>	<u>% Error</u>
15)	% CH ₄ in Feed, C _o	1.0 - 12.6%	± 6%
16)	% C ₂ H ₆ in Effluent, [C ₂ H ₆]	0.02 - 0.2%	± 7%
17)	% C ₂ H ₄ in Effluent, [C ₂ H ₄]	0.01 - 0.1%	± 7%
18)	% C ₂ H ₂ in Effluent, [C ₂ H ₂]	< 0.002 - 0.1%	±10% (when reported)
19)	% Conversion to C ₂ H ₆	0.1 - 6.0%	± 3%
20)	% Conversion to C ₂ H ₄	0.04 - 2.0%	± 3%
21)	% Conversion to C ₂ H ₂	< 0.04 - 1.7%	± 6% (when reported)

Errors in calculated quantities may be estimated by repeated calculation of replicate points, as was done in Chapter 3 for v_d . Alternatively, an upper bound estimate may be obtained by the method of Mickley, Sherwood and Reed.⁽¹³²⁾ The method is illustrated for $(n_e)_o$, v_{en} and v_d calculated from δf_o and $\delta \Delta f_{1/2}$. Let $\delta f_o = (f'_o - f_o) = y$, $\delta \Delta f_{1/2} = x$, $(n_e)_o = n$. Then

$$n = \frac{2y}{f_o} \frac{[(2\pi f_o)^2 + v_{en}^2]}{\eta} \times \frac{10^{-6}}{56.4^2} \quad (\text{A-1.1})$$

and

$$v_{en} = \pi f_o \frac{x}{y} \quad (\text{A-1.2})$$

(from equations (2) and (3))

$$\Delta v_{en} = \frac{\pi f_o}{y} \Delta x - \frac{\pi f_o x}{y^2} \Delta y + \frac{\pi x}{y} \Delta f_o \quad (\text{A-1.3})$$

Taking typical values as $x = 2.84$ MHz, $\Delta x = \pm 0.20$ MHz, $y = 6.82$ MHz,

$\Delta y = \pm 0.20$ MHz, $f_o = 3043$ MHz, $\Delta f_o = \pm 30$ MHz, we find from equations (A-1.2) and (A-1.3)

$$v_{en} = 4 \times 10^9 \text{ per sec} , \quad \Delta v_{en} = \pm 4 \times 10^8 \text{ per sec} \approx \pm 10\%$$

where errors in equation (A-1.3) were added for the worst possible combination of signs $+ - +$ and $- + -$. Similarly,

$$\begin{aligned} \Delta n = & \frac{2y}{f_o \eta} 2v_{en} \frac{10^{-6}}{56.4^2} \cdot \Delta v_{en} \\ & + \frac{2}{f_o \eta} [(2\pi f_o)^2 + v_{en}^2] \cdot \frac{10^{-6}}{56.4^2} \Delta y \\ & - \frac{2y}{f_o^2} \frac{[(2\pi f_o)^2 + v_{en}^2]}{\eta} \cdot \frac{10^{-6}}{56.4^2} \Delta f_o \\ & + \frac{2y}{f_o \eta} 8\pi^2 f_o \frac{10^{-6}}{56.4^2} \cdot \Delta f_o \end{aligned} \quad (\text{A-1.4})$$

A corresponding equation may be derived for v_d based on equation (8). The calculated values for the same set of numbers as was used above for v_{en} are

$$n = 5.55 \times 10^{10} \text{ per cm}^3 , \quad \Delta n = \pm 3.5 \times 10^9 \text{ per cm}^3 = \pm 6.3\%$$

$$v_d = 3.24 \times 10^6 \text{ cm/sec} \quad \Delta v_d = \pm 4.6 \times 10^5 \text{ cm/sec} = \pm 14\%$$

The same type of analysis is applicable to the calculated quantities of Part 2, e.g., α , β and γ shown in Fig. 79. A sophisticated analysis of the question of error propagation in first order kinetic schemes is presented in Proposition I, which should be useful when extremely precise rate constant measurements are sought.

Appendix A-2

CALCULATION OF STEADY-STATE CONCENTRATION PROFILES

Assuming constant $\alpha = \frac{\langle n_+ \rangle}{\langle n_o \rangle + \langle n_+ \rangle} \frac{\mu EL}{D}$, the model⁽⁸⁾ predicts steady-state concentration profiles of the form

$$\theta(\eta, \infty) = K e^{-\alpha \eta} \quad (\text{A-2-1})$$

where

$$K = (1 + \delta + \epsilon) / \left(\delta + \epsilon e^{-\alpha} - \frac{e^{-\alpha}}{\alpha} + \frac{1}{\alpha} \right) \quad (\text{A-2-2})$$

$$\theta = \frac{\langle n_o \rangle + \langle n_+ \rangle}{n_o^o}$$

$$\delta = \frac{\text{Cathode end bulb volume}}{\text{Discharge tube volume}}$$

$$\epsilon = \frac{\text{Anode end bulb volume}}{\text{Discharge tube volume}}$$

$$\eta = \frac{z}{L}, \text{ dimensionless distance from cathode.}$$

The measured $\langle n_e \rangle$ and E for a given η , say η_1 , were used in an iterative scheme to back out $\theta(\eta_1, \infty)$. Initially, it was assumed that $\langle n_e \rangle = \langle n_+ \rangle$, but it turned out that in some cases (e.g., Fig. 22) when $\langle n_o \rangle$ was small, there was no solution. For those cases, an empirical factor $J = \frac{\langle n_+ \rangle}{\langle n_e \rangle}$ was introduced and the value of J closest to 1.0 for which there was a solution was accepted as the correct one. The majority of the cases, however, could be solved with $J = 1.0$. As shown in Fig. 21, two solutions result, of which the one with the lower α is physically significant. The higher value of α appears unreasonable compared to what might be expected at this current from composition measurements.⁽⁴¹⁾

The scheme of calculation was as follows:

- 1) Assume $\theta(\eta_1, \infty)$. Reasonable starting value is

$$\frac{1 + \delta + \epsilon}{\delta} = \lim_{\alpha \rightarrow 0} K$$

- 2) Assume $J = \frac{\langle n_+ \rangle}{\langle n_e \rangle}$. Reasonable starting value is 1.0.

- 3) Use measured $\langle n_e \rangle$ and E at η_1 to calculate

$$\alpha = \frac{\langle n_+ \rangle}{n_o \theta} \frac{\mu EL}{D}$$

E at the central position is an interpolated value.

- 4) Calculate $K = (1 + \delta + \epsilon) / (\delta + \epsilon e^{-\alpha} - \frac{e^{-\alpha}}{\alpha} + \frac{1}{\alpha})$
- 5) Calculate $\theta'(\eta_1, \infty) = K e^{-\alpha \eta}$
- 6) Compare θ' to assumed θ and modify assumed θ until agreement is reached (Fig. 21).
- 7) If no agreement is possible for $J = 1.0$, reduce J in steps until a solution is obtained. The first value of J at which this happens is accepted.

Appendix A-3

MEASUREMENT OF WALL TEMPERATURE

As pointed out in the section on experimental technique, the portion of the discharge tube between the end bulbs was not water cooled. As a result, the wall temperature during the experiments used to rise above room temperature. An attempt was made to estimate the extent of this increase by inserting a glass-sheathed copper-constantan thermocouple such that it barely made contact with the plasma. The readings on this thermocouple rose with time in an approximately exponential manner after the discharge was switched on. The time constant for this rise was as high as 1-2 minutes, indicating that convection from the tube to the ambient air was the predominant process in the heat transfer. For $I = 15$ mA, the final temperature was in no case more than 25°C above room temperature.

At steady-state, since there is no energy going into heating the electrons, neutrals or the wall, the input energy is either convected to the ambient air from the hot outside wall of the tube or radiated as the characteristic spectrum of the discharge. Let \bar{k} = fraction of input energy convected to the air. Then,

$$h \pi r_o (T_w - T_a) = \bar{k} E I \quad (\text{A-3-1})$$

where h = heat transfer coefficient for natural convection to air from horizontal cylinder of outer radius r_o

T_w = wall temperature

T_a = ambient air temperature

Hence
$$\frac{T_w}{T_a} = \left(1 + \frac{\bar{k} E I}{h T_a r_o}\right) \quad (\text{A-3-2})$$

Thus a plot of T_w/T_a vs. $E I$ should provide some information on \bar{k} and hence $(1 - \bar{k})$, the fraction of energy radiated away. Figure 23 shows such a plot for helium discharges under a wide variety of pressures and currents. It is seen that it is approximately linear for low $E I$ with slope corresponding to $\frac{\bar{k}}{h} = 0.016 \text{ m}^2 \text{ }^\circ\text{C/watts}$. Using a value of $h = 6.82 \text{ watts/m}^2 \text{ }^\circ\text{C}$ estimated from Perry,⁽⁴⁵⁾ we get $\bar{k} = 0.11$. This means that nearly 90% of the input energy is radiated away in such discharges. At higher currents, the fraction of energy radiated is even higher.

N.B.: The heat generation term in the energy balance can also be calculated from the electrical conductivity as

$$\begin{aligned} Q &= \frac{EI}{\pi R^2} = \langle \sigma_o \rangle E^2 \\ &= \frac{\langle n_e \rangle e^2}{m_e \nu_{en}} E \end{aligned}$$

The Q calculated from $\langle n_e \rangle$ and ν_{en} measurements comes within 3% of the Q calculated from I measurements.

Appendix A-4

LINEAR PERTURBATION ANALYSIS OF A RESONANT MICROWAVE CAVITY

The propagation of a plane electromagnetic wave of frequency ω is described by the equation

$$\vec{E} = \vec{E}_0 \exp i(\omega t - \vec{k} \cdot \vec{r}) \quad (\text{A-4.1})$$

where \vec{k} is the propagation vector which has a real and imaginary part in a lossy medium such as the plasma. Further, a weakly ionized plasma behaves as a Lorentz gas. Hence, the phenomena of interest can be described by the motion of an "average" electron, as modified by collisions with infinitely heavy neutrals. Application of Newton's second law to such an electron leads to Langevin's equation. All magnetic forces are neglected in writing this equation

$$m_e \frac{d\vec{v}}{dt} + m_e \nu_{en} \vec{v} = -e \vec{E}_0 \exp i(\omega t - \vec{k} \cdot \vec{r}) \quad (\text{A-4.2})$$

Langevin's equation is now solved in conjunction with Maxwell's field equations.

When the amplitude of the oscillatory motion of the electrons is small compared to that of the wave, or if \vec{k} is perpendicular to \vec{E}_0 (transverse polarization), the oscillatory solution for \vec{v} is

$$\vec{v} = -[e \vec{E}_0 \exp i(\omega t - \vec{k} \cdot \vec{r})] / [m_e (i\omega + \nu_{en})] \quad (\text{A-4.3})$$

The current density induced in an electron gas of density n_e is

$$\vec{J} = n_e (-e) \vec{v} \quad (\text{A-4.4})$$

Maxwell's field equations in rationalized MKS units are

$$\vec{\nabla} \times \vec{E} = -\mu_0 \frac{\partial \vec{H}}{\partial t} \quad (\text{A-4.5})$$

$$\vec{\nabla} \times \vec{H} = \vec{J} + \epsilon_0 \frac{\partial \vec{E}}{\partial t} \quad (\text{A-4.6})$$

Eliminating \vec{H} from (A-4.5) and (A-4.6)

$$\vec{\nabla} \times (\vec{\nabla} \times \vec{E}) = -\mu_0 \vec{J} - \frac{1}{c^2} \frac{\partial^2 \vec{E}}{\partial t^2} \quad (\text{A-4.7})$$

Using (A-4.3) and (A-4.4)

$$k^2 \vec{E} = -\frac{n_e e^2}{m_e} \frac{i\omega \mu_0}{(i\omega + \nu_{en})} \vec{E} + \frac{\omega^2}{c^2} \vec{E} \quad (\text{A-4.8})$$

Since $\vec{E} \neq 0$

$$k^2 = \frac{\omega^2}{c^2} \left[1 - \frac{\omega_p^2}{\nu_{en}^2 + \omega^2} \left(1 + i \frac{\nu_{en}}{\omega} \right) \right] \quad (\text{A-4.9})$$

where

$$\omega_p^2 = \frac{n_e e^2}{m_e \epsilon_0} \quad (\text{A-4.10})$$

By analogy with the terminology of optics, the quantity multiplying ω^2/c^2 in equation (A-4.9) may be called the square of the complex index of refraction of the plasma.

Therefore,

$$\bar{\mu} = \left[1 - \frac{\omega_p^2}{\nu_{en}^2 + \omega^2} \left(1 + i \frac{\nu_{en}}{\omega} \right) \right]^{1/2} \quad (\text{A-4.11})$$

If $\frac{\omega_p^2}{\nu_{en}^2 + \omega^2} \ll 1$ and $\nu_{en} \ll \omega$ (low density plasma),

$$\bar{\mu} \approx \left[1 - \frac{\omega_p^2}{2(\nu_{en}^2 + \omega^2)} \right] - i \frac{\omega_p^2}{2(\nu_{en}^2 + \omega^2)} \frac{\nu_{en}}{\omega} \quad (\text{A-4.12})$$

Thus, when $n_e \rightarrow 0$ ($\omega_p \rightarrow 0$), the index of refraction is unity. In this case, the wave propagates through free space. Equation (A-4.12) assumes that ν_{en} is independent of the electron velocity.

A first order perturbation analysis of equation (A-4.12) leads to

$$\frac{\delta f_o}{f_o} = \frac{1}{2} \frac{\omega_{po}^2}{\omega^2 + \nu_{en}^2} \eta \quad (\text{A-4.13})$$

$$\delta\left(\frac{1}{Q}\right) = \frac{\omega_{po}^2}{\omega^2 + \nu_{en}^2} \frac{\nu_{en}}{\omega} \eta \quad (\text{A-4.14})$$

where η is a dimensionless form factor given by

$$\eta = \frac{\int \frac{n_{x,y}}{(n_e)_o} \vec{E}_o \cdot \vec{E}_o \, dV}{\int \vec{E}_o \cdot \vec{E}_o \, dV} \quad (\text{A-4.15})$$

Plots of η for various cavity modes are presented in Ref. (23).

Appendix A-5

ELECTRON-ION RECOMBINATION IN THE AFTERGLOW OF A PULSED
DISCHARGE

In an afterglow plasma where fresh ionization does not occur, electrons can disappear by way of diffusion to the walls (and surface recombination), by volume recombination with ions and by attachment to neutrals. If there is only one species of positive ion, and that species is singly charged, the general equation for the time dependence of n_e is

$$\frac{\partial n_e}{\partial t} = D_a \nabla^2 n_e - \alpha' n_e^2 - \nu_a n_e \quad (\text{A-5.1})$$

(1) (2) (3)

where D_a is the ambipolar diffusion coefficient, α the second order volume recombination coefficient and ν_a the attachment coefficient. D_a , α' and ν_a are functions of electron temperature T_e if a Maxwellian $f_e(\epsilon)$ is assumed.

1) Recombination only: Set terms (1) and (3) of equation (A-5.1) = 0 .

Assuming constant T_e , the electron density n_e decays as

$$\frac{1}{n_e(t)} = \frac{1}{n_e(0)} + \alpha'(t - t_0) \quad (\text{A-5.2})$$

where $n_e(0)$ is the initial density at $t = t_0$.

2) Diffusion only: Set terms (2) and (3) in equation (A-5.1) = 0 .

$$n_e = \sum_i a_i \exp(-t/T_i) \quad (\text{A-5.3})$$

where $T_i = \Lambda_i^2 / a$, Λ_i being the diffusion length for the i^{th} spatial mode.

3) Diffusion and recombination: Set term (3) in (A-5.1) = 0 .

Consider the particular case where recombination is small compared to diffusion. Then the density distribution is determined essentially by the prevailing diffusion mode. If only the fundamental mode is effective,

$$\frac{\partial n_e}{\partial t} = D_a \nabla^2 n_e - \alpha' n_e^2 = - \frac{D_a}{\Lambda^2} n_e - \alpha' n_e^2 \quad (\text{A-5.4})$$

which yields

$$\frac{n_e(t)}{\frac{D_a}{\Lambda^2} + \alpha' n_e(t)} = \frac{n_e(0)}{\frac{D_a}{\Lambda^2} + \alpha' n_e(0)} \exp \left\{ - \frac{D_a}{\Lambda^2} (t - t_0) \right\} \quad (\text{A-5.5})$$

4) Attachment only: Neglect terms (1) and (2) in (A-5.1).

For constant v_a , we get an exponential decrease in density with the period $1/v_a$.

Other cases including those of multiple positive ions and of negative ions are discussed by Hasted. (105)

The $(n_e)_0 - t$ curves in pure Ar (Fig. 66) were analyzed for recombination and diffusion effects. Following Biondi, (133) $1/\bar{n}_e(t)$ was plotted against t . Straight lines were obtained for small values of t , after which the plots curved upward (Fig. A-5.1). The slope of the straight line portions was found to be $3.4 \pm 0.6 \times 10^{-7} \text{ cm}^3/\text{sec}$ and independent of pressure in the range $p_1 = 3.0 - 9.0$ torr. This slope can be interpreted directly as the recombination coefficient, (134)

as $\beta' = \frac{\alpha' n_0 \Lambda^2}{a} \sim 10^6 \gg 1$. The α' value is in fair agreement with Biondi's corrected value of $6 \times 10^{-7} \text{ cm}^3/\text{sec}$ and must be interpreted as applicable to the dissociative recombination process $\text{Ar}_2^+ + e \rightarrow \text{Ar} + \text{Ar}$ as Ar^+ ions are negligibly important in pure Ar discharges. (133) The difference between our value and Biondi's could be because his afterglow had $T_e = T_g$, whereas in our case the electrons could remain hot because there is a d.c. electric field present even after the discharge is "off" (Fig. 40,65). In any event, the fact that α' was in the high range $10^{-6} - 10^{-7}$ and was independent of pressure must be taken as striking verification of Biondi's work.

In pulsed discharges in pure He, microwave measurements were, unfortunately, not possible due to the distorting effect of current oscillations. If the effect of oscillations could be overcome, a comparison with the work of Phelps and Brown (135) in the afterglow of pulsed microwave discharges in pure He may be possible.

One set of readings was obtained in pure CH_4 at $p_1 = 1.5$ torr (Fig. 66). The nonlinearity of the $\log(n_e)_0$ vs. t curve is not pronounced enough to rule out pure diffusion. However, an explanation of the plot in terms of diffusion alone would demand a value of $D_a \approx 170 \text{ cm}^2/\text{sec}$, which appears too low. Since the self-diffusion coefficient of CH_4 at 300°K and 1.5 torr is $114 \text{ cm}^2/\text{sec}$, (103) T_e will have to be approximately equal to T_g to support a low value of a such as $170 \text{ cm}^2/\text{sec}$. As pointed out above, this is unlikely in our afterglow. An explanation of the CH_4 data in terms of recombination (Fig. A-5.1) suggests an α' value of $6.1 \times 10^{-7} \text{ cm}^3/\text{sec}$. In view of the possible presence of a number of other ions like CH_5^+ , CH_3^+ , CH_2^+ ,

etc., it is not clear if this α value applies to the recombination of the CH_4^+ ion.

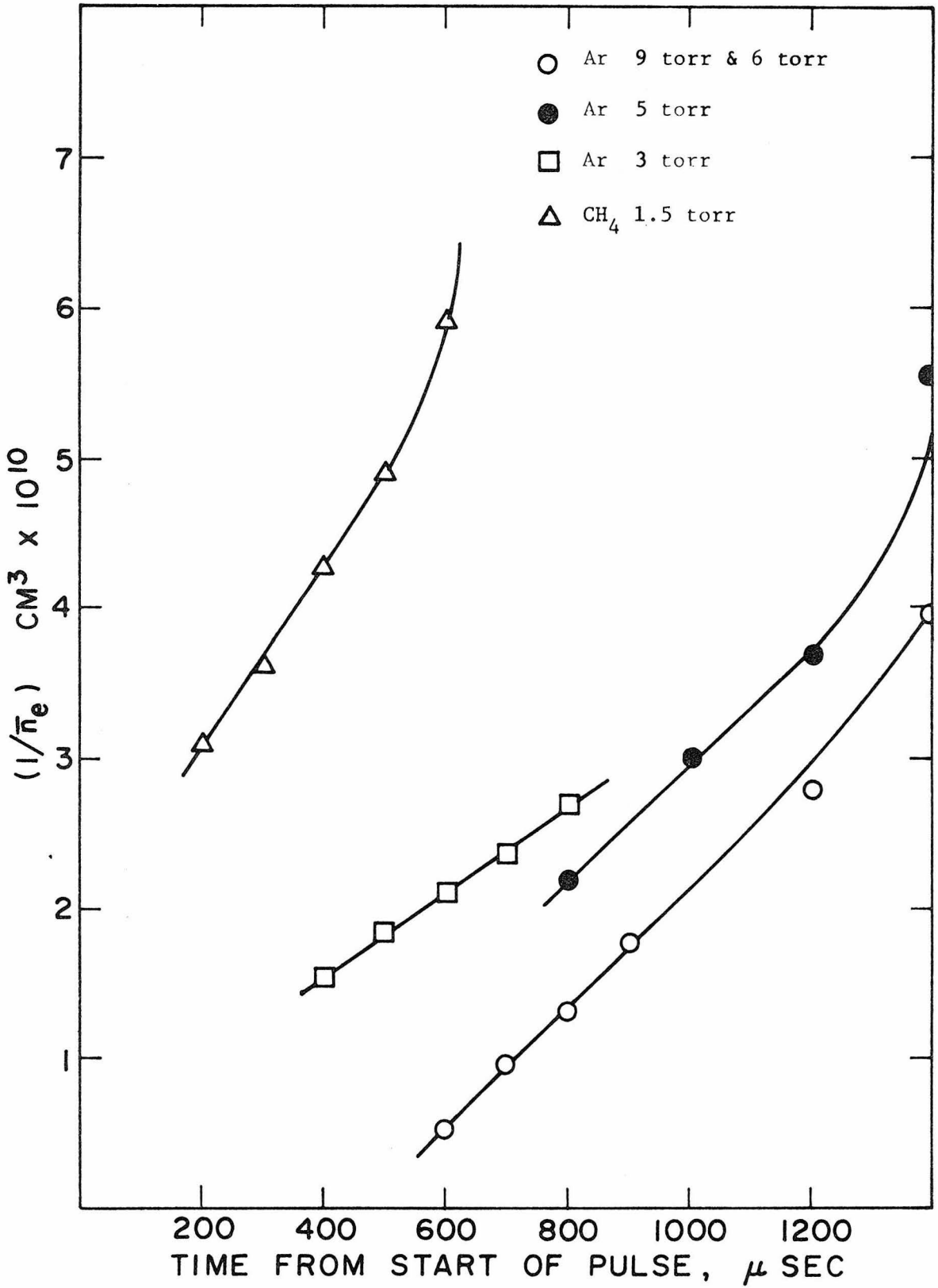


Fig. A-5.1. Test of recombination control in CH_4 and Ar afterglows

Appendix A-6

EVALUATION OF THE INTEGRAL \bar{I} : OF EQUATION (66)

$$\begin{aligned} \bar{I} &= \int_x^{\infty} e^{-\zeta} \zeta^{-1/2} d\zeta \\ &= \int_0^{\infty} e^{-\zeta} \zeta^{-1/2} d\zeta - \int_0^x e^{-\zeta} \zeta^{-1/2} d\zeta \\ &= \Gamma(1/2) - x^{1/2} \Gamma(1/2) \gamma^*\left(\frac{1}{2}, x\right) \end{aligned}$$

where γ^* is a form of the incomplete gamma function which has been tabulated for a limited range of x in Ref. 114.

An asymptotic form of \bar{I} can be obtained for large values of x as shown below.

$$\begin{aligned} \text{Let } u &= \frac{\zeta}{x} - 1 \\ du &= \frac{d\zeta}{x} \end{aligned}$$

$$\begin{aligned} \text{Then } \bar{I} &= \int_0^{\infty} e^{-x(1+u)} x^{-1/2} (1+u)^{-1/2} x du \\ &= x^{1/2} e^{-x} \int_0^{\infty} e^{-xu} (1+u)^{-1/2} du \end{aligned} \tag{A-6.2}$$

Laplace's method (as outlined in Ref. 136) is used for the asymptotic expansion for large x .

Laplace's method: (All variables below have meanings restricted to Appendix A-6).

$$\text{Let } F(x) = \int_0^a \theta(t) \exp(-xt^\alpha) dt$$

where $a > 0$, $\alpha > 0$, $\theta(t) = t^\beta (a_0 + a_1 t + \dots)$, $\beta > -1$

$$\max_{0 < t < a} |t^{-\beta} \phi(t)| \leq M$$

and the series $\sum a_k t^k$ converges for

$$|t| \leq 2h, \quad h > 0 \tag{A-6.3}$$

Then as $x \rightarrow \infty$

$$F(x) = \sum_{n=0}^{\infty} \frac{a_n}{\alpha} \Gamma\left(\frac{\beta + n + 1}{\alpha}\right) x^{-\frac{\beta+n+1}{\alpha}} \tag{A-6.4}$$

In this particular case

$$\phi(u) = \frac{1}{\sqrt{1+u}} = 1 - \frac{1}{2}u + \frac{1}{2} \cdot \frac{3}{2} \cdot \frac{1}{2} u^2 + \dots$$

$$a = \infty > 0, \quad \alpha = 1 > 0, \quad \beta = 0 > -1$$

and

$$\max_{0 < u < \infty} \left| \frac{1}{\sqrt{1+u}} \right| = 1 \quad (\text{Bounded})$$

And the series is convergent for $u < 1$. Hence, as $x \rightarrow \infty$

$$\begin{aligned} \bar{I} &\approx e^{-x} x^{1/2} \sum_{n=0}^{\infty} \Gamma\left(\frac{n+1}{1}\right) x^{-(n+1)} \\ &= e^{-x} x^{1/2} \left[\frac{1}{x} - \frac{1}{2x^2} + \frac{3}{8x^3} + \dots \right] \end{aligned} \tag{A-6.6}$$

Appendix A-7

SIMILARITY CRITERIA FOR GLOW DISCHARGES

The purpose of seeking similarity parameters in glow discharges is, as usual, three-fold.

- 1) Scale up, e.g., in large scale applications of cataphoresis or chemical reaction in plasmas.
- 2) To obtain groups that would enable economy in experimentation.
- 3) As a screen for various postulated mechanisms. One should also distinguish between "electrical" and "chemical" similarity, the latter condition requiring that the concentrations of various species at corresponding points in similar discharges be equal.

In Part I, the use of the similarity parameter pd to correlate V_s and of pR to correlate E/p was explained. These are particular cases of the treatment of electric similarity given in Francis⁽⁵⁾ or Cobine,⁽⁴⁾ where chemical similarity is implicitly assumed and there is no flow of gas. Considering two d.c. discharges with equal V_s , V_n and I whose geometric dimensions bear a ratio of χ , it can be shown that pd and pR must remain constant. Also, $E = \chi E'$, $p = p'/\chi$ (for constant T_g), $E/p = E'/p'$ (for constant T_g) and $T_e = T_e'$. It is less likely that v_d and $f_e(\epsilon)$ are exactly equal in electrically similar discharges. As seen in Part I, chemical similarity may be violated even in discharges in pure rare gases due

to the action of metastables. In gas mixtures, different extents of cataphoresis may lead to the same result even when there is no irreversible chemical reaction.

The parameters $\alpha = \frac{\langle n_+ \rangle}{\langle n_o \rangle + \langle n_+ \rangle} \frac{\mu EL}{D}$ for cataphoresis, $\frac{D\tau}{L^2}$ for longitudinal diffusion and $D\tau/R^2$ for radial diffusion, are examples of chemical similarity parameters in the absence of irreversible reactions.

As seen in Chapters 7-9, chemical reactions in pulsed d.c. discharges can be successfully correlated with the parameter

$$\xi = \frac{\tau}{\tau_I} \int_0^x \bar{n}_e dt, \text{ which reduces to } \tau \bar{n}_e \text{ in the d.c. discharge. } \xi \text{ is}$$

another chemical similarity parameter which assumes electrically similar discharges at least to the extent of maintaining constant α , β and γ . If ionic reactions become important it is possible to derive the parameter $(1 \pm \frac{\tau \mu E}{L})$ by an analysis of the species continuity equations. (137) The positive sign refers to gas flow in the direction of the electric field and the negative sign to the opposite direction of gas flow. In such a case it is possible in principle to change the yield of products by a simple reversal of gas flow. Gas velocities of the order of 10^4 cm/sec are required to get noticeable effects, as this is the order of magnitude of ionic drift velocities. (4)

Appendix A-8

NON-EQUILIBRIUM PLASMA REACTOR FOR NATURAL GAS PROCESSING

The glow discharge hydrocarbon reactions investigated in Part II of the thesis show some promise of being useful for the large scale processing of natural gas to produce C_2 intermediates. Natural gas can contain over 95% CH_4 depending on the location,⁽⁵⁶⁾ and its primary use at present is as a fuel. Unsaturated C_2 's (i.e., ethylene, C_2H_4 and acetylene, C_2H_2) being the starting materials for a large number of organic syntheses, there is a strong economic incentive to find processes that will produce them from the more abundant natural gas. In view of the existence of equilibrium plasma arc processes for C_2H_2 ,⁽⁵⁶⁾ the non-equilibrium plasma process is anticipated to produce C_2H_6 , C_2H_4 and H_2 from CH_4 . A patent application, with the present author as co-inventor,⁽¹³⁸⁾ has been filed. Coupled to existing thermal crackers that produce ethylene from ethane,⁽¹³⁹⁾ it should be possible to develop a non-equilibrium plasma process that converts CH_4 to C_2H_4 (and H_2) with no more than 25-30% formation of side products.

There are two essential conditions that must be met before any large scale development can proceed.

- 1) The selectivity of reaction achieved in the range 1-10 torr by the use of low residence times and currents must be extended to higher pressures ~ 1 atm. It is only at such high pressures that commercial scale throughputs can even be talked about.
- 2) The energy efficiency of the process should be brought down from 80 kwh/(mm³C₂) by a factor of 4 or more. Alternatively, electric power costs should fall by about the same factor relative to other

energy sources.

Interesting possibilities for the geometric configuration of an atmospheric pressure non-equilibrium plasma reactor are crossed flow pulsed and ozonizer discharges⁽¹³⁸⁾ and microwave discharges. The pulsed discharge experiments of Chapter 8 revealed that energy efficiency therein may exceed that of a corresponding d.c. reactor by a factor of 2, as a result of reactions in the afterglow. Further improvements may be effected by utilizing the high field negative glow instead of only the positive column as was done in the present work. It is believed that a practically motivated study could result in a non-equilibrium plasma process at atmospheric pressure that has an energy efficiency of $\sim 20 \text{ kwh}/(\text{nm}^3 \text{C}_2)$ with no loss of selectivity. Under such conditions it would become strongly competitive with existing arc processes for C_2H_2 . The advantage of the former is that a precisely controlled quench would not be necessary to stabilize the products as in equilibrium plasmas.

Ozonizer type silent discharges are being investigated in this laboratory.⁽¹⁴⁰⁾ The advantage of such systems is that they have been extensively used to produce O_3 from atmospheric O_2 , and are relatively well understood. Wulf and Melvin showed in their pioneering work⁽¹⁴¹⁾ that ozonizers are basically similar to low pressure glow discharges and fall into the category of what we would now call non-equilibrium plasmas. The silent discharge has also been used to produce amino acids from mixtures simulating primitive earth atmospheres.

Appendix A-9

PROCEDURE FOR OPERATION OF THE FLAME IONIZATION DETECTOR

1. Set air pressure at 13 p.s.i. to both flames.
2. Set H₂ pressure at 10 p.s.i., one column at a time and let it flow for one minute.
3. Be certain that the electrometer is on all of the time.
4. Push ignitor button on electrometer until both flames "pop".
5. Reduce sense H₂ pressure back to 4-5 p.s.i. which corresponds to about 7 cc/min.
6. Zero the electrometer at attenuation of 1.
 - a. Balance low background on 10,000 with coarse adjustment.
 - b. Balance low background on 1 with fine adjustment.
7. Adjust reference flame to zero recorder.
8. With range selector in S position: bistable mode--either 0 or maximum reading should occur. An in-between reading indicates a malfunctioning electrometer.
9. With the range selector in the T position, there is no input to the electrometer, hence a zero reading should occur.
10. The instrument is now ready for use.

LIST OF REFERENCES

LIST OF REFERENCES

1. I. Langmuir, Phys. Rev. 33, 954 (1929).
2. F. Llewellyn-Jones, The Glow Discharge and an Introduction to Plasma Physics, Methuen, London, 1966.
3. S. C. Brown, Introduction to Electrical Discharges in Gases, Wiley, 1966.
4. J. D. Cobine, Gaseous Conductors--Theory and Applications, Dover, 1958.
5. G. Francis, in S. Flügge ed., Handbuch der Physik XXII, Springer-Verlag, Berlin, 1956.
6. L. Pekarek and V. Krejci, Czech. J. Phys. B. 12 (6), 450 (1962); ibid 13 (12), 881 (1963).
7. K. Patek, Lasers, CRC Press--International Scientific Press, 1967.
8. F. H. Shair and D. S. Remer, J. Appl. Phys. 39, 5762 (1968).
9. R. F. Baddour and R. S. Timmins, The Application of Plasmas to Chemical Processing, M.I.T. Press, 1967.
10. J. M. Anderson, Phys. Fl. 7, 1517 (1964).
11. J. F. Prince and W. W. Robertson, J. Chem. Phys. 45 (7), 2577 (1966).
12. J. L. Peeters, H. W. Rundle and J. M. Deckers, Can. J. of Chem. 44, 2981 (1966).
13. M. A. Biondi and S. C. Brown, Phys. Rev. 75, 1700 (1949).
14. S. C. Brown and D. J. Rose, J. Appl. Phys. 23, 711 (1952).
15. D. J. Rose and S. C. Brown, J. Appl. Phys. 23, 719 (1952).
16. D. J. Rose and S. C. Brown, J. Appl. Phys. 23, 1028 (1952).
17. S. L. Leonard and R. H. Huddleston, Plasma Diagnostic Techniques, Academic Press, N.Y., 1965.
18. M. Sicha, et al, Brit. J. Appl. Phys. 17, 1511 (1966).
19. E. F. Labuda and E. I. Gordon, J. Appl. Phys. 35, 1647 (1964).
20. C. O. Gheorgiu, Rev. Roum. Phys. 14 (1), 61-68, (1969).

21. V. A. Lompe and R. Seeliger, *Ann. Phys.* 15, 300 (1932).
22. H. W. Rundle, K. A. Gillespie, R. M. Yealland, R. Sova and J. M. Deckers, *Can. J. Chem.* 44, 2995 (1966).
23. J. C. Ingraham and S. C. Brown, "Plasma Diagnostics", in R. F. Baddour and R. S. Timmins, ed., The Application of Plasmas to Chemical Processing, M.I.T. Press, 1967.
24. A. L. Lance, Introduction to Microwave Theory and Measurements, McGraw-Hill, N.Y., 1964.
25. J. C. Slater, Microwave Electronics, Van Nostrand, Princeton, N.J., 1950.
26. E. L. Ginzton, Microwave Measurements, McGraw-Hill, N.Y., 1957.
27. International Critical Tables, Vol. 6, National Research Council and McGraw-Hill, 1933.
28. W. Schottky, *Phys. Z.* 25, 342 (1924).
29. N. A. Karelina, *J. Phys. USSR* 6, 218 (1942).
30. B. Klarfeld, *J. Techn. Phys. USSR* 5, 725 (1938).
31. H. Schellenmeier, *Z. Physik* 122, 269 (1944).
32. Yu. B. Golubovskii, et al, *Opt. i Spektroskopiya* 20, 561 (1966).
33. O. Groos, *Z. Physik* 88, 741 (1934).
34. N. E. Bradbury and R. A. Nielson, *Phys. Rev.* 50, 950 (1936).
35. J. S. Townsend, Motions of Electrons in Gases, Oxford: Clarendon Press, 1928.
36. H. W. Allen, *Phys. Rev.* 52, 707 (1937).
37. F. Llewellyn-Jones, Ionization and Breakdown in Gases, Methuen, London, 1957.
38. L. B. Loeb, Basic Processes of Gaseous Electronics, U. of Calif. Press, Berkeley, 1955.
39. N. A. Matveeva, *Acad. Sci. USSR Bull., Phys. Ser. (English translation)* 23, 1009 (1959).
40. A. L. Schmeltekopf, Doctoral Dissertation, Univ. of Texas, Univ. Microfilms, Ann Arbor, 1962.

41. D. S. Remer and F. H. Shair, *Rev. Sci. Instr.* 40 (7), 968 (1969); and D. S. Remer, Ph.D. thesis, Calif. Inst. of Technology, Pasadena 1970.
42. L. B. Headrick and O. S. Duffendack, *Phys. Rev.* 37, 736 (1931).
43. T. P. Sosnowski, *J. Appl. Phys.* 40 (13), 5138 (1969).
44. R. Riesz and G. H. Diecke, *J. Appl. Phys.* 25 (2), 196 (1954).
45. J. H. Perry ed., Chemical Engineers' Handbook, 4th Ed., McGraw-Hill, 1963.
46. P. deWilde, *Ber.* 7, 352 (1874).
47. P. Thenard and A. Thenard, *Compt. Rend.* 78, 219 (1874).
48. R. W. Wood, *Proc. Roy. Soc.* 97A, 455 (1920); *ibid* 102A, 1 (1920).
49. G. M. Schwab and H. Friess, *Naturwiss* 21, 222 (1933).
50. G. Glockner and S. C. Lind, The Electrochemistry of Gases and Other Dielectrics, Wiley, N.Y., 1939.
51. R. L. McCarthy, *J. Chem. Phys.* 22, 1360 (1954).
52. E. J. Hellund, The Plasma State, Reinhold, N.Y., 1961
53. F. K. McTaggart, Plasma Chemistry in Electrical Discharges, Elsevier, N.Y. (1967).
54. B. D. Blaustein, ed., Chemical Reactions in Electrical Discharges, *Advances in Chemistry Series 80*, Am. Chem. Soc., Washington, D.C., 1969.
55. E. R. Riegel, Industrial Chemistry, Reinhold 1937 and 1962.
56. R. E. Kirk and D. F. Othmer, ed., Encyclopedia of Chemical Technology, Interscience, N.Y., 1957.
57. P. H. Dundas and M. L. Thorpe, *Chem. Eng. Prog.* 66 (10), 66 (1970).
58. F. B. Vurzel and L. S. Polak, *Ind. Eng. Chem.* 62 (6), 8 (1970).
59. P. L. Spedding, *Chem. Eng. (London)* 225, CE17 (1969).
60. W. R. Hesp, I. Halasz and O. Gerlach, *J. Appl. Chem.* 17, 306 (1967).
61. E. N. Borisova and E. N. Eremin, *Russian J. of Phys. Chem.* 41 (1), 69 (1967).
62. C. L. Thomas, G. Egloff and J.C. Morrell, *Chem.Rev.* 28, 1 (1941).

63. A. K. Brewer and P. D. Kueck, *J. Phys. Chem.* 35, 1293 (1931).
64. R. F. Baddour and B. R. Bronfin, *Ind. Eng. Chem. Proc. Design and Develop.* 4, 162 (1965).
65. W. H. Rodebusch and W. C. Klingelhoefter, *J. Am. Chem. Soc.* 55, 130 (1933).
66. J. D. Blackwood and F. K. McTaggart, *Australian J. of Chem.* 12, (2), 114 (1959).
67. E. Warburg, *Ann. Physik* 17, 1 (1905).
68. C. S. Stokes and W. W. Knipe, *Ind. Eng. Chem.* 52, 287 (1960).
69. A. V. Grosse, H. W. Leutner and A. C. Stokes, *Res. Inst. Temple Univ. 1st Ann. Rpt.*, Office of Naval Res., Contract 3085(02), 1961.
70. R. Kaiser, Gas Phase Chromatography, Vols. I, II, III, Butterworths, Washington, D.C., 1963.
71. A. J. P. Martin and A. T. James, *Biochem. J.* 50, 679 (1952).
72. P. Schuftan, Die Technische Gasanalyse, S. Hirzel, Leipzig, 1931.
73. N. C. Turner, *Nat. Petrol. News* 35, R234 (1943).
74. C. S. G. Phillips, *Disc. Far. Soc.* 7, 241 (1949).
75. A. B. Littlewood, Gas Chromatography--Principles, Techniques and Applications, Academic Press, N.Y., 1970.
76. R. D. Condon, *Anal. Chem.* 31, 1717 (1959).
77. H. W. Patton, J. S. Lewis and W. I. Kaye, *Anal. Chem.* 27, 170 (1955).
78. T. A. Bellar and J. E. Sigsby Jr., *Environ. Sci. Tech.* 1 (3), 242 (1967).
79. S. A. Greene and H. Pust, *Anal. Chem.* 29, 1055 (1957).
80. O. L. Hollis and W. V. Hayes, *J. Gas Chromatog.* 4, 235 (1966).
81. W. E. Harris and H. W. Habgood, Programmed Temperature Gas Chromatography, Wiley, 1966.
82. A. V. Phelps, in B. D. Blaustein ed., Chemical Reactions in Electrical Discharges, *Advances in Chemistry Series 80*, Am. Chem. Soc., Washington, D.C., 1969.

83. F. Kaufman, in B. D. Blaustein ed., Chemical Reactions in Electrical Discharges, Advances in Chemistry Series 80, Am. Chem. Soc., Washington, D.C., 1969.
84. W. L. Fite, in B. D. Blaustein ed., Chemical Reactions in Electrical Discharges, Advances in Chemistry Series 80, Am. Chem. Soc., Washington, D.C., 1969.
85. W. P. Allis, in S. Flügge ed., Handbuch der Physik XXI, Springer-Verlag, Berlin, 1956.
86. A. G. Engelhardt, A. V. Phelps and C. G. Risk, Phys. Rev. 135, A1566 (1964).
87. D. T. Shaw, J. Appl. Phys. 40 (6), 2412 (1969).
88. D. T. Tuma, Rev. Sci. Instr. 41 (9), 1360 (1970).
89. E. W. McDaniel, Collision Phenomena in Ionized Gases, Wiley, N.Y., 1964.
90. A. G. Engelhardt and A. V. Phelps, Phys. Rev. 131 (5), 2115 (1963).
91. T. E. Sharp and J. T. Dowell, J. Chem. Phys. 46, 1530 (1967).
92. L. J. Kieffer, Atomic Data (USA) 1 (1), 19 (1969); *ibid* 1 (2), 120 (1969).
93. K. K. Corvin and S. J. B. Corrigan, J. Chem. Phys. 50 (6), 2570 (1969).
94. R. G. Buser and J. J. Sullivan, J. Appl. Phys. 41 (2), 472 (1970).
95. J. M. Deckers, et al, Can. J. of Chem. 42, 1792 (1964); *ibid* 44, 2981 (1966); *ibid* 44, 2995 (1966).
96. R. C. L. Bosworth, Phil. Mag. Ser. 7, 39 (298), 847 (1948).
97. O. Levenspiel, Chemical Reaction Engineering--An Introduction to the Design of Chemical Reactors, Wiley, N.Y., 1967.
98. Instruction Manual for Model 160 Series Gas Chromatograph, pg. 37, LOENCO Inc., Altadena, Calif.
99. W. Braun, K. H. Welge and J. R. McNesby, J. Chem. Phys. 45 (7), 2650 (1966); *ibid* 46 (6), 2071 (1967).
100. B. A. Brown, C. R. Howarth and J. D. Thornton, J. Phys. D., Appl. Phys. 3 (11), L67 (1970) and Third Joint Meeting of AIChE and IMIQ, Denver, Colorado, Sept. 1970, Paper 76.
101. F. A. Grant, Can. J. of Res. 28A, 339 (1950).

102. W. A. English and G. C. Hanna, *Can. J. of Phys.* 31, 768 (1953).
103. R. C. Reid and T. K. Sherwood, *The Properties of Gases and Liquids --Their Estimation and Correlation*, McGraw-Hill, 1966, pp.520-567.
104. F. A. Cleland and R. H. Wilhelm, *A.I. Ch.E.J.* 2 (4), 489 (1956).
105. J. B. Hasted, *Physics of Atomic Collisions*, Butterworths, London, 1964.
106. E. W. R. Steacie, *Atomic and Free Radical Reactions*, Vol. I and II, Reinhold, N.Y., 1954.
107. W. A. Chupka and C. Lifshitz, *J. Chem. Phys.* 48 (3), 1109 (1968).
108. B. H. Mahan and R. Mandal, *J. Chem. Phys.* 37 (2), 207 (1962).
109. C. K. Jen, S. N. Foner, E. L. Cochran and V. A. Bowers, *Phys. Rev.* 112, 1169 (1958).
110. A. Shepp, *J. Chem. Phys.* 24, 939 (1956).
111. R. E. Dodd and E. W. R. Steacie, quoted Ref. 106.
112. R. G. W. Norrish and G. Porter, *Disc. Far. Soc.* 2, 97 (1947).
113. G. Porter, *Disc. Far. Soc.* 2, 142 (1947).
114. M. Abramowitz and I. A. Stegun, *Handbook of Mathematical Functions* National Bureau of Standards Applied Math Series 55, Washington, D.C., 1964
115. A. Langer, J. A. Hipple and D. P. Stevenson, *J. Chem. Phys.* 22, 1836 (1954).
116. D. Rapp, et al, *J. Chem. Phys.* 42, 4081 (1965).
117. B. Adamczyk et al, *J. Chem. Phys.* 44, 4640 (1966).
118. H.S.W. Massey, E.H.S. Burhop and H.B. Gilbody, *Electronic and Ionic Impact Phenomena*, Vol. II, Second Edition, Clarendon Press, Oxford, England, 1969, pg. 700.
119. C. E. Melton, *J. Chem. Phys.* 33 (3), 647 (1960).
120. F. N. Harllee, H. M. Rosenstock and J. T. Herron, "A Bibliography on Ion-Molecule Reactions", NBS Tech. Note 291, U.S. Dept. of Commerce, National Bureau of Standards.
121. F. H. Field and J. L. Franklin, *Electron Impact Phenomena and the Properties of Gaseous Ions*, Academic Press, N.Y., 1957.

122. A. L. Lane and A. Kupperman, Rev. Sci. Instr. 39, 126 (1968).
123. I. Langmuir and H. Mott-Smith, Gen. Elec. Rev. 27, 449 (1924);
ibid 538; ibid 616; ibid 762; ibid 810.
124. M. I. Druyvesteyn, Z. Physik 64, 781 (1930).
125. A. Garscadden, Phys. Lett. 29A (5), 265 (1969), and private communication.
126. R. H. Bond, "Directed Electron Velocity Distributions in Rare Gas Discharges Using Guard Ring Probes", Tech. Rpt. 25, Nonr 220(50), U.S. Office of Naval Res. and California Inst. of Technology, June 1965.
127. R. L. F. Boyd and N. D. Twiddy, Proc. Roy Soc. 250A, 53 (1959).
128. N. F. Brockmeier, Paper presented at Third Joint Meeting of AIChE and IMIQ, Denver, Colorado, Sept. 1970.
129. G. Bekefi and S. C. Brown, Am. J. Phys. 29, 404 (1961).
130. J. L. Delcroix, Plasma Physics, Vol. 2, Weakly Ionized Gases. Wiley, N.Y., 1968.
131. R. G. Lindgren and G. R. Gavalas, Phys. Fl. 13 (6), 1499 (1970).
132. H. S. Mickley, T. K. Sherwood and C. E. Reed, Applied Mathematics in Chemical Engineering, McGraw-Hill, N.Y., 1957.
133. M. A. Biondi, Phys. Rev. 129 (3), 1181 (1963).
134. E. P. Gray and D. E. Kerr, Ann. of Phys. 17, 276 (1959).
135. A. V. Phelps and S. C. Brown, Phys. Rev. 86, 102 (1952).
136. M. A. Evgrafov, Asymptotic Estimates and Entire Functions (Translated from the Russian), Gordon and Breach, 1961.
137. A. L. Ravimohan, "The Development of Techniques for the Study of Chemical Reactions in Glow Discharges", California Institute of Technology, Master's Report in Dept. of Chem. Eng., June 1968.
138. F. H. Shair and A. L. Ravimohan, "Non-Equilibrium Plasma Reactor for Natural Gas Processing", USAEC Patent Case No. S-39450 (RL-5366), Sept. 9, 1970.
139. W. L. Faith, D. B. Keyes and R. L. Clark, Industrial Chemicals John Wiley, 1957.

140. R. Bizios, P. Ré, K. G. Donohoe and F. H. Shair, Private communications and laboratory reports.
141. O. Wulf and E. H. Melvin, Phys. Rev. 55 (8), 687 (1939).

AUTHOR INDEX

AUTHOR INDEX

() indicate number on List of References

[] indicate Sections in thesis where references appear

M. Abramowitz	(114)	[9.4]	S. C. Brown	(3)	[1.1]
B. Adamczyk	(117)	[9.5]		(13)	[1.2a]
H. W. Allen	(36)	[3.3b, 3.3c, 3.4]		(14)	[1.2a]
W. P. Allis	(85)	[5.2,10.3]		(15)	[1.2a]
J. M. Anderson	(10)	[1.2a,3.4]		(16)	[1.2a]
R. F. Baddour	(9)	[1.1,5.1a]		(23)	[2.3a, 2.3c,6.2a]
	(23)	[2.3a,2.3c, 6.2a]	E.H.S. Burhop	(118)	[9.5]
	(64)	[5.1a]	R. G. Buser	(94)	[5.2]
G. Befeki	(129)	[10.2]	F. Chen	(17)	[1.2a, 10.2]
T. A. Bellar	(78)	[5.1b]	W. A. Chupka	(107)	[9.1,9.4]
M. A. Biondi	(13)	[1.2a]	R. L. Clark	(139)	[A-8]
	(133)	[A-5]	F. A. Cleland	(104)	[7.6]
R. Bizios	(140)	[A-8]	J. D. Cobine	(4)	[1.1]
J. D. Blackwood	(66)	[5.1a]	E. L. Cochran	(109)	[9.2]
B. D. Blaustein	(54)	[5.1a]	R. D. Condon	(76)	[5.1b]
	(82)	[5.2]	S.J.B. Corrigan	(93)	[5.2]
R. H. Bond	(126)	[10.2]	K. K. Corvin	(93)	[5.2]
E. N. Borisova	(61)	[5.1a,9.2]	J. M. Deckers	(12)	[1.1]
R.C.L. Bosworth	(96)	[6.2a]		(22)	[1.2b]
V. A. Bowers	(109)	[9.2]		(95)	[5.2, 6.2b]
R.L.F. Boyd	(127)	[10.2]	J. L. Delcroix	(130)	[10.3]
N. E. Bradbury	(34)	[3.3b,3.4]	G. H. Diecke	(44)	[4.4a]
W. Braun	(99)	[6.3,9.2, 9.6]	R. E. Dodd	(111)	[9.2]
A. K. Brewer	(63)	[5.1a]	K. G. Donohoe	(140)	[A-8]
N. F. Brockmeier	(128)	[10.2]	J. T. Dowell	(91)	[5.2,9.5]
B. R. Bronfin	(64)	[5.1a]	M. J. Druyvesteyn	(124)	[10.2]
B. A. Brown	(100)	[6.4,8.6, 9.4]	O. S. Duffendack	(42)	[4.1]

P. H. Dundas	(57)	[5.1a]	H. W. Habgood	(81)	[5.1b]
G. Egloff	(62)	[5.1a]	I. Halasz	(60)	[5.1a]
A. G. Engelhardt	(86)	[5.2]	G. C. Hanna	(102)	[7.5]
	(90)	[5.2,10.1a]	F. N. Harllee	(120)	[9.6]
W. A. English	(102)	[7.5]	W. E. Harris	(81)	[5.1b]
E. N. Eremin	(61)	[5.1a,9.2]	J. B. Hasted	(105)	[8.4,A-5]
M. A. Evgrafov	(136)	[A-6]	W. V. Hayes	(80)	[5.1b]
W. L. Faith	(139)	[A-8]	L. B. Headrick	(42)	[4.1]
F. H. Field	(121)	[9.6]	E. J. Hellund	(52)	[5.1a]
W. L. Fite	(84)	[5.2]	J. T. Herron	(120)	[9.6]
S. Flügge	(5)	[1.1,1.2b, 2.1,3.3a, 3.4,5.2]	W. R. Hesp	(60)	[5.1a]
	(85)	[5.2,10.3]	J. A. Hipple	(115)	[9.4]
S. N. Foner	(109)	[9.2]	O. L. Hollis	(80)	[5.1b]
G. Francis	(5)	[1.1,1.2b, 2.1,3.3a, 3.4,5.2]	C. R. Howarth	(100)	[6.4,8.6, 9.4]
J. L. Franklin	(121)	[9.6]	R. H. Huddleston	(17)	[1.2a,10.2]
H. Friess	(49)	[5.1a]	J. C. Ingraham	(23)	[2.3a, 2.3c,6.2a]
A. Garscadden	(125)	[10.2]	A. T. James	(71)	[5.1b]
G. R. Gavalas	(131)	[10.3]	C. K. Jen	(109)	[9.2]
O. Gerlach	(60)	[5.1a]	R. Kaiser	(70)	[5.1b]
C. O. Gheorghiu	(20)	[1.2a]	N. A. Karelina	(29)	[3.3a]
H. B. Gilbody	(118)	[9.5]	F. Kaufman	(83)	[5.2]
K. A. Gillespie	(22)	[1.2b]	W. I. Kaye	(77)	[5.1b]
E. L. Ginzton	(26)	[2.3c]	D. E. Kerr	(134)	[A-5]
G. Glockner	(50)	[5.1a]	D. B. Keyes	(139)	[A-8]
Yu. B. Golubovskii	(32)	[3.3a,3.4]	L. J. Kieffer	(92)	[5.2]
E. I. Gordon	(19)	[1.2a, 3.3b,4.1]	R. E. Kirk	(56)	[5.1a]
F. A. Grant	(101)	[6.4]	B. Klarfeld	(30)	[3.3a]
E. P. Gray	(134)	[A-5]	W. C. Klingelhoefter	(65)	[5.1a]
S. A. Greene	(79)	[5.1b]	W. W. Knipe	(68)	[5.1a]
O. Groos	(33)	[3.3a]	V. Krejci	(6)	[1.1]
A. V. Grosse	(69)	[5.1a]	P. D. Kueck	(63)	[5.1a]
			A. Kupperman	(122)	[9.6]
			E. F. Labuda	(19)	[1.2a, 3.3b,4.1]

A. L. Lance	(24)	[2.3b]	Natl. Research Council	(27)	[2.3c]
A. L. Lane	(122)	[9.6]			
A. Langer	(115)	[9.4]	R. A. Nielson	(34)	[3.3b,3.4]
I. Langmuir	(1)	[1.1]	R.G.W. Norrish	(112)	[9.2]
	(123)	[10.2]	D. F. Othmer	(56)	[5.1a]
S. L. Leonard	(17)	[1.2a,10.2]	K. Patek	(7)	[1.1]
H. W. Leutner	(69)	[5.1a]	H. W. Patton	(77)	[5.1b]
O. Levenspiel	(97)	[6.2a,7.6]	J. L. Peeters	(12)	[1.1]
J. S. Lewis	(77)	[5.1b]		(95)]	[5.2]
C. Lifshitz	(107)	[9.1,9.4]	L. Pekarek	(6)	[1.1]
S. C. Lind	(50)	[5.1a]	J. H. Perry	(45)	[A-3,9.1]
R. G. Lindgren	(131)	[10.3]	A. V. Phelps	(82)	[5.2]
A. B. Littlewood	(75)	[5.1b,6.3]		(86)	[5.2]
F. Llewellyn-Jones	(2)	[1.1,3.4, 5.2,9.4, 10.1a]		(90)	[5.2, 10.1a]
	(37)	[3.4]	C.S.G. Phillips	(135)	[A-5]
L. B. Loeb	(38)	[3.4]	L. S. Polak	(74)	[5.1b]
Loenco, Inc.	(98)	[6.3]	G. Porter	(58)	[5.1a]
V. A. Lompe	(21)	[1.2b,3.3a]		(112)	[9.2]
B. H. Mahan	(108)	[9.2,9.6]	J. F. Prince	(113)	[9.2]
R. Mandal	(108)	[9.2,9.6]		(11)	[1.1,1.2a, 3.3b]
A.J.P. Martin	(71)	[5.1b]	H. Pust	(79)	[5.1b]
H.S.W. Massey	(118)	[9.5]	D. Rapp	(116)	[9.5]
N. A. Matveeva	(39)	[4.1]	A. L. Ravimohan	(137)	[A-7]
R. L. McCarthy	(51)	[5.1a]		(138)	[A-8]
E. W. McDaniel	(89)	[5.2]	P. Re	(140)	[A-8]
J. R. McNesby	(99)	[6.3,9.2, 9.6]	C. E. Reed	(132)	[A-1]
F. K. McTaggart	(53)	[5.1a,9.2]	R. C. Reid	(103)	[7.6]
	(66)	[5.1a]	D. S. Remer	(8)	[1.1,1.2b, 2.1,4.1, 4.2,4.4a, 4.4b,4.5, A-2]
C. E. Melton	(119)	[9.6]		(41)	[4.1,4.4a, 4.5,A-2]
E. H. Melvin	(141)	[A-8]	E. R. Riegel	(55)	[5.1a]
H. S. Mickley	(132)	[A-1]	R. Riesz	(44)	[4.4a]
J. C. Morrell	(62)	[5.1a]	C. G. Risk	(86)	[5.2]
H. Mott-Smith	(123)	[10.2]			

W. W. Robertson	(11)	[1.1,1.2a, 3.3b]	D. P. Stevenson	(115)	[9.4]
W. H. Rodebusch	(65)	[5.1a]	A. C. Stokes	(69)	[5.1a]
D. J. Rose	(14)	[1.2a]	C. S. Stokes	(68)	[5.1a]
	(15)	[1.2a]	J. J. Sullivan	(94)	[5.2]
	(16)	[1.2a]	A. Thenard	(47)	[5.1a]
H. M. Rosenstock	(120)	[9.6]	P. Thenard	(47)	[5.1a]
H. W. Rundle	(12)	[1.1]	C. L. Thomas	(62)	[5.1a]
	(22)	[1.2b]	I. D. Thornton	(100)	[6.4, 8.6,9.4]
	(95)	[5.2]	M. L. Thorpe	(57)	[5.1a]
H. Schellenmeier	(31)	[3.3a]	R. S. Timmins	(9)	[1.1,5.1a]
A. L. Schmeltekopf	(40)	[4.1]	(23)	[2.3a, 2.3c,6.2a]	
W. Schottky	(28)	[2.3c,5.2]	J. S. Townsend	(35)	[3.3b,3.4]
P. Schuftan	(72)	[5.1b]	D. T. Tuma	(88)	[5.2,10.2]
G. M. Schwab	(49)	[5.1a]	N. C. Turner	(73)	[5.1b]
R. Seeliger	(21)	[1.2b,3.3a]	N. D. Twiddy	(127)	[10.2]
F. H. Shair	(8)	[1.1,1.2b, 2.1,4.1, 4.2,4.4a, 4.4b,4.5, A-2]	F. B. Vurzel	(58)	[5.1a]
	(41)	[4.1,4.4a, 4.5,A-2]	E. Warburg	(67)	[5.1a]
	(138)	[A-8]	K. H. Welge	(99)	[6.3, 9.2,9.6]
	(140)	[A-8]	P. de Wilde	(46)	[5.1a]
T. E. Sharp	(91)	[5.2,9.5]	R. H. Wilhelm	(104)	[7.6]
D. T. Shaw	(87)	[5.2]	R. W. Wood	(48)	[5.1a,9.2]
A. Shepp	(110)	[9.2]	O. Wulf	(141)	[A-8]
T. K. Sherwood	(103)	[7.6]	R. M. Yealland	(22)	[1.2b]
	(132)	[A-1]			
M. Sicha	(18)	[1.2a]			
J. E. Sigsby	(78)	[5.1b]			
J. C. Slater	(25)	[2.3b]			
T. P. Sosnowski	(43)	[4.1,4.4a]			
R. Sova	(22)	[1.2b]			
P. L. Spedding	(59)	[5.1a]			
E.W.R. Steacie	(106)	[9.1]			
	(111)	[9.2]			
I. A. Stegun	(114)	[9.4]			

PROPOSITION P-1

The following reprint is an article based on the proposition accepted by the Candidacy Examination Committee consisting of Professors Shair, Gould, Pings and Seinfeld on November 29, 1968.

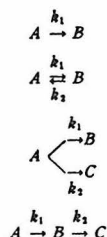
The Accuracy of Kinetic Parameters Estimated from Batch and Integral Reactor Data

A. L. RAYIMOHAN, W. H. CHEN and J. H. SEINFELD

Department of Chemical Engineering, California Institute of Technology, Pasadena, California 91109, U.S.A.

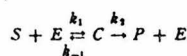
The accuracy of rate constant estimates obtained by minimizing the sum of squares of differences between observed and calculated concentrations is considered. Closed solutions are obtained for some basic types of first order reaction schemes. The results are presented in the form of plots of the dimensionless variance of parameter estimates. The kineticist can use the plots both in analyzing experiments and in planning them for maximum economy. Such advance studies are capable of providing valuable insight into questions of experimental design even when the reaction scheme is unknown.

The estimation of rate constants from experimental concentration-time measurements in batch and tubular flow reactors is an important problem in chemical engineering. Two steps are involved in the overall problem. First, estimates of the rate constants must be obtained. It is now recognized that the correct procedure that must be used is least squares analysis of the measured data. Since, for experimental reasons, the measured quantities are usually the concentrations, the least squares criterion must be applied to the raw concentration vs. time data. This step can be conveniently carried out using quasilinearization^(1,2). It is the object of this paper to consider the second step, namely the analysis of the accuracy of kinetic parameter estimates, for the four reaction schemes:



It is shown that in addition to this type of post-facto analysis, the results can also be used for the systematic planning of kinetic experiments.

Rosenbrock and Storey⁽⁴⁾ present a general technique for the determination of confidence intervals for parameter estimates in ordinary differential equations. Heineken, *et al.*⁽⁵⁾ used this procedure to determine confidence intervals for parameter estimates in the enzymatic reactions



Seinfeld and Gavalas⁽⁶⁾ used quasilinearization to estimate the rate constants and Rosenbrock and Storey's procedure to analyze the estimates in the pyrolytic dehydrogenation of benzene to diphenyl and triphenyl,

On a étudié l'exactitude des estimés relatifs à la constante de vitesse qu'on obtient en minimisant la somme des carrés des différences entre les concentrations observées et celles qu'on a calculées. On obtient des solutions fermées pour certains genres fondamentaux de systèmes de réaction de premier ordre. On présente, sous forme de graphiques, les résultats de la variance sans dimensions des estimés des paramètres. Le préposé à la cinétique peut utiliser les dits graphiques pour analyser le travail expérimental et le planifier pour minimiser son coût. Des études préliminaires de ce genre permettent d'obtenir une connaissance précieuse des questions relatives à la conception de travaux expérimentaux, lorsqu'on ne connaît pas le système de réaction.



The present work represents a continuation of the effort to provide experimental kineticists with easily-interpretable results on the accuracy of rate constant estimates in common reactions.

The general problem may be stated as one of estimating the parameters in a set of ordinary differential Equations⁽⁷⁾. The state of a system is governed by the set of ordinary differential Equations

$$\dot{x}_i = f_i(x, a, t) \quad i = 1, 2, \dots, n \quad x_i(t_0) = x_{i0} \dots (1)$$

which contain p unknown parameters, a_k , $k = 1, 2, \dots, p$. Experimental observations z_j , $j = 1, 2, \dots, m$, are made at R values of t , t_1, t_2, \dots, t_R , and are known functions of the system state, $g_j(x)$, but contain additive random experimental errors η_j ,

$$(z_j)_r = g_j(x(t_r)) + (\eta_j)_r$$

$$j = 1, 2, \dots, m; r = 1, 2, \dots, R \dots (2)$$

The error vectors n_r , corresponding to different sets of measurements are assumed to be statistically independent. The errors in the individual elements of each vector n_r are assumed to be normally distributed with zero mean and covariance matrix M_r . The parameters a are estimated to minimize the weighted sum of squares

$$S^2 = \sum_{r=1}^R [z_r - g(x(a, t_r))]^T M_r^{-1} [z_r - g(x(a, t_r))] \dots (3)$$

where $x(a, t)$ is the solution of Equation (1), with known initial conditions.

We present only the formulas required to compute confidence intervals. If the experimental error variances are small enough for linearization to be valid, the error in the parameter estimates obtained by minimizing S^2 will be normally distributed with zero mean and covariance matrix P . If the initial conditions x_0 are known without error

$$P = H^{-1} \dots (4)$$

Reprinted in Canada from
 THE CANADIAN JOURNAL OF CHEMICAL ENGINEERING
 Vol. 48: 420-427: August 1970
 A Publication of The Chemical Institute of Canada
 151 Slater Street, No. 906, Ottawa 4, Ontario

where

$$H = \sum_{i=1}^n D_i^T G_i^T M_i^{-1} G_i D_i \dots \dots \dots (5)$$

and

$$\begin{aligned} \dot{D} &= AD + B \\ D(t_0) &= 0 \dots \dots \dots (6) \end{aligned}$$

$$A = \{A_{ij}\} = \left(\frac{\partial f_i}{\partial x_j} \right)_{a^*}$$

$$B = \{B_{ij}\} = \left(\frac{\partial f_i}{\partial a_j} \right)_{a^*} \dots \dots \dots (7)$$

$$G = \{G_{ij}\} = \left(\frac{\partial g_i}{\partial x_j} \right)_{a^*}$$

a^* being the value of a minimizing S^2 . Heineken, *et al.*⁽⁵⁾ show that as $R \rightarrow \infty$ the matrix H defined in Equation (5) rapidly approaches

$$Rh = \frac{R}{T - t_0} \int_{t_0}^T D(t)^T G(t)^T M(t)^{-1} G(t) D(t) dt \dots \dots (8)$$

The variance of any linear combination of the a for an arbitrary vector b is $\sigma_b^2 = b^T P b$. Complete details are given by Rosenbrock and Storey⁽⁶⁾.

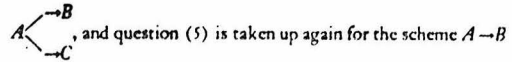
In the analysis to follow we make the assumptions:

1. The initial concentrations are known without error.
2. The initial charge in each case consists of pure A .
3. The concentrations are measured directly.
4. Unless otherwise indicated, the covariance matrix of experimental errors, $M(t)$ has the simple form $\sigma^2 I$.

We examine the effect of the following on the confidence intervals of the rate constant estimates:

1. How many data points R should be taken and over what range in order to attain a given accuracy of parameter estimates.
2. What effect does the level of experimental error have on the problem.
3. Above what value of R can Equation (8) be taken as an adequate representation of Equation (5).
4. How many of the n independent concentrations should be measured, and which ones chosen in the event of a choice being available.
5. What advantage can be gained by measuring more than the independent number of concentrations.
6. Instead of spacing the observation points equally in the time interval (t_0, T) , might it not be advantageous to space the same number of points in a different manner. In particular, what is the effect of spacing them equally in the conversion interval $(1, \xi)$ rather than the corresponding time interval (t_0, T) .
7. If concentration-time data from runs at different temperatures are used to determine the rate constants and activation energies, how accurate would these estimates be. At how many temperatures should observations be taken in order to achieve a given accuracy.

Questions (1) and (2) are answered for all the four reaction schemes. (3) is considered for the schemes $A \rightleftharpoons B$ and $A \rightarrow B \rightarrow C$. (4) and (5) are thoroughly discussed for the scheme



where the matrix of experimental errors $M(t)$ has a form different from the $\sigma^2 I$ usually assumed. The simple scheme $A \rightarrow B$ is also used to illustrate how the same techniques can be used to answer the more complicated questions (6) and (7).

Results

Following Heineken *et al.*, dimensionless parameters of the type $\psi_i = \frac{\sigma_{a_i}^2 R}{k_i^2 \sigma^2}$ were used to correlate the results. Here, k

is the mean value and $\sigma_{a_i}^2$ the variance of an estimated parameter, R the number of data points, and σ^2 the variance of the dimensionless forms of the experimentally measured concentrations. The ψ_i are obtained as diagonal elements of the matrix $PR/\sigma^2 k^2$, where $P \approx h^{-1}/R$ for large R and $P = H^{-1}$ in general. The ψ_i parameter contains information regarding the

accuracy of an estimate (the larger the value of $\frac{k^2}{\sigma_{a_i}^2}$, the more accurate is the estimate), for any given value of the experimental error. It also incorporates the number of observations R , and can be used to decide what value of R is necessary in order to get an acceptable accuracy of the estimate. Plots of ψ_i are therefore a concise and convenient representation of the results of the study. They can be used to plan kinetic experiments which seek to obtain accurate estimates of parameters when approximate values are known from a less sophisticated analysis.

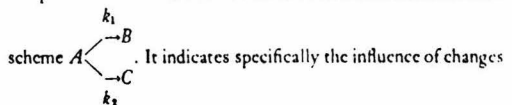
Figure 1 presents $\psi_1 = \frac{\sigma_{a_1}^2 R}{k_1^2 \sigma^2}$ and $\psi_2 = \frac{\sigma_{a_2}^2 R}{k_2^2 \sigma^2}$ versus $k_1 T$ for the isothermal scheme $A \rightleftharpoons B$. The curve of $\psi_1 = \frac{\sigma_{a_1}^2 R}{k_1^2 \sigma^2}$

for the scheme $A \xrightarrow{k_1} B$ is also shown for comparison. Figures 2 and 3 show the same type of plots for $A \rightarrow B \rightarrow C$ and $A \begin{cases} \xrightarrow{k_1} B \\ \xrightarrow{k_2} C \end{cases}$ when the number of components measured is the same as the number of independent components = 2, and these are chosen to be A and B .

Figure 4 illustrates some typical results when the exact formula $P = H^{-1}$ is used for computation instead of the approximation $P = h^{-1}/R$ in the isothermal scheme $A \rightleftharpoons B$. Similar

curves for $A \rightarrow B \rightarrow C$ are shown in Figure 5. Figure 6 is a cross-plot of Figure 5 in which the asymptotic approach to the approximate formula as R increases is clearly seen.

Figure 7 is an attempt to answer the question of how many components and which ones should be measured in the isothermal



in the G matrix on the accuracy of estimation, and D matrix remaining the same and the M matrix continuing to be $\sigma^2 I$. This important question is raised again for the isothermal scheme $A \rightarrow B$, but this time the G matrix is kept constant at col [1 - 1]. The source of variation now is the matrix of experimental errors M . M is taken to be $\begin{pmatrix} \sigma_A^2 & 0 \\ 0 & \sigma_B^2 \end{pmatrix}$, which represents independent measurements on A and B with different variances. This, of course, is a more realistic assumption than $M = \sigma^2 I$. $s = \frac{\sigma_A}{\sigma_B}$ is allowed to vary, and the results are shown in Figure 8.

In Figure 9, the effect of unequal division of the time interval is explored for the isothermal scheme $A \rightarrow B$. When the time interval (t_0, T) is equally divided by R points, it can be shown that

$$\psi_1 = \frac{\sigma_A^2 R}{k_1^2 \sigma_A^2} = \frac{R}{\sum_1^R (k_1 t_r) \exp(-2k_1 t_r)} \dots (9)$$

where

$$t_r = t_0 + \frac{r(T-t_0)}{R} \quad r = 1, \dots, R.$$

When the conversion interval $(1, \xi)$ is equally divided by R points, the corresponding result is

$$\psi_1 = \frac{\sigma_A^2 R}{k_1^2 \sigma_A^2} = \frac{R}{\sum_1^R (x_r \ln x_r)^2} \dots (10)$$

where

$$x_r = 1 - \frac{r(1-\xi)}{R} \quad r = 1, \dots, R$$

and

$$\xi = \exp[-k_1(T-t_0)]$$

As R becomes large, Equations (5) and (8) should converge to the same value.

In Figure 10, the dimensionless variances of the frequency factor and activation energy estimates are plotted against the number of temperatures at which observations are taken.

$$\psi_G = \frac{\sigma_G^2 R}{G^2 \sigma^2} = \frac{h_{22}}{G^2 \sigma^2 |h|}$$

$$\psi_E = \frac{\sigma_E^2 R}{E^2 \sigma^2} = \frac{h_{11}}{E^2 \sigma^2 |h|}$$

where

$$h = \sum_{l=0}^L \left\{ \frac{1}{\sigma^2(T-t_0)} \int_{t_0}^T \begin{bmatrix} D_1^2 & D_1 D_2 \\ D_1 D_2 & D_2^2 \end{bmatrix} dt \right\} \dots (11)$$

It must be noted that Equation (11) represents a hybrid expression which is h from the point of view of each run but is actually

H from the point of view of $\sum_{l=0}^L$. Hence, $P = h^{-1}/R$ and no

division by L is necessary. Very large values of L are experimentally unrealistic as the number of temperatures at which isothermal runs are conducted seldom exceeds 10.

Discussion of results

The discussion of each figure appears below the figure.

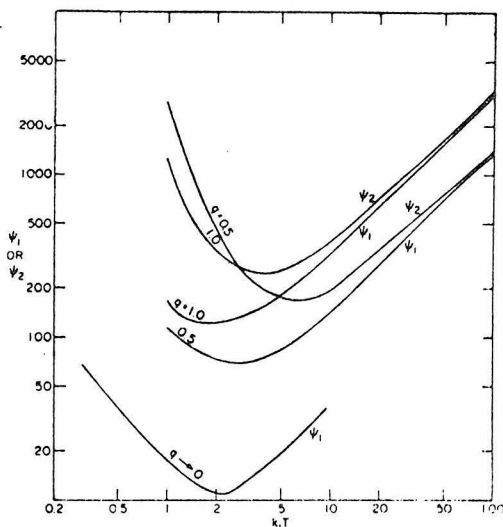


Figure 1—Dimensionless variance of parameter estimates vs. dimensionless time in the reaction scheme $A \xrightleftharpoons[k_2]{k_1} B$, when only component A is measured and the number of observations R is large.

For each value of $q = \frac{k_2}{k_1}$ there exists a minimum value of

ψ_1 and ψ_2 corresponding to a particular $k_1 T$. As q decreases, the value of $k_1 T$ at which the minimum occurs at first increases. This is because as k_2/k_1 decreases, more B is present at equilibrium and it takes longer for the reaction to achieve equilibrium. In order to obtain maximum accuracy it is necessary in this case to continue taking measurements for a longer time. However,

when $\frac{k_2}{k_1}$ becomes very small, the amount of A present at equilibrium tends to zero. Due to the error in measuring A , there is not much point in taking a large number of observations when its concentration is very low. Hence the optimum value of $k_1 T$ starts decreasing as $\frac{k_2}{k_1}$ approaches 0.

For small values of $k_1 T$, k_1 can be estimated more accurately than k_2 . In this range, the smaller the value of q , the greater the accuracy that can be obtained in ψ_1 . Conversely, in this range, the smaller the value of q , the lesser the accuracy that can be obtained in ψ_2 . This is because the smaller the value of q the more significant is the forward reaction. If, on the other hand, measurements are continued for a long time (high $k_1 T$), this difference gets narrowed down. This is because more of the observations are now being taken close to equilibrium and are effectively being wasted.

For small values of $k_1 T$ (small extent of reaction) the dimensionless variance ψ_1 tends to zero, because only the first step in the reaction is important and k_1 can be estimated accurately by a large number of measurements carried out over the interval $(0, T)$. As q increases, the rate of the second reaction relative to the first increases and ψ_1 increases for small values of $k_1 T$. This is because it becomes harder to estimate k_1 from observations over the fixed interval $(0, T)$ due to the increasing effect of the second reaction.

For small values of $k_1 T$, ψ_2 increases rapidly because of the inability to observe the effect of the second reaction which is

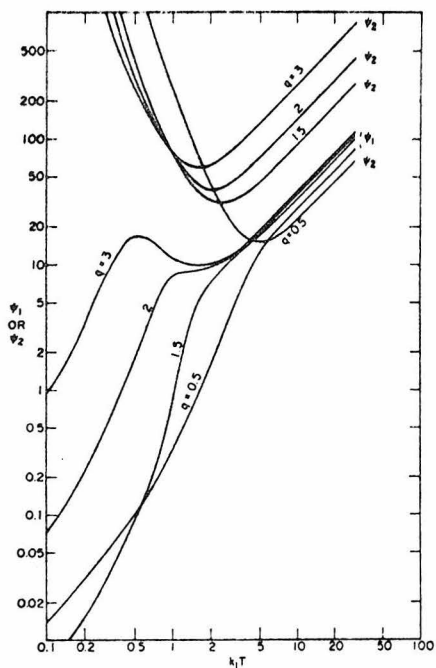


Figure 2—Dimensionless variance of parameter estimates vs. dimensionless time in the reaction scheme $A \xrightarrow{k_1} B \xrightarrow{k_2} C$, when components A and B are measured and the number of observations R is large.

necessary to estimate k_2 . Conversely, ψ_1 , for small k_1T , as q increases, ψ_2 decreases, because the second reaction becomes important.

For large values of k_1T , both ψ_1 and ψ_2 increase with k_1T , the more accurate estimates corresponding to smaller values of q . Smaller values of q correspond to a longer time necessary for complete conversion to C and the ability to obtain more information on a fixed interval $(0, T)$. As a result, the ψ_2 curves exhibit a minimum coupled with a reversal of the dependence on q . For $q = 3$ the ψ_1 curve also exhibits a minimum (a relative minimum) reflecting the trade-off between the increase in ψ_1 at high values of k_1T and the effect of a large k_2/k_1 which causes an increase in ψ_1 for moderate values of k_1T .

Fig 3 For very small and very large values of k_1T both ψ_1 and ψ_2 become large. In the former case it is because neither reaction has proceeded to any appreciable extent. In the latter case, the low accuracy is due to the fact that most of the measurements are being wasted in measuring values of A and B which have, for all practical purposes, long since reached their final values. The trade-off between these two considerations results in a minimum in both the ψ_1 and ψ_2 curves for all values of $q = \frac{k_2}{k_1}$.

As q increases, the value of k_1T corresponding to the minimum value of the ψ_1 and ψ_2 curves decreases. This is a direct consequence of measurements being taken on A and B only. The higher the value of q for a given k_1 , the more important the second reaction becomes. It is then advantageous to take

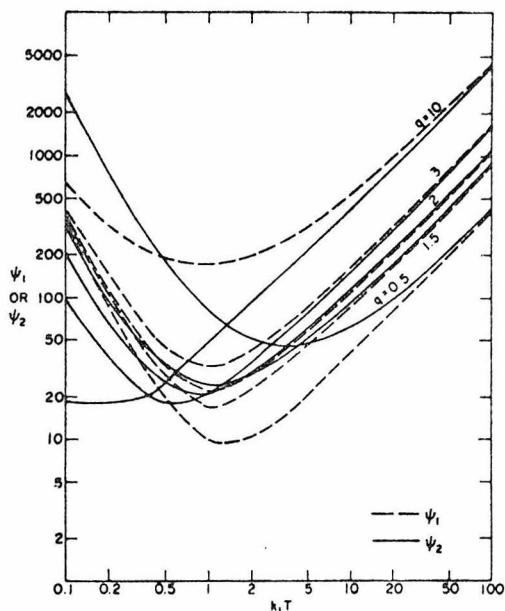


Figure 3—Dimensionless variance of parameter estimates vs. dimensionless time in the reaction scheme $A \xrightarrow{k_1} B \xrightarrow{k_2} C$ when components A and B are measured and the number of observations is large.

measurements on A and B before all the A is converted to C by the second reaction and the value of B becomes static. The optimum value of k_1T therefore becomes smaller as q increases.

For values of q less than about 2, ψ_1 is less than ψ_2 , i.e. k_1 is estimated more accurately than k_2 . But for higher values of q , the situation is exactly the opposite. This effect is important for low values of k_1T , and is again a consequence of the fact that we are observing only A and B. We may think of the measurements on A as determining $(k_1 + k_2)$ and the measurements on B as determining k_1 . As q increases, it becomes less and less profitable to measure B as the predominant reaction is the second one. Hence the k_1 estimates start getting less and less accurate. However, under these circumstances, $(k_1 + k_2)$ becomes very nearly the same as k_2 itself, and therefore the accuracy of the k_2 estimate does not suffer as much. For low values of q , on the other hand, the situation is exactly the opposite; k_2 estimates are poor because we are effectively taking no observations on the second reaction.

Fig 4 In general, as R is increased the accuracy of the estimates of k_1 and k_2 is increased.

For small values of k_1T , smaller values of ψ_1 and ψ_2 are obtained with fewer measurements. This is because ψ_1 and ψ_2 depend on the product of σ^2 and R, and as R decreases, the decrease in R more than compensates for the increase in σ^2 . For large values of k_1T , as R decreases, σ^2 increases faster than R decreases and ψ_1 and ψ_2 increase. At large values of k_1T , ψ_1 and ψ_2 depend very strongly on R, and it is in this range that R should be made as large as possible.

Fig 5 For small values of k_1T and $R = 5, 10, 20$, ψ_1 and ψ_2 are not strongly dependent on R. If $R = \infty$, a significant decrease in ψ_1 and ψ_2 occurs. For large values of k_1T , ψ_1 and ψ_2 are strong functions of R. Thus, if the reaction is allowed to proceed

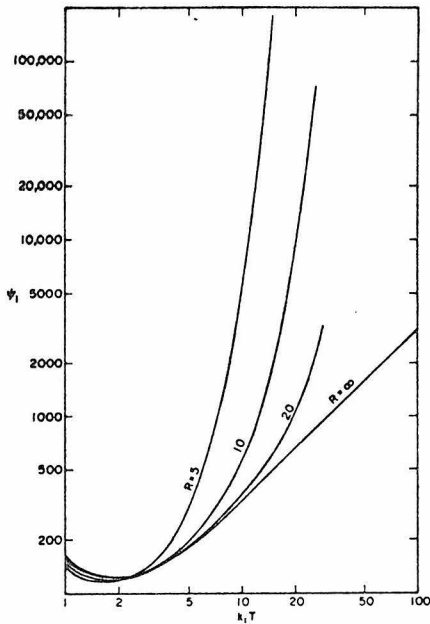


Figure 4—Effect of number of observations R on the dimensionless variance of k_1 estimate vs. dimensionless time in the reaction scheme $A \xrightarrow{k_1} B$ when only component A is measured and $q = \frac{k_2}{k_1} = 1$.

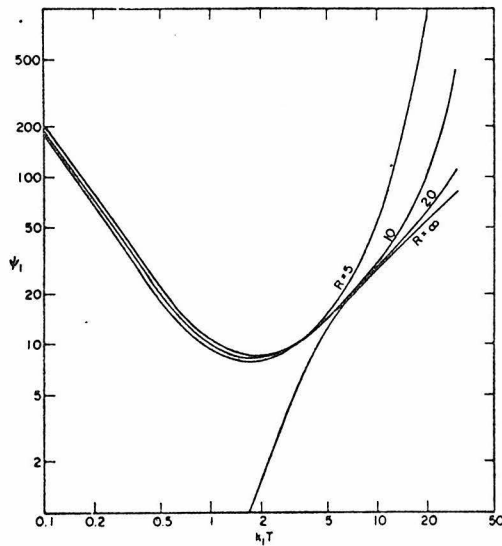


Figure 5—Effect of number of observations R on the dimensionless variance of k_1 estimate vs. dimensionless time in the reaction scheme $A \xrightarrow{k_1} B \xrightarrow{k_2} C$, when components A and B are measured and $q = \frac{k_2}{k_1} = 0.5$.

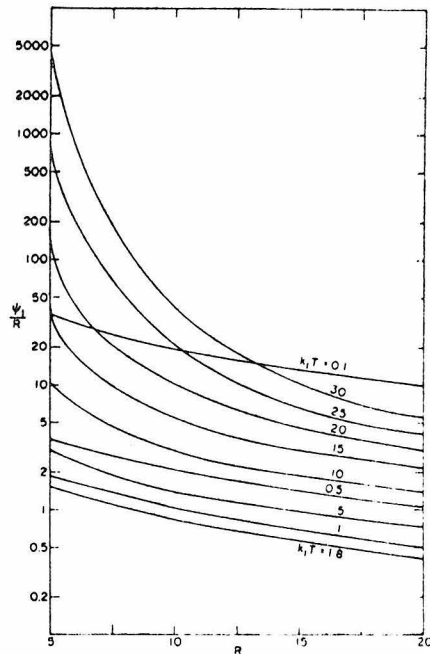


Figure 6—Effect of number of observations R on the accuracy of k_1 estimate in the reaction scheme $A \xrightarrow{k_1} B \xrightarrow{k_2} C$, when components A and B are measured and $q = \frac{k_2}{k_1} = 0.5$ (cross-plot of Figure 5).

substantially toward the complete conversion to C, it is important for a fixed value of T that one make as many measurements as possible. If the reaction is stopped early, then the number of observations is not as important. These conclusions are clearly visible in Figure 6 in which $\frac{\psi_1}{R}$ is plotted against R for constant values of $k_1 T$.

Fig. 7 The number of independent components in a reaction scheme must be equal to the number of independent reactions. Also, they must be chosen in such a way that the stoichiometric matrix A relating them to the extents of the independent reactions be non-singular.

$$\begin{pmatrix} C_1 \\ \vdots \\ C_n \end{pmatrix} = A \begin{pmatrix} \xi_1 \\ \vdots \\ \xi_n \end{pmatrix}$$

In many problems of kinetic parameter estimation, there is a choice regarding which components are to be measured. Seinfeld and Gavalas⁽⁶⁾ come to the conclusion that one should try and measure as many of the R independent concentrations as possible; and that if a choice must be made, intermediates give better parameter estimates than primary constituents.

In the present study, this question was thoroughly examined

for the isothermal scheme $A \begin{cases} \xrightarrow{k_1} B \\ \xrightarrow{k_2} C \end{cases}$. Figure 7 is an example of the

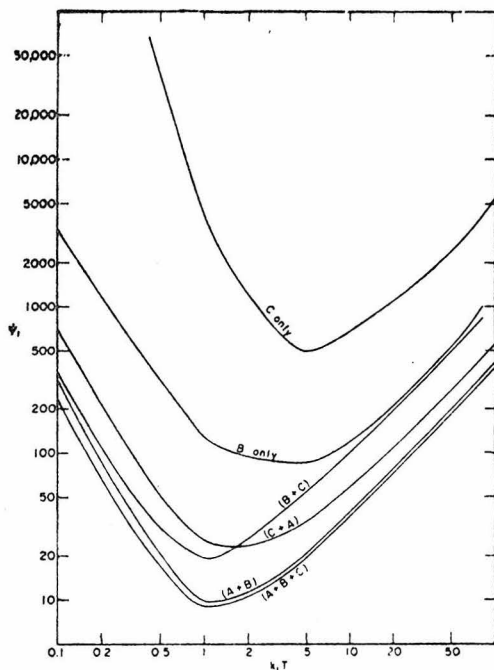


Figure 7—Effect of number of components measured on the dimensionless variance of k_1 estimate vs. dimensionless time in the reaction scheme $A \xrightarrow{k_1} B$, $A \xrightarrow{k_2} C$, when the number of observations R is large and $q = \frac{k_2}{k_1} = 0.5$.

large number of plots that were obtained for various values of $\frac{k_2}{k_1}$. The only conclusion that is valid for all these plots is that the most accurate estimates of k_1 and k_2 are obtained when all the three components are measured. However, a certain combination of two components always comes very close to the $(A + B + C)$ curve. Hence it would appear that there is little advantage in measuring more than the independent number of concentrations when the error matrix M has the form $\sigma^2 I$.

For specific guidance in an actual problem, it is necessary to look at the plot for the relevant value of $\frac{k_2}{k_1}$. Consider, for example, $\frac{k_2}{k_1} = 0.5$ which is illustrated in Figure 7. Further, let us confine our attention to the ψ_1 curves which give information regarding the accuracy of the k_1 estimate. Here, the best two components to measure are obviously A and B . Measuring C and A is better for high values of $k_1 T$, but B and C is better for lower values of $k_1 T$. Near the optimum values of $k_1 T$, there is little to choose between these two combinations.

The best single component to measure is B . Measurement of C alone is likely to lead to extremely inaccurate estimates. Of course, measurement of A alone will not give us k_1 and k_2 separately, a fact that is strikingly evident in the singularity of the $D^T G' G D$ matrix (and hence the H matrix) for that case.

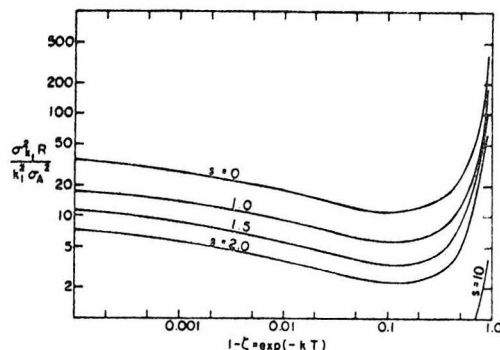


Figure 8—Effect of measuring more than the number of independent components on the dimensionless variance of parameter estimate vs. conversion in the reaction scheme $A \rightarrow B$ when the covariance matrix of errors is $M_i = \begin{pmatrix} \sigma_A^2 & 0 \\ 0 & \sigma_B^2 \end{pmatrix}$.

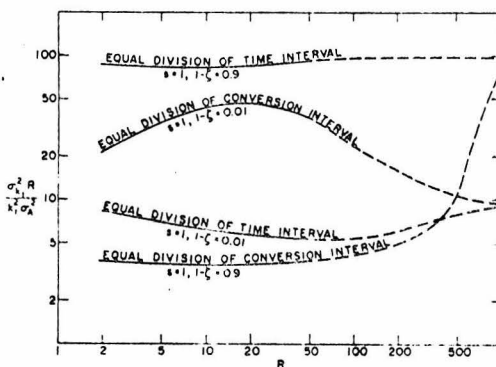


Figure 9—Effect of distribution of experimental observations on the dimensionless variance of parameter estimate vs. number of observations in the reaction scheme $A \rightarrow B$.

The existence of H^{-1} is an essential requirement in the procedure of Rosenbrock and Storey⁽¹⁾. Evidence from the present work confirms that the non-singularity of H is a sufficient condition for the estimability of parameters in a system of first order linear ordinary differential equations.

Fig 8 For a given σ_A and a given number of observations R , the accuracy of estimation improves as s increases. This is correct as increasing s means increasing accuracy of measuring B . The curve for $s = 0$ corresponds to extremely imprecise measurements on B , which is equivalent to measurement of A alone.

Measuring more than the number of independent components is advantageous under all circumstances except $s = 0$. Further, for every value of n , there is a minimum which represents the point at which the reaction must be skipped to get maximum accuracy of estimate.

As $T \rightarrow t_0$ ($\xi \rightarrow 1$), all the curves go up to infinity. This is obvious as there can be no estimates when the reaction is not carried out at all.

Fig 9 The limiting value plotted in Figure 9 is strictly valid for a very large number of observations. This limit is approached

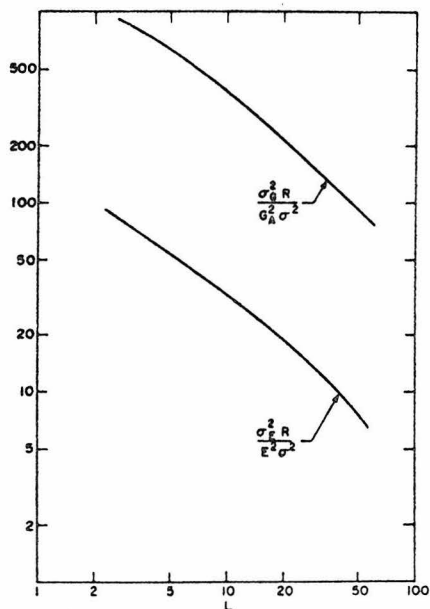


Figure 10—Effect of number of isothermal runs on the dimensionless variances of the frequency factor and activation energy estimates in the scheme $A \xrightarrow{G_A \exp(-E/\theta)} B$

with $G_A T = 10$, $\frac{\theta(0)}{E} = \frac{1}{5}$, $\frac{\theta(L)}{E} = \frac{1}{3}$.

rapidly from the lower side when the time interval (t_0, T) is equally divided. However, if the same number of observations are taken at intervals of equal conversion, the results are profoundly different. For high values of ξ (e.g. 0.9), it is possible to achieve much greater accuracies by this device. For low values of ξ (e.g. 10^{-2}), on the other hand, this must not be done as errors increase greatly. In fact, for low ξ , the limit as $R \rightarrow \infty$ is approached from the upper side. We therefore conclude that taking a finite number of observations at equal conversion intervals will be useful when the reaction has to be stopped far from completion. The physical meaning of this is that when concentrations are changing rapidly, observations must be taken more frequently, but when they are changing slowly, the time period between observations can be lengthened. The experimental kineticist very often makes use of this trick while collecting his data.

Fig. 10 The accuracy of estimation of G_A and E improves almost in direct proportion to the number of temperatures at which observations are taken.

In the limited range considered, the activation energy is estimated more accurately than the frequency factor. This would indicate that non-linear regression of the pooled data yields a better estimate of E than that obtained by regressing the estimated rate constants at different temperatures. In such cases, the technique presented in this paper could be invaluable in assigning confidence limits to the parameters obtained by the non-linear analysis.

Conclusion

The statistical structure of several basic first order reaction schemes was analyzed. No analysis of experimental kinetic data is complete without a good estimate of the accuracy of the rate constants derived therefrom. The first use of the present results is in obtaining such estimates for any desired confidence

level from the computed variance of the rate constant error distribution. The second and more important use is in planning experiments to obtain maximum kinetic information without sacrifice of accuracy. Questions such as how many data points to take and in what range, which components should be measured in the event of a choice being available, and what effect the level of experimental errors has on the problem, were answered. The same technique was also extended to answer some novel questions such as how to distribute the observations in a given time interval, and at how many temperatures isothermal runs must be conducted to get acceptable estimates of the frequency factor and activation energy. The practising chemical engineer should find the procedure extremely useful even when confronted by reaction schemes more complex than the ones considered here. Even if this type of complete analysis is not undertaken, the simple first order schemes should give him a feel for the effects of features like reversibility, parallelism and consecutiveness in the reaction mechanism on the propagation of error.

Acknowledgment

This work was supported by the U.S. Atomic Energy Commission under Project Agreement No. 1 under AT(04-3)-767 and a Chevron Oil Field Research Company Grant.

APPENDIX: THE WORKING EQUATIONS

We will illustrate the details of the analysis for the scheme



Under the assumptions in the introduction, the reaction is described by

$$\frac{dx_1}{dt} = -(k_1 + k_2) x_1; x_1(0) = 1$$

$$\frac{dx_2}{dt} = k_1 x_1; x_2(0) = 0$$

where $x_1 = [A]/[A_0]$ and $x_2 = [B]/[A_0]$ and A and B have been chosen as the independent components. Therefore,

$$x_1 = \exp[-(k_1 + k_2)t]$$

$$x_2 = \frac{k_1}{k_1 + k_2} [1 - \exp\{-(k_1 + k_2)t\}]$$

In this case, $n = 2$, $p = 2$ and D is a 2×2 matrix governed by

$$\frac{dD_{11}}{dt} = -(k_1 + k_2) D_{11} - x_1; D_{11}(0) = 0$$

$$\frac{dD_{12}}{dt} = -(k_1 + k_2) D_{12} - x_1; D_{12}(0) = 0$$

$$\frac{dD_{21}}{dt} = k_1 D_{11} + x_1; D_{21}(0) = 0$$

$$\frac{dD_{22}}{dt} = k_1 D_{12}; D_{22}(0) = 0$$

The integrated forms are

$$D_{11} = -t \exp[-(k_1 + k_2)t]$$

$$D_{12} = -t \exp[-(k_1 + k_2)t]$$

$$D_{21} = \frac{k_1 t}{k_1 + k_2} \exp[-(k_1 + k_2)t] -$$

$$\frac{k_2}{(k_1 + k_2)^2} [\exp\{-(k_1 + k_2)t\} - 1]$$

$$D_{22} = \frac{k_1 t}{k_1 + k_2} \exp[-(k_1 + k_2)t] +$$

$$\frac{k_1}{(k_1 + k_2)^2} [\exp\{-(k_1 + k_2)t\} - 1]$$

When, for example, only A is measured, $G = [1 \ 0]$, and

$$D^T G^T G D = \begin{bmatrix} D_{11}^2 & D_{11} D_{12} \\ D_{11} D_{12} & D_{12}^2 \end{bmatrix}$$

h is now easily obtained from Equation (8). The results of other cases are summarized below.

Isothermal case

a) $A \xrightarrow{k_1} B$, $n = 1$, $p = 1$

$$D = -t \exp(-k_1 t)$$

b) $A \xrightleftharpoons[k_2]{k_1} B$, $n = 1$, $p = 2$

$$D_1 = -\frac{k_2}{(k_1 + k_2)^2} - \frac{k_1}{(k_1 + k_2)^2} t \exp\{-(k_1 + k_2)t\} +$$

$$\frac{k_2}{(k_1 + k_2)^2} \exp\{-(k_1 + k_2)t\}$$

$$D_2 = \frac{k_1}{(k_1 + k_2)^2} - \frac{k_1}{k_1 + k_2} t \exp\{-(k_1 + k_2)t\} -$$

$$\frac{k_1}{(k_1 + k_2)^2} \exp\{-(k_1 + k_2)t\}$$

c) $A \xrightarrow{k_1} B \xrightarrow{k_2} C$, $n = 2$, $p = 2$

$$D_{11} = -t \exp(-k_1 t)$$

$$D_{12} = 0$$

$$D_{21} = \frac{k_1}{k_1 - k_2} t \exp(-k_1 t) + \frac{k_2}{(k_1 - k_2)^2} \exp(-k_1 t)$$

$$- \frac{k_2}{(k_1 - k_2)^2} \exp\{-k_2 t\}$$

$$D_{22} = -\frac{k_1}{k_1 - k_2} t \exp(-k_2 t) + \frac{k_1}{(k_1 - k_2)^2} \exp(-k_2 t)$$

$$- \frac{k_1}{(k_1 - k_2)^2} \exp(-k_1 t)$$

Isothermal runs at different temperatures

If $A \xrightarrow{k_1} B$ and $k_1 = G_A \exp(-E/\theta)$ we will consider the i^{th} experiment with temperature θ_i . Since $n = 1$ and $p = 2$ (G_A and E), D is given by

$$D_1 = -t \exp[-t G_A \exp(-E/\theta_i) - E/\theta_i]$$

$$D_2 = \frac{t G_A}{\theta_i} \exp\left[-t G_A \exp\left(-\frac{E}{\theta_i}\right) - \frac{E}{\theta_i}\right]$$

Nomenclature

a	= p -dimensional parameter vector
b	= arbitrary p -dimensional vector
c	= n -dimensional initial value vector
A, B, C, E, P, S	= components in various reactions
D	= $n \times p$ matrix
E	= activation energy divided by the gas constant
f	= n -dimensional vector function
g	= m -dimensional known function of state variables
G	= $m \times n$ matrix
G_A	= frequency factor
h	= $p \times p$ matrices
H	
k_1, k_2	= rate constants
L	= number of equal divisions of temperature interval
M	= covariance matrix of experimental error
n	= number of independent components
p	= number of parameters to be estimated
P	= covariance matrix of parameter estimates
q	= k_2/k_1
R	= number of equal divisions of the time interval
S^2	= sum of squares being minimized
s	= σ_A/σ_n
t	= time variable
t_0	= lower limit of time interval
T	= upper limit of time interval
x	= n -dimensional state vector
z	= m -dimensional vector of observations
ζ	= extent of an independent reaction
η	= random additive experimental error
θ	= absolute temperature
ξ	= lower limit of conversion interval
$\sigma_A^2, \sigma_B^2, \sigma^2$	= variances of experimental error
$\sigma_{k_1}^2, \sigma_{k_2}^2, \sigma_G^2, \sigma_E^2$	= variances of parameter estimates
Ψ_1, Ψ_2	= dimensionless variances of parameter estimates

References

- (1) Bellman, R. and Kalaba, R., "Quasilinearization and Nonlinear Boundary Value Problems", American Elsevier, New York (1965)
- (2) Donnelly, J. K. and Quon, D., AIChE Tampa Meeting, Paper 19f, May 19-22 (1968).
- (3) Lee, E. S., Ind. Eng. Chem. Fundamentals, 7, No. 1, 152 (1968)
- (4) Rosenbrock, H. H., and Storey, C., "Computational Techniques for Chemical Engineers", Pergamon, New York (1966).
- (5) Heiniken, F. G., Tsuchiya, H. M. and Aris, R., Math. Biosciences, 1, 115 (1967).
- (6) Seinfeld, J. H. and Gavalas, G. R., "Analysis of Kinetic Parameters from Batch and Integral Reaction Experiments", AIChE Journal, 16, 4, 644 (1970).

Manuscript received May 27, 1969; accepted March 24, 1970.

★ ★ ★

PROPOSITION P-2

Reprint from Journal of Physical Chemistry

ABSTRACT

Microwave absorption is proposed as a technique for monitoring the kinetics of liquid reactions in which there is a large difference of dipole moment between the products and the reactants. The absorption is conveniently measured by perturbing the resonance of a microwave cavity.

[Reprinted from the Journal of Physical Chemistry, 74, 2855 (1970).]
 Copyright 1970 by the American Chemical Society and reprinted by permission of the copyright owner.

Application of Microwave Cavity Perturbation Techniques to a Study of the Kinetics of Reactions in the Liquid Phase

by A. L. Ravimohan

Department of Chemical Engineering, California Institute of Technology, Pasadena, California 91109
 (Received March 30, 1970)

Polar liquids are known to have broad absorption bands in the microwave region which arise from orientation of the molecules with increasing electric field E , followed by relaxation to thermal equilibrium as E falls to zero. The absorption is expressed as the loss factor $\tan \delta$, and for a dilute solution of a polar solute in a non-polar solvent it is given¹ by the Debye theory as

$$\tan \delta = \frac{(\epsilon_c + 2)^2}{\epsilon_c} \frac{4\pi\mu^2 c N \nu}{27k_B T \nu_0 [1 + (\nu/\nu_0)^2]} \quad (1)$$

where δ = loss angle, ϵ_c = static dielectric constant, μ = dipole moment of solute molecule, c = concentration of solute in moles per cm³, ν = frequency of radiation, $\nu_0 = 1/2\pi\tau$, where τ = relaxation time of solute in solution, N = Avogadro's number, k_B = Boltzmann constant, and T = absolute temperature of the solution. For a mixture of solutes, $\tan \delta$ is the sum of the loss factors due to the individual solutes. Jackson and Powles² verified eq 1 for solutions of several polar solutes in benzene by measuring resonant frequency shifts and Q factors of cylindrical microwave cavities partially filled with samples of the solution. The proportionality of $\tan \delta$ to the concentration of dipole c , for constant values of other variables in (1), suggests a convenient method of following the kinetics of certain classes of liquid reactions. Consider a reaction in which the reactants have no dipole moments but the products have appreciable μ 's. The time variation of the product concentration, and hence the extent of reaction, can be followed by measuring $\tan \delta$ (and ϵ_c) of the reaction mixture as a function of time. The method would be fast, accurate, and convenient, as no samples have to be withdrawn for analysis. It is especially suited to the study of the early stages of the reaction, when the use of conventional methods³ would be difficult. The chief limitations are that one must stay within the bounds of the Debye theory of dilute solutions and of the linearized theory of microwave cavity perturbation.⁴ In particular, aqueous reactions are ruled out because of the abnormally high absorption of microwaves by water.

The room temperature (22°) liquid phase bromination of benzene with iodine as catalyst was chosen for the present study. C₆H₆, Br₂, and I₂ have no dipole moments, but C₆H₅Br and HBr have dipole moments of 1.52 and 0.78 D, respectively.⁵

Experimental Technique

The two parameters of a liquid that can be obtained from microwave cavity measurements are the static dielectric constant ϵ_c and the loss factor $\tan \delta$. A particular cavity resonance is characterized by the resonant frequency f_0 and the loaded quality factor Q . A liquid placed in a quartz bottle on the axis of the cylindrical cavity introduces a change in both f_0 and Q . As shown by Dunsmuir and Powles⁶ and Slater,⁴ the first-order perturbation solution takes the form

$$\epsilon_c = 1 + \frac{2(f_0 - f_0')}{f_0 \eta} \quad (2)$$

$$\tan \delta = F(R_0, R_1, R_2, \epsilon_b, \epsilon_c) \left(\frac{1}{Q'} - \frac{1}{Q} \right) \quad (3)$$

where η = dimensionless form-factor depending on cavity geometry, R_0 = radius of microwave cavity, R_1 = inner radius of quartz bottle, R_2 = outer radius of quartz bottle, ϵ_b = dielectric constant of bottle material, ϵ_c = dielectric constant of the liquid. When $R_0 \gg R_1$, $R_1 \approx R_2$, and $\epsilon_b \approx \epsilon_c$

$$\tan \delta = G(R_0, R_1, R_2, \epsilon_b) \left(\frac{1}{Q'} - \frac{1}{Q} \right) / \epsilon_c = \text{constant} \left(\frac{1}{Q'} - \frac{1}{Q} \right) / \epsilon_c \quad (4)$$

The method used for the measurement of f_0 and Q was a "transmission" method.⁷ With the circuit of Figure 1, it is possible to obtain a resonance curve in about 20 sec. A faster sweep may be obtained, if necessary, by using an oscilloscope and high-speed photography. f_0

- (1) W. Gordy, *et al.*, "Microwave Spectroscopy," Dover Publications, New York, N. Y., 1966.
- (2) W. Jackson and J. G. Powles, *Trans. Faraday Soc.*, **42A**, 101 (1946).
- (3) K. J. Laidler, "Chemical Kinetics," McGraw-Hill, New York, N. Y., 1965.
- (4) J. C. Slater, "Microwave Electronics," Van Nostrand, Princeton, N. J., 1950.
- (5) N. A. Lange, Ed., "Handbook of Chemistry," 9th ed. McGraw-Hill, New York, N. Y., 1956.
- (6) R. Dunsmuir and J. G. Powles, *Phil. Mag.*, **37**, 747 (1946).
- (7) E. L. Ginzton, "Microwave Measurements," McGraw-Hill, New York, N. Y., 1957.

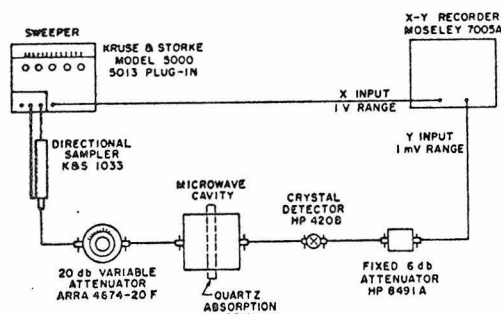


Figure 1. Coaxial circuit for automatic plotting of transmission characteristic of microwave cavity with quartz absorption cell.

and the half-power frequencies f_2 and f_1 are determined directly from the calibrated frequency scale. Now $Q = f_0/(f_2 - f_1)$. The mode of resonance used was TM_{011} , for which η determined empirically from ϵ_0 measurements on standard liquids (benzene and *m*-xylene), was found to be 0.01145.

The reaction studied was



Since the products are formed in equimolar amounts, a quantity proportional to the common product concentration c can be deduced from (1) and (4) as

$$c = \frac{\text{const}}{(\epsilon_0 + 2)^2} \left[\left(\frac{1}{Q_0'} - \frac{\epsilon_0}{\epsilon_0 Q_0'} \right) - \frac{1}{Q} \left(1 - \frac{\epsilon_0}{\epsilon_0} \right) \right] \quad (6)$$

where ϵ_0 is the dielectric constant and Q_0' is the quality factor at zero time, and the $\tan \delta$ of the reaction mixture at zero time has been subtracted out. The reason why Q_0' is not equal to Q is discussed in the next section.

Analytical reagent grade chemicals meeting ACS specifications were used in the work. A known solution of bromine in benzene was prepared and a known weight of iodine dissolved in it. The reaction mixture was poured into the quartz cell which was then closed tightly with a neoprene stopper. Replicated microwave readings were taken at various time intervals, with intermittent shaking of the tube to ensure homogeneity. A test run on the same solution without iodine catalyst revealed that the noncatalytic reaction was negligible under the present conditions. It is believed that the addition reaction is also negligible. Finally, the reaction was stopped after 2.5 hr by pouring the contents into excess KI. Total free halogen was estimated by titration against standard $\text{Na}_2\text{S}_2\text{O}_3$ solution using starch as indicator. This titration provided the means for estimating the constant of eq 6 which is necessary as the microwave absorption data determine only a quantity proportional to the product concentration.

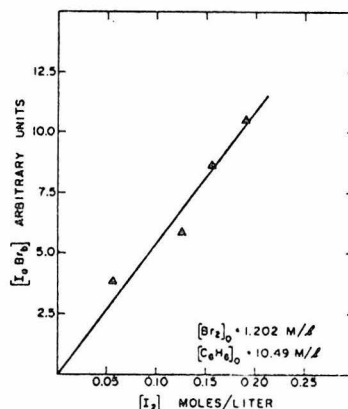


Figure 2. Initial absorption as a function of iodine added.

Discussion of Results

The first noteworthy feature about the results is that there is significant absorption even at zero time, since $Q_0' < Q$. This indicates the instantaneous formation of a species with a dipole moment. A survey of the literature reveals that an intermediate of the type $I_a\text{Br}_2$ has been invoked to explain the catalytic action of iodine on the reaction,⁸⁻¹¹ with the most likely form being IBr . Initial absorption data can therefore be used to obtain relative $I_a\text{Br}_2$ concentrations. Figure 2 shows a plot of this quantity against moles of added iodine. The approximately linear nature of the plot indicates that $K = [I_a\text{Br}_2]/[I_2]^a[\text{Br}_2]^b$ is very high, a result in accordance with the findings of Price and Arntzen.¹⁰ The high K value means that the $I_a\text{Br}_2$ concentration is not affected appreciably by changes in the Br_2 concentration. Hence it is a valid procedure to subtract out the initial reading to get the product concentration, as done in eq 6. If it is assumed that $a = b = 1$, putting $[\text{IBr}] = [I_2]/2$ in eq 1, along with Sheka's¹² value of the dipole moment of IBr (1.21 D), yields $\tau = 4 \times 10^{-10}$ sec, which is quite reasonable. If measurements are made at other frequencies, it is possible to get both μ and τ of the intermediate from microwave data, but this was not done here.

The existence of a $\text{C}_6\text{H}_6\text{-I}_2$ complex with a dipole moment of 0.6 D has been deduced from absorption measurements in the visual range.¹³⁻¹⁵ However, no sig-

- (8) L. Bruner, *Z. Phys. Chem.*, **41**, 514 (1902).
- (9) C. C. Price, *J. Amer. Chem. Soc.*, **58**, 2101 (1936).
- (10) C. C. Price and C. E. Arntzen, *ibid.*, **60**, 2835 (1938).
- (11) P. W. Robertson, *et al.*, *J. Chem. Soc.*, 933 (1949).
- (12) A. L. McClellan, "Tables of Experimental Dipole Moments," W. H. Freeman, San Francisco, Calif., 1963.
- (13) H. A. Benesi and J. H. Hildebrand, *J. Amer. Chem. Soc.*, **71**, 2703 (1949).
- (14) F. Fairbrother, *Nature*, **160**, 87 (1947).
- (15) R. S. Mulliken, *J. Amer. Chem. Soc.*, **72**, 600 (1950).

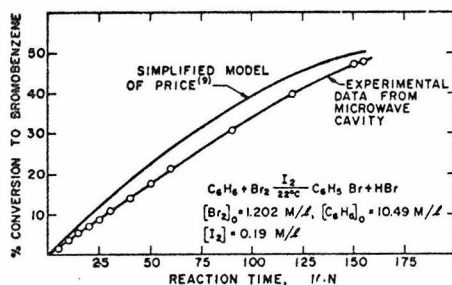


Figure 3. Per cent conversion in substitution reaction as a function of time.

nificant microwave absorption was observed in the present experiments even in saturated solutions of iodine in benzene. This could be either due to the low concentration of the complex or because it has a low ν_0 so that $\nu \ll \nu_0$. Similarly any complex between bromine and benzene was not picked up. In any event, the interpretation of both the initial absorption and kinetic data in the $\text{C}_6\text{H}_6\text{-Br}_2\text{-I}_2$ system was thereby considerably simplified.

Figure 3 shows the conversion in the substitution reaction as a function of time. The order of the reaction with respect to total Br_2 , as determined by the method of Powell,¹⁶ is approximately 0.75. This does

not agree with Price's⁹ value of 1.5, which he derived from some of Bruner's⁸ data. The reason for this disagreement is possibly because the model $dx/dt = k[\text{Br}_2]^{1.5}[\text{I}_2]^{2.5}$ is an oversimplified description of the kinetics of iodine-catalyzed bromosubstitution. In fact, an examination of Bruner's data, *e.g.*, his Table IA reveals that the order with respect to total Br_2 apparently increases with time in the same run. The "order" would thus depend upon which segment of the $x-t$ curve is being considered. The present data fall in a conversion range well below that of (8) for comparable concentrations. Hence there is no real conflict with Bruner's raw data, the only disagreement being with the simplified fits^{9,11,17} before. The microwave absorption method was able to illuminate this abnormal behavior as it is ideally suited for measurements at low product concentrations.

Acknowledgment. The author is thankful to Mr. J. M. Yehle for his invaluable assistance in setting up the microwave circuitry and to Professor F. H. Shair for many helpful discussions. This work was supported by the U. S. Atomic Energy Commission under Project Agreement No. 1 under AT(04-3)-767.

(16) R. E. Powell, quoted by A. A. Frost and R. G. Pearson, "Kinetics and Mechanism," Wiley, New York, N. Y., 1961.

(17) "Tables of Chemical Kinetics-Homogeneous Reactions," Circular 510, National Bureau of Standards, Washington, D. C., 1951.

PROPOSITION P-3

(J. of Optimization Theory and
Applications, in press)

Proposition P-3

OPTIMIZATION OF CHEMICAL REACTION NETWORKS
WITH RESPECT TO FLOW CONFIGURATION

Contents

ABSTRACT

1. Generalization of R. Jackson's approach to include the effects of local mixing in the network
2. Application of the general equations to a particular example

ABSTRACT

R. Jackson treated for the first time an optimization problem in which changes in chemical reactor performance were related to small changes in the mixing pattern or flow configuration. His algebraic structure could handle arbitrary kinetic schemes, but had the severe limitation that only global mixing in the reactor network was considered. In the present paper, it is shown how the approach can be further generalized to take into account local mixing in the network by introducing CSTR's of given volume at a newly defined type of nodal point. Relatively simple algebraic equations are derived, which can be used as a basis for optimizing performance by successive adjustments in the mixing pattern. Finally, the new equations are applied to a simple example, and the results are shown to agree with those obtained by direct calculation.

The proposed technique should be useful in the optimization of arbitrary networks of given chemical reactors with respect to flow configuration, i.e., their mode of interconnection.

1. GENERALIZATION OF R. JACKSON'S APPROACH TO INCLUDE THE EFFECTS OF LOCAL MIXING IN THE NETWORK

Let us consider the chemical reactor network shown in Figure P-3-1, which is a further generalization of the one considered by Jackson⁽¹⁾. It consists of N interconnected reaction paths which behave as ideal tubular reactors with discontinuities at the nodal points. In addition to source and sink points, we now have a third type of discontinuity, which arises because of the introduction of ideal continuous stirred tank reactors (CSTR's) of known volume V_k^n at a finite number of points (n,k) along the reaction paths. This newly defined kind of nodal point accounts for local mixing in the reactor network, while the interconnections account for global mixing. The terms local and global mixing are used here in the same sense as, for example, in Horn and Tsai⁽²⁾. The general network of Figure P-3-1 is capable of modeling almost any mixing pattern that can be visualized for a chemical reactor system.

In the algebra that follows, the notation of Ref. (1) will be followed as far as possible. The objective, as before, is to maximize P , a given scalar function of the combined product flow vector at the termini of the reaction paths.

$$P = F(p) = F \left\{ \sum_{n=1}^N q_{K_n}^n (x_{K_n}^n) \right\} \quad (P-3-1)$$

The maximization is with respect to the positions of the nodal points, which now include points of the type shown in Figure P-3-2. An expression will be obtained linking δP to infinitesimal changes in

the positions x_k^n of nodal points (n,k) , so that performance can be maximized by successive improvements of the x_k^n .

For the CSTR of Figure P-3-2, we can write an algebraic equation for the change in the column vector f , whose components are the flow rates of the independent components of the reaction mixture, as

$$q_k^n(x_k^n) = q_{k-1}^n(x_k^n) - V_k^n \cdot g\{q_k^n(x_k^n)\} \quad (\text{P-3-2})$$

where g is a given vector function accounting for the reaction in the CSTR. g , of course, is related to the f function in tubular reactor 2 by the expression

$$g\{q_k^n(x_k^n)\} = f\{q_k^n(x_k^n)\} / A_2 \quad (\text{P-3-3})$$

where A_2 is the cross-sectional area of tube 2 at x_k^n .

The effect of a small perturbation in the position of the CSTR is to change equation (P-3-2) into

$$q_k^{n*}(x_k^{n*}) = q_{k-1}^{n*}(x_k^{n*}) - V_k^n \cdot g\{q_k^{n*}(x_k^{n*})\} \quad (\text{P-3-4})$$

Putting $x_k^{n*} = x_k^n + \delta x_k^n$, expanding in a Taylor series with only first order terms, and using equation 1 of Ref. (1),

$$\begin{aligned} q_k^{n*}(x_k^{n*}) + \delta x_k^n \cdot f\{q_k^n(x_k^n)\} &= q_{k-1}^{n*}(x_k^n) + \delta x_k^n \cdot f\{q_{k-1}^n(x_k^n)\} \\ &- V_k^n \cdot [g\{q_k^{n*}(x_k^n)\} + \delta x_k^n \cdot g'\{q_k^{n*}(x_k^n)\} \cdot f\{q_k^n(x_k^n)\}] \end{aligned} \quad (\text{P-3-5})$$

where g' is the square matrix obtained by differentiating the g column vector with respect to the elements of the q vector. Subtracting (P-3-2) from (P-3-5) and simplifying,

$$\begin{aligned} & [1 + V_k^n \cdot g' \{q_k^n(x_k^n)\}] \cdot \delta q_k^n(x_k^n) \\ & = \delta q_{k-1}^n(x_k^n) + \delta^{(o)} q_k^n \end{aligned} \quad (P-3-6)$$

where

$$\begin{aligned} \delta^{(o)} q_k^n & = \delta x_k^n \cdot [f \{q_{k-1}^n(x_k^n)\} \\ & - \{1 + V_k^n \cdot g'(q_k^{n*}(x_k^n))\} \cdot f \{q_k^n(x_k^n)\}] \end{aligned} \quad (P-3-7)$$

Equations 10, 11, 12 and 13, and Figure 3 of Ref. (1) are still valid. Hence equation (P-3-6) can be written in the alternative form

$$\begin{aligned} & [1 + V_k^n \cdot g' \{q_k^n(x_k^n)\}] \cdot \delta q_k^n(x_k^n) \\ & - \Lambda_{k-1}^n(x_{k-1}^n) \cdot \delta q_{k-1}^n(x_{k-1}^n) = \delta^{(o)} q_k^n \end{aligned} \quad (P-3-8)$$

Now when the adjoint equations are written, we must consider Case (d) in addition to the cases (a), (b) and (c) considered in Ref. (1).

Case (d): The point $(n, k+1)$ is a CSTR.

The term $\delta q_k^n(x_k^n)$ appears multiplied by the $[1 + V_k^n \cdot g' \{q_k^n(x_k^n)\}]$ matrix, which is assumed to be nonsingular, in the equation with R.H.S. $\delta^{(o)} q_k^n$, and multiplied by $-\Lambda_k^n(x_k^n)$ in the equation with R.H.S.

$$\delta^{(o)} q_{k+1}^n .$$

Understanding that $V_k^n \equiv 0$ unless (n,k) is a CSTR type of nodal point, we can write the adjoint equations as

$$\begin{aligned} & \ell_k^n \cdot [1 + V_k^n \cdot g' \{q_k^n(x_k^n)\}] \\ & = \{ \ell_{k+1}^n \cdot (1 - \sigma_{k+1}^n) + \ell_{k+1}^n \cdot \sigma_{k+1}^n \} \cdot \Lambda_k^n(x_k^n) , \end{aligned}$$

(n,k + 1) source point (P-3-9)

$$\ell_k^n \cdot [1 + V_k^n \cdot g' \{q_k^n(x_k^n)\}] = \ell_{k+1}^n \cdot \Lambda_k^n(x_k^n)$$

(n,k + 1) sink point or CSTR (P-3-10)

$$\ell_k^n \cdot [1 + V_{K_n-1}^n \cdot g' \{q_{K_n-1}^n(x_{K_n-1}^n)\}] = F'(p)$$

(n,K_n) terminal point, n = 1, 2, ... N (P-3-11)

Defining row vectors λ as in equation 26 or Ref. (1) leads to the following boundary conditions.

$$\begin{aligned} & \lambda_k^n(x_{k+1}^n) \cdot [1 + V_k^n \cdot g' \{q_k^n(x_k^n)\}] \\ & = \lambda_{k+1}^n(x_{k+1}^n) \cdot (1 - \sigma_{k+1}^n) + \lambda_{k+1}^n(x_{k+1}^n) \cdot \sigma_{k+1}^n \end{aligned}$$

(n,k + 1) source point (P-3-12)

$$\lambda_k^n(x_{k+1}^n) \cdot [1 + v_k^n \cdot g'\{q_k^n(x_k^n)\}] = \lambda_{k+1}^n(x_{k+1}^n)$$

(n, k + 1) sink point or CSTR (P-3-13)

$$\lambda_{K_n}^n(x_{K_n}^n) \cdot [1 + v_{K_n-1}^n \cdot g'\{q_{K_n-1}^n(x_{K_n-1}^n)\}] = F'(p)$$

(P-3-14)

(n, K_n) terminal point, n = 1, 2, ..., N

Comparing equations (P-3-9) to (P-3-11) with (P-3-12) to

(P-3-14)

$$\lambda_{K_n}^n = \lambda_{K_n}^n(x_{K_n}^n) \quad (P-3-15)$$

$$\lambda_k^n = \beta \cdot \lambda_k^n(x_k^n), \quad k \neq K_n \quad (P-3-16)$$

β is an arbitrary positive constant which arises because equations (P-3-9) and (P-3-10) could as well have been written with a constant multiplying both sides. In qualitative arguments about the sign of δP , the introduction of β makes no significant difference, but its existence becomes important in a numerical calculation.

The equation for the change in the objective function P defined in equation (P-3-1) now takes the form

$$\delta P = \beta \sum_{\text{sources } k} [\lambda_{\tilde{k}}^n(x_{\tilde{k}}^n) - \lambda_k^n(x_k^n)] \cdot \delta \sigma_k^n \cdot q_{k-1}^n(x_k^n)$$

$$+ \beta \sum_{\substack{\text{all non-terminal} \\ \text{points including} \\ \text{CSTR's}}} \delta x_k^n \cdot [\lambda_{k-1}^n(x_k^n) \cdot \{1 + v_{k-1}^n g'(q_{k-1}^n(x_{k-1}^n))\}] \cdot f\{q_{k-1}^n(x_k^n)\} - \lambda_k^n \cdot f\{q_k^n(x_k^n)\}]$$

$$- \beta \sum_{\text{CSTR's } k} \delta x_k^n \cdot [\lambda_k^n(x_k^n) \cdot v_k^n \cdot g'\{q_k^n(x_k^n)\} \cdot f\{q_k^n(x_k^n)\}]$$

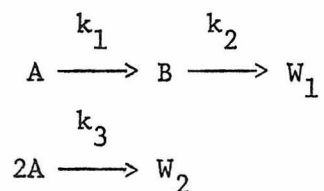
$$+ \sum_{\substack{\text{terminal} \\ \text{points } n}} \delta x_{K_n}^n \cdot \lambda_{K_n}^n(x_{K_n}^n) \cdot [1 + v_{K_n-1}^n \cdot g'\{q_{K_n-1}^n(x_{K_n-1}^n)\}] \cdot f\{q_{K_n}^n(x_{K_n}^n)\}$$

-300-

(P-3-17)

2. APPLICATION OF THE GENERAL EQUATIONS TO A PARTICULAR EXAMPLE

The Van de Vusse⁽³⁾ reaction scheme



affords an interesting example for testing some of the ideas developed in Section 1. Given a tubular reactor x_1x_3 of known length L and cross-sectional area A , and a CSTR of known volume V , the objective is to find the optimum point x_2 to insert the CSTR, so that the flow rate of B at x_3 is maximized. The feed is assumed to consist only of component A , together with any inerts. The reactions occur isothermally, and density changes of the reaction mixture are neglected.

The flow vectors q_1 and q_2 in the two segments of the tubular reactor are determined from the equations

$$dq_k/dx = f(q_k) \quad , \quad k = 1,2 \quad (P-3-18)$$

with the boundary conditions

$$\begin{aligned} q_1(x_1) &= q_0 \\ q_1(x_2) - q_2(x_2) &= V \cdot g\{q_2(x_2)\} \end{aligned} \quad (P-3-19)$$

The corresponding adjoint variables λ_1 and λ_2 are determined from

$$d\lambda_k/dx = -\lambda_k \cdot (\partial f/\partial q_k) \quad , \quad k = 1,2 \quad (P-3-20)$$

with the boundary conditions

$$\lambda_2(x_3) \cdot [1 - V \cdot \partial g / \partial q_2] = F'(p)$$

$$\lambda_2(x_2) = \lambda_1(x_2) \quad (P-3-21)$$

Considering A, B and W_1 as the independent components in the reaction scheme,

$$f = (\rho/q^{(T)}) \cdot \text{col}[\{-k_1 q_k^{(A)} - k_3 q_k^{(A)2} \rho/q^{(T)}\} , \{k_1 q_k^{(A)} - k_2 q_k^{(B)}\} , \{k_2 q_k^{(B)}\}] \quad (P-3-22)$$

where $q^{(T)}$ = total molar flow rate (constant)

ρ = molar density of reaction mixture (constant)

$k = 1, 2$

$$g = (\rho/q^{(T)}) \cdot \text{col}[\{-k_1 q_2^{(A)} - k_3 q_2^{(A)2} \rho/q^{(T)}\} , \{k_1 q_2^{(A)} - k_2 q_2^{(B)}\} , \{k_2 q_2^{(B)}\}]_{x=x_2} \quad (P-3-23)$$

$$q_0 = \text{col}[q_0^{(A)} , 0 , 0] \quad (P-3-24)$$

$$P = q_2^{(B)}(x_3) = [0 \ 1 \ 0]p \quad (P-3-25)$$

$$F'(p) = [0 \ 1 \ 0] \quad (P-3-26)$$

Using equations (P-3-22) through (P-3-26), the systems of differential equations (P-3-18) to (P-3-20) were solved with the respective boundary conditions. In both cases, the results were obtained in closed form for $a_2 = k_2/k_1 = 1$.

δP was then evaluated from the following reduction of equation (P-3-17)

$$\begin{aligned} \delta P &= \beta \cdot \delta x_2 \cdot [\lambda_1(x_2) \cdot f\{q_1(x_2)\} - \lambda_2(x_2) \cdot (1 + V \cdot \partial g / \partial q_2) \\ &\quad \cdot f\{q_2(x_2)\}] + \delta x_3 \cdot [\lambda_2(x_3) \cdot (1 + V \partial g / \partial q_2) \cdot f\{q_2(x_3)\}] \\ &= \delta P_1 + \delta P_2 \end{aligned} \quad (P-3-27)$$

δP_2 , the change in the objective function due to a small increase in the length of the tubular reactor turned out to be

$$\delta P_2 = \delta x_3 \cdot (A\rho/q^{(T)}) \cdot [k_1 q_2^{(A)}(x_3) - k_2 q_2^{(B)}(x_3)] \quad (P-3-28)$$

Thus, it is advantageous to increase the length of the tubular reactor only if $[k_1 q_2^{(A)}(x_3) - k_2 q_2^{(B)}(x_3)] > 0$, a result that is eminently reasonable. In the reaction scheme being considered, B is formed by reaction 1 and destroyed by reaction 2. As long as the former proceeds at a faster rate than the latter, the concentration of B increases. When the rate of reaction 2 becomes greater than that of 1, the concentration of B starts falling off, an undesirable result as far as the optimization is concerned.

δP_1 , the change in the objective function due to a small change in the position of the CSTR, was then evaluated. Numerical results for

$$a_1 = \frac{k_3 q_o^{(A)} \rho}{k_1 q^{(T)}} = 10$$

are shown in Figure (P-3-3). α , the fraction of the mean residence time τ spent in the CSTR was taken to be 0.1 and $k_1 \tau = 1.0$. In order that the results could be compared with those obtained by direct

calculation, it was necessary to integrate $\partial P_1 / \partial x_2$ numerically. The extreme points of the direct calculation were used to determine β and the constant of integration. As seen in Figure (P-3-3), the agreement of the remaining points is excellent. It is believed that the small discrepancy that still exists is due to the approximate nature of the integration procedure used. As the integration becomes more accurate, the results obtained by the two methods coincide.

The optimal position for the CSTR is at $x_2 = 0$, i.e., before the tubular reactor. Physically, this means that when the concentration of A is high, it is more important to suppress its conversion to W_2 by the second order reaction. The CSTR does this by instantaneously dropping the A concentration to a lower value. Later, it is important to suppress the loss of B to W_1 which occurs as a result of the spreading of the residence time distribution. The ideal tubular reactor performs this function admirably, as the residence time distribution in this type of reactor has zero spread. The optimal solution is thus a combination of a CSTR and an ideal tubular reactor.

This example has shown the validity of the technique in situations where local mixing plays an important role. Considering that the problem of computing the adjoint vectors is of the same nature and complexity as that of computing flow vectors, it is possible to visualize applications of the general equations to optimize reactors with respect to more complex flow configurations. The only limitation is the possible singularity of the $[1 + V_k^n \cdot g'\{q_k^n(x_k^n)\}]$ matrix, when the adjoint variables may not be well behaved, although $\partial P / \partial x$ from direct calculation is.

Fig. P-3.1

GENERAL REACTOR NETWORK WITH LOCAL MIXING

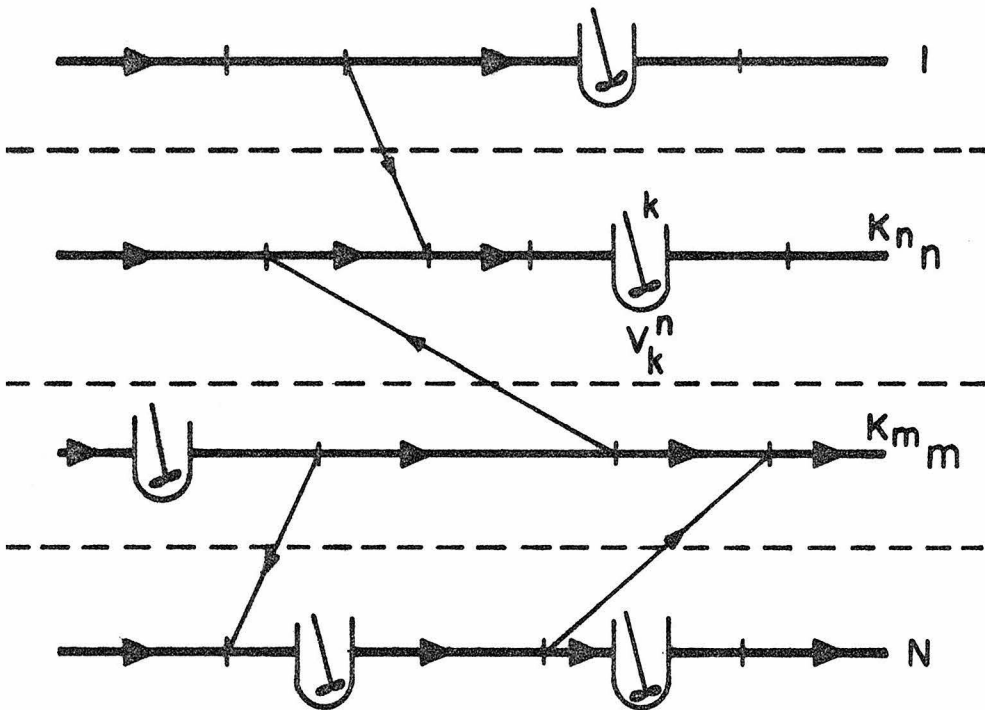


Fig. P-3.2

NODAL POINT OF THE CSTR TYPE

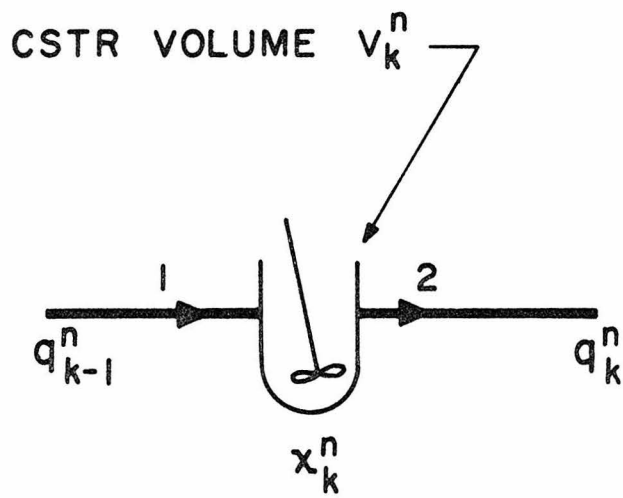
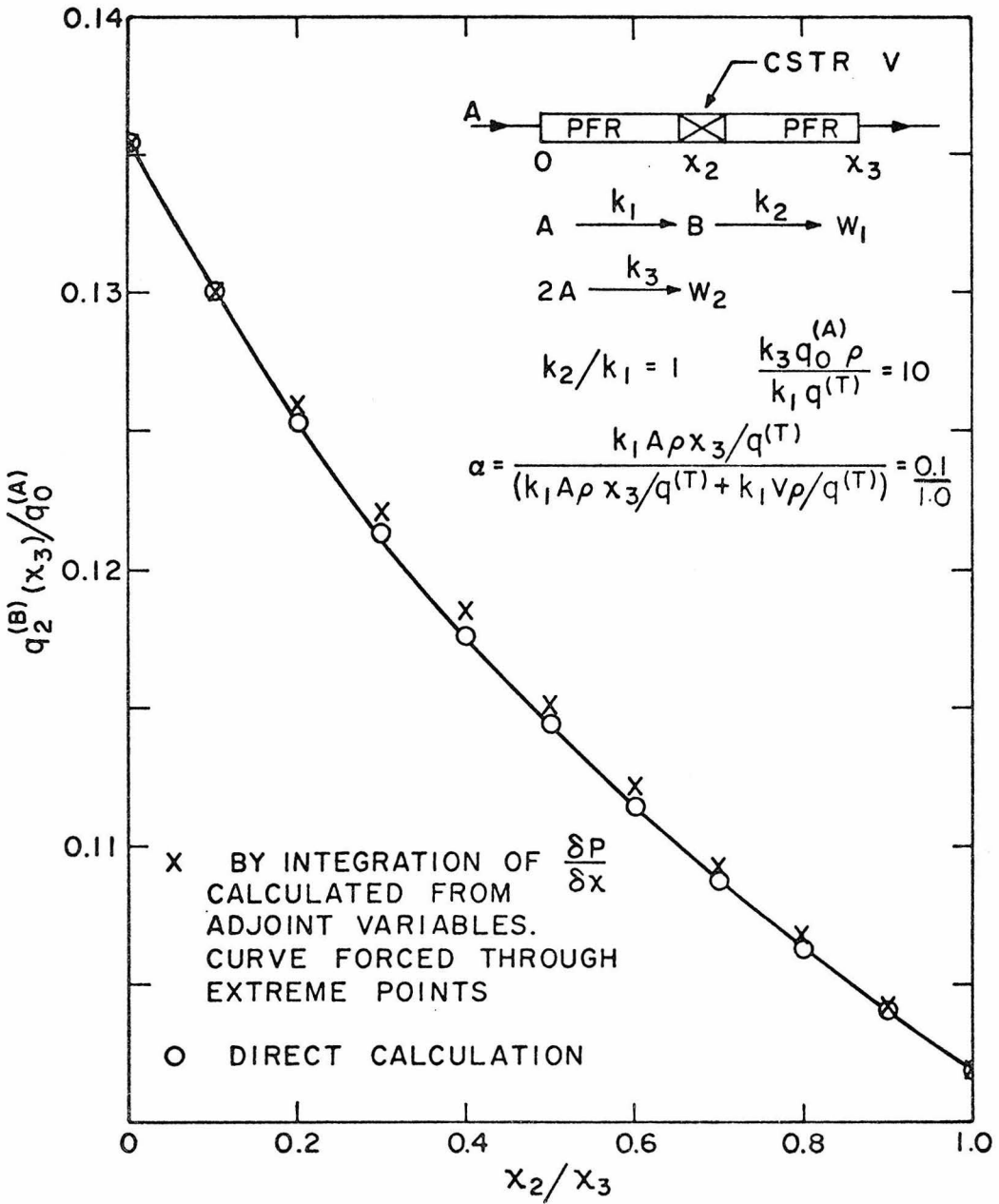


Fig. P-3.3

YIELD AS A FUNCTION OF CSTR POSITION



REFERENCES

- (1) Jackson, R., "Optimization of Chemical Reactors with Respect to Flow Configuration", Journal of Optimization Theory and Applications, Vol. 2, No. 4, 1968.
- (2) Horn, F. J. M., and Tsai, M. J., "The Use of Adjoint Variables in the Development of Improvement Criteria for Chemical Reactors", Journal of Optimization Theory and Applications, Vol. 1, No. 2, 1967.
- (3) Van de Vusse, J. A., "Plugflow Reactor vs. Tank Reactor", Chemical Engineering Science, 19, 994, 1964.

MISCELLANEOUS PUBLICATIONS AND CONFERENCE PRESENTATIONS

Reprinted from

ENVIRONMENTAL
Science & Technology

Vol. 2, December 1968, Pages 1101-1108
Copyright 1968 by the American Chemical
Society and reprinted by permission of
the copyright owner

A Theoretical Model for the Effect of an Acute Air Pollution Episode on a Human Population

S. K. Friedlander

W. M. Keck Engineering Laboratories and Division of Chemistry and Chemical Engineering,
California Institute of Technology, Pasadena, Calif. 91109

An Application of the Model to the 1952 London "Killer" Fog

A. L. Ravimohan

Division of Chemistry and Chemical Engineering,
California Institute of Technology, Pasadena, Calif. 91109

■ A quantitative theory for the increase in the mortality rate accompanying a severe air pollution episode has been developed, based on the following concepts: An individual dies when the activity of the gene-controlled, biochemical reaction steps in his respiratory system reaches a certain critically low value. The activity decays normally as a result of genetic changes in the somatic cells (the aging process); in the presence of severe air pollution, additional decay is produced by cytotoxic agents. The chemical effects depend on the time history of pollutant concentration in the tissue, determined by the rate at which material is transferred from the environment into the respiratory tissue.

A mathematical model based on these concepts was used to correlate the data for mortality rates and concentrations collected during the London "killer" fog of 1952. Three constants with well defined physical meanings appear in the theory. The model may be applicable to the setting of environmental standards and to the development of a strategy for coping with an acute air pollution episode in an urban area.

A major problem in environmental control is the development of rational methods for establishing permissible levels of atmospheric contamination (Breslow, 1967; Sargent, 1967). The criterion most often used in setting standards is human health and well being (Goldsmith, 1968), although esthetic considerations or industrial use may also be invoked. In the development of the California ambient air quality standards, three levels of pollutant concentration were defined in terms of their effects as follows (American Association for the Advancement of Science, 1965):

"I. **Adverse Level.** The first effects of air pollutants are those that will probably cause untoward symptoms or discomfort. Although they are not known to be associated with the development of disease, even in sensitive groups, such effects can disturb the population stability of residential or work communities. The 'adverse' level is one at which eye irritation occurs...."

"II. **Serious Level.** Concentrations of pollutants, or possible combinations of pollutants, that are likely to cause insidious

or chronic disease or significant alteration of physiological functions in a sensitive group define the 'serious' level...."

"III. **Emergency Level.** Levels of pollutants, or combinations of pollutants, and meteorological factors likely to lead to acute sickness or death for a sensitive group of people define the 'emergency' level...."

In setting standards, this set of definitions of contamination levels is used in evaluating data on the effect on human health of a specific pollutant. The data may come from a number of sources and one of the most useful has been the threshold limit values compiled by industrial toxicologists. A report based on the data and taking into account unusually sensitive groups of people is prepared by the staff of the State of California Air Pollution Medical Studies Unit. The report leads eventually to a statement of concentrations and exposure times corresponding to each of the three levels cited above. The report is submitted to a review procedure involving several committees of the State Department of Public Health as well as outside consultants. If it passes the committee review procedure, the proposed standard then goes to the State Board of Health, which, after public hearing, may incorporate it in the State Administrative Code.

An example of the third or "emergency" level of pollution attack often cited (Goldsmith, 1968) occurred in London in 1952; from December 5 to 9 the city was covered by fog, and a temperature inversion resulted in high concentrations of SO₂ and particulates. About 4000 deaths were counted in excess of the usual number for the 3-week period from December 5 to 27. The most severely affected were those with a history of respiratory illness. The excessive mortality was associated with irritation of the respiratory tract by the contaminants.

As shown in the Appendix (Figure A-5) the time history of the contaminant concentration in the 1952 fog episode is roughly of the form of a triangular pulse. The mortality rate for each age group increased rapidly with contaminant concentration until a maximum was reached at roughly the same time as the environmental contaminant concentration; thereafter the mortality rate decayed slowly while contaminant concentration returned to background level. A primary purpose of this paper is to devise a predictive theory which can be used to pass from the contaminant pulse to the pulse in the mortality rate. Viewed in this light, an analogy to the transfer function concept of systems theory becomes evident. The

theory should be sufficiently general to permit incorporation of specific biochemical and toxicological data.

Biology of Aging and Death

Those most severely affected in an acute air pollution episode are the aged and the infirm. Hence, the present approach to the development of a theoretical model has been to modify the theory of aging and death to take into account environmental influences. According to the modern theory of the aging of higher organisms (Szilard, 1959), spontaneous mutations take place in large numbers in the genes of the somatic cells. Curtis (1966, 1967) has stressed the importance of chromosomal aberrations in cells which are seldom renewed, such as those in the brain, muscle, and kidney. Irreversible changes in the cell nucleus tend to be harmful; according to the one gene-one enzyme theory, gene damage would be expected to lead to production of faulty RNA and protein, with a concomitant damage to cell metabolic processes.

Eventually too many cells reach a state in which they are functioning poorly or not at all. At this point homeostasis breaks down, perhaps as a result of bacterial or viral infection, and the creature dies. Thus, according to this model, both aging and death are genetically determined, since the probability of chromosome aberration depends on the structure of the DNA molecules which are inherited by the creature from its parents. The experimental basis for this picture is not well established. Some of the most convincing evidence has been provided by Crowley and Curtis (1963) who studied the development of chromosome aberrations in the liver cells of two inbred strains of mice with markedly different life spans.

The liver cells of normal animals are seldom renewed unless destroyed. Hence, it is argued, the number of chromosome aberrations present at any age represent spontaneous mutations. Working with two strains of inbred mice, Crowley and Curtis destroyed parts of the liver by injection of carbon tetrachloride and sacrificed the animals 72 hours later. At the end of this period, a sufficient amount of regeneration had taken place to permit measurement of the frequency of chromosomal aberrations among the regenerated cells, assumed equal to the incidence present before destruction. The results of experiments with animals of different ages support the hypothesis that animals with higher chromosome aberration rates die at an earlier age.

Burnet (1959, 1965), while accepting Curtis' view of the importance of chromosomal aberrations in nonrenewable tissue, has emphasized the role of mutations among the renewable somatic cells in the aging process. Such cells line the respiratory and intestinal tracts and include the blood cells as well. The rapid turnover of cells exposed to the environment, such as those of the respiratory tract, probably serves to prevent loss of tissue function by replacement before environmental damage takes place. Chronic irritation of respiratory tissue by unfavorable environmental conditions—such as smoking or chronic air pollution—will presumably lead to increased rates of cell turnover. Burnet argues that mutations constantly occur during the replacement process, but probably at a rate so low that their presence would not ordinarily be manifest. The effect can be amplified, however, when a mutant is produced which has a selective proliferative advantage, perhaps as a result of producing antibody against one of the plasma proteins normally present in the internal environment of the individual. Clone descendants of the mutant cell may replace significant numbers of faithful replicas of the original cells composing the tissue, leading to a general

loss of cell and tissue function with time—the aging process. An unfavorable environment leads to increased mutational rates and accelerates the aging process. In the extreme case when the clone descendants of mutant cells proliferate without effective control, the result is malignancy.

Rate of Loss of Gene Function

Respiratory illness is a major cause of death in acute air pollution episodes. In setting up our model, let us assume that we can consider the respiratory system and its breakdown apart. Let us further limit ourselves, for the moment, to a population of genetically identical individuals born at the same instant. At some reference time, each individual possesses n_0 functioning genes among the cells of the respiratory system. These are the genes important to the functioning of the system and do not necessarily include all of the genes located on the chromosomes of the cells of that system. Let n be the number of those genes functioning without error at some time, t , after the reference time. Then for this class of genetically identical individuals we may write an expression for the decay of functioning genes as a result of spontaneous mutations:

$$\frac{dn}{dt} = F(n) \quad (1)$$

It is natural in constructing a theory of this type to assume that the decay rate is linear in the fraction of functioning genes:

$$\frac{dn}{dt} = -\lambda n \quad (2)$$

The first-order rate constant, λ , for respiratory tissue is a function of the rate of cell turnover which, in turn, is genetically determined but modified by the level of chronic air pollution (including smoking). For sufficiently short times (n not too far from n_0) this form is consistent with the approximately linear relationship between chromosome aberrations and time found experimentally for mouse liver by Crowley and Curtis (1963). There appear to be no equivalent data for renewable tissue such as the respiratory system.

According to the genetic theory of aging and death, when n reaches a sufficiently small value, the probability of homeostatic breakdown and death becomes very great. Three important variables determine the age at death: the fraction of inherited defective genes, $1 - x_0$, the first-order rate coefficient, λ , and the fraction of surviving genes at which death takes place, $x^* = n^*/n_0$. In his theory of aging, Szilard (1959) assumes that λ and x^* are the same for all humans and that "the main reason why some adults live shorter lives and others longer is the difference in the number of faults they have inherited." The data of Crowley and Curtis suggest that variations in λ are particularly important in determining age at death, while x^* differs for different inbred populations. The data indicate that values of x_0 for the two populations studied did not vary greatly. For simplicity it is assumed that λ varies for groups of different genetic constitution but that x^* and x_0 are the same for all groups. Variations in the coefficient λ seem plausible on physicochemical grounds and as a result of chronic environmental influences. The parameters x^* and x_0 are kept fixed to preserve the simplicity of the model; methods of generalization will be apparent as the picture is developed.

Integrating Equation 2 from $t = 0$ to $t = t^*$, the age at which $x = x^*$, gives the following expression for the age at death:

$$t^* = \frac{1}{\lambda} \ln x_0/x^* \quad (3)$$

According to this model, all creatures of the same genetic group would be expected to die on the same day. In fact, as pointed out in this connection by Szilard, there is a difference in the ages at death even for identical twins. Kallmann (1957) reports that the mean age difference at death for female identical twins dying above the age of 60 is about 2.6 years. Clearly, the homeostatic state does not crumble at a particular value of x^* . To take this spread into account, we could introduce a probability distribution function for the likelihood that death occurs for various values of x near x^* . We would expect the probability to go from a value near zero for values of x a little less than x^* to unity for values of x a little greater than x^* .

It is possible to speculate concerning the value of x^* . Szilard suggests that the value corresponds to a fraction of functioning cells somewhere between $1/3$ and $1/12$. According to Brody (1955), there is a loss of more than 20% of the brain cells in the human body by the age of 70. This would correspond to a fraction of functioning cells of $1/3$, a considerably larger figure than the one suggested by Szilard. Of course, the figure may vary, depending on the organ system involved. According to Black (1958), for example, the nephron population of the kidney is reduced during the aging process to 60% of the original number.

Effects of Genetic Distribution

The model developed above holds for a cohort of genetically identical individuals. Since human populations are distributed genetically, we would expect a distribution in the gene mutation rate coefficient, λ , leading to a distribution of ages at death different in character from the sharp peak behavior discussed above. For this purpose, it is convenient to introduce a distribution function $f(\lambda)$ defined in such a way that the fraction of the individuals in the original cohort with gene mutation rates between λ and $\lambda + d\lambda$ is given by the expression

$$dw = f(\lambda)d\lambda \quad (4)$$

A possible type of distribution function is shown in Figure 1. The shaded area represents the fraction of the original population surviving at age t , corresponding to all classes with values of $\lambda < (\ln x_0/x^*)/t$. As t increases and the population ages, the shaded area moves to the left and decreases.

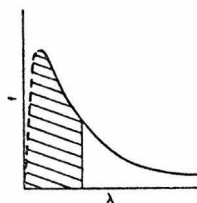


Figure 1. Schematic diagram of distribution function for gene mutation rates for group born at same time

Shaded area. Fraction of population surviving at age t

The mortality rate in terms of the fraction of the original cohort dying at any instant is given by the expression

$$\frac{dy}{dt} = -f(\lambda) \frac{d\lambda}{dt} \quad (5)$$

When Equation 3 holds for the dependence of the age at death on λ , substitution in Equation 5 gives

$$\frac{dy}{dt} = \frac{\lambda f(\lambda)}{t} \quad (6)$$

This expression can be combined with observed results for the cohort mortality rate to obtain the distribution function, $f(\lambda)$. For example, if the cohort mortality rate can be approximated by a power law:

$$\frac{dy}{dt} = Kt^p \quad (7)$$

Then

$$f(\lambda) = K(\ln x_0/x^*)^{p+1} \lambda^{-(p+2)} \quad (8)$$

It is shown below that p is near 4, which means that Equation 8 can hold only for large values of λ .

Effect of Environmental Pollutants

When a chemical contaminant, a cytotoxic agent, is introduced from the environment, cells not damaged by gene mutation (aging) will begin to malfunction. We seek a rational way to weight loss of cell function by environmental damage and by gene mutation to arrive at a criterion for death:

If n is the number of functioning genes in the physiological system at any instant, there will be an equivalent number of biochemical reaction steps controlled by these genes (Tatum, 1959). When mutations occur, a certain number of genes cease to function properly, leading to the blocking of an equivalent number of reaction steps. In our previous model, adapted from Szilard, this is an on-off process: Either the gene (or reaction step) is functioning or it is not. The presence of a chemical contaminant, such as an enzyme inhibitor, may cause deviations of the rate of the reaction step from the range of rates corresponding to normal cell function. In this way a second concept is introduced in addition to the on-off mutation loss process—namely, the extent of the deviation of the rate of a functioning reaction step from the range for normal cell function (Figure 2).

Let γ_i be the activity coefficient for a single reaction step controlled by gene i . The activity coefficient is equal to unity when the organism has never been exposed to an environ-

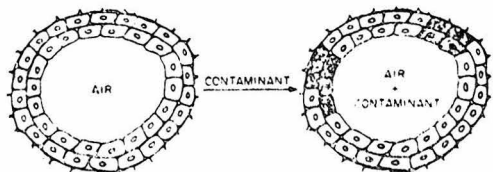


Figure 2. Schematic diagram of effect of contaminant on respiratory tissue

Left. Clonal descendants of mutant cells shown stippled. These cells are presumably not functioning as effectively as unstippled ones, faithful replicas of original cells.

Right. Contaminant absorbed by tissue interferes with metabolic processes.

mental contaminant and is less than unity when the rate of the particular step deviates from the normal range. (Obviously this is not the usual activity coefficient of chemical thermodynamics.) The activity of the gene-controlled metabolic system is defined as follows:

$$a = \sum_1^n \gamma_i = \gamma n \tag{9}$$

where n is now the total number of gene-controlled reaction steps in the system and γ is the average activity coefficient. When $\gamma = 1$, the activity is equal to n , the total number of functioning reaction steps in the system. We can now generalize our criterion for death to take into account environmental damage by assuming that death follows when the activity of the metabolic system falls to a critical value $a^* = n^*$, independent of contaminant concentration or nature.

The activity of the system when exposed to an acute air pollution episode is given by the relation

$$a = \gamma n_0 e^{-\lambda t} \tag{10}$$

Setting $a = a^*$ and differentiating

$$\frac{d\lambda}{dt} = -\frac{\lambda}{t} + \frac{1}{t} \frac{d \ln \gamma}{dt} \tag{11}$$

By Equation 5, $\frac{d\lambda}{dt}$ determines the mortality rate. Hence the effect of the contaminant on mortality rate has been reduced to the determination of how $\ln \gamma$ varies with time as a result of the contaminant. The dependence of γ on the type of contaminant is the molecular or toxicological information referred to in the introduction.

In the Appendix it is shown that mortality data can be correlated if the log of the activity coefficient depends linearly on the contaminant dose

$$\ln \gamma = -\alpha \int_0^t c dt \tag{12}$$

or

$$\frac{d \ln \gamma}{dt} = -\alpha c$$

where α is a proportionality constant and c is the concentration of the contaminant in the tissue. If we substitute Equations 11 and 12 in Equation 5, the mortality rate is given by

$$-f(\lambda) \frac{d\lambda}{dt} = f(\lambda) \left[\frac{\lambda}{t} + \frac{\alpha c}{t} \right] \tag{13}$$

During the time of the pollution episode, it can be assumed that λ and $f(\lambda)$ change relatively little. Introducing Equations 3 and 8 into Equation 13 gives

$$r \approx r_1 + \frac{f_1(\lambda)\alpha c}{t} = r_1 + K[\ln x_0/x^*]^{-1} t^{p+1} \alpha c \tag{14}$$

where r_1 is the mortality rate at t_1 , the time when the episode began. The second term on the right represents the increase in the mortality rate resulting from the contaminant. The increase depends on the rate at which the contaminant accumulates in the respiratory tissue and is determined by an equation of mass transfer. Assuming that the respiratory tissue acts as a single compartment for the storage of contaminant, the mass transfer equation for an inert species can be written (Hatch and Swann, 1961):

$$V \frac{dc}{dt} = U(c_e - c) \tag{15}$$

where c = concentration of contaminant in the body compartment, and c_e = contaminant concentration in the inspired air. The volume of respiratory tissue is designated V and the over-all mass transfer coefficient, U , is discussed by Hatch and Swann (1961). It depends, among other variables, on the gas or particle diffusion coefficient, aerodynamic patterns, and gas solubility. This equation can be solved for c if the time history of the pollutant concentration in the environment is known. The situation becomes more complicated when the contaminant reacts chemically in the tissue. As shown in the Appendix, it is necessary to modify the rate equation for an inert species to correlate the experimental data.

Further Remarks on Model

A model was proposed for the response of a human population to an environmental pollutant. It was based on the genetic theory of aging and death and a mechanism was provided for the effect of an environmental pollutant, a cytotoxic agent which interferes with the gene-controlled metabolic processes. This general approach to the problem should be stressed, since the details are likely to require modification.

In our simple theory, it was assumed that death occurs as a result of the breakdown of homeostatic processes when the gene activity function, a , for the cardio-pulmonary system, reaches a critical value, $a^* = n^*$. The theory can be extended to the prediction of morbidity rates by choosing values of $a > n^*$ as a lower cutoff, below which all individuals are classified as ill.

From a theory of this type, it would be possible to predict in detail the effect of an acute air pollution episode on a human population. It might then be possible to decide which fraction of the population is most susceptible to a given type of contaminant and to take measures to shield or evacuate the population and control the contaminant level. In conjunction with benefit-cost analyses of the type proposed by Thomas (1964) and meteorological data, the theory may lead to improved methods for setting limits on atmospheric emissions. In particular, one might be able to answer the following question: "How much would it cost to reduce the probable number of deaths as a result of acute air pollution episodes to N per year in a given urban location?" As a step in this direction, the model is applied to the famous London fog of 1952 in the Appendix.

Appendix—An Application of the Model

On the morning of December 5, 1952, unusual meteorological conditions in the Thames Valley, including Greater London, led to the development of a temperature inversion and the accumulation of a fog containing smoke, SO_2 , and other pollutants (Committee of Departmental Officers, 1954). Maximum concentrations of 4.46 mg. per cu. meter of smoke and 1.34 p.p.m. of SO_2 , about ten times the pre-episode value, were recorded during December 6 to 8. On the morning of the 9th, a southwest wind gradually dispersed the fog.

A sharp increase in the mortality rate for Greater London occurred during the period of the episode. This was followed by a rapid fall to a level still significantly above that for the weeks preceding the episode. In all, it was estimated that some 4000 extra deaths could be attributed to the pollution episode. Postmortem examinations indicated that the components of the fog produced irritation of the bronchi and bronchioles and so accelerated death among those already suffering from diseases of the respiratory and circulatory systems (Committee of Departmental Officers, 1954). This conclusion is consistent with the model discussed above. A detailed breakdown of

deaths by age group and cause is available only for the London Administrative County (LAC) (Glasgow Conference, 1953). Since pollution was most serious in the LAC, it was decided to use these figures to test the model.

Death rates in the model appear as dy/dt , the fraction of the original population of any age group which dies in a given time interval. It is therefore necessary to calculate the original population distribution—that is, the population at the time of birth of each age group. This was done in the following manner:

1. The nationwide statistics for the distribution of population in 1952 according to age group were obtained from the United Nations (1955). The number of people in the age groups 25 to 34, 35 to 44, 45 to 54, 55 to 64, 65 to 74, and 75+ in the LAC was calculated.

2. The nationwide statistics for specific death rate as a function of age (Figure A-1) were used to back-calculate by a numerical integration procedure the population of each group at the time of birth. This, of course, depends on the assumption that the specific death rate curve of Figure A-1 has remained constant over time.

3. The results of 2 were used to convert the death statistics of the Glasgow Conference to the form dy/dt .

The death rate in the form dy/dt has a mean value r_1 before the pollution episode. The log-log plot of r_1 vs. age yields a straight line with slope $p = 3.8$ (Figure A-2), which compares well with a value of 3.9 obtained from the corresponding national figures. Lines are shown in Figure A-2 for circulatory and respiratory causes, assuming that a certain constant fraction of the total death rate can be attributed to each of these causes. These fractions were obtained from the Glasgow Conference, and may change drastically during the pollution episode, but it can be assumed that at any given time they do not change appreciably from one age group to another. The lines of Figure A-2 also yield the values of K by Equation 7.

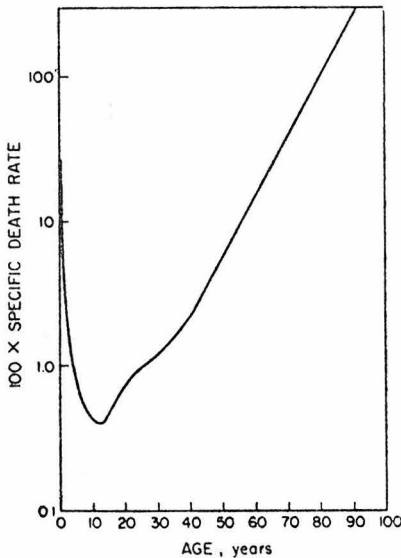


Figure A-1. Specific death rate as a function of age for England and Wales, 1953

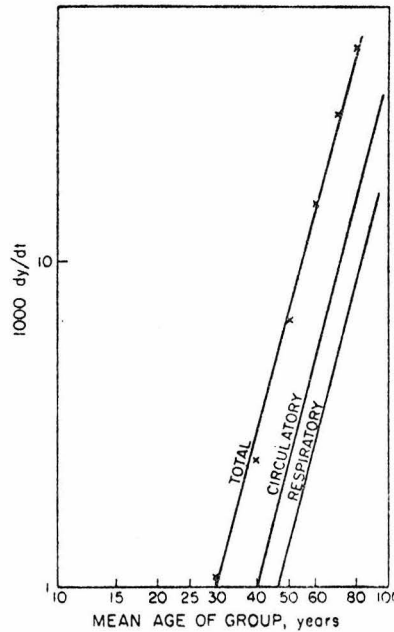


Figure A-2. Fractional death rate based on population of group at birth as a function of age group before air pollution episode

London Administrative County. Slope $p = 3.8$

At any time, according to Equation 14, a log-log plot of $(r - r_1)$ vs. age group should yield a straight line of slope $= (p + 1)$. Figures A-3 and A-4 present such straight lines for the 3 weeks ending December 13, 20, and 27. Reasonably good straight lines are obtained, and the slope is approximately 4.8 $(= 3.8 + 1)$. This conclusion is true even for the death rate broken down into respiratory and circulatory causes (Figure A-4) by using the data of the Glasgow Conference (1953), as was done for obtaining Figure A-2. The intercepts yield the values of $G = K_1[\ln x_0/x^*]^{-1} \alpha c$ as a function of time. To test the model more completely, it is necessary to have values of G for each day between December 6 and 13. These were obtained by assuming that the daily breakdown of total death rates given by Logan (1953) is the same for all age groups.

Based on the experimental observations (Committee of Departmental Officers, 1954), the concentration of pollutant in the atmosphere behaves approximately as follows (Figure A-5):

$$c_e \beta(t - t_1) \quad t_1 < t < t_2 \quad (\text{A-1a})$$

$$c_e = \beta(t_2 - t_1) \quad t_2 < t < t_2' \quad (\text{A-1b})$$

$$c_e = -\beta[t - (t_2 + t_2' - t_1)] \quad t_2' < t < (t_2 + t_2' - t_1) \quad (\text{A-1c})$$

Next it is assumed that the following laws apply to the concentration c of pollutant in the tissue,

$$V \frac{dc}{dt} = U(c_e - c) \quad c < c_e \quad (\text{15})$$

$$\frac{dc}{dt} = -kc \quad c \geq c_e \quad (\text{A-2})$$

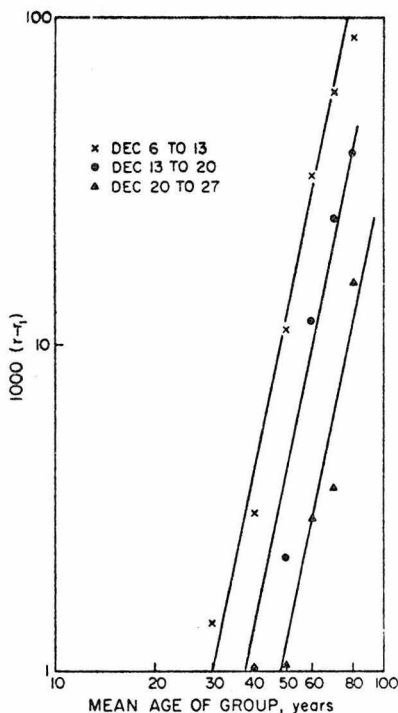


Figure A-3. Increase in death rate (all causes) over pre-episode value as a function of age group

Lines have slope of 4.8 = (p + 1)

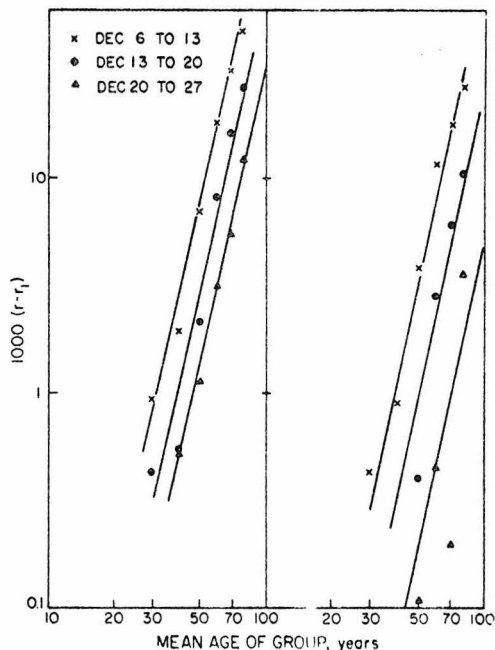


Figure A-4. Increase in death rate over pre-episode value as a function of age group

Left. Respiratory death rate
Right. Death rate due to circulatory causes
Lines have slope of 4.8 (= p + 1)

Equation 15 is applicable to the transfer of an inert (nonreacting) material from the gas to the tissue; U should be considered an average value over the time of interest. During the clearance period, which corresponds roughly to $c \geq c_a$, Equation A-2 is introduced. This is equivalent to the assumption that an independent mechanism is responsible for the elimination of contaminant from the system. The exponential decay law derived from Equation A-2 is of the form usually encountered in the literature on the clearance of particles from the respiratory system (Morrow, Gibb, *et al.*, 1967). The primary justification for the use of these equations at present is in the success of the model in correlating experimental data.

The concentration c is given by

$$c = \beta \frac{V}{U} \left[\frac{U}{V} (t - t_1) - 1 + e^{-U(t-t_1)/V} \right] \quad t_1 < t < t_2 \quad (\text{A-3a})$$

$$c = c_{h'} [t - t_2 e^{-U/V(t-t_2)} + e^{-U(t-t_2)/V}] \quad t_2 < t < t_2' \quad (\text{A-3b})$$

$$c = c_{max} e^{-k(t-t_2')} \quad t_2' < t < (t_2 + t_2' - t_1) \quad (\text{A-3c})$$

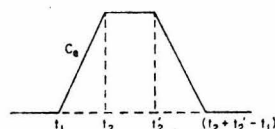


Figure A-5. Approximate form of SO_2 and particulate concentration-time history curves for 1952 London fog

where c_{max} is the maximum concentration of the pollutant in the tissue. This occurs soon after $t = t_2'$, and has been assumed to occur at $t = t_2'$.

Since $G = K[\ln x_0/x^*]^{-1} \alpha c = \text{const.} \times c$, the G values can be used to estimate the constants U/V , $\alpha[\ln x_0/x^*]^{-1}$, and k . The best values were found by trial and error (Table I) and were used to calculate "theoretical" values of the death rates. Figures A-6 and A-7 show the theoretical curves as well as the observed points. Figure A-8 is a plot of $(r - r_1) t^{-(p+1)}$ vs. time. The model predicts that the value of this parameter should be the same for all age groups at any given time. In spite of the considerable scatter among the points, the agree-

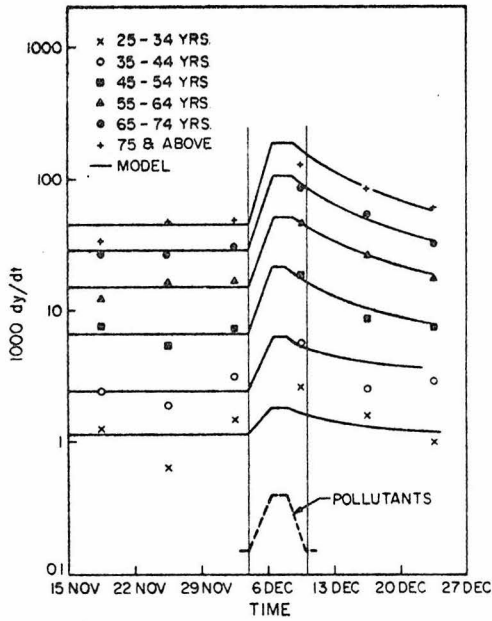


Figure A-6. Fractional death rates (all causes) as a function of time for different age groups, with lines calculated from theoretical model

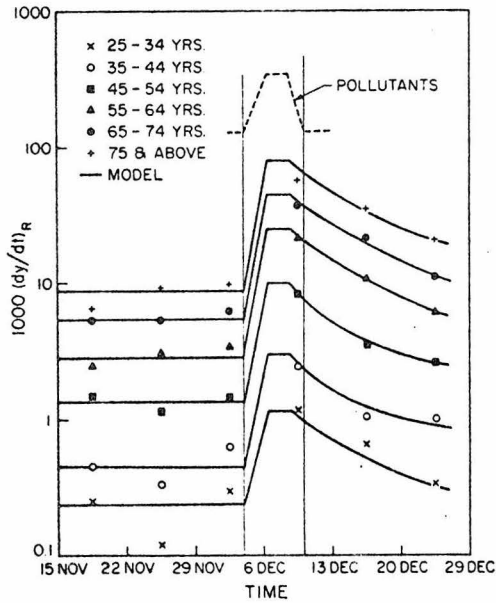


Figure A-7. Fractional death rates (respiratory causes) as a function of time for different age groups, with lines calculated from theoretical model

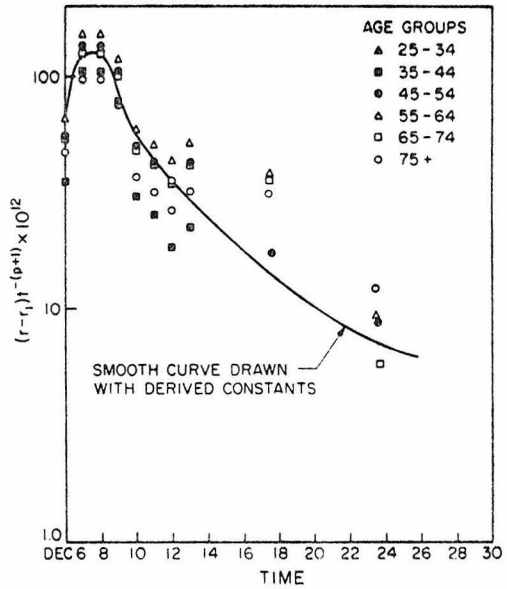


Figure A-8. Age-invariant death rate parameter as a function of time

According to theoretical model all data points should fall on single curve

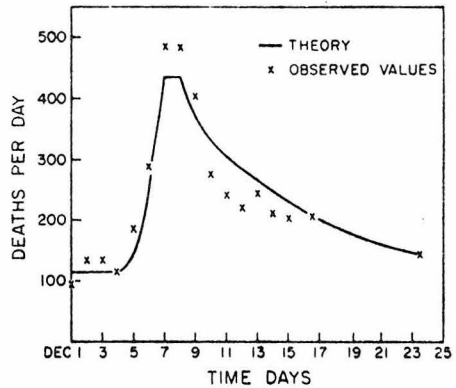


Figure A-9. Total number of deaths per day for all ages over 25 compared with calculated values

London Administrative County, December 1952 (total population 3,700,000)

Table I. Summary of Values of Constants for 1952 London Smog Episode

$$\frac{U}{V} = 5 \text{ days}^{-1}$$

$$k = 0.18 \text{ day}^{-1}$$

$$p = 3.8$$

$$K = 2.5 \times 10^{-9} (\text{year})^{-p-1} \text{ for all causes}$$

$$= 8 \times 10^{-10} (\text{year})^{-p-1} \text{ for circulatory diseases}$$

$$= 4.6 \times 10^{-10} (\text{year})^{-p-1} \text{ for respiratory diseases}$$

$$\beta = 0.5 \text{ p.p.m./day for SO}_2$$

$$\alpha [\ln (x_0/x^*)]^{-1} = 0.036 \text{ year}^{-1} (\text{p.p.m. SO}_2)^{-1}$$

ment with theory is not bad, considering the large number of uncertainties in the data and the calculations. Finally, Figure A-9 presents the death rates due to all causes and in all age groups above 25. Agreement with the curve predicted by the model is good.

Both SO₂ and particulate concentrations followed roughly the same course in their concentration-time history, and the two have been considered together as a single environmental contaminant in the calculations. Values of α and β are expressed in terms of SO₂ concentrations; these values would have to be modified for different particulate concentrations or properties, as would values of U/V and k . The values of the constants are summarized in Table I.

Nomenclature

- c = tissue contaminant concentration expressed either as actual concentration or as equivalent equilibrium gas-phase concentration or tension
- c_e = atmospheric contaminant concentration expressed in same units as c
- F = functional dependence of gene decay rate on n
- f = cohort distribution function of genetic decay rates
- f_1 = value of f when air pollution episode begins
- $G = K [\ln x_0/x^*]^{-1} \alpha c$
- k = first-order decay rate for contaminant in tissue
- K = proportionality constant in power law form of mortality rate
- n = number of genes functioning without error at any time
- n_0 = number of genes functioning without error at some given reference time
- n^* = number of genes functioning without error at which death occurs
- p = age exponent in power law form of mortality rate
- r = mortality rate, dy/dt
- r_1 = mortality rate at time pollution episode begins
- t = time or age of cohort
- t_1 = time at which air pollution episode begins
- t_2 = time at which pollutant concentration levels off
- t_2' = time at which pollutant concentration begins to decrease
- t^* = age at death
- U = over-all mass transfer coefficient
- V = volume of tissue in which contaminant is absorbed
- w = fraction of individuals in a cohort (group born at the same time) with gene mutation rates $< \lambda$

- x_0 = fraction of defective genes present at some given reference time
- x^* = fraction of surviving genes at which death takes place
- y = fraction dead of individuals in a cohort

GREEK LETTERS

- α = proportionality coefficient between $\ln \tau$ and the dose
- β = slope of atmospheric concentration vs. time curve for environmental contaminant
- γ = average activity coefficient for a cell or group of cells in the presence of a cytotoxic agent
- λ = first-order rate constant of genetic decay
- τ = dummy time variable

Literature Cited

Air Conservation Commission, American Association for the Advancement of Science, Washington, D. C., "Air Conservation," 1965.

Black, D. A. K., "Renal Function in Respiratory Failure," in "Colloquia on Ageing," G. E. W. Wolstenholme and M. O'Connor, eds., Vol. 4, p. 264, J. & A. Churchill, London, 1958.

Breslow, L., *Arch. Environ. Health* **14**, 232 (1967).

Brody, H., *J. Comp. Neurol.* **102**, 511 (1955).

Burnet, F. M., *Brit. Med. J.* **1**, 338 (1965).

Burnet, F. M., "The Clonal Selection Theory of Acquired Immunity," p. 186, Cambridge University Press, Cambridge, 1959.

Committee of Departmental Officers and Expert Advisers Appointed by the Minister of Health, "Mortality and Morbidity during the London Fog of December 1952," Report 95, H. M. Stationery Office, London, 1954.

Crowley, C., Curtis, H. J., *Proc. Natl. Acad. Sci.* **49**, 626 (1963).

Curtis, H. J., "Biological Mechanisms of Aging," p. 69, Charles C Thomas, Springfield, Ill., 1966.

Curtis, H. J., "Radiation and Ageing," in "Aspects of the Biology of Ageing," Symposia of the Society for Experimental Biology, No. XXI, p. 51, Cambridge University Press, Cambridge, 1967.

Glasgow Conference, National Smoke Abatement Society, Proceedings, 1953.

Goldsmith, J. R., "Effects of Air Pollution on Human Health," in "Air Pollution," A. C. Stern, ed., p. 547, Academic Press, New York, 1968.

Hatch, T. F., Swann, H., "Absorption and Storage of Vapors and Gases in Relation to Cardiorespiratory Performance," in "Inhaled Particles and Vapors," C. N. Davies, ed., p. 267, Pergamon Press, New York, 1961.

Kallmann, F. J., "Twin Data on the Genetics of Ageing," in "Colloquia on Ageing," Vol. 3, p. 131, J. & A. Churchill, London, 1957.

Logan, W. P. D., *Lancet* **1953**, 336-8 (Feb. 14, 1953).

Morrow, P. E., Gibb, F. R., Gazioglu, K., "Clearance of Dust from the Lower Respiratory Tract of Man. An Experimental Study," in "Inhaled Particles and Vapors," C. N. Davies, ed., Vol. II, p. 351, Pergamon Press, Oxford, 1967.

Sargent, F., *Arch. Environ. Health* **14**, 35 (1967).

Szilard, L., *Proc. Natl. Acad. Sci.* **45**, 30 (1959).

Tatum, E. L., *Science* **129**, 1711 (1959).

Thomas, H. A., Jr., *J. Am. Water Works Assoc.* **56**, 1087 (1964).

United Nations Demographic Yearbook, 1955.

Received for review June 25, 1968. Accepted October 31, 1968. Research supported in part by the National Air Pollution Control Administration.

CORRESPONDENCE

Precise Estimation of Reaction Orders

In two recent papers (2, 3) (the earlier one coauthored by Watson), Kittrell and Mezaki present a method for analyzing isothermal, constant volume kinetic data of irreversible reactions. In my comments on these two papers, I shall use the nomenclature of Reference 2.

Working with a transformed variable $z^{(\lambda)}$ defined by Equation 1, Kittrell *et al.* minimize the sum of squares $S(\lambda)$ (Equation 2) with respect to the parameters k and n :

$$z^{(\lambda)} = \begin{cases} \frac{y^{(\lambda)} - 1}{\lambda y^{\lambda-1}} & \lambda \neq 0 \\ j \ln y & \lambda = 0 \end{cases} \quad (1)$$

where $y = (1 - x)^{-1}$, $\lambda = (n - 1)$
 j = geometric mean of the N values of y

$$S(\lambda) = \sum_{i=1}^N (z_i^{(\lambda)} - bt_i)^2 \quad (2)$$

where $b = kC_{A0}^\lambda j^{1-\lambda}$

The estimates of n and k thus obtained are claimed to be maximum likelihood estimates. This claim is based on the assumption that $y^{(\lambda)}$ [hence $z^{(\lambda)}$] is a variable which simultaneously achieves

- (i) Linearity of the model
- (ii) Equal variance at all points (homoscedasticity)
- (iii) Normality of error distribution
- (iv) Independence of observations

Kittrell, Mezaki, and Watson (3) cite the paper by Box and Cox (1) to justify the choice of the transformation. A careful reading of that paper reveals the following: "We have supposed that after suitable transformation from y to $y^{(\lambda)}$: (a) the expected values of the transformed observations are described by a model of simple structure; (b) the error variance is constant; and (c) the observations are normally distributed. Then we have shown that the maximized likelihood for λ , and also the approximate contribution to the posterior distribution of λ , are each proportional to a negative power of the residual sum of squares for the variate $z^{(\lambda)} = y^{(\lambda)}/j^{1/\lambda}$. The 'over-all' procedure seeks a set of transformation parameters for which (a), (b), and (c) are simultaneously satisfied, and sample information on all three aspects goes into the choice . . . The above procedure depends on specific assumptions, but it would be quite wrong for fruitful application to regard the assumptions as final. The proper attitude of skeptical optimism is accurately expressed by saying that we tentatively

entertain the basis for analysis, rather than that we assume it. The checking of the plausibility of the present procedure is discussed in Section 5."

It is apparent that Kittrell and Mezaki, in their numerical examples, make no attempt to use sample information to check the "plausibility" of the assumptions (as was intended by Box and Cox). Indeed, in the absence of multiple observations at a given time, it is impossible to conduct either Bartlett's test or the Neyman-Pearson test to check assumptions (ii) and (iii), respectively. Assumption (i), on the other hand, is true by definition of $z^{(\lambda)}$.

It is therefore unjustifiable *a priori* to regard the estimates of n and k as maximum likelihood estimates. Further, if the choice were given to the experimenter, he would in all probability make the assumptions (ii) to (iv) apply to his observations (the C_A 's) rather than to an artificially defined variable such as $y^{(\lambda)}$ or $z^{(\lambda)}$. [Obviously they cannot be true of both the C_A 's and the $y^{(\lambda)}$'s.] He would do this for lack of further statistical information on the errors. The criterion that now leads to maximum likelihood estimates is

$$Min_{k,n} S'(k,n) = \sum_i (C_A - C_{A \text{ cal}})^2 \quad (3)$$

$$\text{where } C_{A \text{ cal}} = \begin{cases} [C_{A0}^{1-n} - (n-1)kt]^{1/(1-n)} & n \neq 1 \\ C_{A0} \exp(-kt) & n = 1 \end{cases}$$

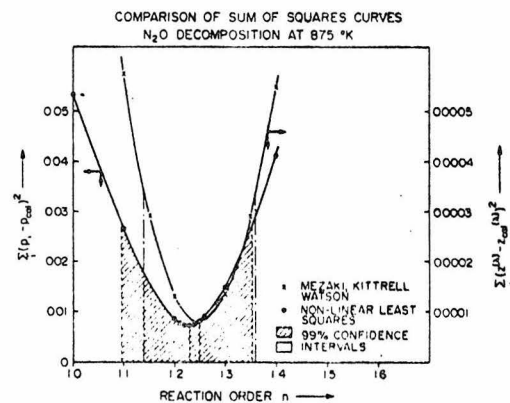


Figure 1. Comparison of sum of squares curves for N_2O decomposition at $875^\circ K$. p_1 represents the partial pressure of N_2O , which was measured by Pease (4)

We can now subject the data to a nonlinear squares analysis, in the light of Equation 3. For the decomposition of N_2O at 875 °K, the results of such an analysis are compared in Table I and Figure 1 with the results obtained by Kittrell, Mezaki, and Watson for the same data points. No significant difference in computing time was noticed.

TABLE I. COMPARISON OF PARAMETER ESTIMATES AND 99% CONFIDENCE INTERVALS FOR N_2O DECOMPOSITION AT 875 °K.
[Data from Pease (4)]

	Kittrell, Mezaki, and Watson	Nonlinear least squares with C_A 's
$k \times 10^4$	(1.45 ± 0.38)	(1.31 ± 0.54)
n	(1.25 ± 0.11)	(1.23 ± 0.13)
Units of k are $\left(\frac{kg}{cm^2}\right)^{1-n} \text{sec}^{-1}$.		

It is seen that the results differ not only in the parameter estimates, but more importantly in the confidence limits. The confidence limits with the nonlinear analysis, also computed by the procedure of Box and Cox, are seen to be less optimistic than those of Kittrell and Mezaki. The nonlinear analysis performed here does not involve differentiation of the data to obtain reaction rates. Hence the difference in the results cannot be due to computational errors. The only explanation is that the basic assumptions are different in the two cases. Kittrell and Mezaki use a least squares criterion on a transformed variable $z(\lambda)$, and claim without further justification that this leads to maximum likelihood estimates. It is my contention that in the absence of further statistical information on the errors, the experimenter is better off using a least squares criterion on the observed variable C_A and performing a nonlinear analysis as above.

The only specific complaint which Dr. Kittrell expresses in his reply to my comments (which follow on page 78) seems to be that I did not carry out a residuals test on the data. Table II shows the results of such a test, using the same example as before—the decomposition of

TABLE II. ANALYSIS OF VARIANCE OF N_2O DECOMPOSITION DATA AT 875 °K^a
[Data from Pease (4)]

Source of Variation	Degrees of Freedom	Mean Squares, $\left(\frac{kg}{cm^2}\right)^2$	
		Least squares analysis of transformed variable of Kittrell and Mezaki	Nonlinear least squares analysis of observed variable Ravimohan
Due to model (2 parameters)	1	$\frac{278.86}{1} = 278.86$	$\frac{223.17}{1} = 223.17$
Residual	4	$\frac{5.40}{4} = 1.35$	$\frac{0.0942}{4} = 0.0235$
Ratio of mean sum of squares due to model to the mean residual		$\frac{278.86}{1.35} = 206.56$	$\frac{223.17}{0.0235} = 9950.0$

^a The deviations have been taken from the $t = 0$ value of the observed variable p_t .

N_2O at 875 °K, with data taken from Pease (4). The fit is shown to be much better when the raw untransformed observations are used for the analysis as I suggested above. The plausibility of the assumptions regarding $z(\lambda)$ thus remain unverified, even approximately. The experimenter can still ask whether, if at all, it helps him to shift the assumptions from the observed variable to an artificially defined variable, $z(\lambda)$.

REFERENCES

- (1) Box, G. E. P., and Cox, D. R., *J. Royal Statist. Soc., Series B*, **26** (2), 211 (1966).
- (2) Kittrell, J. R., and Mezaki, Reiji, Ch. 10 In "Applied Kinetics and Chemical Reaction Engineering," R. L. Goring and V. W. Weekman, Eds., American Chemical Society Publications, Washington, D.C. (1967).
- (3) Kittrell, J. R., Mezaki, Reiji, and Watson, C. C., *IND. ENG. CHEM.*, **58** (5), 51 (1966).
- (4) Pease, R. N., *J. Chem. Phys.*, **7**, 769 (1939).

A. L. RAVIMOHAN

Division of Chemical Engineering
California Institute of Technology
Pasadena, Calif.

Replies to Comments of A. L. Ravimohan

Mr. Ravimohan apparently has three primary criticisms of the paper in question (1). He asserts (a) we did not realize that the Box-Cox transformation does not guarantee maximum likelihood estimates of a reaction order; (b) we did not utilize sample information to test the transformed error variable for normality, independence, and constancy of variance; and (c) in the absence of any numerical information to the contrary, the experimenter should assume that the reactant concentrations possess these three properties rather than any transformation of the concentration.

I believe that we belabored point (a) sufficiently in the paper. We stated twice on page 53 and once on page 54 that the transformations only achieve errors with an independent, normal distribution of constant variance to the extent that it is possible. On page 59 we say, "The method . . . transforms the dependent variable to achieve an error distribution as consistent as possible with the assumptions inherent in a least squares analysis. Hence, if these assumptions are fulfilled, the maximum likelihood estimates of the reaction order and the transformed rate constant are obtained . . ." A similar statement may be found on page 123 of Ravimohan's Reference 2.

Concerning point (b), we did not formally test the plausibility of these assumptions; Mr. Ravimohan pointed out that since insufficient data exist, such tests are impossible. It might be pointed out that sufficient data are seldom available from kinetic experiments to conduct these particular statistical tests rigorously. We did, however, use residuals to approximately test these assump-

tions (see our examples). The residual tests we used are those covered in Draper and Smith, "Applied Regression Analysis," pp 86-103, Wiley, New York, N.Y. (1966). These attempt to specify whether the transformed variable or the untransformed variable has constant variance, etc., and are quite distinct from the analysis of variance contained in Mr. Ravimohan's Table II on page 77. Since the residual sum of squares is being minimized in obtaining Ravimohan's entry of Table II, it is not surprising to find a smaller residual mean square is obtained by nonlinear least squares; this is the preferred method, however, only if all data are of equal precision.

The criticism of point (c) is quite subjective. If the experimenter feels that C_A has the correct properties, then the unweighted nonlinear least squares analysis is quite appropriate. Similarly, the transformation in C_A often has been used to stabilize error variance. (Our procedure approximately reduces to this for a first-order reaction.) However, if no prior knowledge of the error distribution is available, our procedure will be quite valuable in parameter estimation; the point and interval estimates should approach those of the above weighting procedures if those procedures are appropriate.

REFERENCE

- (1) Kittrell, J. R., Mezaki, R., and Watson, C. C., *IND. ENG. CHEM.*, **58** (5), 51 (1966).

J. R. KITTRELL

*Chevron Research Co.
Richmond, Calif.*

For the precise determination of reaction orders of power function rate models, Ravimohan recommends the use of nonlinear squares analysis for integral rate equations rather than the use of linear least squares analysis for a transformed variable. The reason for this recommendation is that two basic assumptions imposed upon the error variance of the transformed variable (constant error variance at all experimental points and normality of error distribution) are not justified for the transformed variable exemplified by Kittrell *et al.* (1).

In many cases of kinetic study, not enough data have been gathered to obtain the accurate information concerning the behavior of error variance of the dependent variable. With unweighted nonlinear least squares one can approximately maximize the likelihood function. Thus we obtain the most precise estimates of parameters only when we do know the nature of error variance. In any event, one can check the "plausibility" of these assumptions after a trial fit by using simple tests such as residual plots. If the assumptions are found to be inappropriate, then perhaps a nonlinear model of the original observations should be used.

The confidence intervals of nonlinear parameter estimates shown in Table I of Ravimohan's correspondence give some information relative to the allowable range of

parameter estimates. For this case, however, it would be more adequate to show the joint confidence regions for parameter estimates.

With limited knowledge on error variance, it would be rather difficult to judge which estimation method is superior. Nevertheless, the use of a transformed variable reported in Reference 1 seems to furnish more accurate estimates of parameters in any situations of error variance of the dependent variable.

The most important assumption made in these analyses is that the kinetic model is correct. This could lead to more problems in the analysis than any of the other assumptions, especially if the model is not correct.

Acknowledgment

I am indebted to W. J. Hill for his valuable suggestions.

REFERENCE

- (1) Kittrell, J. R., Mezaki, Reiji, and Watson, C. C., *IND. ENG. CHEM.*, **58** (5), 51 (1966).

REIJI MEZAKI

*Department of Engineering and Applied Science
Yale University
New Haven, Conn.*

Reprinted from



Vol. 61, May 1969, Pages 76-78
Copyright 1969 by the American Chemical Society and reprinted by permission of the copyright owner

Abstract Submitted

For the 1970 Plasma Physics Meeting of
The American Physical Society held at Washington, D.C.

November 4-7, 1970

Physical Review
Analytic Subject Index
Number 35.5

Bulletin Subject Heading in
which paper should be placed:
Gas Discharges

Electron Density, Collision Frequency and Electric Field Measurements in D.C. Discharges in Pure Rare Gases and their Binary Mixtures.* A.L. Ravimohan and F.H. Shair, California Institute of Technology. A TM_{011} Microwave Cavity was used to measure the radially averaged electron density n_e and the electron-neutral collision frequency ν_{en} in d.c. glow discharge positive columns. Electric field E was measured by measuring the floating potential across pairs of probes in the plasma. The pure gases studied were He, Ne and Ar at pressures of 1-8 torr and discharge currents of 5-20 mA. The calculated values of the electron drift velocity v_d in He and Ne are substantially lower than the Bradbury and Nielson¹ drift tube values, indicating substantial effect of metastables in the range of p and I investigated. Discharges in He-Ar and He-Ne mixtures at $p = 2-5$ torr and $I = 15$ mA exhibit time and space dependent values of n_e, ν_{en}, E due to the effect of cataphoresis. The results indicate that the Shair and Remer² model is a reasonable description of the phenomenon of cataphoresis in these mixtures with He where the impurity (Ar or Ne) content is in the range of 2-20%.

*Work supported by the U.S. Atomic Energy Comm.

¹N.E. Bradbury and R.A. Nielson, Phys. Rev. 50, 950 (1936)

²F.H. Shair and D.S. Remer, J. Appl. Phys. 39, 5762 (1968)

Submitted by

Dr. F. H. Shair
2330 Glen Canyon
Altadena, Cal. 91001

Abstract Submitted

For the 1970 Plasma Physics Meeting of
The American Physical Society held at Washington, D.C.
November 4-7, 1970

Physical Review
Analytic Subject Index
Number 35.5

Bulletin Subject Heading in
which paper should be placed:
Gas Discharges

Kinetics of Methane Conversion in an Argon Positive Column Plasma*. A.L. Ravimohan and F.H. Shair, California Institute of Technology. By employing a flow system with low residence times ($\sim 30-50$ millisecc) and discharges with low power inputs ($\sim 10^{-1}$ watts/cm³) it is possible to convert up to 5% of the methane selectively into ethane, ethylene and hydrogen, with negligible formation of solid and liquid products. The percentage of methane in the feed affects the product distribution with best results achieved at a CH₄ concentration of approx. 20%. Electron densities in the discharge were simultaneously measured by perturbation of the resonance of a TM₀₁₀ microwave cavity. A mechanism is proposed to correlate the data and to derive integrated cross-sections for electron-impact dissociative steps such as CH₄+e → CH₃+H+e and CH₄+e → CH₂+H₂+e. Experimental work continues on pulsed d.c. discharges where the residence time in the discharge zone is effectively reduced even further.

*Work supported by the U.S. Atomic Energy Comm.

Submitted by

Dr. F. H. Shair
2330 Glen Canyon Rd.
Altadena, Calif. 91001

Abstract of paper to be presented
at the Los Angeles National Meeting
of the American Chemical Society
March 28 - April 2, 1971

REACTIONS OF METHANE IN THE POSITIVE COLUMN OF
A PULSED D.C. GLOW DISCHARGE*

Arakali L. Ravimohan and Fredrick H. Shair, Department of Chem. Eng.,
California Institute of Technology, Pasadena, California, 91109

In a previous investigation¹ it was shown how it is possible to convert CH_4 selectively into C_2H_6 , C_2H_4 and H_2 in a d.c. discharge flow system with low residence times and low power inputs. This suggested the use of a pulsed power supply on the same type of system as a means to reducing the effective residence time even further. Results will be presented of experiments conducted at 3-9 torr using both argon and helium as carrier gases, with pulse durations ~ 1 millisecc and pulse intervals $\sim 20-50$ millisecc. When the average residence time in the discharge tube is of the same order of magnitude as the pulse interval, the reaction is exceptionally clean, with no trace of by-products, either in the solid, liquid or gas phase. Pulse current was measured with a current probe, and was typically 1-10 mA (peak). A TM_{010} microwave cavity was also used to obtain the transient electron densities in the discharge, which varied between 10^9 and 10^{10} electrons/cc. The results are consistent with a free radical mechanism with electron impact dissociation as the initiating step.

¹A. L. Ravimohan and F. H. Shair, Paper presented at the 1970 Annual Meeting of the Div. of Plasma Phys. of the Am. Phys. Soc., Washington, D.C., Nov. 4-7, 1970

*Work supported by the U.S. Atomic Energy Commission under Project Agreement No. 1 under AT(04-3)-767

Kinetics: Gas Phase or Plasma Chemistry